Small Esters, Ketones, and Amines with Large Amplitude Motions

Von der Fakultät für Mathematik, Informatik und Naturwissenschaften der RWTH Aachen University zur Erlangung des akademischen Grades einer Doktorin der Naturwissenschaften genehmigte Dissertation

vorgelegt von

Dipl.-Chem.

Ha Vinh Lam Nguyen

aus Hanoi

(Vietnam)

Berichter: Universitätsprofessor Dr. rer. nat. W. Stahl

Universitätsprofessor Dr. rer. nat. A. Lüchow

Tag der mündlichen Prüfung: 08.03.2012

Diese Dissertation ist auf den Internetseiten der Hochschulbibliothek online verfügbar.

For the thorn birds.

Yesterday is history. Tomorrow is mystery. But today is the gift. That's why it's called PRESENT.

Grand Master Oogway (Kung Fu Panda)

Acknowledgement

I owe my deepest gratitude to Prof. Dr. rer. nat. W. Stahl who has always leaded and helped me since many years not only in my study but also in my life. From the small research projects to my diploma thesis, from my first paper to this dissertation would not have been successful without his help. I would like to thank for his advice on life and for every story he told me. There were some long ones, sometimes only one or two sentences, but every time I received meaningful lessons.

I would like to thank Prof. Dr. rer. nat. A. Lüchow for the advise in quantum chemical questions. It is a pleasure to thank Dr. I. Kleiner for the excellent cooperation, for her support and the nice discussions for many papers, meetings, and proposes.

My dear colleagues - my lovely girlfriends, D. Lucht, H. Mouhib, L. Sutikdja, Y. Zhao, L. Tulimat, have always supported me during my work and shared weal and woe like a real family. I would like to thank them for their helpful hints and support.

I am indebted to my parents who brought me up, give me a sufficient and happy life, and guided me to study in the wonderful country, Germany. This thesis would not have been possible without their support. I would like to show my gratitude to Minh, my sister, for her love and amusement which brought me many experience of life.

I thank my small family for the smile, the care, and the endless love which gave me energy and belief in my work and my life.

I am deeply grateful to all of my friends in the beautiful city Aachen who made the habitation here one of the most beautiful time in my life.

At last, I would like to thank the past days. Not only the happy days but also the blue days have brought me more and more love for today.

Cảm ơn thầy, GSTSKH W. Stahl, người trong bao nhiêu năm qua đã luôn dìu dắt, giúp đỡ em không chỉ trong học tập. Từ những nghiên cứu nhỏ đến luận văn tốt nghiệp thạc sĩ, từ những bài báo đầu tiên đến đến luận văn tiến sĩ này, tất cả sẽ không thể thành công như thế nếu không có sự chỉ dẫn tận tình của thầy. Cảm ơn thầy về những lời khuyên trong cuộc sống, cảm ơn thầy về những câu chuyện thầy kể, lúc dài, khi chỉ một hai câu, nhưng luôn cho em những bài học đầy ý nghĩa.

Cảm ơn GSTSKH A. Lüchow về những chỉ bảo tận tình của thầy mỗi khi em gặp khó khăn. Cảm ơn TS I. Kleiner về những dự án chung và những bài báo tuyệt vời.

Cảm ơn Daniela, Halima, Lilian, Yueyue, Layla, những cô bạn đồng nghiệp, những cô bạn gái đáng yêu đã luôn giúp tớ trong công việc cũng như luôn sẻ chia về tinh thần như một gia đình thật sự.

Cảm ơn bố mẹ đã nuôi dạy con lớn khôn, cho con một cuộc sống đủ đầy và hạnh phúc, cho con học ở đất nước Đức xinh đẹp để con có được thành công, để hôm nay có luận văn tốt nghiệp này. Cảm ơn bố mẹ đã luôn ở bên con những khi vui cũng như những lúc khó khăn, động viên và hỗ trợ con cả về tinh thần và vật chất để con có thể tập trung hoàn thành tốt công việc của mình.

Cảm ơn dì Minh đã chăm sóc cho bố mẹ trong suốt thời gian chị đi học. Không có em, chắc chắn chị không thể yên tâm làm việc và cũng không thể viết được một luận văn tiến sĩ mà chị rất hài lòng. Cảm ơn em về tình yêu và những chia sẻ đã cho chị nhiều trải nghiệm về cuộc sống và bản thân mình.

Cảm ơn gia đình nhỏ của tôi vì những nụ cười, sự quan tâm và tình yêu vô bờ bến đã đem lại cho tôi niềm tin và nghị lực trong công việc.

Cảm ơn thành phố Aachen xinh đẹp với những người bạn đã làm cho quãng thời gian ở đây trở thành một trong những khoảng thời gian đẹp nhất của cuộc đời tôi.

Và cuối cùng, xin cảm ơn những ngày đã qua! Những ngày hạnh phúc cũng như khổ đau đều cho tôi thêm yêu cuộc sống và thêm yêu ngày hôm nay.

Contents

Chapter 3

Vinyl acetate

Quantum chemical calculations and improvement of the fit

Chapter 4

Isopropenyl acetate

Two rotors and C$_1$ frame symmetry

Chapter 5

Methyl propionate

Two rotors and C$_S$ frame symmetry

Chapter 6

Diethyl ketone

Two equivalent rotors and C$_{2v}$ frame symmetry

Chapter 7

Acetone

New aspects of the internal rotation in acetone

B. Nitrogen inversion tunneling

Chapter 8

Diethyl amine

The effects of nitrogen inversion tunneling, methyl internal rotation, and ^{14}N quadrupole coupling

Chapter 9

Methyl *tert*-butyl amine

Nitrogen inversion tunneling, ^{14}N quadrupole coupling, and internal rotation in an almost prolate symmetric top (κ = −0.994)

Chapter 10

Triethyl amine

Conformational landscape – the wind mill structure found in an oblate symmetric top

Conclusion   **144**

Appendix

Introduction

The rotational energy levels of a rigid body are completely determined by its three principal moments of inertia. However, for many molecules this simple rigid body approach is often not sufficient, since there are effects like centrifugal distortion, small amplitude motions (e.g. vibrations), and large amplitude motions which make it necessary to modify the simple rigid rotor model. This thesis deals with investigations on small molecules which exhibits important type of large amplitude motions, internal rotation and nitrogen inversion tunneling, by a combination of molecular beam Fourier transform microwave (MB-FTMW) spectroscopy and quantum chemical calculations.

MB-FTMW spectroscopy is an excellent tool to study molecular structure and dynamics. By this way a large number of molecules were investigated. The classical method to determine the molecular structure is isotopic substitution which was applied for the first assignment of almost every small molecule like hydrogen cyanide HCN,[1] cyanamid NH_2–CN,[2] diazomethane CH_2=N=N,[3] formaldehyde,[4,5] to somewhat larger molecules like methanol,[6] formamide,[7,8] ethanol,[9] glycol aldehyd,[10,11] etc. Surprisingly, only very few simple esters, ketones, and amines were among them, though they are very important class in chemistry. This might be due to the fact that even small esters, ketones, and amines contain quite a large number of atoms which makes them too big for classical structure determination by isotopic substitution. Moreover, even under molecular beam conditions usually several conformers exist. For those molecules, conformers can be identified by comparing the experimental data with quantum chemical calculations carried out using the program *Gaussian03*[12] and *Gaussian09*[13] package. Different methods like Møller-Plesset perturbation theory of second order (MP2) and B3LYP density function of theory and basis sets were chosen and compared. Frequency calculations were carried out in addition to structure optimizations. In many molecules energy potential curve and energy potential surface were calculated to study the interaction in the molecules. Theory to quantum chemical calculations has been reported in many books (e.g. Cramer[14]) and papers (e.g. ref.[15,16]) and therefore will not be repeated here.

The combination of microwave spectroscopy and quantum chemical calculations was a successful method to assign the rotational spectrum with splittings due to internal rotation of *trans* ethyl acetate (Chapter 1, published in *J. Mol. Spectrosc.* **257**, 111 (2009)), allyl acetate

(Chapter 2, published in *Mol. Phys.* **108**, 763 (2010)), vinyl acetate (Chapter 3), isopropenyl acetate (Chapter 4, published in *J. Mol. Spectrosc.* **264**, 120 (2010)), and methyl propionate (Chapter 5, submitted to *Mol. Phys.* 2012). In all cases structure optimization and energy potential curve were carried out for identify the conformer. Two ketones, diethyl ketone (Chapter 6, published in *Chem. Phys. Chem.* **12**, 1900 (2011)) and acetone (Chapter 7), were also investigated. Here, the energy potential surfaces were additionally calculated to study the interaction between two equivalent internal methyl rotors.

For assignment of molecules with nitrogen inversion tunnelling like diethyl amine (Chapter 8, published in *J. Chem. Phys.* **135**, 024310 (2011), doi:10.1063/1.3607992) and methyl *tert-*butyl amine (Chapter 9) only structure optimization and frequency calculations were necessary. In the case of triethyl amine (Chapter 10, paper in progress) many geometries can be generated by rotating the three ethyl groups. Quantum chemical calculations turned out to be very helpful to determine the possible stable conformers and carried out an orientation for the spectrum assignment.

Experimental setup

All spectra used throughout this thesis were recorded using two MB-FTMW spectrometers in the frequency ranges 4 to 26.5 GHz and 26.5 to 40 GHz. They are modified versions of those described in ref. [17,18] and ref. [19], respectively. All substances were obtained from Merck Schuchardt OHG, Hohenbrunn, Germany, and used without further purification. A gas mixture containing 1% substance in helium at a total pressure of 100 to 200 hPa was used throughout. We have chosen helium as a carrier gas because the cooling is not as effective as with argon or neon and therefore also higher J levels can still be observed.

The spectrometers can be operated in two different modes, the high resolution mode and the scan mode. In the high resolution mode all lines are split into doublets due to the Doppler effect. The molecular transition frequency is the center frequency. The splitting depends on both, the center frequency and the velocity of the molecular beam. In the scan mode a series of overlapping spectra taken in the high resolution mode are automatically recorded and only the presence of lines is indicated in a broad band scan.

References

[1]J. W. Simmons, W. E. Anderson, W. Gordy, *Phys. Rev.* **77**, 77 (1950).

[2]J. K. Tyler and J. Sheridan, *Proc. Chem. Soc.* 155 (1959).

[3]A. P. Cox, L. F. Thomas, J. Sheridan, *Nature* **181**, 1000 (1958).

[4]R. B. Lawrence and M. W. P. Strandberg, *Phys. Rev.* 83, 363 (1951).

[5]H. Hirakawa, T. Oko, K. Shimoda, *J. Phys. Soc. Japan* **11**, 1207 (1956).

[6]R. H. Hughes, W. E. Good, D. K. Coles, *Phys. Rev.* **84**, 418 (1951).

[7]R. J. Kurland, *Bull. Am. Phys. Soc.* **1**, 12 (1956).

[8]C. C. Costain and J. M. Dowling, *J. Chem. Phys.* **32**, 158 (1960).

[9]L. M. Imanov, Ch. O. Kadzhark, I. D. Isaev, *Opt. Spectrosc.* **18**, 194 (1965).

[10]M. A. Simons and R. C. Woods, *Symp. Mol. Struct. & Spectrosc. Ohio* 47 (1969).

[11]K. M. Marstokk and H. Møllendal, *J. Mol. Struct.* **5**, 205 (1970).

[12]Gaussian 03, Revision D.02, M. J. Frisch, G. W. Trucks, H. B. Schlegel, G. E. Scuseria, M. A. Robb, J. R. Cheeseman, J. A. Montgomery, Jr., T. Vreven, K. N. Kudin, J. C. Burant, J. M. Millam, S. S. Iyengar, J. Tomasi, V. Barone, B. Mennucci, M. Cossi, G. Scalmani, N. Rega, G. A. Petersson, H. Nakatsuji, M. Hada, M. Ehara, K. Toyota, R. Fukuda, J. Hasegawa, M. Ishida, T. Nakajima, Y. Honda, O. Kitao, H. Nakai, M. Klene, X. Li, J. E. Knox, H. P. Hratchian, J. B. Cross, V. Bakken, C. Adamo, J. Jaramillo, R. Gomperts, R. E. Stratmann, O. Yazyev, A. J. Austin, R. Cammi, C. Pomelli, J. W. Ochterski, P. Y. Ayala, K. Morokuma, G. A. Voth, P. Salvador, J. J. Dannenberg, V. G. Zakrzewski, S. Dapprich, A. D. Daniels, M. C. Strain, O. Farkas, D. K. Malick, A. D. Rabuck, K. Raghavachari, J. B. Foresman, J. V. Ortiz, Q. Cui, A. G. Baboul, S. Clifford, J. Cioslowski, B. B. Stefanov, G. Liu, A. Liashenko, P. Piskorz, I. Komaromi, R. L. Martin, D. J. Fox, T. Keith, M. A. Al-Laham, C. Y. Peng, A. Nanayakkara, M. Challacombe, P. M. W. Gill, B. Johnson, W. Chen, M. W. Wong, C. Gonzalez, J. A. Pople, Gaussian, Inc., Wallingford CT, 2004.

[13]Gaussian 09, Revision A.02, M. J. Frisch, G. W. Trucks, H. B. Schlegel, G. E. Scuseria, M. A. Robb, J. R. Cheeseman, G. Scalmani, V. Barone, B. Mennucci, G. A. Petersson, H. Nakatsuji, M. Caricato, X. Li, H. P. Hratchian, A. F. Izmaylov, J. Bloino, G. Zheng, J. L. Sonnenberg, M. Hada, M. Ehara, K. Toyota, R. Fukuda, J. Hasegawa, M. Ishida, T. Nakajima, Y. Honda, O. Kitao, H. Nakai, T. Vreven, J. A. Montgomery, Jr., J. E. Peralta, F. Ogliaro, M. Bearpark, J. J. Heyd, E. Brothers, K. N. Kudin, V. N. Staroverov, R. Kobayashi, J. Normand, K. Raghavachari, A. Rendell, J. C. Burant, S. S. Iyengar, J. Tomasi, M. Cossi, N. Rega, J. M. Millam, M. Klene, J. E. Knox, J. B. Cross, V. Bakken, C. Adamo, J. Jaramillo, R. Gomperts, R. E. Stratmann, O. Yazyev, A. J. Austin, R. Cammi, C. Pomelli, J. W. Ochterski, R. L. Martin, K. Morokuma, V. G. Zakrzewski, G. A. Voth, P. Salvador, J. J. Dannenberg, S. Dapprich, A. D. Daniels, O. Farkas, J. B. Foresman, J. V. Ortiz, J. Cioslowski, D. J. Fox, Gaussian, Inc., Wallingford CT, 2009.

[14]C. J. Cramer, Essentials of Computational Chemistry, Wiley, Chichester, 2002, 2nd edition.

[15]C. Møller and M. S. Plesset, *Phys. Rev.* **46**, 618 (1934).

[16]A. D. Becker, *Phys. Rev. A* **38**, 3098 (1988).

[17]U. Andresen, H. Dreizler, J.-U. Grabow, W. Stahl, *Rev. Sci. Instrum.* **61**, 3694 (1990).

[18]J.-U. Grabow, W. Stahl, H. Dreizler, *Rev. Sci. Instrum.* **67**, 4072 (1996).

[19]I. Merke, W. Stahl, H. Dreizler, *Z. Naturforsch.* **49a**, 490 (1994).

A. Internal rotation

Introduction

Internal rotation is a large amplitude motion where an internal rotor, e.g. a methyl group, rotates with respect to the rest of the molecules, usually denoted as the frame. The internal rotor can be symmetric or asymmetric and the torsional potential can have different numbers of equivalent minima. Most frequent are methyl groups attached to an asymmetric frame for which a threefold potential is found.[1] The height of the potential barrier varies in a wide range depending on the rotor and the frame. The quantum chemical prediction of torsional barriers is even with modern methods still difficult and experimental results are important for benchmark calculations.

The structure of methanol, **CH₃OH**, a very important molecule in chemistry and industry, has been determined by Hughes, Good, and Coles already in 1951,[2] but the internal rotation was reported for the first time 17 years later by Lees and Baker.[3] The results were improved by De Lucia et al. in 1989.[4] In contrast, the barrier to internal rotation of 1190 ± 40 cal/mol ($398(14)$ cm^{-1}) in acetaldehyde, **CH₃CHO**, was given for the first time already in 1956 by Lin and Kilb.[5] The analysis was improved by Bauder,[6] Liang,[7] and Maes et al.[8] A further molecule, methyl formate, HCOO**CH₃**, has been measured for the first time in 1959 by Curl in the microwave region.[9] The barrier to internal rotation of the methyl group was determined to be $V_3 = 416(14)$ cm^{-1}. Thereafter, the spectral analysis has been improved by investigations of Plummer,[10] Demaison,[11] Oesterling,[12] and Oka et al.[13] The methyl group of acetic acid, **CH₃COOH**, an isomer of methyl formate, also shows internal rotation.[14,15] The barrier of 497 cal/mol (174 cm^{-1}) has been determined by Tabor[16] in 1957 and was improved by Krischer and Saegebarth to be $168.16(17)$ cm^{-1}.[17] Some larger molecules with methyl internal rotation like ethyl methyl ether, C₂H₅–O–**CH₃**,[18,19] ethyl methyl ketone,[20,21] C₂H₅–(C=O)–**CH₃**, methyl vinyl ketone,[22,23] CH₂=CH–(C=O)–**CH₃**, m-cresol,[24] CH₃–C₆H₄–OH, and *cis* N-methyl formamide, **CH₃**–NH–CHO,[25] have also been investigated. Several molecules with two methyl internal rotors like acetone (for details see Chapter 7), dimethyl ether,[26,27] and methyl acetate were also studied very extensively. The barrier to internal rotation of two equivalent methyl groups in dimethyl ether was reported by Lutz and Dreizler to be 2545 cal/mol (890 cm^{-1}),[27] which is similar to the barrier found in ethyl methyl

ether.[19] Methyl acetate, **CH₃–COO–CH₃,** is the smallest acetate which was investigated for the first time by Sheridan and Bauder[28] and reanalyzed by Tudorie et al.[29] The barrier of 422.148(55) cm^{-1} of the methoxy methyl group [29] is in reasonable agreement with the barrier found for the methyl group in methyl formate. A few molecules with more than two methyl internal rotors such as trimethyl silyl iodide, **(CH₃)₃SiI,**[30] or mesityl oxide, **CH₃–(C=O)–CH=C(CH₃)₂,**[31] have also been studied.

Many internal rotors are asymmetric. A typical example is the primary amino group –NH₂. The spectrum of ethyl amine has been analyzed by Fischer and Botskor first for the *trans* conformer in 1982,[32] later also for the *gauch* conformer.[33] An appropriate program had been developed for fitting the spectrum of this molecule. The water molecule can also be an interesting asymmetric rotor. It plays this role in a couple of complexes like water–carbon oxide,[34] phenol–water,[35] and quinuclidine–water.[36]

The smaller the barrier to internal rotation, the larger the splittings in the spectrum are.[1] Knowledge about internal rotation is essential for the assignment of spectra in astrophysics. Many small molecules have been detected in space and a lot of them show internal rotation. Most identifications of molecules in space were based on recording the spectra in the laboratory and observations of interstellar surveys by means of microwave, milimeterwave or submilimeterwave telescopes. For example, methanol has been found in Orion A by Lovas et al.[37] Acetaldehyde was detected for the first time in Sgr B2 [38] and then in the cold dust cloud TMC-1 and L134N.[39] The first detection of interstellar acetic acid was carried out by Mehringer et al.[40] In 1975, Churchwell and Winnerwisser reported on the detection of the AE doublet of the $1_{10} \leftarrow 1_{11}$ transition of methyl formate in Sgr B2.[41] This molecule was also found in Orion-KL besides methanol, dimethyl ether, acetonitril, etc.[42] Larger molecules like ethyl methyl ether (in the hot core region W51e2)[43] and acetone [44] have also been detected.

In this thesis only internal rotation of C_{3v} symmetric methyl groups in different molecular systems are investigated. For an one-rotor molecule, all rotational lines split into A and E components. In the case of two internal rotors, the A species splits into doublets, which will be called the AA-AE doublet, and the E species into triplets, called the EA-EE-EE* triplets. It should be noted that within the local mode symmetry label $\Gamma_1\Gamma_2$ the first letter Γ_1 is associated with the lower torsional barrier, while Γ_2 belongs to the higher barrier. For molecules with two equivalent rotors, AA-AE-EE-EE* quartets arise in the spectrum, since the AE and EA species are degenerated (see Figure I).[45] Filled circles in Figure I symbolize the non-rotating states and round arrows the rotating states.
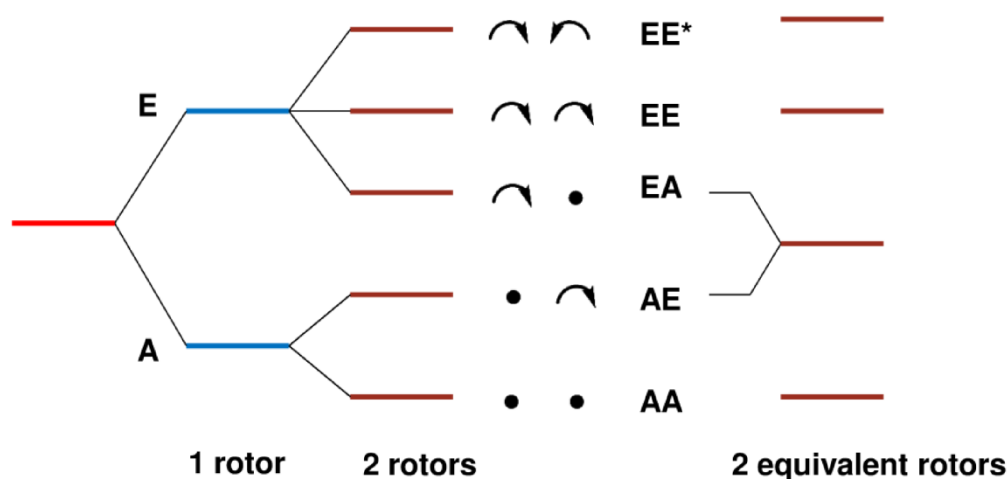
FIG. I Splittings due to internal rotation in the rotational spectrum of molecules with one rotor, two non-equivalent rotors or two equivalent rotors.

Several programs have been developed to treat internal rotation. A widely used program for fitting spectra with splittings due to symmetric internal rotors is XIAM developed by Hartwig.[46] The XIAM code uses the Internal Axis Method (IAM) and can fit rotational spectra of molecules with up to three internal rotors. Many molecular parameters such as the rotational and centrifugal distortion constants, the V_3 and higher potential terms, the angles which determine the internal rotor axis within the principal axis system, the moment of inertia of the internal rotor as well as some top-top kinetic and potential coupling terms like F_{12}, V_{cc}, and V_{ss} can be fitted. Moreover, nuclear quadrupole interaction of up to one coupling nucleus can be treated in a first order approximation. This is sufficient to fit the hyperfine structure of nuclei with relatively small quadrupole moments like ^{14}N.

Within the XIAM code the internal rotation problem is set up in the principal axis system. Subsequently, the Hamiltonian matrix is transformed into individual rho axis systems for each internal rotor in order to eliminate Coriolis coupling terms. In the rho axis system the eigenvalues are conveniently calculated in the product basis of symmetric top functions for the overall rotation and planar rotor functions for the torsion. Finally, the eigenvalue matrix is transformed back to the principal axis system.

Since XIAM is very user-friendly and extremely fast due to suitable basis transformations and matrix factorization,[47] it became one of the most used program for fitting the rotational spectra of many molecules with internal rotation. Some of them are 2-methyl thiazole,[48] methanol dimer,[49] trans-2-epoxybutane,[50] and recently assigned molecules like cyclopropyl methyl silane,[51] o-fluorotoluene,[52] o-tolunitrile,[53] o- and m-toluidine[54] etc. This program has

been used throughout the internal rotation part of this thesis to fit the microwave spectra of all investigated molecules.

A further program which is also well-known for treating internal rotation problems is BELGI, written by Kleiner et al. BELGI exists currently as BELGI-C_S for molecules with one[55] or two internal rotors of C_{3v} symmetry[29] and a C_S frame symmetry and BELGI-C_1 for one rotor and a C_1 frame symmetry.[56,57] BELGI can fit rotational transitions with J_{max} = 30, up to two vibrational states, and up to 80 parameters for each vibrational state. BELGI-C_S has been extensively tested with acetaldehyde.[58,59] Later, other molecules like acetic acide [60,61] and ^{13}C-methyl formate (HCOO–$^{13}CH_3$)[62] were also fitted using this program. The BELGI-C_S-2tops code has been recently tested on methyl acetate.[29] Unlike XIAM, BELGI uses the rho-axis system method (RAM). It does not treat nuclear quadrupole coupling. Some comparative studies of both programs have been carried out within this thesis.

Program Erham, written by Groner,[63] is another program which is often used to fit rotational spectra of molecules with one or two internal rotors up to J_{max} = 120. In contrast to XIAM and BELGI, the internal rotors are not restricted to C_{3v} symmetric. The frame symmetry can be C_S or C_1 for single rotors or non-equivalent rotors and C_2, C_{2v}, or C_S for equivalent rotors. Erham sets up and solves an **E**ffective **R**otational **HAM**iltonian.[47] Therefore, the physical meaning of the fitted parameters is less clear than in the other two programs. Like XIAM, Erham is very fast and fitting even a big data set takes only a few seconds. The transition frequencies can be usually fitted close to experimental accuracy. However, it is difficult to extract the rotational barrier. Dimethyl ether has been the first molecule that was fitted using this program, first by Groner[64] and then by Endres et al.[65] Acetone is another molecule with two equivalent internal rotors which was studied very extensively with Erham (for details see Chapter 7). Erham has also been used to fit the spectra of many molecules with only one rotor like methyl carbamate,[66] pyruvic acid,[67] methyl formate,[68] and pyruvonitrile.[69]

This chapter deals with studies on small but important carbonyl compounds like esters and ketones showing internal rotation. At the beginning, acetates with one internal rotor, the acetyl methyl group, and different frame symmetry were investigated. We started with ethyl acetate, one of the smallest saturated acetates, and assigned the *trans* C_S conformer including the internal rotation of the acetyl methyl group. Here, the frame has C_S symmetry. In a next step, the microwave spectra of two unsaturated esters, vinyl acetate and allyl acetate, were measured. Several molecules with two internal rotors like isopropenyl acetate (non-equivalent
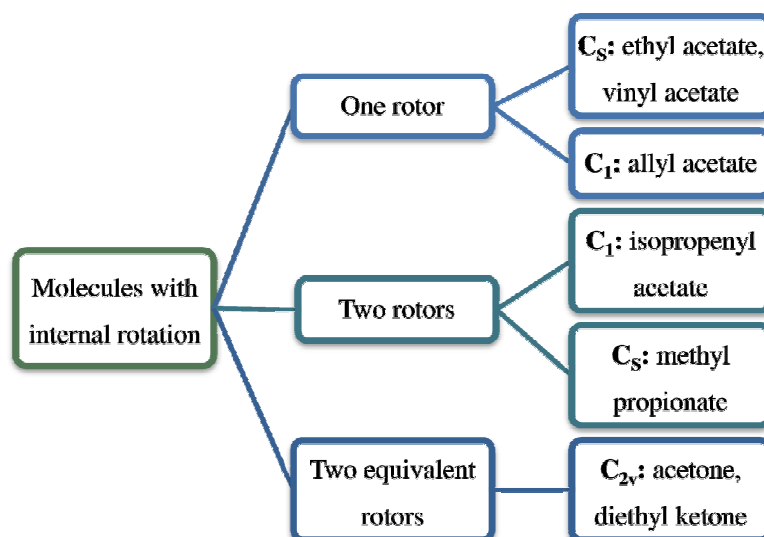
FIG. II Molecules with one or two (non-equivalent or equivalent) internal rotors and different frame symmetry investigated in this thesis.

rotors, C_1 frame symmetry), methyl propionate (non-equivalent rotors, C_S frame symmetry), diethyl ketone, and acetone (equivalent rotors, C_{2v} frame symmetry) were investigated. The concept is given in Figure II. Three well-known internal rotation programs XIAM, BELGI, and Erham were used to fit the microwave spectra of these molecules for comparative studies.

References

[1] W. Gordy and R. L. Cook, Microwave Molecular Spectra, John Wiley & Sons, New York, 1984, 3rd edition.

[2] R. H. Hughes, W. E. Good, D. K. Coles, *Phys. Rev.* **84**, 418 (1951).

[3] R. M. Lees and J. G. Baker, *J. Chem. Phys.* **48**, 5299 (1968).

[4] F. C. De Lucia, E. Herbst, T. Anderson, P. Helminger, *J. Mol. Spectrosc.* **134**, 395 (1989).

[5] C. C. Lin and R. W. Kilb, *J. Chem. Phys.* **24**, 631 (1956).

[6] A. Bauder and Hs. H. Günthard, *J. Mol. Spectrosc.* **60**, 290 (1976).

[7] W. Liang, J. G. Baker, E. Herbst, R. A. Booker, F. C. De Lucia, *J. Mol. Spectrosc.* **120**, 298 (1986).

[8] H. Maes, G. Wlodarczak, D. Boucher, J. Demaison, *Z. Naturforsch.* **42a**, 97 (1987).

[9] R. F. Curl, *J. Chem. Phys.* **30**, 1529 (1959).

[10] G. M. Plummer, G. A. Blake, E. Herbst, F. C. De Lucia, *Astrophys. J. Suppl.* **55**, 633 (**1984**).

[11] J. Demaison, D. Boucher, A. Dubrulle, B. P. Van Eijck, *J. Mol. Spectrosc.* **102**, 260 (1983).

[12] L. C. Oesterling, S. Albert, F. C. De Lucia, K. V. L. N. Sastry, E. Herbst, *Astrophys. J.* **521**, 255 (1999).

[13] K. Oka, Y. Karakawa, H. Odashima, K.Takagi, S. Tsunekawa, *J. Mol. Spectrosc.* **210**, 196 (2001).

[14] B. P. Van Eijck, J. Van Ophensden, M. M. M. Van Schaik, E. Van Zoeren, *J. Mol. Spectrosc.* **86**, 465 (1981).

[15] Demaison, A. Dubrulle, D. Boucher, J. Burie, B. P. van Eijck, *J. Mol. Spectrosc.* **94**, 211 (1982).

[16]W. J. Tabor, *J. Chem. Phys.* **27**, 974 (1957).

[17]C. C. Krischer and E. Saegebarth, *J. Chem. Phys.* **54**, 4553 (1971)

[18](a) M. Hayashi, H. Imaishi, K. Ohno, H. Murata, *Bull. Chem. Soc. Japan* **44**, 872 (1971); (b) S. Tsunekawa, Y. Kinai, Y. Kondo, H. Odashima, K. Takagi, *Molecules* **8**, 103 (2003); (c) U. Fuchs, G. Winnewisser, P. Groner, F. De Lucia, E. Herbst, *Astrophys. J. Suppl.* **144**, 277 (2003).

[19]M. Hayashi and K. Kuwada, *J. Mol. Struct.* **28**, 147 (1975).

[20]L. Pierce, C. K. Chang, M. Hayashi, R. Nelson, *J. Mol. Spectrosc.* **32**, 449 (1969).

[21]N. M. Pozdeev, A. K. Mamleev, L. N. Gunderova, R. V. Galeev, *J. Struc. Chem.* **29**, 52 (1988).
[22]P. D. Foster, V. M. Rao, R. F. Curl, Jr., *J. Chem. Phys.* **43**, 1064 (1965).

[23]A. C. Fantoni, W. Caminati, R. Meyer, *Chem. Phys. Lett.* **133**, 27 (1987).

[24]A. Hellweg, C. Hättig, I. Merke, W. Stahl, *J. Chem. Phys.* **124**, 204305 (2006).

[25]A. C. Fantoni, W. Caminati, H. Hartwig, W. Stahl, *Mol. Struct.* **612**, 305 (2002).

[26](a) U. Blukis, P. H. Kasai, R. J. Myers, *J. Chem. Phys.* **38**, 2753 (1963); (b) J. R. Durig, Y. S. Li, P. Groner, *J. Mol. Spectrosc.* **62**, 159 (1976). (c) W. Neustock, A. Guarnieri, J. Demaison, G. Wlodarczak, *Z. Naturforsch.* **45a**, 702, 1990.

[27]H. Lutz and H. Dreizler, *Z. Naturforsch.* **30a**, 1782 (1975).

[28]J. Sheridan, W. Bossert, A. Bauder, *J. Mol. Spectrosc.* **80**, 1 (1980).

[29]M. Tudorie, I. Kleiner, J. T. Hougen, S. Melandri, L. W. Sutikdja, W. Stahl, *J. Mol. Spectrosc.* **269**, 211 (2011).

[30]I. Merke, A. Lüchow, W. Stahl, *J. Mol. Struct.* **780**, 295 (2006).

[31]Q. Lejeune, master thesis at the RWTH Aachen University under supervision of H. Mouhib and Prof. W. Stahl, **2011**.

[32]E. Fischer and I. Botskor, *J. Mol. Spectrosc.* **91**, 116 (1982).

[33]E. Fischer and I. Botskor, *J. Mol. Spectrosc.* **104**, 226 (1984).

[34]G. Columberg, A. Bauder, N. Heineking, W. Stahl, J. Makarewicz, *Mol. Phys.* **93**, 215 (1998).

[35]M. Gerhards, M. Schmitt, K. Kleinermanns, W. Stahl, *J. Chem. Phys.* **104**, 967 (1996).

[36]D. Consalvo and W. Stahl, *J. Mol. Spectrosc.* **174**, 520 (1995).

[37]F. J. Lovas, D. R. Johnson, D. Buhl, L. E. Snyder, *Astrophys. J.* **209**, 770 (1976).

[38]M. B. Bell, H. E. Matthews, P. A. Feldman, *Astron. Astrophys.* **127**, 420 (1983).

[39]H. E. Matthews, P. Friberg, W.M. Irvine, *Astron. Astrophys.* **290**, 609 (1985).

[40]D. M. Mehringer, L. E. Snyder, Y. Miao, F. J. Lovas, *Astrophys. J.* **480**, 71 (1997).

[41]E. Churchwell and G. Winnewisser, *Astron. Astrophys.* **45,** 229 (1975).

[42]C. W. Lee, S. H. Cho, S. M. Lee, *Astrophys. J.* **551**, 333 (2001).

[43]G. W. Fuchs, U. Fuchs, T. F. Giesen, F. Wyrowski, *Astron. Astrophys.* **444**, 521 (2005).

[44]F. Combes, M. Gerin, A. Wootten, G. Wlodarczak, F. Clausset, P. J. Encrenaz, *Astron. Astrophys.* **180**, 13 (1987).

[45]H. Dreizler, *Z. Naturforsch.* **16a**, 1354 (1961).

[46]H. Hartwig and H. Dreizler, *Z. Naturforsch.* **51a**, 923 (1996).

[47]Instructions for the programs XIAM, Erham and BELGI. The programs are available at the web-site of Prof. Kisiel http://www.ifpan.edu.pl/~kisiel/prospe.htm.

[48]J.-U. Grabow, H. Hartwig, N. Heineking, W. Jäger, H. Mäder, H. W. Nicolaisen, W. Stahl, *Mol. Struct.* **612**, 349 (2002).

[49]F. J. Lovas and H. Hartwig, *J. Mol. Spectrosc.* **185**, 98 (1997).

[50]M. R. Emptage, *J. Chem. Phys.* **47**, 1293 (1967).

[51]M. D. Foellmer, J. M. Murray, M. M. Serafin, A. L. Steber, R. A. Peebles, S. A. Peebles, J. L. Eichenberger, G. A. Guirgis, C.J. Wurrey, J. R. Durig, *J. Phys. Chem. A* **113**, 6077 (2009).

[52]S. Jacobsen, U. Andresen, H. Mäder, *Structural Chemistry* **14**, 217 (2003).

[53]N. Hansen, H. Mäder, T. Bruhn, *Mol. Phys.* **97**, 587 (1999).

[54]R. G. Bird and D. W. Pratt, *J. Mol. Spectrosc.* **266**, 81 (2011).

[55]J. T. Hougen, I. Kleiner, and M. Godefroid, *J. Mol. Spectrosc.* **163**, 559 (1994).

[56]I. Kleiner and J. T. Hougen, *J. Chem. Phys.* **119**, 5505 (2003).

[57]R. J. Lavrich, A. R. Hight Walker, D. F. Plusquellic, I. Kleiner, R. D. Suenram, J. T. Hougen, G. T. Fraser, *J. Chem. Phys.* **119**, 5497 (2003).

[58](a) I. Kleiner, J. T. Hougen, R. D. Suenram, F. J. Lovas, M. Godefroid, *J. Mol. Spectrosc.* **153**, 578 (1992); (b) S. P. Belov, M. Yu. Tretyakov, I. Kleiner, J. T. Hougen, *J. Mol. Spectrosc.* **160**, 61 (1993); (c) I. Kleiner, F. J. Lovas, M. Godefroid, *J. Phys. Chem.* **25**, 1113 (1996).

[59]I. Kleiner, J. T. Hougen, J.-U. Grabow, S. P. Belov, M. Y. Tretyakov, J. Cosleou, *J. Mol. Spectrosc.* **179**, 41 (1996).

[60]V. V. Ilyushin, E. A. Alekseev, S. F. Dyubko, S. V. Podnos, I. Kleiner, L. Margulès, G. Wlodarczak, J. Demaison, J. Cosléou, B. Maté, E. N. Karyakin, G. Yu. Golubiatnikov, G. T. Fraser, R. D. Suenram, J. T. Hougen, *J. Mol. Spectrosc.* **205**, 286 (2001).

[61]V. V. Ilyushin, E. A. Alekseev, S. F. Dyubko, I. Kleiner, *J. Mol. Spectrosc.* **220**, 170 (*2003*).

[62]M. Carvajal, L. Margulès, B. Tercero, K. Demyk, I. Kleiner, J. C. Guillemin, V. Lattanzi, A. Walters, J. Demaison, G. Wlodarczak, T. R. Huet, H. Møllendal, V. V. Ilyushin, J. Cernicharo, *Astron. Astrophys.* **500,** 1109 (2009).

[63]P. Groner, *J. Chem. Phys.* **107**, 4483 (1997).

[64]P. Groner, S. Albert, E. Herbst, F. C. De Lucia, *Astrophys. J.* **500**, 1059 (1998).

[65]C. P. Endres, B. J. Drouin, J. C. Pearson, H. S. P. Müller, F. Lewen, S. Schlemmer, T. F. Giesen, *Astron. Astrophys.* **504**, 635 (2009).

[66]P. Groner, M. Winnewisser, I. R. Medvedev, F. C. De Lucia, E. Herbst, K. V. L. N. Sastry, *Astrophys. J. Suppl. Ser.* **169**, 28 (2007).

[67]Z. Kisiel, L. Pszczólkowski, E. Bialkowska-Jaworska, S. B. Charnley, *J. Mol. Spectrosc.* **241**, 220 (2007).

[68]A. Maeda, F. C. De Lucia, E. Herbst, *J. Mol. Spectrosc.* **251**, 293 (2008).

[69]A. Krasnicki, L. Pszczólkowski, Z. Kisiel, *J. Mol. Spectrosc.* **260**, 57 (2010).

Chapter 1

ETHYL ACETATE

One rotor and C_S frame symmetry

1. Introduction

Ethyl acetate, $CH_3-COO-CH_2-CH_3$, is a widely used solvent and it is also abundant in many fruits contributing to their odors. From a chemical point of view it is a small aliphatic ester, obtained by condensation of ethanol and acetic acid using some acid as a catalyst. Surprisingly, to our knowledge only one electron diffraction study[1] deals with the structure of this important molecule in the gas phase and no microwave studies have been reported.

Sugino et al.[1] suggested that ethyl acetate exists in two conformers, the *trans* conformer which has C_S symmetry with all heavy atoms being located within the mirror plane, and a *gauche* conformer with C_1 symmetry. Both conformers are shown in Figure 1. Here, the microwave studies on the *trans* conformer will be reported.

Ethyl acetate has two methyl groups that could show internal rotation. For the acetyl methyl group, we expected a low barrier to internal rotation on the order of 100 cm^{-1}, similar to the barrier of 99.559(83) cm^{-1} found in methyl acetate.[2] For the ethyl methyl group, the barrier was expected to be considerably higher, on the order of 1000 cm^{-1}, as found for the ethyl methyl group in ethyl fluoride (1171.3(14) cm^{-1}).[3]

The motivation for this work was predominantly the interest in accurate internal rotation parameters of the acetyl methyl group. A further motivation was a comparison of two different computer programs, BELGI-C_S and XIAM. Both of them treat internal rotation effects in rotational spectra using the rho axis method (RAM) and the combined axis method (CAM), respectively.

2. Quantum chemistry

In order to get rotational constants and also the angle between the internal rotor axis and the *a* axis as starting values for assigning the spectra, theoretical calculations were carried out at the workstation cluster of the Center for Computing and Communication at the RWTH Aachen
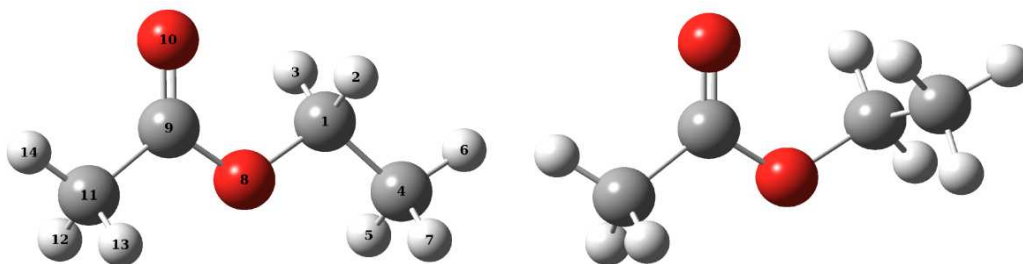
FIG. 1 The *trans* (left-hand side) and *gauche* conformers (right-hand side) of ethyl acetate.

University using the program package *Gaussian03*. In all cases a fully optimized structure was obtained. Also the dipole moment components were calculated to get an impression of the relative strength of *a*-, *b*-, and *c*-type transitions.

At first we focused our calculations on the *trans* conformer to compare the results of DFT and MP2 calculations with various basis sets. From former DFT studies given by Nagy et al.[4] two stable conformers of ethyl acetate were known. Our calculations with different start geometries and full relaxation of all structural parameters yielded three conformers. The results are summarized in Table 1. The nuclear coordinates in the principal axes system of all conformers calculated at the MP2/6-311++G(d,p) level are given in the Appendix in Table A-1.

The *cis* conformer has an energy of about 33 kJ/mol (referred to the calculations at the MP2/6-311++G(d,p) level) above the *trans* conformer and appears unlikely to be visible under molecular beam conditions. Therefore we only concentrate on the *trans* and *gauche* ester. It should be considered that the torsional force constant of the CO**O–C** bond is quite low and sometimes a rotation of both molecule fragments around this bond still improves the rotational constants. Therefore, we decided to calculate a potential curve of ethyl acetate by freezing the dihedral angle $\varphi = \angle(C_4, C_1, O_8, C_9)$ at certain fixed values while all other parameters were optimized. In this case we calculated a half rotation of 180° (due to the symmetry) with a 10° step width. The curve was parametrized. The corresponding potential curve is shown in Figure 2, the Fourier coefficients are given in Table 2. This potential curve has two minima, which confirm that only two stable conformers, the *trans* ($\varphi = 0°$) and the *gauche* conformer ($\varphi = \pm100°$), exist. These conformers have almost the same stabilization energy value. The energy difference is only about 0.5 kJ/mol. Therefore, both of them should be present in the microwave spectrum. Another *trans* C_S configuration at $\varphi = 180°$ represents a maximum in the potential curve.

Table 1

Rotational constants (in GHz), dipole moments (in Debye), and stabilization energies of ethyl acetate (*trans* and *gauche* conformer) obtained by DFT and MP2 methods using the *Gaussian03* package.

Nr.	Method / Basis set	E / Hartree	A	B	C	μ_a	μ_b	μ_c
	trans conformer							
1	B3LYP/6-31++G(d,p)	−307.7324997	8.3797	2.0686	1.7122	1.189	1.794	0.000
2	B3LYP/6-311++G(d,p)	−307.8042029	8.4184	2.0738	1.7172	1.165	1.735	0.000
3	B3LYP/cc-PVTZ	−307.8287645	8.4576	2.0827	1.7246	1.076	1.699	0.000
4	MP2/6-311G(d,p)	−306.9328341	8.3958	2.1069	1.7390	0.897	1.846	0.000
5	MP2/6-311++G(d,p)	−306.9455003	8.3907	2.0994	1.7339	0.986	1.934	0.000
6	MP2/cc-PVTZ	−306.9893138	8.4491	2.1134	1.7452	0.930	1.919	0.000
	gauche conformer							
7	B3LYP/6-311++G(d,p)	−307.8035757	7.3909	2.2752	2.0174	0.612	1.793	0.131
8	MP2/6-311++G(d,p)	−306.9453084	7.2396	2.3602	2.0830	0.339	1.925	0.308
	cis conformer							
9	B3LYP/6-311++G(d,p)	−307.7920838	7.9554	2.0946	1.7113	2.692	3.939	0.000
10	MP2/6-311++G(d,p)	−306.9328339	7.9442	2.1184	1.7269	2.834	4.411	0.001

Table 2

Potential functions for the rotation around the dihedral angle $\varphi = \angle(C_4, C_1, O_8, C_9)$. Energies were calculated in a 10° grid and parametrized as a Fourier series $V(\varphi) = a_0 + \sum_{i=1}^{15} a_i \cos(i\varphi)$. The Fourier coefficients a_i are given for the MP2/6-311++G(d,p) level of theory.

i	a_i / Hartree
0	−306.942052098
1	−0.004431972
2	0.002959686
3	−0.002017752
4	−0.000077978
5	0.000145391
6	0.000003748
7	−0.000065279
8	0.000036275
9	−0.000001937
10	0.000003161
11	−0.000007544
12	0.000008470
13	−0.000005678
14	0.000004814
15	−0.000004089
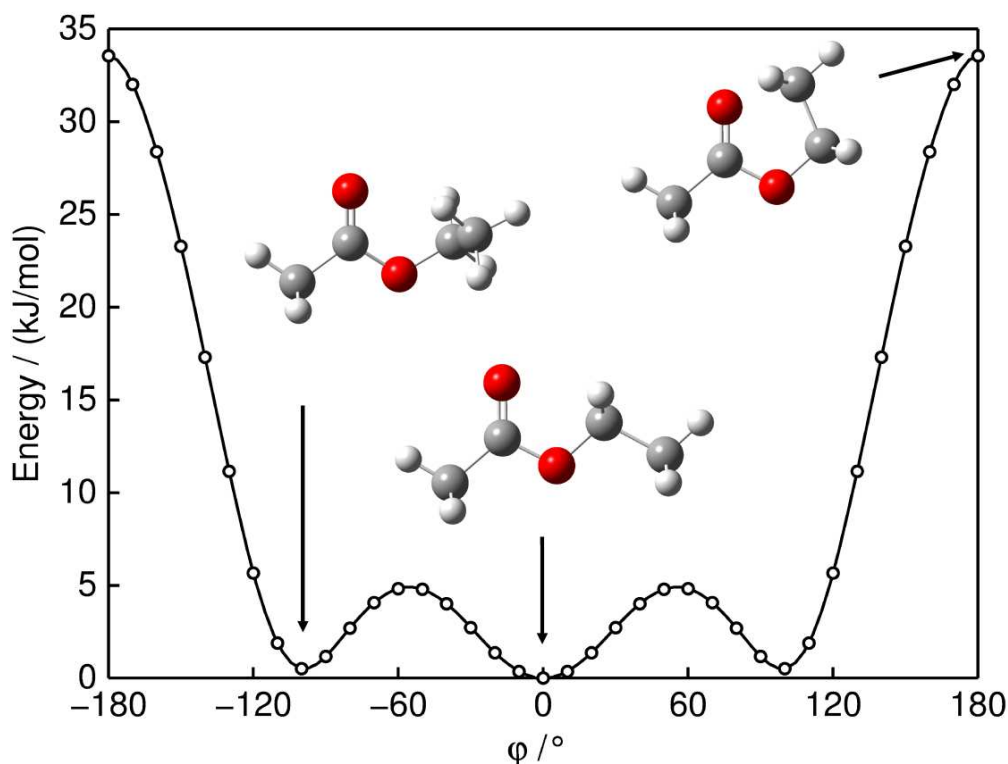
FIG. 2 The potential curve of ethyl acetate obtained by rotating the ethyl group. The relative energy with respect to the lowest energy *trans* conformer (E = −306.9455003 Hartree) is given.

3. Microwave spectrum

3.1. Spectral assignment

All spectra were recorded using two MB-FTMW spectrometers described in ref. [17,18] and ref. [19] in the experimental setup section. At the beginning of our measurements broadband scans in the frequency range from 10.0 to 11.9 GHz were carried out. In total 65 lines were found. Many of them were quite strong. All lines were remeasured in the high resolution mode and almost all of them were broadened, some lines were clearly split by up to some 100 kHz. A typical spectrum is shown in Figure 3. The instrumental resolution was 0.8 kHz, typical experimental line width 12 kHz.

In ethyl acetate the rotational lines are split due to two large amplitude motions, the internal rotation of the acetyl methyl group and the ethyl methyl group. For the acetyl methyl group we assumed the barrier to internal rotation to be almost the same as Sheridan et al.[2] found for the acetyl methyl group in methyl acetate, which is 99.559(83) cm^{-1}. This is a rather low barrier and we expected very large A-E splittings from a few MHz to a few GHz, depending on the respective transition.

The internal rotation of the ethyl methyl group should be comparable to that in ethyl fluoride[3] and ethyl chloride,[5] where a barrier of 1171.3(14) cm^{-1} and 1260(4) cm^{-1}, respectively, was found. This would cause only broadened lines or narrow splittings for those transitions observable in the molecular beam and it explains the broadened and split lines we observed.

At first we tried to assign the A species spectrum (referred to the acetyl methyl group) by treating it as an effective rigid rotor spectrum. Therefore, we used rotational constants obtained from quantum chemical calculations on various levels of theory for the *trans* conformer (see Table 1). By trial and error some *a*-type *R* branch transitions of the *trans* conformer could be identified yielding the B and C rotational constants. Later, some *b*-type *Q* branch transitions were assigned and also the A constant was fixed. This enabled us to predict the whole rigid rotor spectrum with sufficient accuracy to find all remaining A species lines and, subsequently, to fit the (effective) quartic centrifugal distortion constants. The standard deviation after fitting 60 A species transitions was 3 kHz, which is almost our experimental accuracy. It should be noted that despite an intense search no *c*-type transitions were found, which means that the *c* dipole moment component is near zero and which confirms that we indeed observed the *trans* conformer with a mirror plane perpendicular to the *c* axis.

In a next step we predicted both, the A and E species transitions (referred to the acetyl methyl group) using the program XIAM. The barrier was taken from methyl acetate,[2] approximately 100 cm^{-1}. The angle between the internal rotor axis and the inertial *a* axis were calculated from the optimized *ab initio* geometry on the MP2/6-311++G(d,p) level to be approximately 45°. The start value of the inertia of the methyl group was chosen to be 3.2 uÅ^2, which we considered to be a reasonable value found in many molecules where methyl internal rotation has been analyzed. The predicted spectrum was in close agreement with lines we observed in our scan. The assignment was straight forward for the *a*-type *R* branch transitions, where the A-E splittings were only on the order of 10 to 100 MHz. The assignment of *b*-type *Q* branch lines, split by a few 100 MHz up to a few GHz, was more difficult. Here, the search for lines which form closed cycles in the energy level diagram turned out to be very helpful. Finally, 60 A species and 66 E species lines could be assigned and fitted with the program XIAM to a standard deviation of 18.5 kHz (see Fit I in Table 3). In a second fit with XIAM (Fit II in Table 3) the internal rotation parameters were fixed to the values obtained from Fit I and only the A species lines were fitted to a standard deviation of 2.8 kHz, which is close to the experimental accuracy. The same data set was fitted again with the program BELGI-C$_S$ using the Rho Axis Method (RAM) with 15 parameters to experimental accuracy with a standard
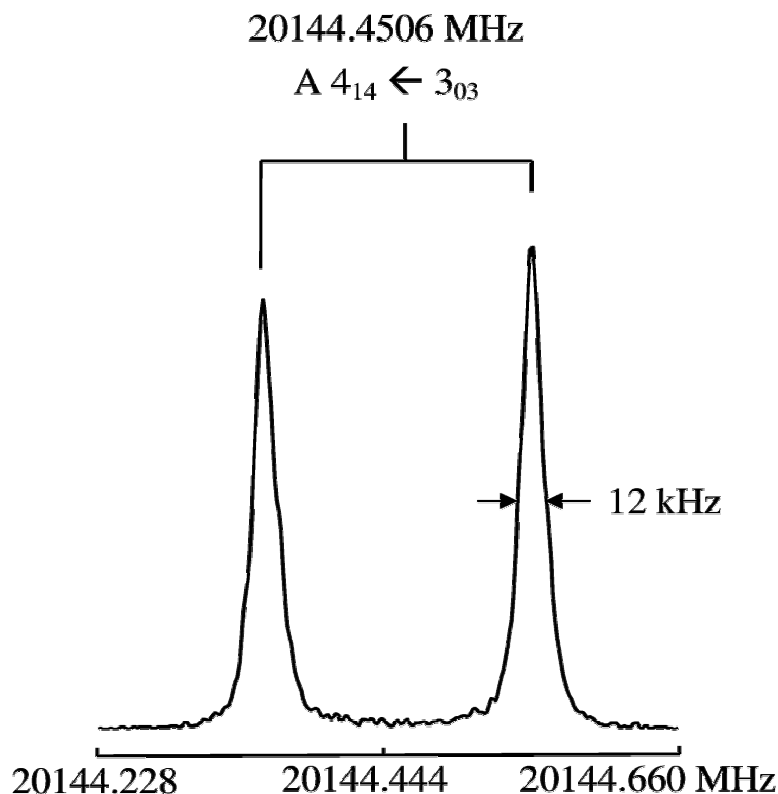
FIG. 3 A typical spectrum of the *trans* conformer of ethyl acetate. The experimental resolution was 0.8 kHz, the typical experimental line width 12 kHz as indicated in the spectrum. The large splitting is due to the Doppler effect. For this spectrum 22 FIDs were co-added.

deviation of only 2.3 kHz (Fit III, Table 3). Levels up to $J = 19$ and $K_a = 4$ were included in the fit. Fit results are given in Table 3 and 4. A complete list of all fitted transitions is found in the Appendix (Table A-2 and A-3).

The internal rotation of the ethyl methyl group causes the A species lines of the acetyl methyl group to split into doublets ($|\sigma_1,\sigma_2> = |0,0>$, $|0,\pm1>$) and the E species lines into triplets ($|\pm1,0>$, $|\pm1,\pm1>$, $|\pm1,\mp1>$). Here, the torsional states are labeled by the torsional symmetries σ_1 and σ_2 of group I and II.[6] Sample calculations with XIAM have shown that the splittings of the A species lines are usually too narrow to be resolved. However, the E species lines of some selected transitions were split by up to 80 kHz. A typical splitting is shown in Figure 4. With the splittings observed for 9 E species and one A species transitions and keeping all other parameters fixed we found the barrier of the ethyl methyl group to be $V_3 = 1061.4(68)$ cm^{-1}. Here, the angle between the internal rotor axis and the principal a and b axis were first taken from the *ab initio* geometry on the MP2/6-311++G(d,p) level and fitted to be $\angle(i,a) = 155.9(38)°$ and $\angle(i,b) = 65.9(38)°$. All fitted transitions are given in Table A-4 in the Appendix.
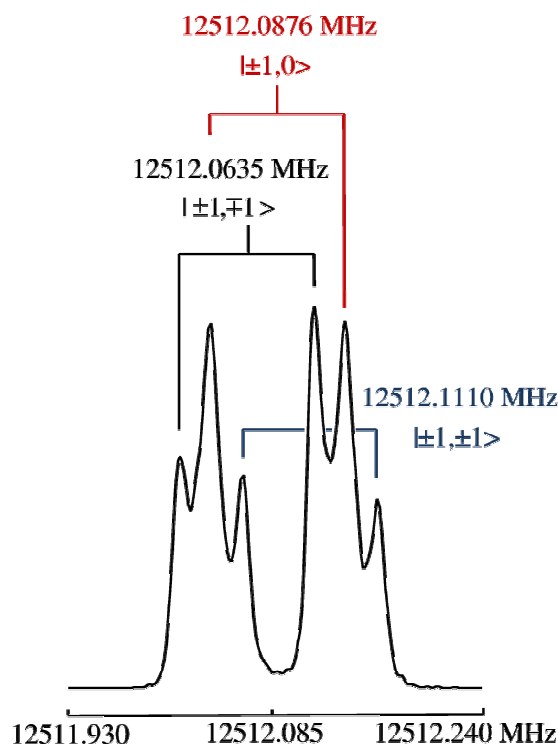
FIG. 4 The $3_{03} \leftarrow 2_{11}$ E species transition of *trans* ethyl acetate. The splitting is due to the internal rotation of the ethyl methyl group. Doppler splittings are indicated by brackets.

3.2. The XIAM and the BELGI-C$_S$ codes

The microwave spectrum of ethyl acetate has been analyzed by means of two different programs, XIAM and BELGI-C$_S$. XIAM sets up the Hamiltonian in the principal axis system of the entire molecule. The internal rotation operator of each top is set up in its own rho axes system and after diagonalization, the resulting eigenvalues are transformed (rotated) into the principal axis system. Only centrifugal distortion constants, but no higher order coupling terms between internal rotation and overall rotation are implemented. A global fit of A and E species transitions is possible (Fit I, Table 3). However, in cases with rather low barriers E species transitions are not satisfactorily predicted. The standard deviation is 18.5 kHz, much larger than our experimental accuracy. The situation can be improved by fitting the A species transitions separately, whereas all parameters are fixed to the values obtained from the global fit. This method significantly reduces the uncertainties in the fit (Fit II, Table 3), however, only the A species lines could be fitted within the experimental accuracy.

As an alternative, a global fit with BELGI-C$_S$ was carried out. In this program the calculations are carried out in the rho axes system (also referred in the literature often as RAM for "rho axis method"), and all parameters obtained in the fit are referred to this axes system. The

method based on the work of Kirtman,[7] Lees and Baker,[8] and Herbst et al.[9] takes its name from the choice of the axis system, the rho axis system, which is related to the principal axis system by a rotation chosen to eliminate the $-2FP_\gamma\rho_xJ_x$ and $-2FP_\gamma\rho_yJ_y$ coupling terms in the kinetic energy operator where F is the internal rotation constant, P_γ is the internal angular momentum, $\mathbf{J}_x$ and $\mathbf{J}_y$ are the usual x and y components of the global rotation angular momentum, and ρ is a vector that expresses the coupling between the angular momentum of the internal rotation P_γ and the global rotation $\mathbf{J}$. Unlike XIAM, BELGI-C_S which was used successfully to describe the spectra for internal rotors with very low internal rotation barriers ($V_3 \cong 25$ cm^{-1}) such as acetamide,[10] and also for peptide mimetics such as the ethylacetamidoacetate molecule[11] and the N-acetyl alanine methyl ester,[12] allows for fitting many higher order terms not only in the total angular momentum $\mathbf{J}$, but also in the angular momentum of the internal rotor $\mathbf{P}_\gamma$ and in cross-terms between them. BELGI-C_S uses a two-step diagonalisation procedure in which the first step is the diagonalisation of the torsional Hamiltonian consisting of the one dimensional potential function $V(\gamma)$ together with a torsion-rotation kinetic operator diagonal in K, the rotational quantum number. A first set of torsional calculations, one for each K values, is carried out using a 21 x 21 torsional basis set: $|K\, v_t\, \sigma> = \exp[i(3k+\sigma)\gamma]$ where v_t is the principal torsional quantum number and k is an integer running from -10 to $+10$ for BELGI-C_S. For XIAM this indices k runs from -15 to 15. This basis is then reduced by discarding all but the nine lowest torsional eigenfunctions for each K. Finally the torsional eigenfunctions are multiplied by the symmetric top rotational function $|J, K, M>$ to form a basis set which is then used to diagonalize, in the second step, the zeroth-order asymmetric rotor terms and higher order terms in the Hamiltonian.

In order to compare the results from BELGI-C_S referring to a rho axes system with the more usual constants given in a principal axis system, some transformations can be made. A_{RAM}, B_{RAM}, C_{RAM}, and D_{ab} are proportional to the elements of the inverse inertia tensor. Diagonalizing it by rotation around the c axis by an angle θ_{RAM} yields the PAM constants A and B:

$$A = \tfrac{1}{2}(A_{RAM} + B_{RAM} + \sqrt{(A_{RAM} - B_{RAM})^2 + 4D_{ab}^2}) \qquad (1)$$

$$B = \tfrac{1}{2}(A_{RAM} + B_{RAM} - \sqrt{(A_{RAM} - B_{RAM})^2 + 4D_{ab}^2}) \qquad (2)$$

with

$$\tan(2\theta_{RAM}) = \frac{2D_{ab}}{(A_{RAM} - B_{RAM})}. \tag{3}$$

For the *trans* ethyl acetate molecule this is 13°.

The centrifugal distortion constant D_J has the same meaning in both coordinate systems, because the $\mathbf{J}^4$ operator is invariant under rotation.

To determine the rotational constant F_0 of the internal rotor, we start with the definition of the $\vec{\rho}$ vector $\vec{\rho} = (\rho_a, \rho_b, \rho_c)$. Its elements are defined by

$$\rho_a = \frac{\lambda_a I_\gamma}{I_a}, \quad \rho_b = \frac{\lambda_b I_\gamma}{I_b}, \quad \rho_c = \frac{\lambda_c I_\gamma}{I_c}, \tag{4}$$

where I_a, I_b, I_c are the principal moments of inertia of the entire molecule and I_γ is the moment of inertia of the internal rotor. λ_a, λ_b, λ_c are the direction cosines between the internal rotor axis and the principal axes a, b, c, with

$$\lambda_a^2 + \lambda_b^2 + \lambda_c^2 = 1. \tag{5}$$

The relations (4) may also be expressed with the respective rotational constants A, B, C, and F_0 of the molecule and the internal rotor

$$\rho_a = \frac{\lambda_a A}{F_0}, \quad \rho_b = \frac{\lambda_b B}{F_0}, \quad \rho_c = \frac{\lambda_c C}{F_0}. \tag{6}$$

Note that in relation (6) above, the definition of F_0 is different from that of the "reduced" F given in Eq. (9) of ref. [13]:

$$F = \frac{\hbar^2}{2rI_\gamma} \text{ with } r = 1 - I_\alpha(\frac{\lambda_a^2}{I_a} + \frac{\lambda_b^2}{I_b} + \frac{\lambda_c^2}{I_c}).$$

The length of the vector $\vec{\rho}$ is given by

$$\rho = \sqrt{\rho_a^2 + \rho_b^2 + \rho_c^2}. \tag{7}$$

In our case $\lambda_c = 0$, and with (5), (6), and (7) we obtain

$$\rho^2 F_0^2 = \lambda_a^2(A^2 - B^2) + B^2. \tag{8}$$

The *a* component of $\vec{\rho}$ is available from

$$\rho_a = \rho \cos\theta_{RAM} \ , \tag{9}$$

and with (6) we find

$$\lambda_a = \frac{F_0 \rho_a}{A} \ . \tag{10}$$

The system of equations (8) and (10) may be solved to yield

$$F_0 = \frac{B}{\rho\sqrt{1 - \dfrac{A^2 - B^2}{A^2}\cos^2\theta_{RAM}}} \tag{11}$$

and

$$\lambda_a = \sqrt{\frac{\rho^2 F_0^2 - B^2}{A^2 - B^2}} \ . \tag{12}$$

From (11) and (12) the angle between the internal rotor axis and the inertial a axis is obtained by

$$\angle(i,a) = \arccos\lambda_a . \tag{13}$$

All results, obtained with XIAM, BELGI-C$_S$, and by theoretical calculations, referred to the principal axis system, are summarized in Table 3.

4. Results and discussion

The standard deviation is in the same order for the A species for both programs, XIAM (see Fit II in Table 3) and BELGI-C$_S$, but it is much smaller for the E species in the fit of BELGI-C$_S$ (Fit I and Fit III in Table 3). Therefore the predictive power of BELGI-C$_S$ is much better than XIAM. However, for assignment purposes XIAM is in some aspects more convenient to use since it is somewhat faster than BELGI-C$_S$.

The torsional barrier determined for the acetyl methyl rotor is 99.57(11) cm^{-1} using BELGI-C$_S$ and 97.7844(45) cm^{-1} using XIAM. These differences are within a few percent. The discrepancies are, however, larger than the standard deviation of the parameters by one order of magnitude and are likely a result of systematic errors in the models. The differences between the methyl rotor angles are only about 0.011° by comparing the two methods. Also the agreement with the theoretical results allows to conclude, that we indeed observed the *trans* conformer of ethyl acetate.

Table 3

Molecular constants of *trans* ethyl acetate obtained with the program XIAM and comparison with results of the program BELGI-C_S and quantum chemical calculations.

Para-meter	Unit	Fit I XIAM	Fit II XIAM	Fit III BELGI-C_S	Calc.[b]
A	GHz	8.4491579(34)	8.44915544(55)	8.41174(28)[a]	8.391
B	GHz	2.0923861(26)	2.09238732(10)	2.094799(70)[a]	2.099
C	GHz	1.7330504(16)	1.733050895(87)	1.734069(58)[a]	1.734
Δ_J	kHz	0.1827(26)	0.18940(65)		
Δ_{JK}	kHz	1.288(24)	1.2548 (40)		
Δ_K	kHz	9.73(38)	9.740 (60)		
δ_J	kHz	0.0390(13)	0.04181(25)		
δ_K	kHz	0.771(67)	0.652(13)		
D_{pi2J}	kHz	200.71(36)	200.71 (fixed)		
D_{pi2-}	kHz	114.52(22)	114.52 (fixed)		
V_3	GHz	2931.50(14)	2931.50 (fixed)	2984.9(30)	
	kJ/mol	1.169762(54)		1.1910(12) [c]	
	cm^{-1}	97.7844 (45)		99.57(10) [c]	
F_0	GHz	153.5445(70)	153.5445 (fixed)	159.98(13)	
I_γ	uÅ^2	3.29142(15)[d]	3.29142 (fixed)	3.1590(25)	
$\angle$(i,a)	°	43.0647(5)	43.0647 (fixed)	43.0537(5)	44.75
$\angle$(i,b)	°	46.9353(5)[e]	46.9353 (fixed)	46.9463(5)	45.24
$\angle$(i,c)	°	90.00 (fixed)[f]	90.00 (fixed)	90.00 (fixed)	90.00
s[g]		8.182277		8.109929	
σ	kHz	18.5	2.8	2.3	
N_A/N_E		60/66	60/0	60/66	
N_{tot}		126	60	126	

All constants refer to the principal axis system, for the centrifugal distortion constants Watson's A reduction and a I^r representations was used.
[a] Obtained by transformation from the rho axis system to the principal axis system, see text.
[b] Calculation on MP2/6-311++G(d,p) level using *Gaussian03*.
[c] Hindering potential, calculated from value in frequency units.
[d] Moment of inertia I_γ of the internal rotor, calculated from its rotational constant F.
[e] Calculated from $\angle$(i,b) = 90° − $\angle$(i,a).
[f] Fixed due to symmetry.
[g] Reduced barrier $s = \dfrac{4V_3}{9F}$.

For the *trans* conformer, different methods and basis sets were used. By comparison the experimental rotational constants with the calculated ones (Figure 5), we found that the calculated B and C constant matched quite well the experimental constants in all cases, especially at the MP2/6-311++G(d,p) level of theory (number 6 in Figure 5). The A constant depends strongly on the chosen method and basis set. The best agreement was achieved at the cc-PVTZ basis set. However, the MP2 method yielded better rotational constants than the

Table 4

Molecular constants of *trans* ethyl acetate obtained by a global fit using program BELGI-C$_S$.

Operator[a]	Constant[b]	Unit[c]	Value
P_a^2	A	GHz	8.08735(41)
P_b^2	B	GHz	2.419190(32)
P_c^2	C	GHz	1.73406873(89)
$\{P_a,P_b\}$	D_{ab}	GHz	−1.394249(60)
$-P^4$	D_J	kHz	0.1812(5)
$-P^2P_a^2$	D_{JK}	kHz	−0.349(17)
$-2P^2(P_b^2-P_c^2)$	δ_J	kHz	0.0372(1)
P_γ^2	F	GHz	163.58(13)
$(1/2)(1-\cos3\gamma)$	V_3	GHz	2984.9(30)
P_aP_γ	ρ	unitless	0.039446(19)
$P_a^3P_\gamma$	k_1	MHz	−0.2110(31)
$(1-\cos3\gamma)P_a^2$	K_5	MHz	114.6(12)
$(1-\cos3\gamma)P^2$	F_V	MHz	−3.531(45)
$(1-\cos3\gamma)(P_b^2-P_c^2)$	C_2	MHz	−1.781(45)
$(1-\cos3\gamma)\{P_a,P_b\}$	D_{ab}	MHz	−6.69(17)

[a] All constants refer to a rho-axis system, therefore the inertia tensor is not diagonal and the constants cannot be directly compared to those of a principal axis system. P_a, P_b, P_c are the components of the overall rotation angular momentum, P_γ is the angular momentum of the internal rotor rotating around the internal rotor axis by an angle γ. $\{u,v\}$ is the anti commutator $uv + vu$.
[b] The product of the parameter and operator from a given row yields the term actually used in the vibration-rotation-torsion Hamiltonian, except for F, ρ, and A, which occur in the Hamiltonian in the form $F(P_\gamma-\rho P_a)^2 + AP_a^2$.
[c] Values of the parameters from the present fit. Statistical uncertainties are shown as one standard uncertainty in the last digit.

DFT method. Furthermore, it should be noted that the experimental data are obtained from the vibrational ground state. In contrast, the values from *Gaussian03* are equilibrium data. The assignment of the *trans* conformer is also supported by the absence of *c*-type transitions, which indicates that a mirror plane perpendicular to the *c* axis is present. Finally, we can also note that the fit achieved with BELGI-C$_S$, which reproduced the experimental data within experimental accuracy, did not required any out-of-plan type terms of symmetry A_2.

It should be noted, that with both, XIAM and BELGI-C$_S$, a strong correlation between V_3 and I_γ is present which is due to the fact that only $v_t = 0$ ground torsional state transitions are included in the analysis. However, both programs converged at almost the same I_γ. We can compare the internal rotation parameters with those of the acetyl methyl group of methyl acetate.[2] Here, V_3 and I_γ are 99.559(83) cm^{-1} and 3.2085(26) uÅ^2, respectively. For ethyl acetate we found 99.57(10) cm^{-1} and 3.1590(25) uÅ^2. This is almost the same and there seems
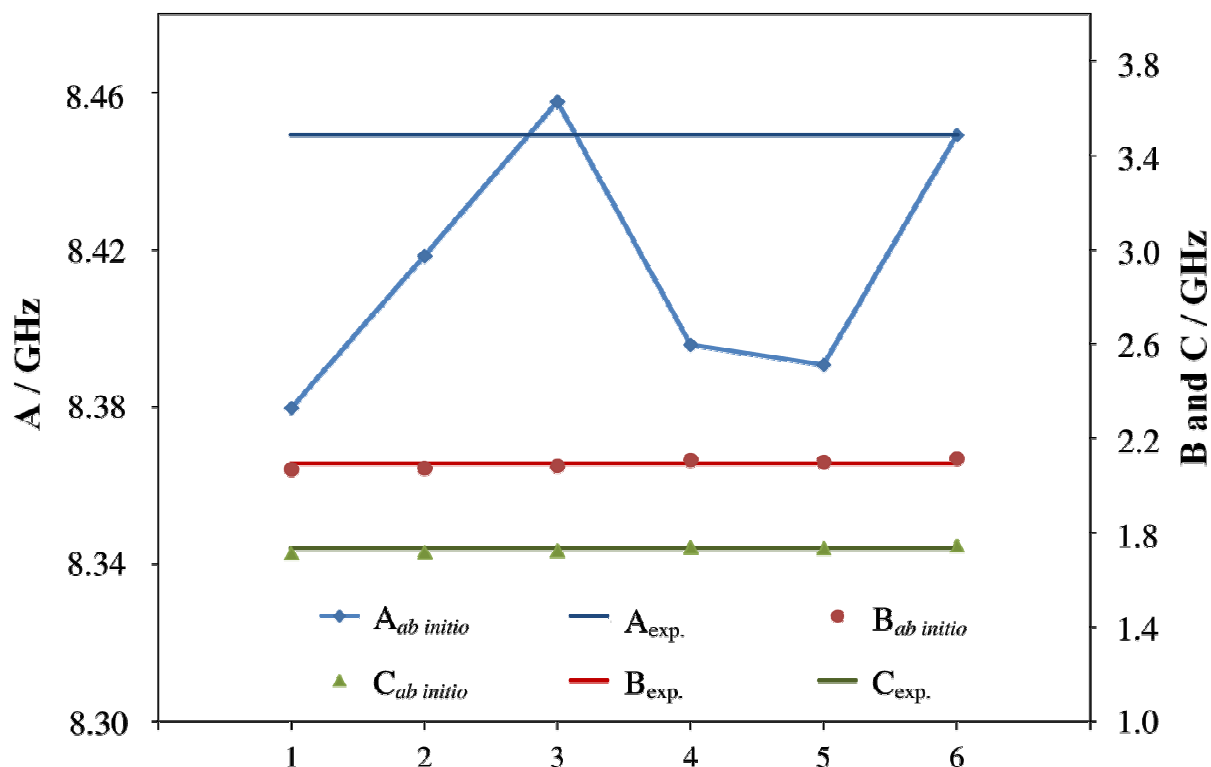
FIG. 5 Comparison of the calculated rotational constants ($A_{ab\ initio}$, $B_{ab\ initio}$, and $C_{ab\ initio}$) at different methods and basis sets (for the corresponding number see Table 1) with the experimental rotational constants ($A_{exp.}$, $B_{exp.}$, and $C_{exp.}$). The experimental rotational constants exactly the calculated one almost exactly by calculation at the MP2/cc-PVTZ level.

to be no influence of the alkyl group in alkyl esters. This also holds for bigger alkyl groups like in isoamyl acetate[14] and n-butyl acetate.[15]

The barrier of the ethyl methyl group is 1061.4(68) cm^{-1}, which is quite close to the barrier of 1260(4) cm^{-1} found in ethyl chloride[5] and 1171.3(14) cm^{-1} in ethyl fluoride.[3] Therefore, we conclude that a substitution from halogen atoms to carbonyl group does not affect the barrier to internal rotation of ethyl methyl groups significantly. Further discussion will be reported later in Chapter 8.

Finally it should be mentioned that only about 30% of all measured lines could be assigned. The still unassigned lines might be due to the *gauche* or other conformers, to excited torsional states, and also due to other vibrational states. Also some lines probably arise from isotopomeres of strong lines of *trans* ethyl acetate. We will continue for a complete assignment of the ethyl acetate spectrum in a near future.

5. Conclusion

The Fourier transform microwave spectrum of ethyl acetate has been measured under molecular beam conditions. The *trans* conformer, where all heavy atoms are located within a mirror plane, was identified after analyzing the spectrum by comparison with quantum chemical results. The barrier to internal rotation of the acetyl methyl group was found to be only 97.7844(45) cm^{-1} by fitting with the program XIAM and 99.57(10) cm^{-1} using the program BELGI-C$_S$. The parameters obtained with both programs are in reasonable agreement. The standard deviation is on the same order of 3 kHz for the A species, but for the E species BELGI-C$_S$ appears to be much better. Therefore, BELGI-C$_S$ has a better predictive power, however, for assignment purposes XIAM is more user-friendly and faster. For the methyl torsion in the ethyl group a barrier of 1061.4(68) cm^{-1} was determined. A comparison between two theoretical approaches treating the internal rotation, the so-called RAM (Rho-Axis-Method) and CAM (Combine-Axis-Method), was performed.

Acknowledgments

Publication statement

Part of this work is published in Journal of Molecular Spectroscopy under D. Jelisavac, D. Cortés-Gómez, H. V. L. Nguyen, L. W. Sutikdja, W. Stahl, I. Kleiner, *J. Mol. Spectrosc.* **257**, 111 (2009).

References

[1]M.Sugino, H. Takeuchi, T. Egawa, S. Konaka, *J. Mol. Struct.* **245**, 357 (1991).

[2]J. Sheridan, W. Bossert, A. Bauder, *J. Mol. Spectrosc.* **80**, 1 (1980).

[3]E. Fliege, H. Dreizler, J. Demaison, D. Boucher, J. Burie, A. Dubrulle, *J. Chem. Phys.* **78**, 3541 (1983).

[4]P. I. Nagy, F. R. Tejada, J. G. Sarver, W. S. Messer, Jr., *J. Phys. Chem. A* 10173 (2004).

[5]W. Stahl, H. Dreizler, M. Hayashi, *Z. Naturforsch.* **38a**, 1010 (1983).

[6]N. Ohashi, J. T. Hougen, R. D. Suenram, F. J. Lovas, Y. Kawashima, M. Fujitake, J. Pyka, *J. Mol. Spectrosc.* **227**, 28 (2004).

[7]B. Kirtman, *J. Chem. Phys.* **37**, 2516 (1962).

[8]R. M. Lees and J. G. Baker, *J. Chem. Phys.* **48**, 5299 (1968).

[9]E. Herbst, J. K. Messer, F. C. DeLucia, P. Helminger, *J. Mol. Spectrosc.* **108**, 42 (1984).

[10]V. Ilyushin, E. A. Alekseev, S. F. Dyubko, I. Kleiner, J. T. Hougen, *J. Mol. Spectrosc.* **227**, 115 (2004).

[11]R. J. Lavrich, A. R. Hight Walker, D. F. Plusquellic, I. Kleiner, R. D. Suenram, J. T. Hougen, G. T. Fraser, *J. Chem. Phys.* **119**, 5487 (2003).

[12]D. F. Plusquellic, I. Kleiner, J. Demaison, R. D. Suenram, R. J. Lavrich, F. J. Lovas, G. T. Fraser, V. V. Ilyushin, *J. Chem. Phys.* **125**, 104312 (2006).

[13]J. T. Hougen, I. Kleiner, M. Godefroid, *J. Mol. Spectrosc.* **163**, 559 (1994).

[14]L. W. Sutikdja, D. Jelisavac, W. Stahl, I. Kleiner, submitted to *Mol. Phys.* **2012**.

[15]T. Attig, diploma thesis at the RWTH Aachen University under supervision of L. W. Sutikdja and Prof. W. Stahl, **2011**.

Chapter 2

ALLYL ACETATE

One rotor and C_1 frame symmetry

1. Introduction

MB-FTMW spectroscopy is an excellent tool to study the structure and dynamics of molecules in the gas phase. By this way a large number of molecules has been investigated, but surprisingly, as discussed in Chapter 1, only very few esters were among them, though they are a very important class of compounds in chemistry. This might be due to the fact that even small esters contain quite a large number of atoms which makes them too big for classical structure determination by isotopic substitution. Moreover, even under molecular beam conditions usually several conformers exist. We tried to identify conformers of esters by comparing the experimental data with quantum chemical calculations and succeeded for some aliphatic esters such as ethyl acetate (see Chapter 1).

Among the esters allyl acetate, CH_3–COO–CH_2–CH=CH_2, is one of the smallest unsaturated ester with an interesting dynamics. Our interest in large amplitude motions motivated us to investigate this molecule. The acetyl methyl group shows internal rotation. From investigations on methyl acetate,[1] where a barrier of the acetate methyl group of 99.559(83) cm^{-1} was observed, and from our studies on ethyl acetate (Chapter 1), where we found a barrier of 97.7844(45) cm^{-1}, we expected also in this case a rather low hindering barrier on the order of 100 cm^{-1}. This could additionally increase the complexity of the spectra and makes assignment difficult. On the other hand we could not exclude to observe a different value since an interaction with the double bond appeared possible.

Furthermore, our quantum chemical calculations on allyl acetate, carried out before beginning the experimental work, made us curious. A conformer with the ethylene group bent against the plane containing the ester group was predicted, whereas our intuition told us that all heavy atoms should be located in a mirror plane. For the latter geometry the theoretical calculations predicted a local maximum in the potential. We expected that a microwave study would allow us to decide which structure is the correct one.
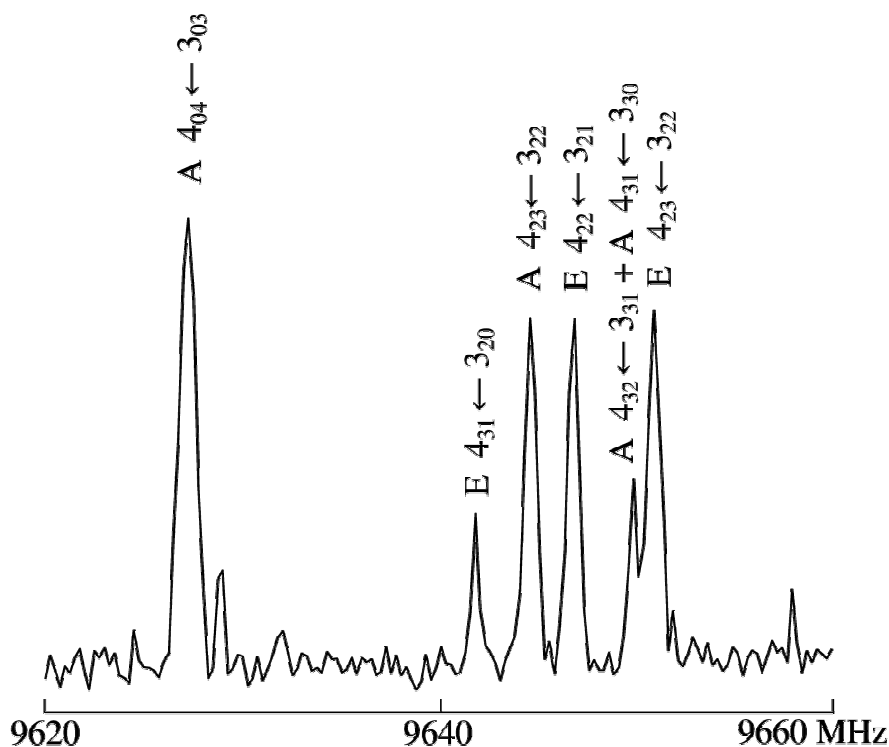
FIG. 1 A typical scan of allyl acetate. The spectral range of 40 MHz was covered by overlapping spectra with a step width of 250 kHz. For each single measure 50 FIDs were co-added.

2. Microwave spectrum

We started our investigations by recording broadband scans in the frequency range from 9.3 to 10.0 GHz using the MB-FTMW spectrometer described in ref. [17,18] in the experimental setup section. Additionally, during the process of spectral assignment some smaller ranges on the order of 100 to 200 MHz were scanned. An example is given in Figure 1. In total 274 lines were found, many of them were quite strong. All lines were remeasured in the high resolution mode of the spectrometer. The line width was approximately 8 kHz. The line positions can be determined with an accuracy of 1 kHz for strong lines and 5 kHz for weaker lines. A typical spectrum is shown in Figure 2.

At the beginning of our studies on allyl acetate, we assumed that the C_S conformer with a symmetry plane (conformer C_S, shown in Figure 3) should exist and it should be the most stable one. Taking this mirror plane as a constraint in quantum chemical calculations (see next section), we predicted the rotational constants and tried to use them for assigning the spectrum. However, we found that the experimental and the theoretical spectra did not match at all. Without this constraint, using the program *Gaussian03* a fully optimized structure with the MP2 method and the 6-311++G(d,p) basis set was obtained, where the plane of the vinyl

$$A\ 4_{04} \leftarrow 3_{03}$$

$$9627.2408\ \text{MHz}$$

8 kHz

9627.091   9627.240   9627.390 MHz
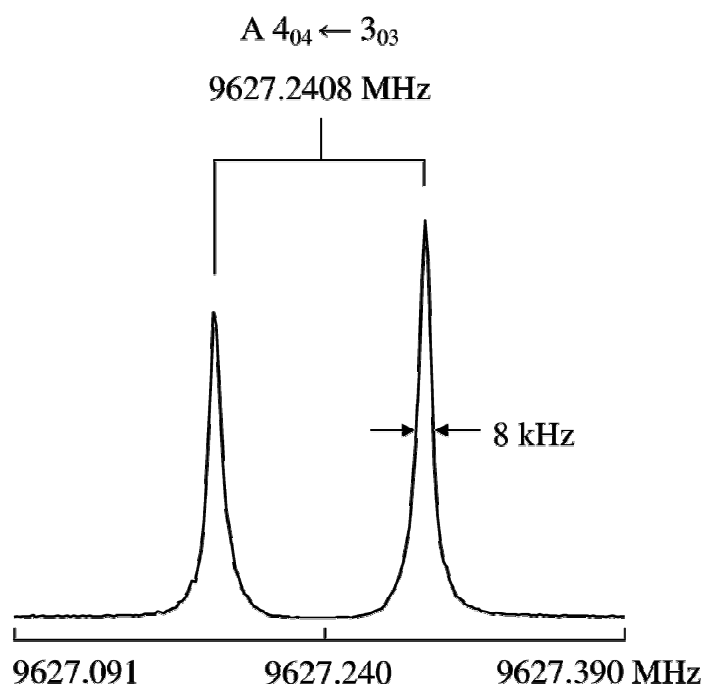
FIG. 2 A typical spectrum of allyl acetate. The experimental resolution was 0.8 kHz, the typical experimental line width 8 kHz as indicated in the spectrum. The large splitting is due to the Doppler effect. For this spectrum 60 FIDs were co-added.

group was bent by an angle of 121.57° against the ester group (conformer I, shown in Figure 4). We tried again to assign the spectrum with the new rotational constants (see Table 1) and succeeded. However, the calculated and the experimental rotational constants differed by up to 2.5 %. The origin of this will be discussed in section 4.

We started the assignment with the lines of the A species, which could be treated as an effective rigid rotor spectrum. On the basis of the rotational constants obtained by quantum chemical calculations we predicted the spectrum with the program XIAM. By trial and error the typical pattern of the a-type $4 \leftarrow 3$ R branch could be identified. Fitting these lines with XIAM yielded already quite accurate B and C rotational constant, which were still improved by including other a-type R branches. Finally, also b-type Q branch transitions were identified, which enabled us to fit the A constant as well.

It should be noted that by our quantum chemical calculations the c dipole moment component is predicted to be small but not zero. Therefore we were surprised that no c-type transitions could be found at all in the scans. After the spectrum had been assigned we were able to measure some c-type transitions using polarizing pulses with a power of 1 or 2 W, whereas for a- and b-type transitions a few mW turned out to be sufficient. The existence of c-type
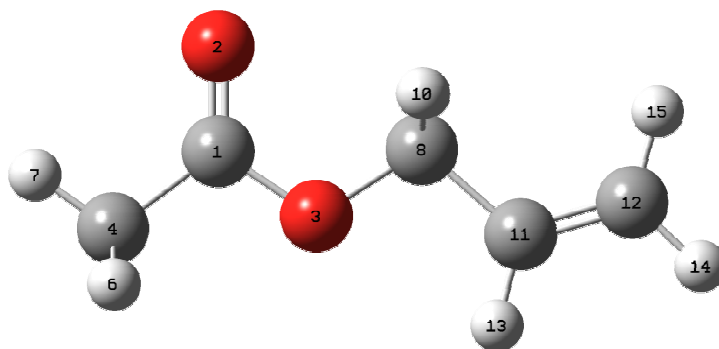
FIG. 3 The planar geometry (conformer C_S) of allyl acetate
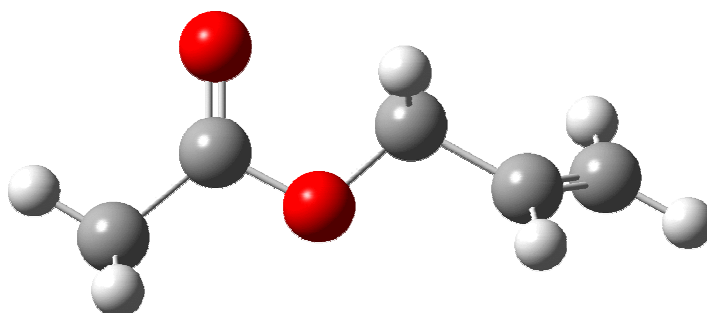
FIG. 4 The bent conformer (conformer I) of allyl acetate from optimization at the MP2/6-311++G(d,p) level. The dihedral angel $\varphi_1 = \angle(C_{12}, C_{11}, C_8, O_3)$ is 121.57° (see section 3).

transitions proofs that no mirror plane is present within the conformer studied. It should also be noted that the c-type transitions were not split, which indicates that no tunneling of the vinyl group through the plane of the ester group occurs on the time scale of our experiment. A list of some c-type transitions is given in the Appendix (Table B-1). The observed c-type transitions were, however, very weak and we did not include them in our fits.

In allyl acetate the rotational lines are split due to internal rotation of the acetyl methyl group, which has a low barrier to internal rotation. Thus, we expected very large A-E splittings from a few MHz up to 1 GHz or more, depending on the respective transition. The E species transitions were predicted using the XIAM code. The barrier to internal rotation was assumed to be approximately 100 cm^{-1} as in ethyl acetate (Chapter 1) and also in methyl acetate.[1] The moment of inertia of the methyl group was first chosen to be 3.2 uÅ^2, which we considered to be a reasonable value found in many molecules with methyl internal rotation. The angles between the internal rotor axis and the principal inertial axes of the molecule were calculated from the *ab initio* geometry shown in Figure 4. Its Cartesian coordinates are found in the Appendix (Table B-2). The angles are given in Table 1.

Table 1

Molecular constants in the PAM system of allyl acetate from different fits and quantum chemical calculations.

Parameter	Unit	Fit I BELGI-C$_1$	Fit II XIAM	Fit III XIAM	Calc. I[d]	Exp.– Calc.[e]	Dev. [%]	Calc. II[f]	Exp.– Calc.[e]	Dev. [%]
A	GHz	7.67929(30)[a]	7.7034352(67)	7.70343360(35)	7.511	0.192	2.49	7.698	0.005	0.06
B	GHz	1.2691224(98)[a]	1.2678319(59)	1.267831492(71)	1.277	–0.009	0.71	1.266	0.002	0.15
C	GHz	1.14203856(61)[a]	1.1415254(63)	1.141526125(76)	1.150	–0.008	0.79	1.137	0.005	0.43
Δ_J	kHz		0.1399(34)	0.13953(17)						
Δ_{JK}	kHz		–1.195(33)	–1.1808(18)						
Δ_K	kHz		32.56(62)	32.337(32)						
δ_J	kHz		0.0045(24)	0.00246(13)						
δ_K	kHz		–0.41 (35)	–0.392(18)						
D_{pi2J}	kHz		87.34(85)	87.34 (fixed)						
D_{pi2-}	kHz		47.89(93)	47.89 (fixed)						
V_3	GHz	2955.3(44)	2940.74(35)	2940.74 (fixed)						
	kJ/mol	1.1793(18)[c]	1.17345 (14)							
	cm^{-1}	98.58(15)[c]	98.093(12)							
F_0	GHz	158.621(82)	153.589(15)	153.589 (fixed)						
I_γ	uÅ^2	3.1861(17)[b]	3.29046 (33)	3.29046 (fixed)						
$\angle$(i,a)	°	44.45601(64)	44.4871(33)	44. 4871 (fixed)	46.73	–2.24		45.73	–1.24	
$\angle$(i,b)	°	134.15842(61)	134.8143(57)	134. 8143 (fixed)	136.46	–1.65		135.43	–0.62	
$\angle$(i,c)	°	85.68777(84)	85.832(17)	85. 832 (fixed)	86.04	–0.21		85.82	0.01	
σ	kHz	2.3	54.0	2.7						
N_A/N_E		109/62	109/62	109/0						
N_{tot}		171	171	109						

Note: All constants refer to the principal axis system, for the centrifugal distortion constants Watson's A reduction and a I^r representations was used.
[a] Obtained by transformation from rho axis system to principal axis system, see text.
[b] Moment of inertia I_γ of the internal rotor, calculated from its rotational constant F_0.
[c] Hindering potential, calculated from value in frequency units.
[d] Calculation on MP2/6-311++G(d,p) level using *Gaussian03*.
[e] With respect to Fit II
[f] Same as Calc. I with empirical correction, see section 4.

We started the assignment of the E species lines with those lines which were predicted to be close to the respective A species transitions. This holds for the *a*-type *R* branch transitions, where the A-E splittings were only on order of 10 to 100 MHz. After fitting the internal rotation parameters and thereby improving our predictions, also *b*-type *Q* branch transitions could be assigned, which were split by several 100 MHz up to 1 GHz. In some cases scanning a small range of 5 MHz was necessary to find the lines.

Using the XIAM code the barrier to internal rotation was determined to be 98.093(12) cm^{-1}. This can be compared to the barrier of the acetyl methyl group of methyl acetate which is 99.559(83) cm^{-1} and to the barrier of 97.7844(45) cm^{-1} which was found for ethyl acetate. All barriers are very close together and obviously, the double bond of allyl acetate does not affect the internal rotation.

Finally, 109 A species and 62 E species lines were assigned and fitted again with the program BELGI-C$_1$ using the Rho Axis Method (RAM). This code allows us to calculate and fit transitions for asymmetric top molecules containing one C$_{3v}$ internal rotor (like the CH$_3$ group) and having a C$_1$ point group symmetry at equilibrium. The BELGI-C$_1$ code was used only twice up to now and the fit can be compared to a perturbation treatment in the PAM axis system used in the JB95 code.[2,3] The results are shown in Table 1 and Table 2. A complete list of all fitted transitions is given in the Appendix (Table B-3 and B-4).

3. Quantum chemistry

For an unambiguous identification of the assigned conformer quantum chemical calculations on MP2/6-311++G(d,p) level were carried out. From calculations on ethyl acetate (Chapter 1) and other esters like ethyl pivalate[4] and ethyl isovalerate[5] we know that this method gives reliable rotational constants.

In the case of allyl acetate many start geometries can be generated by rotating a part of the molecule around the C$_8$–O$_{11}$ and O$_3$–C$_8$ bonds. All of them are *trans* geometries. Rotation around the C$_1$–O$_3$ bond yields *cis* geometries of allyl acetate which are much higher in energy and are unlikely to be observed under molecular beam conditions.[6] Therefore we will not discuss them here and only concentrate on the *trans* ester throughout this text.

In total, 36 different start geometries were created by varying the dihedral angles $\varphi_1 = \angle$(C$_{12}$, C$_{11}$, C$_8$, O$_3$) and $\varphi_2 = \angle$(C$_{11}$, C$_8$, O$_3$, C$_1$) in each case from $-180°$ to $120°$ in a grid of $60°$. Atom numbers are given in Figure 3. The MP2/6-311++G(d,p) level was used to optimize all

Table 2

Molecular constants in the RAM system of allyl acetate obtained by a global fit using the program BELGI-C_1.

Operator[a]	Constant[b]	Unit[c]	Value
P_a^2	A	GHz	7.51535(31)
P_b^2	B	GHz	1.14266690(55)
P_c^2	C	GHz	1.4324355(43)
$\{P_a,P_b\}$	D_{ab}	GHz	–0.0423367(81)
$\{P_a,P_c\}$	D_{ac}	GHz	1.011141(13)
$-P^4$	Δ_J	kHz	0.19522(16)
$-P^2P_a^2$	Δ_{JK}	kHz	–4.1206(37)
$-P_a^4$	Δ_K	kHz	33.975(51)
$-2P^2(P_b^2-P_c^2)$	δ_J	kHz	–0.03006(13)
$- [P_a^2,(P_b^2-P_c^2)]$	δ_K	kHz	0.6391(48)
P_γ^2	F	GHz	160.61(19)
		cm^{-1}	5.3575(62)
$(1/2)(1-\cos3\gamma)$	V_3	GHz	2955.3(44)
		cm^{-1}	98.58(15)
P_aP_γ	ρ	unitless	0.035007(18)
$(1-\cos3\gamma)P_a^2$	k_5	MHz	71.55(87)
$(1-\cos3\gamma)P^2$	F_V	MHz	–1.6286(59)
$(1-\cos3\gamma)(P_b^2-P_c^2)$	c_2	MHz	0.7132(61)
$(1-\cos3\gamma)\{P_a,P_b\}$	d_{ab}	MHz	5.5(56)
$(1-\cos3\gamma)\{P_a,P_c\}$	d_{ac}	MHz	3.857(36)
	$N_A/N_E/N_{tot}$		109 / 62 / 171
	$\sigma_A/\sigma_E/\sigma_{tot}$	kHz	2.7 / 1.2 / 2.3

[a] All constants refer to a rho-axis system, therefore the inertia tensor is not diagonal and the constants cannot be directly compared to those of a principal axis system. P_a, P_b, P_c are the components of the overall rotation angular momentum, P_γ is the angular momentum of the internal rotor rotating around the internal rotor axis by an angle γ. $\{u,v\}$ is the anti commutator $uv + vu$.
[b] The product of the parameter and operator from a given row yields the term actually used in the vibration-rotation-torsion Hamiltonian, except for F, ρ, and A, which occur in the Hamiltonian in the form $F(P_\gamma-\rho P_a)^2 + AP_a^2$.
$N_A/N_E/N_{tot}$ are the numbers of A transitions, E transitions, and the total number of transitions. $\sigma_A/\sigma_E/\sigma_{tot}$ are the respective standard deviations.
[c] Values of the parameters from the present fit. Statistical uncertainties are shown as one standard uncertainty in the last digit.

start geometries. Only 6 conformers were found and indicated in Figure 5 with their relative electronic energies. The rotational constants, stabilization energies, dihedral angles φ_1 and φ_2, and dipole moments are given in Table 3. The nuclear coordinates in the principal axes system are found in the Appendix (Table B-5). In contrast to our initial assumption most of the conformers do not have a symmetry plane and exist as enantiomeric pairs. Frequency calculations have shown that the intuitively predicted conformer, conformer C_S, is a saddle point of second order with a vibration around the C_1–C_4 and a vibration around the C_8–C_{11} bond rather than a stable conformer.

Table 3

The rotational constants, stabilization energies, dihedral angles φ_1 and φ_2, and dipole moments of 6 conformers of allyl acetate obtained from quantum chemical calculations.

Conf.	rel. E^a / kJ/mol	φ_1^b / °	φ_2^b / °	$|\mu_a|^c$ / D	$|\mu_b|^c$ / D	$|\mu_c|^c$ / D	A / GHz	B / GHz	C / GHz
C_S	10.9331	180.0	180.0	0.449	1.913	0.000	8.369	1.237	1.092
I/I*^{d}	1.0528	±121.5	±177.1	0.810	1.919	0.079	7.514	1.277	1.150
I/I*^{e}		±129.0	±129.0				7.511	1.277	1.514
II	3.6492	0.0	180.0	0.906	1.664	0.000	6.165	1.514	1.234
III	3.4352	−3.2	−86.4	0.167	0.442	1.829	4.777	1.767	1.693
IV	0.8268	115.3	−82.9	0.113	1.550	0.877	5.295	1.695	1.494
V	0.0000	114.8	−76.4	0.227	1.928	0.247	6.327	1.452	1.365

^{a} Relative stabilization energies calculated at the MP2/6-311++G(d,p) level with respect to the lowest energy conformers V at −344.9182358 Hartree.

^{b} Dihedral angles $\varphi_1 = \angle(C_{12}, C_{11}, C_8, O_3)$ and $\varphi_2 = \angle(C_{11}, C_8, O_3, C_1)$.

^{c} Dipole moments in principal axes.

^{d} Conformer I and I* are chiral enantiomers which cannot be distinguished by MB-FTMW spectroscopy.

^{e} Empirical correction by adjusting the dihedral angle φ_1 for best agreement with experimental rotational constants, see text.
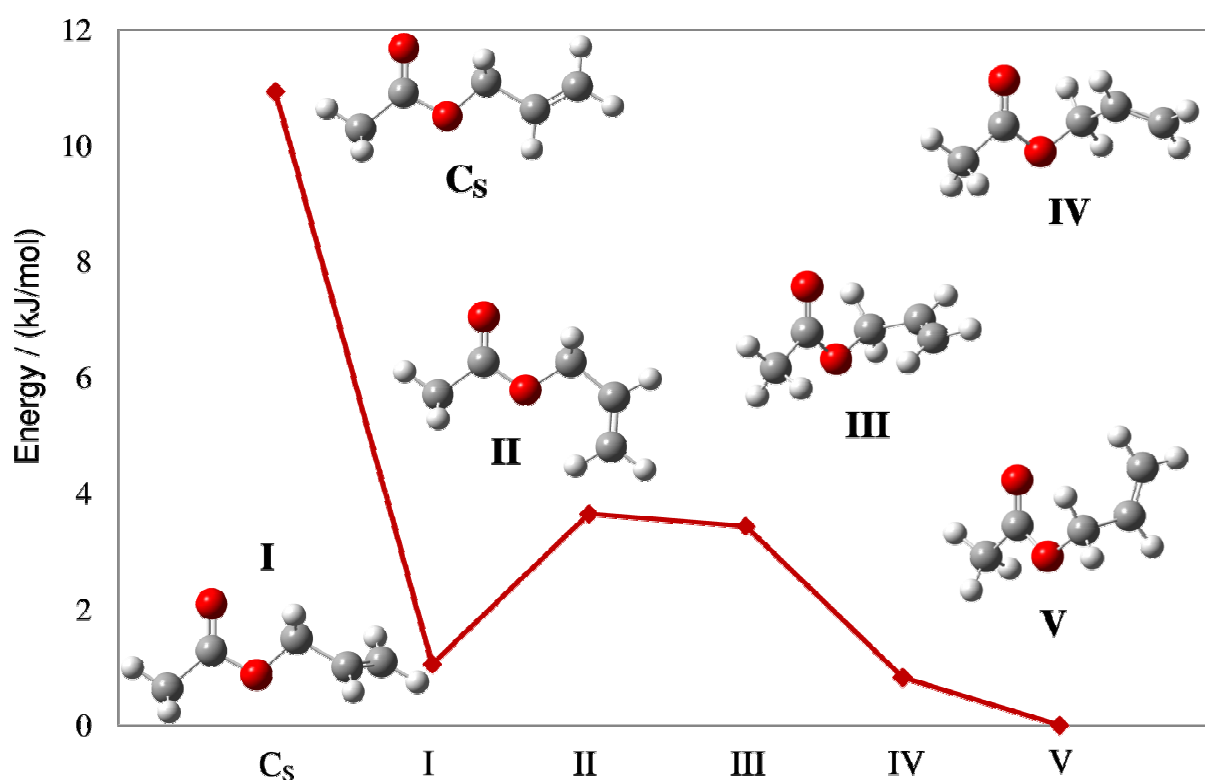
FIG. 5 Different conformers of allyl acetate. The stabilization energy values are relative to the most stable conformer V (−344.9182358 Hartree). Only one enantiomer of conformers I, III, IV, and V are indicated.

In a next step the potential curve of allyl acetate was calculated by freezing the dihedral angle $\varphi_1 = \angle(C_{12}, C_{11}, C_8, O_3)$ at certain fixed values while all other parameters were optimized. In this case we calculated a full rotation of 360° with a 10° step width. The corresponding potential surface is shown in Figure 6.

Obviously, three conformers are generated by this rotation. Conformer I and I* are a pair of enantiomers with the same rotational constants. A further conformer (conformer II) is less stable and should have a symmetry plane. We also indicated a non-stable conformer at $\varphi_1 = \pm 180°$ (conformer C_S) which is also of C_S symmetry. As can be recognized from Figure 6 the dihedral angle φ_1 for the energy minimum is $\pm 121.57°$ for the conformers I/I*.

In Figure 7 the rotational constants in dependence on the dihedral angle φ_1 are drawn. The range from 115° to 130° was enlarged by varying the dihedral angle φ_1 in a grid of 1° instead of 10°. The rotational constants are shown in Figure 8. The experimental rotational constants matched the calculated one exactly at $\varphi_1 \approx +129°$, not at +121.57°, i.e. the rotational constants of conformer I/I* as obtained by full optimization are not the best ones. This will be discussed in the next section.

4. Results and discussion

The microwave spectrum of allyl acetate has been assigned with the programs XIAM and BELGI-C_1. As discussed in Chapter 1, XIAM is very user-friendly and easier to use for assignment purposes, whereas BELGI-C_1 is usually a better model to treat the internal rotation problem for low barrier molecules very accurately. A comparison of XIAM and BELGI has been given in Chapter 1 and will not be repeated here again in detail. With XIAM a global fit of the A and E species was carried out (Fit II in Table 1). A standard deviation of 54.0 kHz was obtained for 171 lines with $J_{max} = 15$ and $K_{a\,max} = 6$ (5) for the A (E) species, respectively. In a second fit with XIAM (Fit III in Table 1) the internal rotation parameters were fixed to the values obtained from Fit II and only the A species lines were fitted. Here a standard deviation of 2.7 kHz was found, which is close to the experimental accuracy. A global fit with BELGI-C_1 allowed to fit together the A species with a standard deviation of 2.7 kHz and the E species with 1.2 kHz. The overall standard deviation is 2.3 kHz which indicated that the model used in BELGI-C_1 almost perfectly describes the observed spectrum. The reason for the better standard deviations obtained by the BELGI-C_1 code is that it uses a global approach dealing with the total set of torsional v_t states (to a certain truncation level)
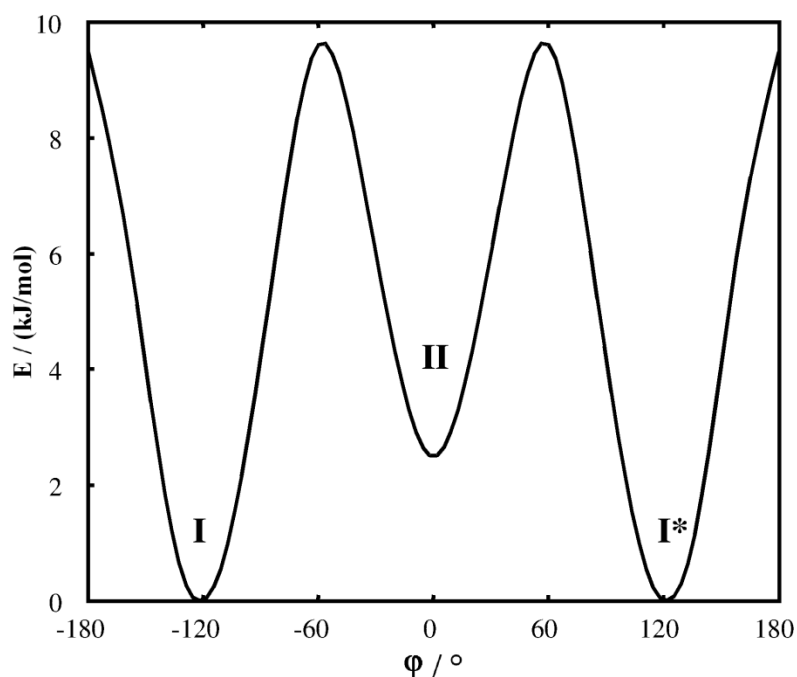
FIG. 6 The potential curve of allyl acetate obtained by rotating the vinyl group. The relative energy with respect to the lowest energy conformers I/I* (–344.9178348 Hartree) is given. Conformer I* is the enantiomer of conformer I with the same rotational constants. Conformer II is the only stable conformer with a symmetry plane. The maxima at ±180° represent the non-stable conformer C_S.
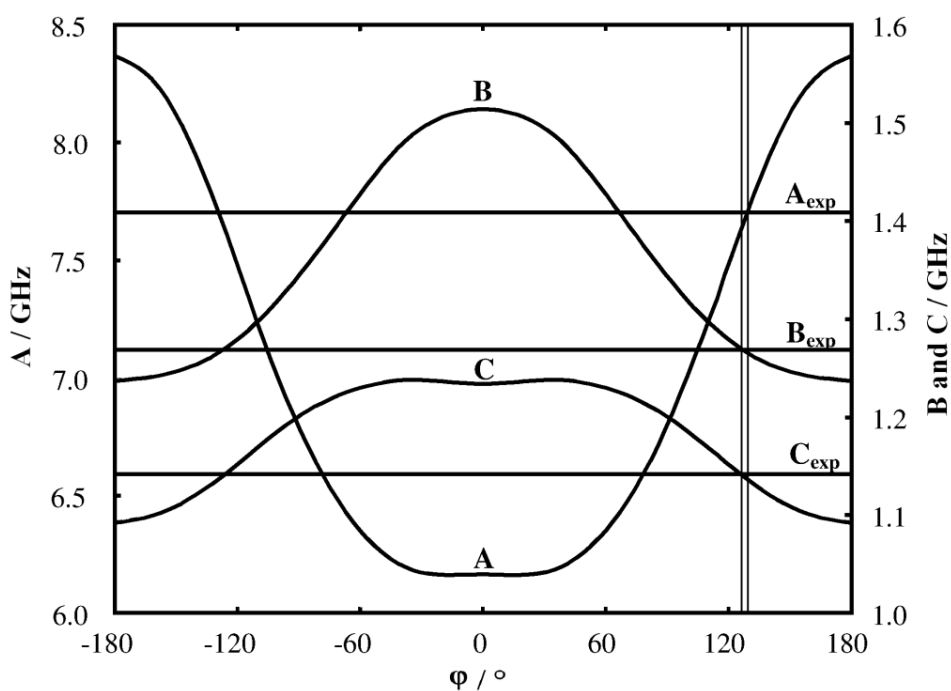
FIG. 7 Comparison of the calculated rotational constants (A, B, C) for different dihedral angel φ_1 with the experimental rotational constants (A_{exp}, B_{exp}, C_{exp}). The A rotational constant is described at the left scale and the B and C rotational constants at the right scale. The horizontal lines are the experimental rotational constants. The vertical lines show the position where the calculated and the experimental data have the best agreement.
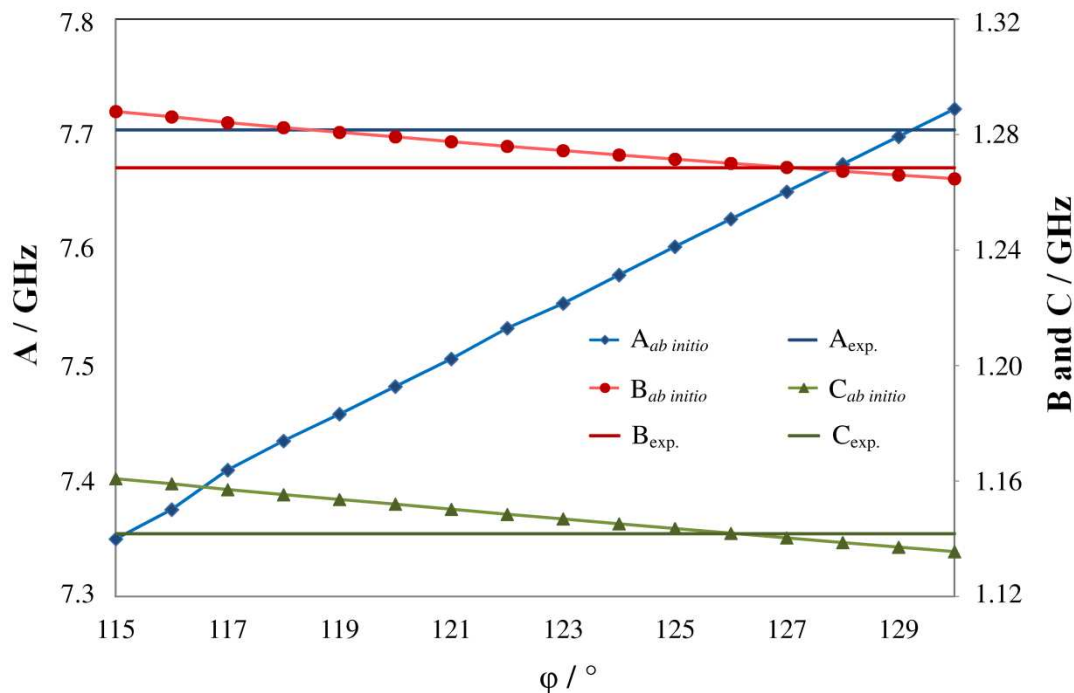
FIG. 8 Comparison of the calculated rotational constants (A, B, C) for different dihedral angel φ_1 in the range from 115° to 130° in a grid of 1° with the experimental rotational constants (A_{exp}, B_{exp}, C_{exp}). The experimental rotational constants matched exactly at $\varphi_1 \approx +129°$.

associated with the internal rotation and using one Hamiltonian and one set of parameters to fit the data. The model used in BELGI does therefore include all torsion-rotation interaction between different torsional states. On the other hand, in the local method used in XIAM, each torsional state is treated separately using its own Hamiltonian. In XIAM, certain off-diagonal matrix elements in v_t are thus neglected (after removal by van Vleck transformations) which is a good assumption only in the high barrier limit. In the present case, the so called reduced barrier height $s = 4V_3/9F$ is small (8.17) and thus the effect of those matrix elements are important and cannot be neglected.

It should be noted that in Table 2, we needed two terms which are symmetry allowed only for a C_1 internal rotor molecule. The D_{ac} parameter (multiplying the $P_aP_c + P_cP_a$ operator), which essentially allows for the fact that the methyl top axis is not required by symmetry to lay in the principal axis ab plane, is actually rather large. We also needed d_{ac}, which is its torsional dependence.

Furthermore, the internal rotation problem in BELGI-C_1 is treated in the rho axis system (RAM system) and consequently, all parameters obtained also refer to this coordinate system. The original parameters from the BELGI-C_1 fit are given in Table 2. To compare these values

with those obtained from XIAM, which refer to a principal axis system (PAM system), all BELGI-C_1 parameters given in Table 2 were transformed from the rho axis system to the principal axis system (Fit I in Table 1).

To facilitate this transformation, in a first step the tensor formed by the diagonal A, B, and C rotational constants and the off-diagonal elements D_{ab}, D_{bc}, and D_{ac} is diagonalized yielding A, B, and C in the PAM system as well as the transformation matrix v. The transformation matrix is used to calculate the elements of the rho vector $\rho_a = \rho \cdot v_{11}$, $\rho_b = \rho \cdot v_{12}$, and $\rho_c = \rho \cdot v_{13}$ in the PAM system. In a next step the moment of inertia of the methyl group F_0 and the direction cosines λ_{ia}, λ_{ib}, λ_{ic} between the internal rotor axis and the principal axes a, b, and c are calculated

$$F_0 = \sqrt{\frac{1}{\frac{\rho_a^2}{A^2} + \frac{\rho_b^2}{B^2} + \frac{\rho_c^2}{C^2}}} \ ,$$

$$\lambda_{ia} = \rho_a \cdot \frac{F_0}{A}, \quad \lambda_{ib} = \rho_b \cdot \frac{F_0}{B}, \quad \lambda_{ic} = \rho_c \cdot \frac{F_0}{C} \ .$$

The barrier to internal rotation of the acetate methyl group is 98.55(13) cm^{-1} and 98.093(12) cm^{-1} and the moments of inertia of the methyl group were fitted to yield 3.1861(17) uÅ^2 and 3.29046 (33) uÅ^2 using BELGI-C_1 and XIAM, respectively. Here, the BELGI-C_1 value appears somewhat smaller, whereas the XIAM value is slightly too high if compared with the methyl rotors in methyl acetate (3.2085(26) uÅ^2)[1] and ethyl acetate (3.16067(76) uÅ^2). However this discrepancy may also indicate that non-rigidity effects are important for I_γ and these effects are treated very differently by the two methods. In the BELGI code, deviations of the C_{3v} symmetry for the methyl group is taken into account by higher-order interaction terms, whereas in XIAM only some higher (fourth order) coupling terms between internal rotation and overall rotation are implemented.

By comparing the experimental rotational constants with the calculated ones of conformer I, we found that the B and C constants have a relative deviation of 0.8%, but for the A constant it is 2.49% which corresponds to an absolute deviation of approximately 200 MHz (see Table 1, Calc. I). However, the ground state constants derived experimentally cannot be directly compared to the computed *ab initio* constants at equilibrium. In the case of *cis* methyl formate molecule HCOOCH$_3$, another molecule containing an internal rotor, the theoretical vibration-rotation interaction α constants deduced from the *ab initio* cubic force field were

combined with the known experimental ground state rotational constants to yield the semi-experimental equilibrium rotational constants to be compared with the equilibrium constants. The correction did not exceed 1.5% for methyl formate,[7] thus less than the 2.49% observed in the case of allyl acetate. In order to obtain a better agreement between the observed and the *ab initio* rotational constants, we rotated the molecular fragments around φ_1 with a step width of 1° and tried to find the angle where the deviation of the rotational constants becomes a minimum. We found that at $\varphi_1 = 129°$ the deviations of A, B, and C are below 0.5% (see Table 1, Calc. II). The difference of approximately 7.5° is probably due to the small torsional force constant causing a rather flat minimum. Here very small interactions between both molecular fragments might cause rather large changes in φ_1. A much better quantum chemical method and a larger basis set might increase accuracy by treating these small interactions more correctly. Also the angles between the internal rotor axis and the principal axes of inertia are improved by this empirical correction.

Finally it should be mentioned that only about 40% of all measured lines could be assigned. The still unassigned lines might be due to the conformers IV and V which have even lower stabilization energy than the assigned conformer I. Also some lines probably arise from strong lines of isotopologues of the assigned conformer. However, due to the complexity of the spectrum, none of these species could be presently assigned.

5. Conclusion

The Fourier transform microwave spectrum of allyl acetate has been measured under molecular beam conditions. By comparing the experimental data with quantum chemical calculations we identified one conformer of C_1 symmetry, in which the ethylene group is bent by an angle of approximately 129° against the plane of the C–COO–C backbone. Large A-E splittings (in some cases up to 1 GHz) of all lines due to internal rotation of the acetate methyl group were found. Analyzing the spectrum with the programs XIAM and BELGI-C_1 yielded a torsional barrier of only 98.093(12) cm^{-1} and 98.58(15) cm^{-1}, respectively. Similar to the case of ethyl acetate, both programs can fit the A species transitions to the experimental accuracy, however, the predictive power of BELGI-C_1 turned out to be better for the E species.

Acknowledgments

Publication statement

Part of this work is published in Molecular Physics under H. V. L. Nguyen, H. Mouhib, W. Stahl, I. Kleiner, *Mol. Phys.* **108**, 763 (2010).

References

[1]J. Sheridan, W. Bossert, A. Bauder, *J. Mol. Spectrosc.* **80**, 1 (1980).

[2]R. J. Lavrich, A. R. Hight Walker, D. F. Plusquellic, I. Kleiner, R. D. Suenram , J. T. Hougen, G. T. Fraser, *J. Chem. Phys.* **119**, 5497 (2003).

[3]D. F. Plusquellic , I. Kleiner, J. Demaison, R. D. Suenram, R. J. Lavrich, F. J. Lovas, G. T. Fraser, V. V. Ilyushin, *J. Chem. Phys.* **125**, 104312 (2006).

[4]H. Mouhib, Y. Zhao, W. Stahl, *J. Mol. Spectrosc.* **261**, 59 (2010).

[5]H. Mouhib, D. Jelisavac, L. W. Sutikdja, E. Isaak, W. Stahl, *J. Phys. Chem. A* **115**, 118 (2011).

[6]M. Oki and H. Nakanishi, *Bul. Chem. Soc. Japan* **43**, 2558 (1970).

[7]J. Demaison, L. Margulès, I. Kleiner, A. G. Császár, *J. Mol. Spectrosc.* **259**, 70 (2010).

Chapter 3

VINYL ACETATE

Quantum chemical calculations and improvement of the fit

1. Introduction

The microwave spectroscopic investigations on allyl acetate (Chapter 2) have shown that the barrier to internal rotation of the acetyl methyl group is 98.093(12) cm^{-1}, almost the same as the barrier of 99.559(83) cm^{-1} and 97.7844 (45) cm^{-1} found for methyl acetate[1] and ethyl acetate (Chapter 1), respectively. Obviously, the allyl group does not affect the rotation of the acetyl methyl group. However, in the case of allyl acetate the double bond is far away from the internal methyl rotor. Therefore, it is interesting to study vinyl acetate, where the double bond is attached directly to the carboxyl group and electronic interactions could be possible.

The free-jet millimeter absorption spectrum of vinyl acetate has already been investigated by Caminati et al.[2] A global fit using the program XIAM was carried out. Unfortunately, the experimental accuracy was not good enough for a reasonable comparison with our own microwave spectroscopic data on methyl acetate,[3] ethyl acetate (Chapter 1), and allyl acetate (Chapter 2). A standard deviation of 0.08 MHz was reported when 14 parameters were fitted. Therefore we decided to remeasure vinyl acetate by MB-FTMW spectroscopy. By reanalysis of the spectrum using two programs, XIAM and Erham, we expected to achieve a better standard deviation as well as to determine the molecular parameters with higher accuracy. Quantum chemical calculations should also be improved.

2. Quantum chemistry

Quantum chemical calculations at the MP2/6-311++G(d,p) level of theory in the studies on vinyl acetate in ref. [2] have shown that three conformers are stable. Unlike allyl acetate, the most stable conformer has a symmetry plane, i.e. all heavy atoms are located on a mirror plane (see Figure 1). However, it should be noted that the vinyl group is tilted with a small angle of 4.5° against the ester group. Therefore, we decided to study the conformers in more detail by calculating a potential curve of vinyl acetate using the *Gaussian03* package with two different basis sets, MP2/6-311++G(d,p) and in addition MP2/6-311++G. The investigation
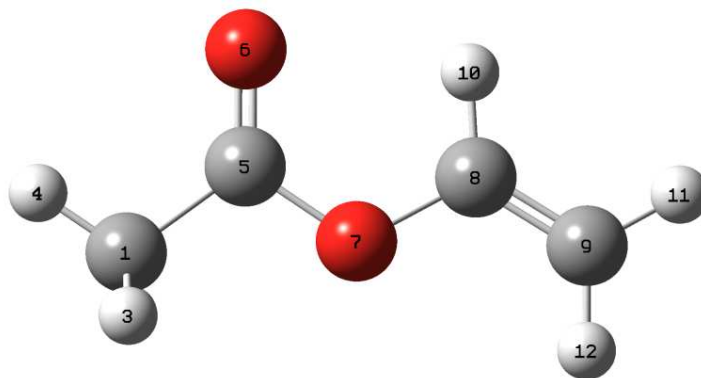
FIG. 1 Geometry of the most stable *trans* conformer I of vinyl acetate.

on ethyl acetate (Chapter 1) and theoretical studies of Oki and Nakanishi[4] have shown that *cis* esters are always much higher in energy and cannot be observed in the molecular beam. Therefore, we focused only on the *trans* conformer of vinyl acetate. The dihedral angle $\varphi = \angle(C_9, C_8, O_7, C_5)$ were frozen at a certain fixed values while all other parameters were allowed to relax. Due to symmetry, only a rotation of 180° in a grid of 10° was needed. The parameterized potential curve is shown in Figure 2, the Fourier coefficients are given in Table 1.

In agreement with the quantum chemical studies of Caminati et al.[2] the potential curve at the MP2/6-311++G(d,p) level shows two possible *trans* conformers. Conformer I has a C_S symmetry and is the most stable one. Conformer II/II* at about $\varphi = \pm 160°$ is a pair of enantiomers. The stabilization energy is approximately 12.6 kJ/mol higher than that one of conformer I. Therefore, conformer II/II* is unlikely to be observed under molecular beam conditions. It should be noted that in both cases, the energy minima are extremely flat. For this reason it is difficult to determine the exact dihedral angles of these conformers.

In contrast to the results of calculations at the MP2/6-311++G(d,p) level, the potential curve calculated with the 6-311++G basis set and the same method shows clearly four minima at $\varphi = \pm 30°$ and $\varphi = \pm 130°$. Conformer I becomes a local maximum. In principal, a tunneling between the two enantiomers at $\varphi = +30°$ and $-30°$ could be possible. However, we did not expect that splittings can be observed in the rotational spectrum, since the tunneling barrier is only 0.55 kJ/mol and the lowest energy level is probably higher. The stabilization energy of conformer II/II* and also the maximum at $\varphi = \pm 180°$ are lower than those obtained with the 6-311++G(d,p) basis set. Nevertheless, the stabilization energy of 8.25 kJ/mol is too high for an observation in the molecular beam. The Cartesian coordinates of conformer I and II calculated at the MP2/6-311++G(d,p) level are given in Table C-1 in the Appendix.
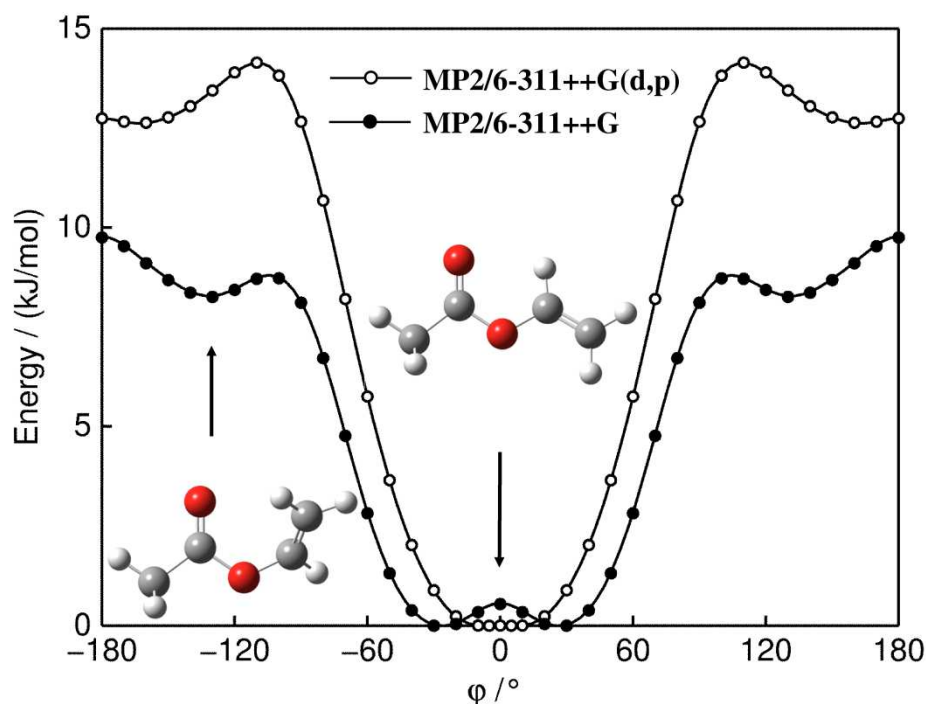
FIG. 2 The potential curve of vinyl acetate obtained by rotating the vinyl group around the O_7–C_8 bond. The MP2 method and two different basis sets were chosen. The relative energy with respect to the lowest energy conformer (E = −305.72213457 Hartree and E = −305.27460397 Hartree for the MP2/6-311++G(d,p) and the MP2/6-311++G level, respectively) is given.

Table 1

Potential functions for the rotation around the dihedral angle $\varphi = \angle(C_9, C_8, O_7, C_5)$. Energies were calculated in a 10° grid and parametrized as a Fourier series $V(\varphi) = a_0 + \sum\limits_{i=1}^{15} a_i \cos(i\varphi)$.

	MP2/6-311++G(d,p)		MP2/6-311++G	
	Hartree	cm^{-1}	Hartree	cm^{-1}
a_0	−305.718818038		−305.27250037	
a_1	−0.002631125	−577.4651	−0.00189374	−415.6274
a_2	−0.001184979	−260.0728	−0.00054718	−120.0912
a_3	0.000226180	49.6408	0.00012473	27.3746
a_4	0.000285334	62.6236	0.00039815	87.3829
a_5	−0.000029032	−6.3718	0.00000929	2.0387
a_6	−0.000019362	−4.2495	−0.00002554	−5.6058
a_7	0.000009582	2.1030	0.00000404	0.8862
a_8	0.000016336	3.5853	0.00001957	4.2960
a_9	0.000000244	0.0536	0.00000351	0.7695
a_{10}	0.000005674	1.2453	0.00000666	1.4619
a_{11}	−0.000001776	−0.3898	−0.00000210	−0.4618
a_{12}	0.000003099	0.6802	0.00000274	0.6018
a_{13}	0.000000355	0.0779	0.00000091	0.1991
a_{14}	0.000001628	0.3573	0.00000170	0.3729
a_{15}	−0.000000431	−0.0946	−0.00000013	−0.0292

3. Microwave spectrum

The acetyl methyl group in vinyl acetate shows large amplitude motion. The barrier to internal rotation was determined by Caminati et al.[2] to be 1.855(1) kJ/mol, i.e. 155.62(9) cm^{-1}. It is somewhat higher than the barrier found in methyl acetate, ethyl acetate, and allyl acetate. However, the barrier is still relatively low if compared to ethyl fluoride (1171.3 cm^{-1}).[5] Therefore, wide A-E splittings were observed. The rotational constants and the barrier from ref. [2] were used to predict the rotational spectrum in the range from 9 to 20 GHz. Using a modified version of the MB-FTMW spectrometer described in ref. [17,18] in the experimental setup section, 25 A species and 31 E species rotational transitions were remeasured. All lines are very intensive. The line width is in the range of 20 to 30 kHz, much larger than the value of 12 kHz found for ethyl acetate (Chapter 1) and allyl acetate (Chapter 2). In some cases, splitting in the order of about 10 kHz could be resolved. We attribute these splittings and the large line widths to spin-spin and spin-rotation coupling of the protons. The line position can be determined with an accuracy of 2 kHz.

In a next step, 56 remeasured lines were fitted with the programs XIAM. The fitted parameters are given in Fit I, Table 2. A list of all transition frequencies is given in the Appendix (Table C-2). In a second fit with XIAM (Fit II in Table 2) the internal rotation parameters were fixed to the values obtained from Fit I and only the A species lines were fitted.

As an alternative, a global fit with the program Erham was carried out. In this case, a standard deviation of only 1.2 kHz was found which is very close to the experimental accuracy. The parameters fitted with Erham are given in Fit III (Table 2) and all fitted transitions in Table C-3.

4. Result and discussion

Using the program XIAM, the rotational constants were determined to be A = 9.42529(13) MHz, B = 2.241298(24) MHz, and C = 1.831877(24) MHz, comparing to A = 9.40186(4) MHz, B = 2.241742(6) MHz, and C = 1.832332(7) MHz found in the previous investigation. The B and C rotational constants match the values calculated at the MP2/6-311++G(d,p) level almost exactly. The A rotational constant differs by 130 MHz, however, the relative deviation is only 1.4%. Totally, 25 A and 31 E species lines could be fitted with a standard deviation of 29.9 kHz (Fit I in Table 2). Though the standard deviation became much better with our new

Table 2

Molecular parameters of vinyl acetate obtained by a fit using programs XIAM, Erham, and quantum chemical calculations.

Parameter[a]	Unit	Fit I XIAM	Fit II XIAM	Fit III Erham	Fit IV Caminati et al.
A	GHz	9.42649(50)	9.42648141(31)	9.4012638(13)	9.40186(4)
B	GHz	2.241347(30)	2.24133757(19)	2.24171194(22)	2.241742(6)
C	GHz	1.831926(30)	1.83192476(15)	1.83242629(27)	1.832332(7)
Δ_J	kHz	0.285(28)	0.1746(27)	0.1679(27)	0.15(1)
Δ_{JK}	kHz	2.12(19)	1.929(16)	1.803(17)	1.84(1)
Δ_K	kHz	6.86(67)	6.352(34)	7.27(28)	10.7(6)
δ_J	kHz	0.0438(82)	0.0366(16)	0.0372(11)	–0.0347(7)
δ_K	kHz	2.14(77)	0.870(53)	0.244(77)	–0.0071(4)
V_3	cm^{-1}	157.78(13)			155.62(9)
	kJ/mol	1.8874(13)			1.855(1)
I_α	uÅ^2	3.1522 (27)		3.371(11)	3.215(2)
$\angle$(i,a)	°	41.3759(96)		37.90(21)	41.05(1)
$\angle$(i,b)	°	48.6241(96)		52.10(21)	48.95(1)
$\angle$(i,c)	°	90.0 (fixed)^c		90.0 (fixed)^c	90.0 (fixed)^c
D_{pi2J}	MHz	0.0648(46)			11(1)
D_{pi2K}	MHz	–3.841(77)			–1.7(1)
ρ				0.050319(42)	
β	°			10.517(77)	
ϵ_{10}	GHz			–4.4465(17)	
$[G_a]_{10}$	MHz			82.75(24)	
$[G_b]_{10}$	MHz			3.17(32)	
$[A–(B+C)/2]_{10}$	MHz			2.4036(81)	
$[(B+C)/2]_{10}$	kHz			–55.2(63)	
$[(B–C)/4]_{10}$	kHz			–18.2(31)	
$[\Delta_{JK}]_{10}$	kHz			3.43(12)	
$[\Delta_K]_{10}$	kHz			4.70(16)	
σ	MHz	0.0299	0.0013	0.0012	0.08
N_{tot}		56	25	56	101

[a] For the nomenclature of the parameters fitted with Erham, see ref. [6].
[b] Calculated at the MP2/6-311++G(d,p) level of theory.
[c] Due to C_S symmetry.

data set (comparing to the value of 0.08 MHz found by Caminati et al. [2]), we were not able to fit all transitions to experimental accuracy. A better standard deviation is currently not possible due to the limitations of the XIAM code. The fit can be improved by fixing the internal rotational parameters to the values obtained from the global fit and only A species transitions were fitted. The standard deviation is significantly reduced to 1.3 kHz (Fit II in Table 2). However, the predictive power for the E species lines is still unsatisfactory.

The global fit with the program Erham yielded a standard deviation of 1.2 kHz. The B and C rotational constants, the centrifugal distortion constants, and also the angles between the internal rotor axes and the inertial axes obtained with Erham have reasonable agreement to the values fitted with XIAM. Using the Erham code, some more effective tunneling parameters were fitted, but unfortunately, the barrier to internal rotation V_3 is not given.

The internal rotation barrier of the acetyl methyl group in vinyl acetate was determined to be 157.78(13) cm^{-1}. Comparing to the value of 98.093(12) cm^{-1} found for allyl acetate the barrier rises significantly. In this case, the vinyl group is attached directly to the oxygen atome whereas in the case of allyl acetate a CH_2- group is in between. This might cause some electronic effects which will be discussed later in Chapter 4 in details.

Finally, quantum chemical calculations at the MP2/6-311++G level show that the most stable conformer is at $\varphi = \pm 30°$ and the *trans* C_S conformer at $\varphi = 0°$ is probably a transition state. We tried to measure *c*-type transitions using polarizing pulses with a power of 2 W, whereas *b*-type transitions are over-polarized already with a few mW. The absence of *c*-type transitions suggests that the *effective* structure of vinyl acetate has a C_S symmetry. However, due to the low dipole moment of only 0.316 Debye in the *c* direction and a tunneling between the two enantiomers at $\varphi = +30°$ and $–30°$ is possible, by the absence of *c*-type transitions it is difficult to decide whether the output power is not sufficient, a tunneling process exists or the real molecular structure has a mirror plane.

5. Conclusion

The rotational spectrum of vinyl acetate was reanalyzed by MB-FTMW spectroscopy and two program codes XIAM and Erham. The standard deviation has been significantly improved comparing to the previous work by Caminati et al. The program Erham enables to fit the whole data set to experimental accuracy. However, some effective tunneling parameters had to be fitted while the barrier to internal rotation is not obtained. XIAM can fit the A species to a standard deviation of only 1.3 kHz. For the E species, the predictive power of XIAM is not satisfactory. The potential curve by rotating the vinyl group was carried out with the MP2 method using two different basis sets. Calculations using the 6-311++G(d,p) basis set shows an extremely flat minimum and the C_S geometry as the stable conformer, whereas the 6-311++G basis set yields a double minima potential where the vinyl group is titled against the ester frame by an angle of approximately 30°. The absence of *c*-type transitions suggests an effective C_S structure at the energy minimum.

Acknowledgments

References

[1]J. Sheridan, W. Bossert, A. Bauder, *J. Mol. Spectrosc.* **80**, 1 (1980).

[2]B. Velino, A. Maris, S. Melandri, W. Caminati, *J. Mol. Spectrosc.* **256**, 228 (2009).

[3]M. Tudorie, I. Kleiner, J. T. Hougen, S. Melandri, L. W. Sutikdja, W. Stahl, *J. Mol. Spectrosc.* **269**, 211 (2011).

[4]M. Oki and H. Nakanishi, *Bul. Chem. Soc. Japan* **107**, 4483 (1997).

[5]E. Fliege, H. Dreizler, J. Demaison, D. Boucher, J. Burie, A. Dubrulle, *J. Chem. Phys.* **78**, 3541 (1983).

[6]P. Groner, S. Albert, E. Herbst, F. C. D. Lucia, F. J. Lovas, B. J. Drouin, J. C. Pearson, *ApJS* **142**, 145 (2002).

Chapter 4

ISOPROPENYL ACETATE

Two rotors and C_1 frame symmetry

1. Introduction

Internal rotation is an interesting type of large amplitude motion and therefore a motivation for a part of this thesis. The more internal rotors a molecule has, the more complex the microwave spectrum is. In the case of allyl acetate (Chapter 2), there is only one methyl group, the acetyl methyl group, which shows internal rotation. All rotational transitions split into A-E doublets and it causes a doubling of all lines in the spectrum. Due to the low barrier of only 98.58(15) cm^{-1}, the splitting is very large (in some cases up to 1 GHz). The microwave spectrum is slightly more complicate in the case of ethyl acetate (Chapter 1). Ethyl acetate contains two methyl groups with internal rotation, the acetyl methyl group and the ethyl methyl group. The barrier of the acetyl methyl group is also on the order of 100 cm^{-1}. As a consequence, large A-E splittings were found in the spectrum. The ethyl methyl group, $CH_3-COO-CH_2-\mathbf{CH_3}$, has a much higher barrier of 1061.4(68) cm^{-1}. The splittings due to internal rotation of this methyl group are very narrow and could be only resolved for a few transitions.

The microwave spectrum becomes more interesting if the barrier to internal rotation of the second methyl group is lower than that of the ethyl methyl group in ethyl acetate, so that considerably larger splittings can be observed. This motivated us to study isopropenyl acetate, $CH_3-COO-C(CH_3)=CH_2$, an isomer of allyl acetate. When Hirota studied the microwave spectrum of propene,[1] $CH_3-CH=CH_2$, he found a barrier to methyl rotation of 698.4(5) cm^{-1}. Since the situation in the isopropenyl group is similar, we expected also to be able to resolve the splittings due to the isopropenyl methyl group. From our knowledge about methyl acetate, investigated by Sheridan et al.,[2] and our own studies on ethyl acetate and allyl acetate, the barrier to internal rotation of the acetyl methyl group is always around 100 cm^{-1}. Therefore, also in the case of isopropenyl acetate a rather low hindering barrier on the order of 100 cm^{-1} was expected. The interesting dynamics due to coupling between two internal rotations was studied and will be reported in this chapter.
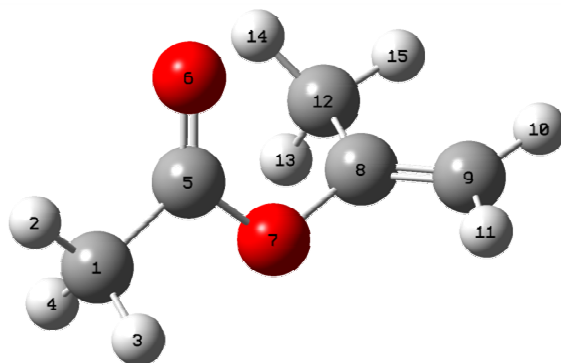
FIG. 1 Geometry of the observed conformer of isopropenyl acetate.

From our studies on allyl acetate, we learned that the vinyl group was not located within the plane formed by the ester group, but tilted by an angle of 129° against it. However, in the case of vinyl acetate,[3] the vinyl group is located within the symmetry plane of the molecule. This is a further motivation to investigate isopropenyl acetate. We were interested to find out whether in this case the isopropenyl group is tilted against the ester group or not.

2. Quantum chemistry

In order to have reasonable rotational constants for spectral assignment we carried out a structure optimization at the MP2/6-311++G(d,p) level using the *Gaussian03* package. This level of theory had been used for similar molecules before and usually yielded rotational constants which were quite close (approximately 1%) to the experimental ones. A better agreement cannot be expected, because the calculated rotational constants refer to the equilibrium internuclear distances whereas the experimental constants are usually effective constants averaged by the zero point vibration. Besides the rotational constants also the angles $\angle(i,g)$, $g = a, b, c$ between the internal rotor axes and the inertial axes were calculated from the *ab initio* geometry, since they can directly be compared to our experimental data. The rotational constants and the angles are given in Table 1, the optimized geometry is shown in Figure 1, the cartesian coordinates are found in the Appendix (Table D-1).

In this work we were only interested in the *trans* conformer of the ester. *cis* esters are known to be much higher in energy and are therefore usually not observed under molecular beam conditions.

In contrast to our initial assumption the optimized structure had no symmetry plane and the isopropenyl group was tilted out of the plane of the ester group. Therefore, we decided to calculate a potential curve where the dihedral angle $\varphi = \angle(C_5, O_7, C_8, C_9)$ (for atom numbers
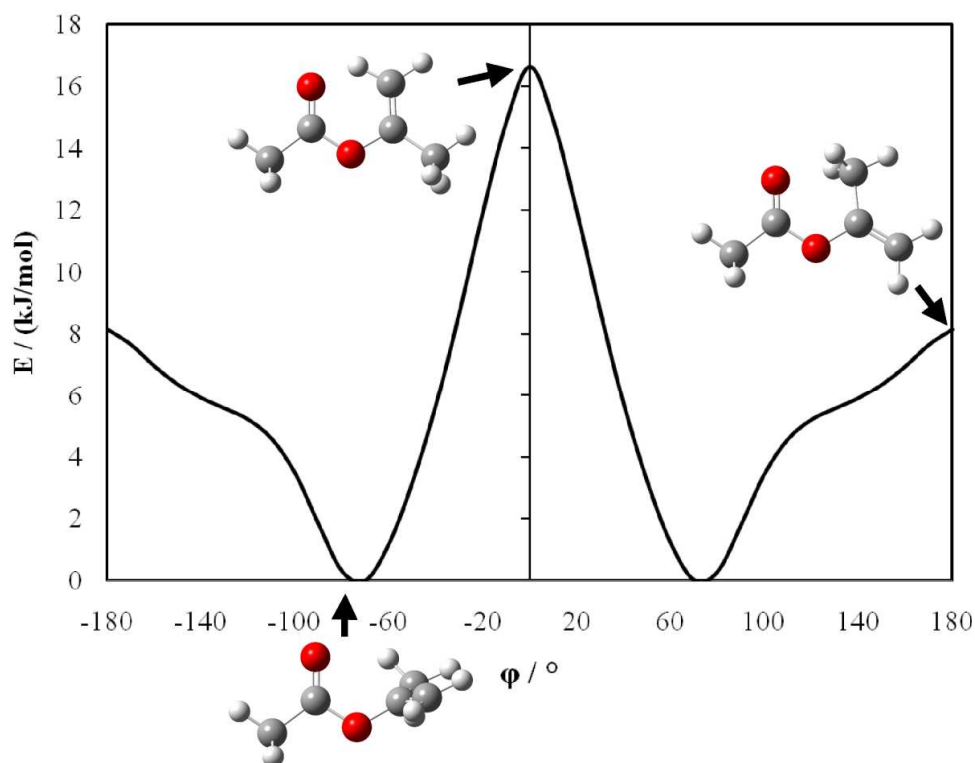
FIG. 2 The potential curve of isopropenyl acetate obtained by rotating the isopropenyl group. The relative energy with respect to the lowest energy conformer (E = −344.9237793 Hartree) is given.

see Figure 1) was varied while all other geometry parameters were allowed to relax. The result is shown in Figure 2. The curve has been parametrized by a Fourier expansion given in Table 2. The potential energy minima at $\varphi \approx \pm 70°$ represent a pair of enantiomers. The same result is obtained by global structure optimization. Two C_S geometries at $0°$ and $\pm 180°$ represent maxima in the potential curve and can be definitely excluded as stable conformers.

We also calculated the potential functions of the internal rotation of the isopropenyl methyl group and the acetyl methyl group in a similar manner. Again, the potential curves were parametrized by Fourier expansions. The Fourier coefficients are summarized in Table 2. Usually, the potential is given by the Fourier expansion

$$V(\alpha) = \frac{V_3}{2}(1 - \cos 3\alpha) + \frac{V_6}{2}(1 - \cos 6\alpha) + ...$$

It should be noted that the V_n potential (n = 3, 6, ...) is given by $V_n = 2\,|a_n|$. For the isopropenyl methyl group we found a V_3 barrier of 656.2 cm^{-1} with a V_6 contribution below 2%. The acetyl methyl group yielded a V_3 barrier of 120.5 cm^{-1}. Here a significant V_6 term of 24.7 cm^{-1} was found, which is 20% of V_3. As a consequence, the potential curve is a distorted cosine function with broadened minima and narrow maxima.

3. Microwave spectrum

3.1. Symmetry labels

According to our quantum chemical calculations the point group of the isopropenyl acetate molecule is C_1, i.e. it has no symmetry plane. There are two internal rotors, the acetyl methyl group with a rather low hindering barrier and the isopropenyl methyl group with a high barrier. The molecular symmetry group is isomorphic to the direct product group[5] $C_3^{(1)} \otimes C_3^{(2)}$. Both C_3 symmetry groups involved have three one-dimensional symmetry species A, E_a, E_b. We will label the rotorsional wave functions by AA, $AE = AE_a + AE_b$, $EA = E_aA + E_bA$, $EE = E_aE_a + E_bE_b$, and $EE^* = E_aE_b + E_bE_a$. In a species $\Gamma_1\Gamma_2$ the acetyl methyl group will be represented by Γ_1 and the isopropenyl methyl group by Γ_2. Due to the low barrier of the acetyl methyl group all spectral lines show wide splittings into an A and an E component. The A component is split under the influence of the isopropenyl methyl group into a narrow AA, AE doublet, the E species splits into a narrow EA, EE, EE* triplet.

3.2. Spectral assignment

All spectra were recorded using the MB-FTMW spectrometer in the frequency range 4 to 26.5 GHz described in ref. [17,18] in the experimental setup section. We started our experimental studies with a broadband scan recorded in the frequency range 9.3 to 14.5 GHz. Within this range, a total of 120 multiplets were found. All lines were remeasured in the high resolution mode. The line width was in the range from 10 to 25 kHz, the line positions can be determined with an accuracy of 1 kHz for strong lines and 5 kHz for weaker lines. Almost all lines appeared as AA, AE doublets or as EA, EE, EE* triplets. A typical spectrum of the AA, AE doublet and EA, EE, EE* triplet is shown in Figure 3 and Figure 4, respectively.

We found that some triplets, also the one in Figure 4, show a narrow additional splitting on the order of 20 kHz. Under the influence of inhomogeneous magnetic fields these splittings vanished. We therefore attributed it to proton spin-spin or spin-rotation coupling as will be discussed below.

In a first step we tried to fit the AA components separately with a rigid rotor program. It should be mentioned that *b*- and *c*-type transitions were quite strong whereas *a*-type lines turned out to be very weak and could not be observed in the scan at all. After the AA components had been assigned, a complete spectrum with all torsional components was
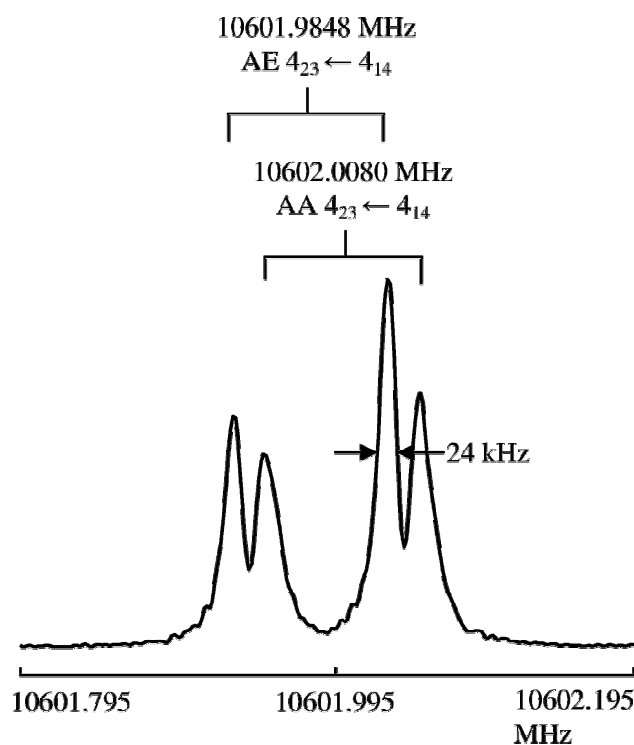
FIG. 3 A typical A species $4_{23} \leftarrow 4_{14}$ transition of isopropenyl acetate. The experimental resolution was 0.8 kHz, the typical experimental line width 24 kHz as indicated in the spectrum. The large splitting is due to the Doppler effect (indicated by brackets). For this spectrum 58 FIDs were co-added.

predicted using the XIAM code. In a first approach we assumed the barrier of the acetyl methyl group to be approximately 100 cm^{-1} as found in methyl acetate,[2] ethyl acetate, or allyl acetate, but no agreement with the observed spectrum was found. Then we successively increased the barrier up to 135 cm^{-1}, where finally the observed and calculated spectra roughly matched. We fitted 50 transitions with 247 torsional components using the XIAM code. Since the A-E splitting caused by the acetyl methyl group is very large, whereas the splittings within the AA-AE doublets and the EA-EE-EE* triplets are rather small, we only fitted the *absolute line positions* of the AA and the EA lines. For the other species we fitted the AA-AE, EA-EE, and EA-EE* *splittings* referred to AA and EA, respectively. The *narrow splittings*, which contain the information of the *high barrier*, could be fitted almost within the experimental uncertainty. On the other hand, the large splittings, determined by the low barrier, could be reproduced only within 10 to 350 kHz, which is on the same order of magnitude as the small splitting. Therefore, fitting all absolute positions of all lines would not allow to determine the high barrier. The resulting molecular parameters are given in Table 1. A list of all fitted lines is available in the Appendix (Table D-2 and D-3). The standard deviation of the fit is 75.5 kHz. This is much larger than our experimental uncertainty which is estimated to be
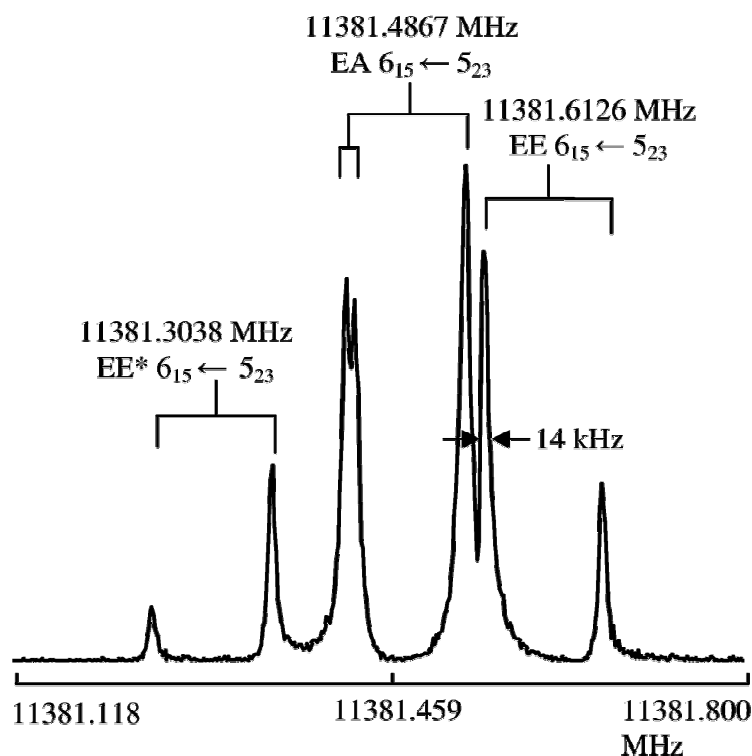
FIG. 4 A typical E species $6_{15} \leftarrow 5_{23}$ transition of isopropenyl acetate. Doppler splittings are indicated by wide brackets. The splitting indicated by small brackets is due to the spin-spin or spin-rotation-coupling. For this spectrum 120 FIDs were co- added.

approximately 2 kHz. This discrepancy is due to the limitations of the XIAM code. In order to check for a correct assignment we fitted the same data set also with the Erham code and found a standard deviation of 2.3 kHz which is very close to experimental accuracy. The parameters fitted with Erham are also given in Table 1. A list of all fitted lines is given in the Appendix (Table D-4 and D-5). The agreement between the rotational and centrifugal distortion constants, and also the angles between the internal rotor axes and the inertial axes obtained with XIAM and Erham is quite good. Unfortunately, the Erham code does not provide information on the potential barrier V_3 but only on more effective tunneling parameters.

4. Results and discussion

Our studies revealed some interesting aspects of the isopropenyl acetate molecule which are different from our initial ideas. In contrast to our assumption, but in agreement with our quantum chemical calculations, isopropenyl acetate has no mirror plane. This has been confirmed by the observation of *c*-type AA species transitions. Moreover, more than 95% of all measured transitions could be assigned. Therefore, it must be assumed that only one conformer exists under molecular beam conditions. This is consistent with our attempts to

Table 1

Molecular parameters of isopropenyl acetate obtained by a fit using programs XIAM, Erham, and quantum chemical calculations.

Parameter	Unit	XIAM (Obs.)	Erham	*ab initio*	Obs.–Calc.
		Rotational and centrifugal distortion parameters			
A	GHz	4.992199(46)	4.98543162(35)	4.950	0.042
B	GHz	1.804480(20)	1.80464157(14)	1.802	0.002
C	GHz	1.651355(18)	1.65156421(15)	1.656	–0.005
Δ_J	kHz	0.447(39)	0.4440(17)		
Δ_{JK}	kHz	2.618(51)	2.5143(29)		
Δ_K	kHz	–1.79(82)	–1.633(37)		
δ_J	kHz	–0.0342(18)	–0.03991(15)		
Δ_K	kHz	–1.79(82)	–1.633(37)		
		Torsional parameters of the acetyl methyl group			
V_3	GHz	4057.69(12)			
	kJ/mol	1.619144 (45)			
	cm^{-1}	135.3498(38)		120.5	14.9
I_γ	uÅ^2	3.1586 (fixed)	3.1380(60)		
$\angle(i,a)$	°	152.1715(67)	152.641(14)	150.4	1.8
$\angle(i,b)$	°	108.125(46)	107.702(55)	108.7	–0.6
$\angle(i,c)$	°	110.369(43)	110.156(33)	112.1	–1.7
D_{pi2J}	kHz	29.9(28)			
D_{pi2-}	kHz	–1136.8(85)			
ρ			0.01574(32)		
α	°		160.58(12)		
β	°		50.47(32)		
ϵ_{10}	MHz		–5862(22)		
$[G_a]_{10}$	MHz		–2.54(49)		
$[G_b]_{10}$	MHz		–0.485(96)		
$[(B+C)/2]_{10}$	kHz		–14.63(15)		
$[A–(B+C)/2]_{10}$	kHz		–447(23)		
$[(B–C)/4]_{10}$	kHz		–1.69(35)		
$[\Delta_K]_{10}$	kHz		–0.615(38)		
$[\delta_J]_{10}$	kHz		–0.001300(72)		
$[\delta_K]_{10}$	kHz		–0.0137(63)		

find other conformers by quantum chemical calculations, where also only one conformer (as a pair of two enantiomers) was found.

The barrier to internal rotation of the acetyl methyl group was found to be approximately 135 cm^{-1}, which is surprisingly high if compared to other acetates like methyl acetate,[2] ethyl acetate, and allyl acetate, where the barrier is always on the order of 100 cm^{-1}. However, it

Table 1 continued

Parameter	Unit	XIAM (obs.)	Erham	*ab initio*	Obs.–Calc.
		Torsional parameters of the isopropenyl methyl group			
V_3	GHz	21337(217)			
	kJ/mol	8.514(87)			
	cm^{-1}	711.7(73)		656.2	55.5
I_γ	uÅ^2	3.1586 (fixed)	3.582(62)		
$\angle(i,a)$	°	74.4(13)	73.53(18)	74.1	0.3
$\angle(i,b)$	°	24.8(22)	26.51(15)	27.4	–2.6
$\angle(i,c)$	°	108.8(20)	110.16(12)	111.7	–2.9
ρ			0.01574(32)		
α	°		160.58(12)		
β	°		50.47(32)		
ϵ_{01}	MHz		–3.118(77)		
		Statistical information			
σ	kHz	75.5	2.3		
N_{tot}		247	247		

[a] For the nomenclature of the parameters fitted with Erham, see ref. [6].
[b] The meaning of $[G_a]_{10}$ and $[G_b]_{10}$ is (1,0,-1,0,0,1) and (1,0,-1,1,0,0), respectively, in the (IQ1,IQ2,MEG,KAP,JP,KP) notation used in the Erham program instructions available in ref. [7]. Finally, it should be mentioned that besides the splittings due to internal rotation

should be mentioned that in the case of vinyl acetate[3] a barrier of 155.1(1) cm^{-1} was found, which is still higher than the barrier found in isopropenyl acetate. Obviously, in both cases there is some delocalization of π-electrons which extends from the vinyl double bond to the ester group, which increases the potential barrier. In the case of allyl acetate the vinyl group is not involved in delocalization and the barrier remains near 100 cm^{-1}. However, we will continue our work on esters to study this feature in detail.

For the isopropenyl methyl group we found a barrier of 711.7(73) cm^{-1}. This is somewhat smaller than we expected at the beginning of our studies. However, it is in reasonable agreement with the barrier of 698.4(5) cm^{-1} reported by Hirota for propene,[1] where the local environment of the methyl group is similar.

Finally, it should be mentioned that besides the splittings due to internal rotation additional very narrow splittings were observed. These splittings changed their appearance or they disappeared when the measurements were carried out in the presence of an inhomogeneous magnetic field ranging from one to five times the strength of the earth's magnetic field. Therefore we concluded that these extra splittings arise from proton spin-rotation and spin-spin coupling. It is surprising that the lines are influenced by those low external magnetic

Table 2

Parametrized potential functions calculated on MP2/6-311++G(d,p) level. The total electronic energy is given by the Fourier expansion $E = a_0 + \sum_{n \geq 1} a_n \cos(n\varphi)$.

	Hartree	kJ/mol	cm^{-1}
	rotation of the entire isopropenyl group		
a_0	−344.9215097		
a_1	0.0005181	1.360	113.7
a_2	0.0018659	4.899	409.5
a_3	0.0010433	2.739	229.0
a_4	0.0003623	0.951	79.5
a_5	−0.0000846	−0.222	−18.6
a_6	0.0001161	0.305	25.5
a_7	0.0000994	0.261	21.8
a_8	0.0000669	0.176	14.7
	rotation of the acetyl methyl group		
a_0	−344.9235593		
a_3	−0.0002746	−0.721	−60.3
a_6	0.0000562	0.148	12.3
a_{12}	0.0000069	0.018	1.5
	rotation of the isopropenyl methyl group		
a_0	−344.922297		
a_3	0.001495	3.925	328.1
a_6	0.000029	0.076	6.4

fields since it is often believed that in closed-shell molecules Zeeman effects due to the earth's magnetic field cannot be observed at all.

5. Conclusion

The Fourier transform microwave spectrum of isopropenyl acetate has been measured under molecular beam conditions. The experimental data as well as quantum chemical calculations have shown that this molecule exists as only one conformer of C_1 symmetry, in which the vinyl group is tilted by an angle of approximately 70° against the plane containing the ester group. Due to internal rotation of the acetyl methyl group, we found large A-E splittings of all lines (from a few MHz up to 1 GHz or more). We also were able to resolve the splitting due to the internal rotation of the second isopropenyl methyl group. The A species lines split into doublets and the E species lines into triplets. These splittings vary from 10 kHz up to 1 MHz, much smaller than the splittings due to the acetyl methyl group. By analyzing the spectrum

with the program XIAM, a torsional barriers of 135.3498(38) cm^{-1} and 711.7(73) cm^{-1} for the acetyl methyl group and the isopropenyl methyl group, respectively, were observed. All lines in the spectrum were also fitted with the program Erham to a standard deviation of only 2.3 kHz.

Acknowledgments

Part of this work is derived from the bachelor thesis of R. Missong with the title "Mikrowellenspektroskopische Untersuchungen an Isopropenylacetat" and the student research project of J. Broda and C. Willems. Furthermore, we would like to thank P. Groner for making his Erham code available to the spectroscopic community.

Publication statement

This work is published in the Journal of Molecular Spectroscopy under H. V. L. Nguyen and W. Stahl, *J. Mol. Spectrosc.* **264**, 120 (2010).

References

[1] E. Hirota, *J. Chem. Phys.* **45**, 1984 (1966).

[2] J. Sheridan, W. Bossert, A. Bauder, *J. Mol. Spectrosc.* **80**, 1 (1980).

[3] B. Velino, A. Maris, S. Melandri, W. Caminati, *J. Mol. Spectrosc.* **256**, 228 (2009).

[4] M. Oki, H. Nakanishi, *Bul. Chem. Soc. Japan* **43**, 2558 (1970).

[5] H. Dreizler, *Z. Naturforsch.* **16a**, 1354 (1961).

[6] P. Groner, S. Albert, E. Herbst, F. C. D. Lucia, F. J. Lovas, B. J. Drouin, and J. C. Pearson, *ApJS* **142**, 145 (2002).

[7] P. Groner, Instructions for program ERHAM, available at http://www.ifpan.edu.pl/~kisiel/prospe.htm.

Chapter 5

METHYL PROPIONATE

Two rotors and C_S frame symmetry

1. Introduction

Methyl propionate, $CH_3–CH_2–COO–CH_3$, is a small aliphatic ester which is found in nature where it contributes to the flavor of fruits. Therefore, it is also used as perfuming agent and for flavoring. Further, it plays an important role as a solvent. Despite its widespread use almost nothing is known about its conformers and its internal dynamics. Therefore, we considered it worthwhile to study methyl propionate by a combination of MB-FTMW spectroscopy and quantum chemical calculations.

Before methyl propionate was investigated, ethyl acetate was measured and fitted with the program BELGI-C_S for one top (Chapter 1). We found a barrier to internal rotation of the acetate methyl group of 99.57(11) cm^{-1} which is relatively low. Moreover, methyl acetate has been originally measured by Sheridan et al.[1] and was remeasured and reanalyzed by Tudorie et al.[2] with the new computer code BELGI-C_S for two-top molecules. A similar barrier of 101.740(30) cm^{-1} was found for the acetate methyl group whereas the methoxy methyl group showed a considerably higher barrier of 422.148(55) cm^{-1}. In the case of methyl propionate there are obviously two methyl groups which could show splittings due to internal rotation. We will refer to the **CH_3CH$_2$CO-** methyl group as the propionyl methyl group, the -**OCH$_3$** methyl group will be called the methoxy methyl group throughout this text. For the propionyl methyl group we expected a barrier to internal rotation on the order of 800 cm^{-1}, as it was observed in diethyl ketone (Chapter 6) and methyl ethyl ketone.[3] For the methoxy methyl group we assumed an intermediate barrier on the order of 425 cm^{-1}, as in the case of methyl acetate.[1]

This is the first time that the BELGI-C_S-2tops code for two-top molecules is applied to a system with one intermediate and one high barrier. The results will be compared with those obtained with the XIAM code. The XIAM code and the BELGI-C_S code were compared for several one-top molecules such as ethyl acetate (Chapter 1) and allyl acetate (Chapter 2), but such a comparison was never done for two-top molecules so far.
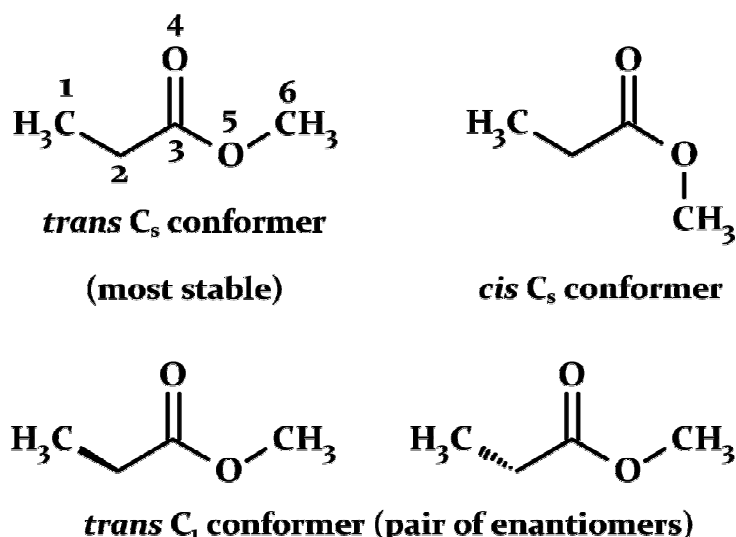
FIG. 1 Possible conformers of methyl propionate.

2. Quantum chemistry

Before the microwave spectrum was recorded, we started our study on methyl propionate with quantum chemical calculations to determine the possible conformers. These calculations are always helpful for the structure determination of large molecules where classical methods like isotopic substitution turn out to be difficult.

By rotating the entire $-OCH_3$ group around the C_3-O_5 bond, *trans* and *cis* conformers can be generated (see Figure 1, for atom numbers see the *trans* C_S conformer). Theoretical studies[4] and also our own observations on ethyl acetate (Chapter 1) have shown that *cis* esters are usually much higher in energy than *trans* esters. Therefore, *cis* esters are unlikely to be observed under molecular beam conditions and we decided to concentrate on the *trans* ester throughout this study.

As a next step, the ethyl group was rotated around the C_2-C_3 bond. A potential curve was calculated where the dihedral angle $\varphi = \angle(C_1, C_2, C_3, O_5)$ was varied within a $10°$ step width while all other geometry parameters were optimized. All calculations were carried out at the MP2/6-311++G(d,p) level of theory using the *Gaussian03* package. The 6-311++G(d,p) basis set was chosen, since it turned out to yield quite reasonable results for some other esters like ethyl acetate (Chapter 1), allyl acetate (Chapter 2), isopropenyl acetate (Chapter 4), and ethyl pivalate.[5] The potential curve is given in Figure 2, the Fourier coefficients of the potential function are found in the Appendix (Table E-1). Obviously, there are two possible conformers
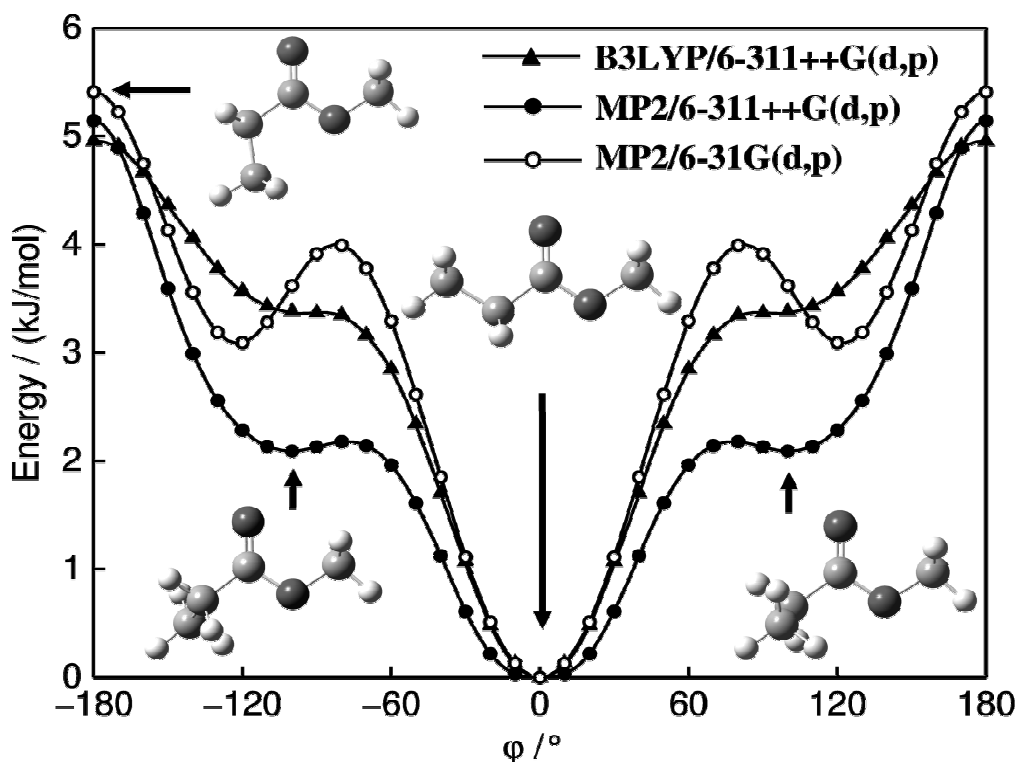
FIG. 2 The potential curve of methyl propionate obtained by rotating the ethyl group around the C_2–C_3 bond (for atom number see Figure 2). Different methods and basis sets were chosen. The relative energies with respect to the lowest energy conformer (E = −306.9413386 Hartree, −306.803613 Hartree, and −307.7994651 Hartree for the MP2/6-311++G(d,p), MP2/6-31G(d,p), and B3LYP/6-311++G(d,p) level, respectively) are given.

for the *trans* methyl propionate. Fully optimized structures and frequency calculations showed that both of them are true minima rather than saddle points.

The most stable conformer has C_S symmetry whereas the *trans* C_1 conformer exists as an enantiomeric pair at $\varphi \approx \pm 100°$. Another *trans* configuration with C_S symmetry at $\varphi = \pm 180°$ turned out to be a transition state. It should be noted that the two local minima of the potential curve, which present the *trans* C_1 conformers, are very shallow. The difference between these minima and the next local maxima at $\varphi \approx \pm 80°$ is only 0.09 kJ/mol. Due to the low temperature in the molecular beam the *trans* C_1 conformer is difficult to be seen in the molecular beam, since its stabilization energy is about 2.1 kJ/mol above the energy of the most stable *trans* C_S conformer. The Cartesian coordinates of both conformers are given in Table E-2 in the Appendix.

From the quantum chemical calculations on ethyl valerate,[6] ethyl methyl butyrate,[7] ethyl isovalerate,[8] and diethyl ketone (Chapter 6) we found that in these cases the MP2/6-
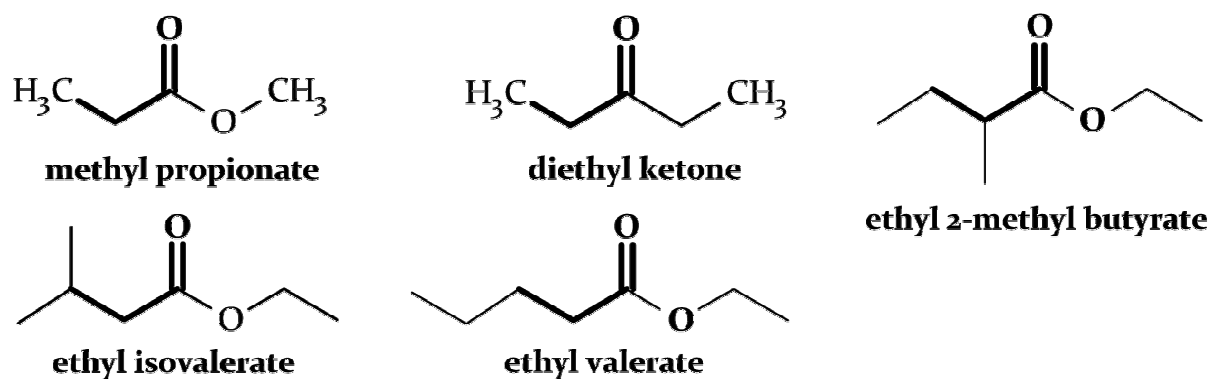
FIG. 3 Similar structure found in methyl propionate and some other molecules. In all cases, the CH–CH$_2$—C=O bond has a low torsional force constant.

311++G(d,p) basis set is not in good agreement with the experimental results. Methyl propionate has a similar structure as these molecules, which is illustrated with bold printed bonds in Figure 3. The C_2–C_3 bond seems to be very flexible. The correspondent dihedral angle depends strongly on the chosen basis set. Therefore, we decided to repeat the whole calculations with another basis set 6-31G(d,p) since it turned out to give the best results in the case of ethyl isovalerate, ethyl valerate, and ethyl methyl butyrate. Results of these calculations (see Figure 2) have shown, that the *trans* C_S conformer at $\varphi = 0°$ is still the most stable one. The transition state at $\varphi = \pm 180°$ has a slightly higher energy, but in between the whole potential curve has changed. The *trans* C_1 conformer moved from $\varphi \approx \pm 100°$ to $\varphi \approx \pm 120°$. The corresponding minima become sharper. The difference to the next local maxima rises to 0.90 kJ/mol.

Finally, density theory calculations were carried out. We used the B3LYP functional in combination with the 6-311++G(d,p) basis set which gave reliable results in the case of ethyl acetate (Chapter 1) and also diethyl ketone (see Chapter 6). Here, the potential curve for the rotation around the C_2–C_3 bond looks similar to the curve obtained at the MP2/6-311++G(d,p) level, however, the secondary minima are less pronounced but higher in energy.

We also calculated the barrier to internal rotation of both methyl groups by rotating the methyl groups around the O_5–C_6 and the C_1–C_2 bonds, respectively. These calculations were exclusively performed at the MP2/6-311++G(d,p) level of theory. The data were collected in a 10° grid and parametrized by Fourier coefficients. These are also given in Table E-3 in the Appendix. The calculated V_3 potentials were found to be 509.2 cm^{-1} and 956.2 cm^{-1} for the methoxy and the propionyl methyl group, respectively.
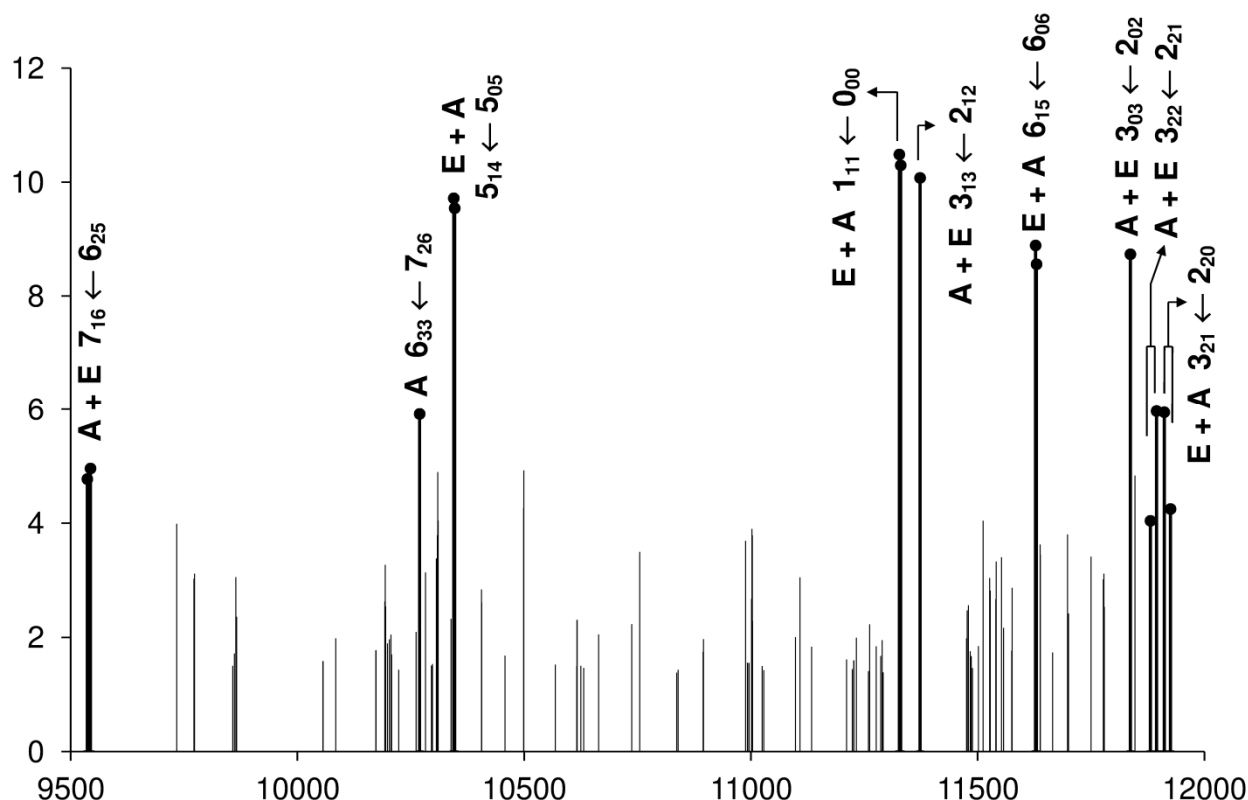
FIG. 4 Broadband scan of methyl propionate in the range of 9.5 to 12.0 GHz. The spectral range of 2.5 GHz was covered by overlapping spectra with a step width of 0.25 MHz. For each single measurement 50 FIDs were co-added. The assigned transitions $J'_{Ka'Kc'} \leftarrow J''_{Ka''Kc''}$ are marked with black points. A and E species refer to the larger splittings due to internal rotation of the methoxy methyl group. The intensities are given in arbitrary units on a logarithmic scale.

3. Microwave spectrum

3.1. Spectral assignment

The spectrum of methyl propionate was recorded with the MB-FTMW spectrometer described in ref. [17,18] in the experimental setup section. At the beginning of our experimental investigation a broadband scan in the frequency range from 9.5 to 12.0 GHz was recorded as shown in Figure 4. The spectral lines were subsequently remeasured in the high resolution mode of the spectrometer. The line widths were usually from 20 to 25 kHz and the estimated accuracy of the line position is approximately 4 kHz. For more details see Chapter 6.

Though there are different results by using different methods and basis sets, all quantum chemical calculations yielded two possible conformers of *trans* methyl propionate. At the MP2/6-311++G(d,p) level, the potential energy of the *trans* C_1 conformer is approximately
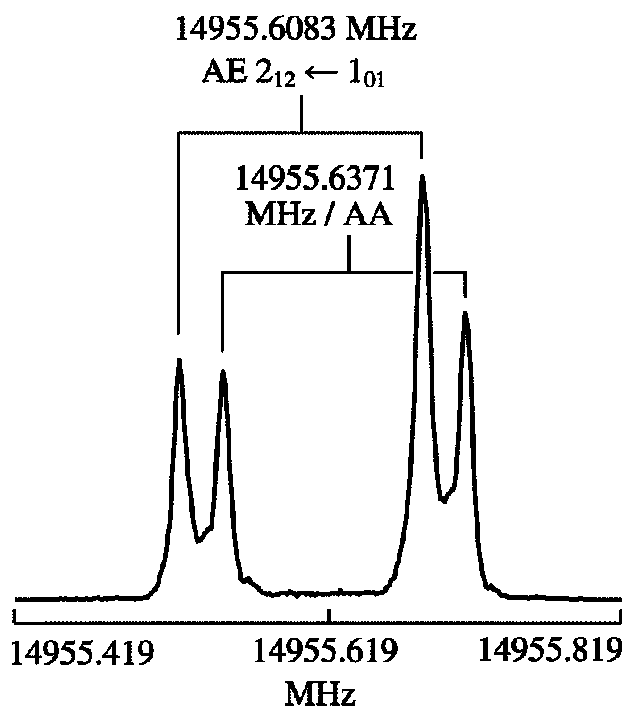
FIG. 5 A typical AA and AE species $2_{12} \leftarrow 1_{01}$ transition of methyl propionate. The experimental resolution was 4 kHz, the typical line width approximately 20 kHz (FWHH). The large splitting is due to the Doppler effect (indicated by brackets). For this spectrum 53 FIDs were co-added.

2.1 kJ/mol higher than that of the *trans* C_S conformer. Other quantum chemical calculations predicted even higher energies. A simple calculation of the Boltzmann factor with an assumed beam temperature of 10 K yields a population ratio of $1.1 \cdot 10^{-11}$. Even if the temperature, which determines the conformer equilibrium, is probably higher than the rotational temperature of 10 K, it appears unlikely that the *trans* C_1 conformer can be observed in the beam, and only rotational lines of the *trans* C_S conformer should be present in the spectrum. Figure 4 shows some strong lines and many lines with much lower intensity. We attribute the low intensity lines to ^{13}C isotopologues with the possibility for the ^{13}C atom to go at four different places within the molecule. We decided to use only the intensive lines to assign the *trans* C_S main conformer.

There are two methyl groups in methyl propionate which show internal rotation. It was clear that the torsion of the methoxy methyl group should cause a wide splitting into an A and an E component. The A components should be additionally split into two torsional components due to the internal rotation of the propionyl methyl group, which will be labeled as the AA, AE doublets. The E components split into three components which are called the EA, EE, and EE* triplets. Examples for the doublet and the triplet structure are given in Figure 5 and
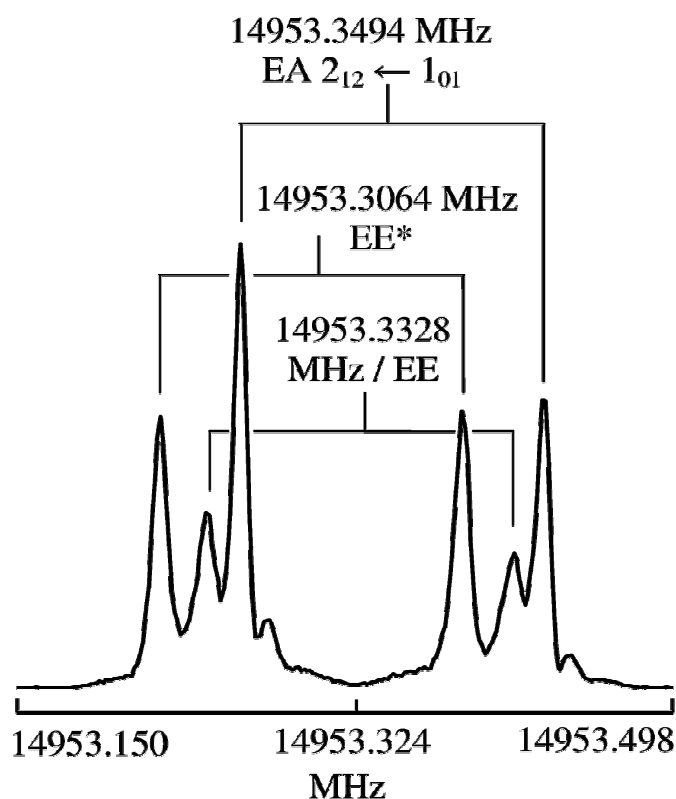
FIG. 6 A typical EA, EE, and EE* species $2_{12} \leftarrow 1_{01}$ transition of methyl propionate. For this spectrum 53 FIDs were co-added.

Figure 6, respectively. These local mode symmetry labels are the same as described in Chaper 4 and will not be repeated here in detail. The first letter of the symmetry label refers to the methoxy methyl group, the second letter to the propionyl methyl group. Since the torsional barrier of the propionyl methyl group is higher than that one of the methoxy methyl group, the splittings caused by the propionyl methyl group should be much narrower. It should be noted that in all calculations using BELGI-C_S-2tops the symmetry labels are based on the permutation-inversion group G_{18}. For the line designation the local mode symmetry labels correspond to the G_{18} symmetry labels by $AA \leftrightarrow A1/A2$, $AE \leftrightarrow E1$, $EA \leftrightarrow E2$, $EE \leftrightarrow E3$, and $EE^* \leftrightarrow E4$.

From quantum chemical calculations the rotational constants and also internal rotation parameters were roughly known. We used the rotational constants from the MP2/6-311++G(d,p) calculation to predict the AA species lines with a rigid rotor program and could assign all AA components within the broadband scan (Figure 4). In a next step, the program XIAM was used to predict a complete spectrum with all torsional components using the expected barriers of $V_3 = 425$ cm^{-1} and 800 cm^{-1} for the methoxy and the propionyl methyl

group, respectively. The theoretical spectrum predicted a AA-AE splitting in the order of a few MHz, whereas the AA-AE and the EA-EE-EE* splittings are only a few ten kHz. All lines were remeasured in the high resolution mode.

Finally the same set of transitions was fitted using the BELGI-C_S-2tops code. Lines were weighted in the least squares fit (as usual) by the inverse of the square of the estimated measurement error of 4 kHz. In total, 61 transitions with 282 torsional components were fitted for the ground torsional state $v_t = 0$ of the *trans* C_S methyl propionate molecule.

3.2. The XIAM and the BELGI-C_S-2tops codes

In this study we used two different codes which can deal with a two-top internal rotor molecule spectrum. The first code is XIAM which has been described several times in the literature (see the introduction of section A). XIAM is a combined axis method (CAM) which sets up the rotation-torsion Hamiltonian in the rho-axis system (RAM) for each top, than converts the RAM parameters into principal axis system (PAM) parameters.

The second code, BELGI-C_S-2tops, has been recently developed to fit the high-resolution torsion-rotation spectra of molecules with two inequivalent methyl rotors and a plane of symmetry at equilibrium. This program was applied to methyl acetate, CH_3COOCH_3,[2] and allowed us to reproduce more than 800 microwave and millimeter-wave measurements on ground-state transitions for this molecule, leading to root-mean-square deviations of 4 kHz for the microwave lines and of 40 kHz for the millimeter-wave lines, i.e., to residuals essentially equal to the experimental measurement errors.

As described in ref. [2], the BELGI-C_S-2tops program is closely related to a program for fitting the microwave spectrum of N-methylacetamide, $CH_3NH(C=O)CH_3$,[9] which has been used only for this special purpose. We differ from the code used in ref. [9] mainly by the fact that we adopted a two-step diagonalization procedure in order to have a faster code. The two-step diagonalization procedure is similar to that one used by Herbst et al.[10] However, we differ from it by using a "modified PAM",[11] instead of the RAM approach,[12] which requires placing the z axis nearly parallel to "the" top axis. The PAM approach is well suited to problems with small ρ values[11] as methyl propionate.

In the first step, only the lowest order pure torsional operators of the Hamiltonian are considered (see eq. (3) of ref. [2] and eq. (6) of ref. [9])

$$H_{tor} = [F_1 \, p_{\alpha 1}{}^2 + (1/2)V_{31}(1-\cos 3\alpha_1) + F_2 \, p_{\alpha 2}{}^2 + (1/2)V_{32}(1-\cos 3\alpha_2)] + F_{12} \, p_{\alpha 1} \, p_{\alpha 2}$$

$$+ V_{12s} \, \sin 3\alpha_1 \, \sin 3\alpha_2 + V_{12c} \, (1-\cos 3\alpha_1) \, (1-\cos 3\alpha_2) , \qquad (1)$$

where the subscripts *1* and *2* designate the two inequivalent tops, respectively.

The basis set for our first (torsional) diagonalization step consists of products of exponentials of the form $(2\pi)^{-1}\exp(3k_1+\sigma_1)i\alpha_1 \exp(3k_2+\sigma_2)i\alpha_2$ with the integers $|k_1|$ and $|k_2|$ both less than a basis set cutoff parameter *ktronc*. In the present calculation, like for methyl acetate, we set *ktronc* = 10, which means that 441 torsional basis functions are used in this first step. Following this diagonalization, we kept the lowest 42 = (2*ktronc*+1)×2 torsional energy levels and wave functions for use in the second step. This corresponds (for similar torsional ladders in the two tops) to keeping somewhat more than the first six torsional levels for each top, together with all their combination levels.

The second step of the procedure consists of diagonalizing the rest of the torsion-rotation Hamiltonian (i.e. $H_{rot} + H_{tor-rot}$ described in eq. (6) of ref. [9]). As explained in ref. [2], terms in this Hamiltonian can be constructed by taking symmetry-allowed and Hermitian products of a rotational factor (chosen from operators of the form $J_x{}^n J_y{}^m J_z{}^s$, where *m*, *n*, and *s* are integer exponents) and a torsional factor for each top *i = 1, 2* (constructed in turn from products of operators of the form $P_{\alpha i}{}^m$, $\cos 3n\alpha_i$, $\sin 3s\alpha_i$, where *m*, *n*, and *s* again represent integers). Details of the calculation are given in ref. [2] and we will not repeat them here.

4. Results and discussion

The 282 torsional components for methyl propionate were fitted with the XIAM code, floating the rotational parameters A, B, C, Δ_J, Δ_{JK}, Δ_K, δ_J, δ_K, the two barrier heights $V_{3,1}$ and $V_{3,2}$ for each top, the angles $\angle(i_1,a)$ and $\angle(i_2,a)$ between the two methyl rotors and the principal *a* axis, and two higher order parameters $D_{\text{pi}2J,1}$ and $D_{\text{pi}2-,1}$, while the moment of inertia of the two tops $I_{\gamma,1}$ and $I_{\gamma,2}$ values were kept fixed. The molecular parameters from the XIAM code are shown in the third column of Table 1. They allow us to reproduce the data with a root-mean-square (rms) deviation of 3.4 kHz, close to experimental accuracy.

The BELGI-C_S-2tops code provides a fit with similar quality (rms = 3.3 kHz) floating 12 parameters, the rotational and 4 centrifugal distorsion parameters (*A, B, C, D_J, D_{JK}, D_K, δ_J*), the two barrier heights V_{31} and V_{32}, one $J(J+1)$ dependence (V_{32J}), as well as the rotation-torsion coupling term q_1 which multiplies the operator $J_z \, p_1$ (equivalent to the term $-2F_1\rho_{1a}$ for

top 1 term in the RAM approach) and r_1 which multiplies the operator $J_x p_1$ (equivalent to the term $-2F_1\rho_{1b}$) . The internal rotation constants for top 1 (F_1) and for top 2 (F_2) are kept fixed to values derived from XIAM. The internal rotation constant F_{12}, (multiplying the top-top kinetic energy interaction operator $p_1 p_2$ was fixed to a value of -0.50 cm^{-1} derived from the structure (see eqs. 10-14 of ref. [9]) whereas the two top-top interaction constants of the next higher order in the potential energy (V_{12s} and V_{12c}) were fixed to zero. Qualitatively speaking, these low order potential energy constants could not all be determined because the present data set only contains information on the torsional ground state, and because the two torsional barriers are rather high ($s = 4V_3/9F \approx 34$ and 65 for top 1 and 2, respectively). Getting a convergence for the fit was difficult with the BELGI code using the present data set, due to the high correlation existing between the various parameters, especially between V_{31}, V_{32}, q_1, r_1, q_2, and r_2. After a number of trials, we decided to keep the q_2 and r_2 parameters fixed (which correspond to the top with the higher barrier and smaller internal rotation splittings) to values calculated from the quantities $-2F_2\rho_{2a}$ and $-2F_2\rho_{2b}$, respectively, using the direction cosine from the XIAM code. Our best fit was however obtained for a value of the q_2 parameter slightly smaller. The set of parameters used to get our final fit is shown in Table 2.

The list of frequencies fitted with the BELGI-C$_S$-2tops code and XIAM, along with the residuals, are given in Table E-4. We found the barrier of the methoxy methyl group of 429.324(23) cm^{-1} to be in good agreement with the assumed barrier of 422.148(55) cm^{-1} reported for methyl acetate.[2] Also the barrier of 820.46(99) cm^{-1} of the propionyl methyl group matches the barriers of 795(10) cm^{-1} and 771.93(27) cm^{-1} observed for methyl ethyl ketone[3] and diethyl ketone (Chapter 6), respectively. Comparing the experimental barriers with those obtained by quantum chemical calculations shows that the latter ones are by approximately 16.5% and 18.6% too high.

We found that in the case of methyl propionate both programs, BELGI-C$_S$-2tops and XIAM, are suitable to analyze the spectrum almost to experimental accuracy. The rotational constants obtained with both programs reasonably agree, however, they do not agree within the standard errors. The *ab initio* A rotational constant differs by 32.6 MHz (0.34%), the B and C constant match the experimental values almost exactly with deviations of -4.5 MHz (-0.21%) and -1.5 MHz (-0.08%), respectively. A better agreement cannot be expected since the *ab initio* data refer to the equilibrium structure whereas the experimental data yield rotational constants for the ground vibrational state and no corrections have been made. The centrifugal

Table 1

Spectroscopic constants of methyl propionate referred to the **PAM** system.

Constant	Unit	XIAM	BELGI-C$_S$-2tops[a]	Calc.[b]	Exp.[c] – Calc. (%)
A	GHz	9.515022(35)	9.51687(21)	9.4824	0.0326 (0.34%)
B	GHz	2.147746(40)	2.148733(52)	2.1522	–0.0045 (–0.21%)
C	GHz	1.811769(35)	1.814411(45)	1.8133	–0.0015 (–0.08%)
Δ_J	kHz	0.18577(87)	0.18527(61)		
Δ_{JK}	kHz	0.9968(72)			
Δ_K	kHz	4.936(40)			
δ_J	kHz	0.02803(16)			
δ_K	kHz	–0.271(22)			
$V_{3,1}$	cm^{-1}	429.324(23)	428.537 (15)	509.2	–79.9 (–18.6%)
$I_{\gamma,1}$	uÅ^2	3.15862 (fixed)[d]	3.19871(70)	3.217	
$\angle(i_1,a)$	°	156.356(19)	154.827(21)	149.86	6.50
$\angle(i_1,b)$	°	66.356(19)	64.827(21)	59.86	6.50
$\angle(i_1,c)$	°	90.0 (fixed)[e]	90.0 (fixed)	90.00	
$D_{pi2J,1}$	kHz	27.7(29)			
$D_{pi2-,1}$	kHz	–70.6(13)			
s_1		33.8215 (derived)	33.7595		
$V_{3,2}$	cm^{-1}	820.46(99)	819.97 (25)	956.2	–135.7 (–16.5%)
$I_{\gamma,2}$	uÅ^2	3.15862 (fixed)[d]	3.25155(11)	3.161	
$\angle(i_2,a)$	°	32.53(46)	34.4583(22)	33.83	–1.30
$\angle(i_2,b)$	°	57.46(46)	55.5417(22)	56.17	1.29
$\angle(i_2,c)$	°	90.0 (fixed)[e]	90.0 (fixed)	89.95	
s_2		65.0381 (derived)	64.9988		
σ/N[f]	kHz	3.4 / 282	3.3 / 282		
σ_A/N_A[g]	kHz		3.4 / 55		
σ_{E1}/N_{E1}	kHz		2.6 / 55		
σ_{E2}/N_{E2}	kHz		3.6 / 58		
σ_{E3}/N_{E3}	kHz		3.4 / 57		
σ_{E4}/N_{E4}	kHz		3.4 / 55		

[a] BELGI-C$_S$-2tops constants are transformed into PAM constants using eqs. 10 - 14 of ref. [9].
[b] Calculation at the MP2/6-311++G(d,p) level using the program *Gaussian03*.
[c] With respect to the XIAM fit.
[d] Derived from F_0 = 160 GHz (fixed).
[e] Due to symmetry.
[f] Standard deviation of the fit / total number of lines.
[g] Standard deviation / number of lines of each symmetry species.

distortion constants Δ_J, Δ_{JK}, Δ_K, and δ_J of XIAM and D_J, D_{JK}, D_K, and δ_J of BELGI-C$_S$-2tops refer to different coordinate systems and cannot be directly compared. No attempts were made to obtain these constants by quantum chemical calculations.

Table 2

Spectroscopic constants of methyl propionate obtained with the program BELGI-C_S-2Tops.

Operator[a]	Parameter[b]	Value[c] / cm^{-1}
J_z^2	A	0.3471830 (48)
J_x^2	B	0.0721304 (17)
J_y^2	C	0.0605222 (15)
$-J^4$	Δ_J	6.180(21)·10^{-9}
$-J^2 J_z^2$	Δ_{JK}	30.17(16)·10^{-9}
$-J_z^4$	Δ_K	167.2(13)·10^{-9}
$-2J^2(J_x^2 - J_y^2)$	δ_J	0.9294(50)·10^{-9}
p_1^2	F_1	5.6417[d]
p_2^2	F_2	5.60674[d]
$p_1\,p_2$	F_{12}	−0.50[d]
$(1/2)(1-\cos3\alpha_1)$	$V_{3,1}$	428.537 (15)
$(1/2)(1-\cos3\alpha_1)J^2$	$V_{3,1J}$	−0.0002903 (90)
$(1/2)(1-\cos3\alpha_2)$	$V_{3,2}$	819.97 (25)
$J_z\,p_1$	q_1	0.590664(92)
$J_z\,p_2$	q_2	0.54[d]
$J_x\,p_1$	r_1	−0.053176(56)
$J_x\,p_2$	r_2	−0.0734 [d]

[a] Operator which the parameter multiplies in the program.
[b] Notation of eq. (6) and Table 3 of ref. [9], except for A, B, and C where the prime was removed.
[c] Value of the parameter obtained from the final least-squares fit, with one standard uncertainty given in parentheses.
[d] Fixed to values calculated from the structure and using the direction cosines from the XIAM code, see also text. Note that F_{12} is named f_{12} in eq. (6) of ref. [9].

5. Conclusion

We report on the rotational spectra of the most abundant conformer of methyl propionate, $CH_3CH_2COOCH_3$, recorded with a Fourier transform microwave spectrometer under molecular beam conditions. We present accurate rotational constants and centrifugal distortion constants. For the propionyl **CH_3**CH_2CO- methyl group and the methoxy -O**CH_3** methyl group barriers of 820.46(99) cm^{-1} and 429.324(23) cm^{-1}, respectively, were found. For spectral analysis two different computer programs were used, the RAM based code BELGI-C_S-2tops and the CAM based code XIAM. The results are compared. The experimental work was supplemented by quantum chemical calculations. Potential energy functions for the rotation of the terminal methyl groups and also of the entire ethyl group were parametrized.

Acknowledgments

Publication statement

This work is submitted to the Dijon HRMS special issue of Molecular Physics by H. V. L. Nguyen, W. Stahl, I. Kleiner, **2012**.

References

[1] J. Sheridan, W. Bossert, A. Bauder, *J. Mol. Spectrosc.* **80**, 1 (1980).

[2] M. Tudorie, I. Kleiner, J. T. Hougen, S. Melandri, L. W. Sutikdja, W. Stahl, *J. Mol. Spectrosc.* **269**, 211 (2011).

[3] N. M. Pozdeev, A. K. Mamleev, L. N. Gunderova, R. V. Galeev, *J. Struct. Chem.* **29**, 52 (1988).

[4] M. Oki and H. Nakanishi, *Bul. Chem. Soc. Japan* **43**, 2558 (1970).

[5] H. Mouhib, Y. Zhao, W. Stahl, *J. Mol. Spectrosc.* **261**, 59 (2010).

[6] H. Mouhib and W. Stahl, accepted in *Chem. Phys. Chem.*

[7] H. Mouhib, dissertation at the RWTH Aachen University under supervision of Prof. W. Stahl, **2012**.

[8] H. Mouhib, D. Jelisavac, L. W. Sutikdja, E. Isaak, W. Stahl, *J. Phys. Chem. A* **115**, 118 (2011).

[9] N. Ohashi, J. T. Hougen, R. D. Suenram, F. J. Lovas, Y. Kawashima, M. Fujitake, J. Pyka, *J. Mol. Spectrosc.* **227**, 28 (2004).

[10] E. Herbst, J. K. Messer, F. C. De Lucia, P. Helminger, *J. Mol. Spectrosc.* **108**, 42 (1984).

[11] C. C. Lin and J. D. Swalen, *Rev. Mod. Phys.* **31**, 841 (1959).

[12] J.T. Hougen, I. Kleiner, M. Godefroid, *J. Mol. Spectrosc.* **163**, 559 (1994).

Chapter 6

DIETHYL KETONE

Two equivalent rotors and C_{2v} frame symmetry

1. Introduction

From the studies on methyl propionate (Chapter 5) we know that the barrier to internal rotation of the ethyl methyl group **CH$_3$**-CH$_2$-COO-CH$_3$ is much lower than in the case of ethyl acetate (Chapter 1). Therefore, splittings due to internal rotation of this methyl group could be resolved to a large extent. The coupling of two internal rotors with different barriers were studied and yielded many interesting results. The methoxy methyl group in methyl propionate has an immediate barrier to internal rotation of 428.263(24) cm^{-1} whereas the ethyl methyl group has a high barrier of 817.8(12) cm^{-1}.

It is interesting to study a similar system, but with two equivalent internal rotors. To create such a system, we replaced the oxygen atom in methyl propionate by a CH$_2$-group and obtained diethyl ketone, CH$_3$–CH$_2$–CO–CH$_2$–CH$_3$. In the studies of Pozdeev et. al. on the microwave spectrum of ethyl methyl ketone, CH$_3$–CH$_2$–CO–CH$_3$,[1] a barrier to methyl internal rotation of the ethyl methyl group of 795(10) cm^{-1} was found. This barrier is also very close to the barrier of 817.8(12) cm^{-1} found for the ethyl methyl group in methyl propionate. In the case of diethyl ketone, the situation is similar to ethyl methyl ketone. Therefore, we expected to be able to resolve the splitting due to the internal rotation of the two equivalent methyl groups. We were also interested to find out, whether the barrier significantly changes.

Furthermore, like the esters, which were studied in this thesis, ketones represent a very important class of chemical compounds in chemistry, industry, and pharmacy. They are widely used as solvents or intermediates for chemical reactions. Surprisingly, there are only very few studies on the molecular geometries of ketones in the gas phase. The most simple aliphatic ketone acetone has been investigated already very early.[2,3] Also microwave studies on trifluoroacetone[4] and methyl vinyl ketone[5] have been reported in the past. To the best of our knowledge, no larger aliphatic ketones with more than four carbon atoms have been studied in the microwave region before. Acetyl acetone,[6] a ketone with two carbonyl groups,

and the cyclic ketones acetophenone,[7] phenyl acetone,[8] benzophenone,[9] and 2-indanone[10] have also been published.

Diethyl ketone is also an interesting molecule concerning its symmetry properties. We were interested to find out how the two ethyl groups are oriented. By rotating both ethyl groups around the O=C−C− bonds many geometries of diethyl ketone can be generated. It is an interesting question how many geometries correspond to energy minima and which of those conformers can be observed under molecular beam conditions. Moreover, it is interesting to find out, whether the stable conformers have C_{2v}, C_2, or C_S symmetry or whether they have no symmetry at all (C_1). We tried to answer these questions by studying diethyl ketone by a combination of MB-FTMW spectroscopy and quantum chemical calculations.

2. Quantum chemistry

In order to predict the conformers of diethyl ketone and their respective rotational constants, quantum chemical calculations were carried out using the *Gaussian03* program package. We started with a planar heavy atom geometry similar to that one shown in Figure 1 and optimized it at the MP2/6-311++G(d,p) level of theory. This method and basis set was chosen since it turned out to be reliable in a number of similar cases, e.g. ethyl acetate (Chapter 1), isopropenyl acetate (Chapter 4) and ethyl pivalate.[11] In contrast to our initial assumption, the optimized structure was lacking a symmetry plane and a C_2 symmetry instead of a C_{2v} symmetry was obtained. Both ethyl groups were tilted against each other by an angle of approximately 24°. This result induced us to study the torsional behavior of the ethyl groups in more detail and we calculated a two-dimensional energy surface as a function of the torsional angles $\varphi_1 = \angle(O_2, C_1, C_3, C_4)$ and $\varphi_2 = \angle(O_2, C_1, C_{10}, C_{11})$. For the atom numbers see Figure 1. To define the dihedral angle $\varphi = \angle(A, B, C, D)$ we look from C along the CB bond onto B. If BCD spans the same plane as ABC, φ is zero. If the BCD plane is rotated counterclockwise against the ABC plane, φ is positive, for a clockwise rotation of the BCD plane against the ABC plane, φ is negative. With this definition, the geometries represented by (φ_1, φ_2), $(-\varphi_1, -\varphi_2)$, (φ_2, φ_1), and $(-\varphi_2, -\varphi_1)$ have the same potential energy. We optimized the geometry with φ_1 and φ_2 fixed at certain values in a grid of 10°. The corresponding energies were parametrized with a two-dimensional Fourier expansion based on terms, having the correct symmetry of the angles φ_1, φ_2. The corresponding coefficients are reported in Table F-1 in the Appendix. Finally, using the Fourier coefficients the energy surface was drawn as a contour plot given in Figure 2. It is obvious that in the region centered at $\varphi_1 = 0°$,
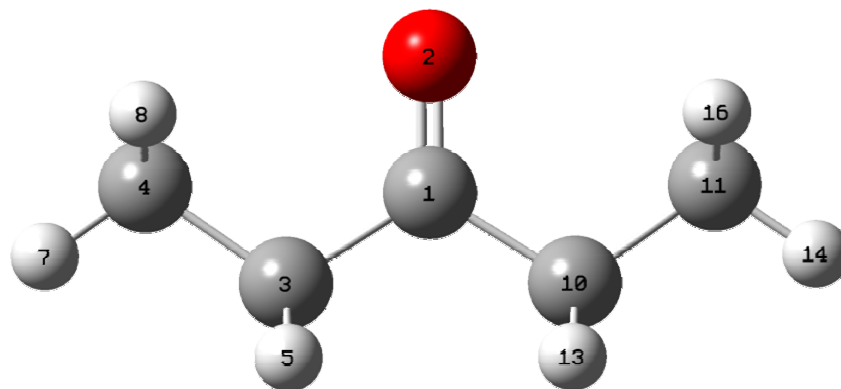
FIG. 1 Geometry of the observed conformer (most stable) of diethyl ketone with C_{2v} symmetry.

$\varphi_2 = 0°$ a broad energy minimum exists. To study this in detail, a one-dimensional energy plot along the diagonal from $\varphi_1 = -180°$, $\varphi_2 = -180°$ to $\varphi_1 = 180°$, $\varphi_2 = 180°$ was calculated (Figure 3). Also here it can be recognized that the potential is very flat in the range $\varphi_1 = \varphi_2 = -20°$ to $+20°$. We recalculated this region within a grid of $1°$ and also plotted the result in Figure 3 with an enlarged scale. Clearly, two minima are found at $\varphi_1 = \varphi_2 \approx -12$ and $+12°$, which correspond to the fully optimized structure at the MP2/6-311++G(d,p) level of theory. The local maximum at $\varphi_1 = \varphi_2 = 0°$ is only 0.3 kJ/mol above these minima. We also show an energy plot along the diagonal starting from $\varphi_1 = -180°$, $\varphi_2 = 180°$ to $\varphi_1 = 180°$, $\varphi_2 = -180°$. Here, a narrow minimum exists (Figure 4). We repeated the optimization using density functional theory at the restricted B3LYP/6-311++G(d,p) level. Here, we found indeed a C_{2v} symmetry. For comparison, we also repeated the calculation of a complete two-dimensional energy surface at this level of theory (Figure 5) and two one-dimensional energy plots along the same diagonals (Figure 6 and Figure 7). The corresponding coefficients are reported in Table F-2. In Figure 6, a broad energy minimum is found around $\varphi_1 = \varphi_2 = 0°$, whereas the minima at $\varphi_1 = \varphi_2 \approx \pm 12°$ do not occur.

Finally, we calculated a potential energy curve for the rotation of the methyl groups, since these caused splittings of the rotational lines and the three-fold hindering potential V_3 could be determined from the experimental data. Here, we also used the MP2/6-311++G(d,p) level of theory. In order to obtain a symmetry plane, the dihedral angles φ_1 and φ_2 were set to $0°$. The dihedral angle $\alpha = \angle(C_1, C_{10}, C_{11}, H_{14})$, which determines the rotation angle of one of the methyl groups was also fixed, whereas all other parameters were allowed to relax. Calculations were carried out at different angles α within a grid of $10°$ and the data were

parametrized with an expansion $V = V_0 + (V_3/2)(\cos 3\alpha) + (V_6/2)(\cos 6\alpha)$. The offset V_0 was determined to be –271.045845 Hartree, V_3 is 10.90 kJ/mol (911.3 cm^{-1}), V_6 is 0.073 kJ/mol (6.1 cm^{-1}). The V_6 contribution to the three-fold V_3 potential is less than 1%.

3. Microwave spectrum

3.1. Symmetry labels

We will start this section with some remarks on the rotorsional symmetry labels used throughout this chapter. The rotorsional states of an asymmetric molecule with two *non-equivalent* internal rotors can be classified within the direct product group $C_3^{(1)} \otimes C_3^{(2)}$, where the subgroups $C_3^{(1)}$ and $C_3^{(2)}$ refer to the symmetry of the torsional wave functions of the first and the second internal rotor, respectively.[12] The symmetry species of the rotorsional states are AA, $AE = AE_a + AE_b$, $EA = E_aA + E_bA$, $EE = E_aE_a + E_bE_b$, and $EE^* = E_aE_b + E_bE_a$ (see Chapter 4). For convenience we introduced the abbreviated symmetry labels AA, AE, EA, EE, and EE*. These labels can still be used in the case of diethyl ketone, in which the two internal rotors are *equivalent* due to the C_2 or C_{2v} symmetry of the molecular frame. However, it has to be considered that the EA states coincide with the AE states. Therefore, we will consistently use the label AE. Summarized, all transition frequencies split into four torsional components due to the internal rotation of two equivalent methyl groups. As a consequence, only quartets instead of quintets could be observed in the microwave spectrum.

3.2. Spectral assignment

Two MB-FTMW spectrometers were used for this study. They were modified versions of those described in ref. [17,18] and ref. [19] in the experimental setup section.

At the beginning of our experimental studies a broadband scan with the spectrometer described in ref. [19] in the frequency range from 31.4 GHz to 36.0 GHz was recorded. Only 20 lines were found. In a first step, a prediction of the AA components with a rigid rotor program was carried out starting with the calculated rotational constants of the planar conformer obtained at the MP2 level. By comparing the observed and the predicted spectra, all 20 transitions could be assigned and three rotational constants were determined with a standard deviation of 467 kHz. This is in the same order as the resolution of the spectrometer when it is used in the scan mode. It should be mentioned that only *b*-type transitions could be observed. The centrifugal distortion constants were not fitted because the resolution in the scan mode is in the order of about 500 kHz, much larger than the order of the centrifugal
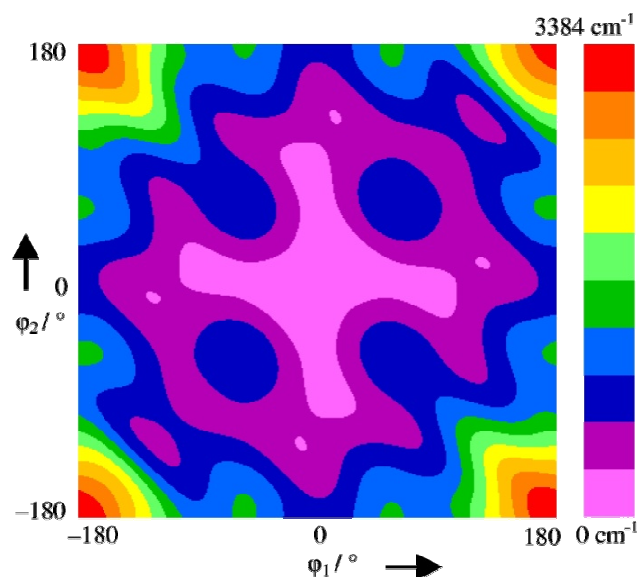
FIG. 2 The potential surface of diethyl ketone obtained by rotating both ethyl groups calculated at the MP2/6-311++G(d,p) level of theory.
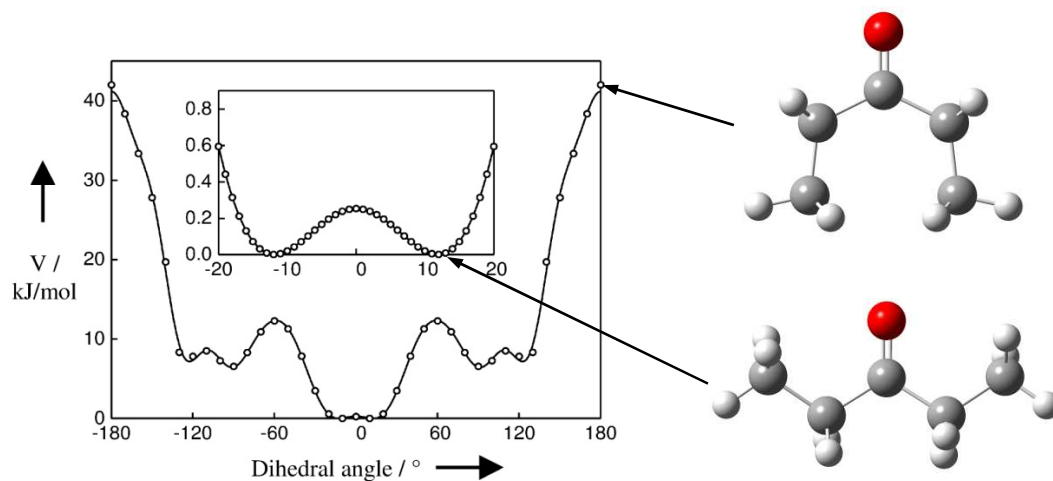
FIG. 3 The potential curve along the diagonal shown in Figure 3 from

$$\varphi_1 = \varphi_2 = -180° \text{ to } \varphi_1 = \varphi_2 = 180°.$$
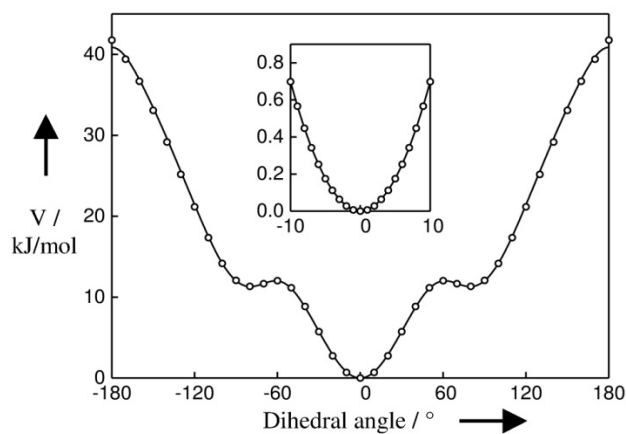
FIG. 4 The potential curve along the diagonal shown in Figure 3 from

$$(\varphi_1, \varphi_2) = (-180°, 180°) \text{ to } (\varphi_1, \varphi_2) = (180°, -180°).$$
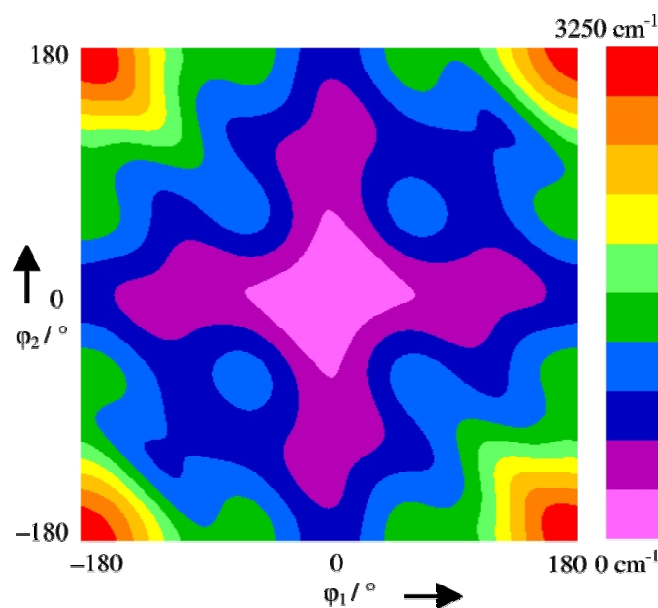
FIG. 5 The potential surface of diethyl ketone obtained by rotating both ethyl groups calculated at the B3LYP/6-311++G(d,p) level of theory.
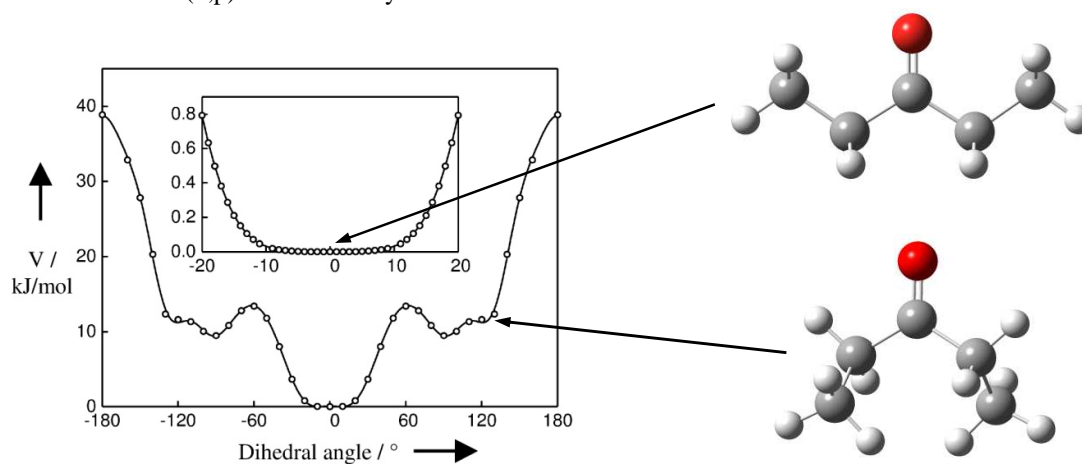
FIG. 6 The potential curve along the diagonal shown in Figure 5 from

$\varphi_1 = \varphi_2 = -180°$ to $\varphi_1 = \varphi_2 = 180°$.
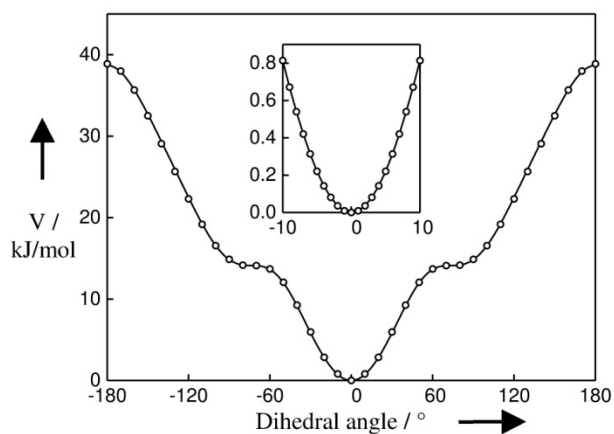
FIG. 7 The potential curve along the diagonal shown in Figure 5 from

$(\varphi_1, \varphi_2) = (-180°, 180°)$ to $(\varphi_1, \varphi_2) = (180°, -180°)$.
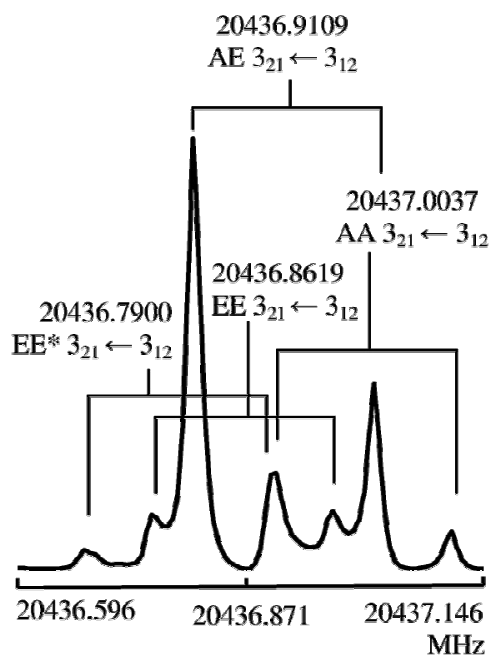
FIG. 8 The $3_{21} \leftarrow 3_{12}$ transition of diethyl ketone. The experimental resolution was 4 kHz, the typical experimental line width 24 kHz. The large splitting is due to the Doppler effect (indicated by brackets). For this spectrum 74 FIDs were co-added.

distortion constants. In the range from 31.4 GHz to 36.0 GHz no measurements in the high resolution mode were carried out, since the lines turned out too weak for an analysis of their torsional fine structure. However, the observed transitions and the preliminary rotational constants obtained from the fit are given in the Appendix in Table F-3.

We used these preliminary rotational constants to predict the spectrum of the AA species lines of diethyl ketone in the frequency range from 5 GHz to 26.5 GHz and measured the predicted transitions directly in the high resolution mode with the spectrometer described in ref. [17,18] (experimental setup section). A typical spectrum is shown in Figure 8. Almost all lines turned out to be multiplets. Some lines (also that one presented in Figure 8) appeared clearly as AA, AE, EE, and EE* quartets. Many lines appeared just as triplets due to a very small splitting between the EE and the EE* species (in some cases lower than 1 kHz) and could not be resolved even in the high resolution mode. Due to this reason, the line width was in the range from 10 to 25 kHz and the line positions could be determined with an accuracy of about 4 kHz. This is larger than the usual accuracy which we could achieve with our spectrometers.

For the analysis of the torsional fine structure a complete spectrum with all torsional components was predicted using the XIAM code. In a first step, we assumed the barrier of both methyl groups to be approximately 800 cm^{-1}, similar to the barrier of the **CH$_3$–CH$_2$–CO**

methyl group in ethyl methyl ketone.[1] The splittings between the different symmetry species of the observed and calculated spectra matched almost exactly. We could assign all lines of the four species on the basis of these splittings. Totally, 54 transitions with 199 torsional components were fitted using the XIAM code to a standard deviation of only 3.9 kHz. It should be noted that most of the lines have a line width of about 20 kHz, much larger than the line width of 2 kHz at 12 GHz observed for the $1 \leftarrow 0$ transition of carbonyl sulfide.[13] Also in other compounds additionally broadened lines were found, e.g. the line width was 12 kHz in the cases of ethyl acetate (Chapter 1) and allyl acetate (Chapter 2). However, in the case of diethyl ketone an even bigger broadening was observed. Moreover, many lines, even strong lines, have additional narrow splittings, which we attribute to magnetic coupling effects of the 10 protons present in the molecule. However, small splittings could also arise from the double minimum potential calculated on the MP2/6-311++G(d,p) level (see Figure 3). Due to the broadened lines, the line positions could be determined only with an accuracy of about 4 kHz, which is by a factor of 2 worse than the accuracy of 2 kHz which we achieved in the cases of allyl acetate and ethyl acetate. However, using the program XIAM, all lines could be fitted within experimental accuracy. The fitted molecular parameters are shown in Table 1. A frequency list of all transitions with their torsional components is given in the Appendix (Table F-4).

4. Results and Discussion

We measured and assigned the rotational spectrum of diethyl ketone. From the experimental data we determined the rotational and centrifugal distortion constants, as well as the torsional constants of the methyl groups. The experimental constants were compared to those obtained by quantum chemical methods. Moreover, two-dimensional potential energy surfaces for the rotation of the two ethyl groups and a potential curve for the rotation of the methyl groups were calculated by theoretical methods.

An fully optimized *ab initio* geometry calculated at the MP2/6-311++G(d,p) level of theory yielded a geometry without a mirror plane. The A rotational constant was found to be 76 MHz too small if compared to the experimental value, whereas the B and the C constant agreed within 2 MHz. The observed planar moment $P_{cc} = I_a + I_b - I_c$ is 0.590 uÅ^2 smaller than the calculated value. This is quite unusual, since due to out-of-plane vibrations the experimental planar moment is expected to be bigger than the calculated one. If the same MP2 calculation is carried out with $\varphi_1 = \varphi_2 = 0°$ as a constraint, a geometry with an *ab* mirror plane is obtained

Table 1

Molecular parameters of diethyl ketone obtained by a fit using program XIAM and quantum chemical calculations.

Para-meter	Unit	XIAM (Obs.)	MP2[a]	Obs.–MP2[a]	MP2[b]	Obs.–MP2[b]	DFT	Obs.–DFT
A	GHz	8.89243817(17)	8.876	0.016	8.816	0.076	8.937	–0.045
B	GHz	1.95419705(12)	1.956	–0.002	1.956	–0.002	1.933	0.021
C	GHz	1.67014354(12)	1.669	0.001	1.672	–0.002	1.653	0.017
Δ_J	kHz	0.17346(26)						
Δ_{JK}	kHz	0.5955(44)						
Δ_K	kHz	3.9704(86)						
δ_J	kHz	0.02473(20)						
δ_K	kHz	0.125(17)						
V_3	GHz	23141.8(79)						
	kJ/mol	9.2343(32)						
	cm^{-1}	771.93(27)	911	–139				
I_γ	uÅ^2	3.1586 (fixed) [c]						
$\angle$(i,a)	°	34.12(13)	34.77	–0.65	34.32	–0.20	33.95	0.17
$\angle$(i,b)	°	55.88(13)	55.23	0.65	56.48	–0.60	56.05	–0.37
$\angle$(i,c)	°	90.0 (fixed)	90.0	0.00	96.56	–6.56	89.95	0.05
P_{cc}[d]	uÅ^2	12.849	12.507	0.342	13.439	–0.590	12.262	0.587
N_{tot}		199						
σ	kHz	3.5						

[a] Geometry fixed at $\varphi_1 = \varphi_2 = 0°$.
[b] Optimized geometry ($\varphi_1 = \varphi_2 \approx 12°$).
[c] Derived from $F_0 = 160$ GHz (fixed).
[d] $P_{cc} = I_a + I_b - I_c$.

and the agreement between observed and calculated rotational constants has significantly improved. In this case the A constant is only 16 MHz too small, and B and C still agree within 2 MHz. Now the experimental planar moment P_{cc} is 0.342 uÅ^2 bigger than the calculated value, which is reasonable considering strong out-of-plane torsions of the ethyl groups. Finally, a DFT calculation carried out at the B3LYP/6-311++G(d,p) level without any constraint yielded also a geometry with an *ab* mirror plane. Here, the agreement between the observed and calculated rotational constants was worse than for the MP2 calculation using the $\varphi_1 = \varphi_2 = 0°$ constraint, however, the observed planar moment turned out to be 0.587 uÅ^2 bigger than the calculated one, which is still a reasonable deviation. Obviously, the experimental rotational constants are in better agreement with a C_{2v} geometry containing a mirror plane rather than a C_2 structure without a symmetry plane. For both, a C_{2v} and a C_2 geometry, the dipole moment vector is in *b* direction. Therefore, the absence of *a*- and *c*-type transitions does not rule out the existence of an *ab* mirror plane.

Two-dimensional potential surfaces calculated on the MP2 (Figure 2) and DFT level (Figure 5) predict a very broad global minimum near $\varphi_1 = \varphi_2 = 0°$. However, if the more detailed energy diagrams along the $\varphi_1 = \varphi_2$ diagonals are considered, it is found, that in the case of the MP2 calculation (Figure 3) a double minimum potential with a local maximum at $\varphi_1 = \varphi_2 = 0°$ and two minima at $\varphi_1 = \varphi_2 \approx \pm12°$ exist. These minima correspond to the C_2 geometry found after optimizing all structure parameters at the MP2 level. Sample calculations using a simple rotator-on-an-arc model with an arc of $\Delta\varphi = \pm10°$ and the rotor being one ethyl group rotating against a rigid frame have shown, that the lowest torsional energy level is above the local energy maximum of approximately 0.3 kJ/mol. Therefore, the lowest torsional wave function and accordingly, the corresponding probability density has a maximum at $\varphi_1 = \varphi_2 = 0°$. Therefore, the *effective* structure might be C_{2v}. In contrast to the MP2 $\varphi_1 = \varphi_2$ diagonal, the DFT calculations (Figure 6) show a simple global minimum at $\varphi_1 = \varphi_2 = 0°$ resulting directly in a C_{2v} geometry of the diethyl ketone molecule. However, it should be mentioned that also here the minimum is extremely broad covering a range of $\Delta\varphi = \pm10°$.

Internal rotation of two equivalent methyl groups gave rise to a quartet structure of all rotational transitions. The torsional parameters were fitted to give a V_3 potential of 771.93(27) cm^{-1} and an angle between the internal rotor axis and the *a* axis of $\angle(i,a) = 34.12(13)°$. The V_3 potential is very similar to the barrier height of 795(10) cm^{-1} reported for methyl ethyl ketone, but it is 18% lower than the value of 911.3 cm^{-1} predicted by quantum chemical calculations carried out at the MP2 level of theory. The angle $\angle(i,a)$ is in excellent agreement with the angle of 34.77° calculated with the MP2 method using the $\varphi_1 = \varphi_2 = 0°$ constraint. Both potential curves (Figure 3 and Figure 6) show local minima at approximately $\varphi_1 = \varphi_2 = 90°$. Therefore, at least one other conformer might exist. Checking these points with harmonic frequency calculations at the MP2/6-311++G(d,p) level have shown that they are saddle points rather than local minima. Even if they would represent another stable conformer it would be approximately 8 kJ/mol above the $\varphi_1 = \varphi_2 = 0°$ conformer and therefore unlikely to be observed under molecular beam conditions. This existence of only one conformer is also supported by the fact that almost all observed lines were assigned to the $\varphi_1 = \varphi_2 = 0°$ conformer and only a very few weak lines remained unassigned.

5. Conclusion

The microwave spectrum of diethyl ketone has been analyzed. Almost all lines were split into narrow quartets in a range from 10 kHz up to 2 MHz, arising from the hindered rotation of the two equivalent terminal methyl groups. In a global analysis using the XIAM code, which is based on the rho axis method, three rotational constants, five quartic centrifugal distortion constants, the torsional barrier of the terminal methyl groups, and the angles between the principal inertial axes and the internal rotor axes were determined. The methyl torsional barrier was found to be $771.93(27)$ cm^{-1}. In total, 199 lines were fitted to a standard deviation of 3.5 kHz. By combining these results with quantum chemical calculations it has been deduced that the diethyl ketone has an effective structure with C_{2v} symmetry. Whether this effective structure corresponds to a C_{2v} or a C_2 *equilibrium* geometry is still uncertain. This might become a subject of future studies with more advanced quantum chemical methods. However, the potential for the bending motions of the ethyl group out of the mirror plane turned out to be extraordinarily broad. The barrier to internal rotation of the methyl groups were found to be in good agreement with the barrier reported for the $\mathbf{CH_3}$-CH_2-CO methyl group of methyl ethyl ketone.

Acknowledgments

Publication statement

This work is published in ChemPhysChem under H. V. L. Nguyen and W. Stahl, *Chem. Phys. Chem.* **12**, 1900 (2011).

References

[1]N. M. Pozdeev, A. K. Mamleev, L. N. Gunderova, R. V. Galeev, *J. Struc. Chem.* **29**, 52 (1988).
[2]J. D. Swalen and C. C. Costain, *J. Chem. Phys.* **31**, 1562 (1959).
[3]R. Peter and H. Dreizler, *Z. Naturforsch.* **204**, 301 (1965).
[4]L. Evangelisti, L. B. Favero, A. Maris, S. Melandri, A. Vega-Toribio, A. Lesarri, W. Caminati, *J. Mol. Spec.* **259**, 65 (2010).

[5]A. C. Fantoni, W. Caminati, R. Meyer, *Chem. Phys. Lett.* **133**, 27 (1987).

[6]W. Caminati and J.-U. Grabow, *J. Am. Chem. Soc.* **128**, 854 (2006).

[7]M. Onda, Y. Kohama, K. Suga, I. Yamaguchi, *J. Mol. Str.* **442**, 19 (1998).

[8]M. J. Tubergen, R. J. Lavrich, D. F. Plusquellic, R. D. Suenram, *J. Phys. Chem. A* **110**, 13188 (2006).

[9]A. Maris, S. Melandri, W. Caminati, P. G. Favero, *Chem. Phys. Lett.* **256**, 509 (1996).

[10]S. Blanco, J. C. Lopez, A. B. Gomez, J. L. Alonso, *Mol. Phys.* **97**, 853 (1999).

[11]H. Mouhib, Y. Zhao, W. Stahl, *J. Mol. Spectrosc.* **261**, 59 (2010).

[12]H. Dreizler, *Z. Naturforsch.* **16a**, 1354 (1961).

[13]J.-U. Grabow and W. Stahl, *Z. Naturforsch.* **45a**, 1043 (1990).

Chapter 7

ACETONE

New aspects of the internal rotation in acetone

1. Introduction

Acetone is the smallest ketone which plays an important role in industry and chemistry. It is a reactant in many syntheses, for example in the preparation of polymethyl methacrylate (acrylic glass). Furthermore, acetone is a popular solvent and extractant for natural resin, colophony, fat, oil etc., and is widely used as nail polish remover. In radio astronomy acetone has been detected in the interstellar space for the first time in 1987.[1] The complicated rotational spectrum of acetone has been treated by a lot of previous investigations. The first microwave spectroscopic study on acetone has been carried out already in 1959 by Swalen and Costain.[2] Afterwards, many analyses on the spectrum of acetone were reported by Peter and Dreizler (1965),[3] Nelson and Pierce (1965),[4] Vacherand et al. (1986),[5] Oldag and Sutter (1992)[6] etc. Two equivalent methyl groups in acetone show internal rotation. The barrier was determined to be 264.7(8) cm^{-1}.[3] Due to the difficulty to fit the rotational transitions, new program codes were written especially for this molecule.[5,7] However, there are still many interesting aspects remaining, for example the improvement of the quantum chemical calculations and the quality of the fit, the interaction between two methyl groups, and spin-spin and spin-rotation coupling of six protons, which can be investigated in more detail now. Therefore, we decided to reanalysis the microwave spectrum of acetone in combination with quantum chemical calculations and compared them with a closely related molecule, pinacolone.

2. Quantum chemistry

Theoretical calculations on the structure of acetone have been done very early.[8,9] The Hartree-Fock calculations of Bowers and Schäfer using the 4-21G basis in 1980 suggest three possible conformers, the eclipsed – eclipsed, staggered – staggered, and staggered – eclipsed confor-mations.[9] Considerably fewer attempts have been made to obtain the complete two-dimensional potential energy surface though these calculations would be very helpful for studying the strongly coupled large amplitude motions of the two methyl groups. In the work
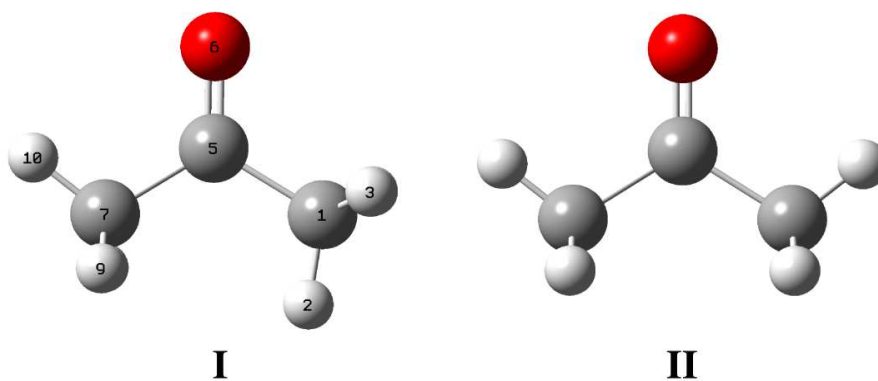
FIG. 1 Optimized structures of acetone at the MP2/6-311++G(d,p) level.

of Crighton and Bell,[10] some SCF calculations on the potential energy surface with a semi-rigid model and structure optimizations at the 3-21G basis were carried out. Four years later, Ozkabak et al.[11] were able to calculate the energy surface with different methods and larger basis sets, i.e. HF/DZ, HF/6-31G(d,p), and MP2/6-31G(d,p). The most recent detailed calculations are those of Smeyer et al.[12] using the same methods (MP2/HF) and basis set (6-31G(d,p)). Only seven selected values of the torsional angels were chosen and calculated. They discussed ellipsoidal rather than circular isoenergetic contour lines in the region of the equilibrium position.

The importance of the methyl torsional interactions in acetone induced us to recalculate the energy potential surface with the MP2 method, which includes corrections for electron correlation and using a larger basis set 6-311++G(d,p). The structure optimization at this level of theory yielded only two conformers, the eclipsed-staggered (conformer I) and the eclipsed-eclipsed conformer (conformer II) with respect to the C=O- bond (Figure 1). Additional frequency calculations have shown that conformer I is a saddle point rather than a stable conformer. The Cartesian coordinates of these conformers are reported in the Appendix (Table G-1)

The two-dimensional energy surface were calculated as a function of the torsional angles $\varphi_1 = \angle(H_2, C_1, C_5, O_6)$ and $\varphi_2 = \angle(O_6, C_5, C_7, H_{10})$. The atom numbers are given in Figure 1. φ_1 and φ_2 were fixed at certain values in a grid of 10° while all other geometry parameters were optimized. Due to the approximate C_{3v} symmetry of the methyl groups, only rotation angles from 0° to 110° were needed. The energy values were parametrized with a two-dimensional Fourier expansion. The energy surface was drawn with these Fourier coefficients as a contour plot given in Figure 2. The Fourier coefficients are given in the Appendix (Table G-2).
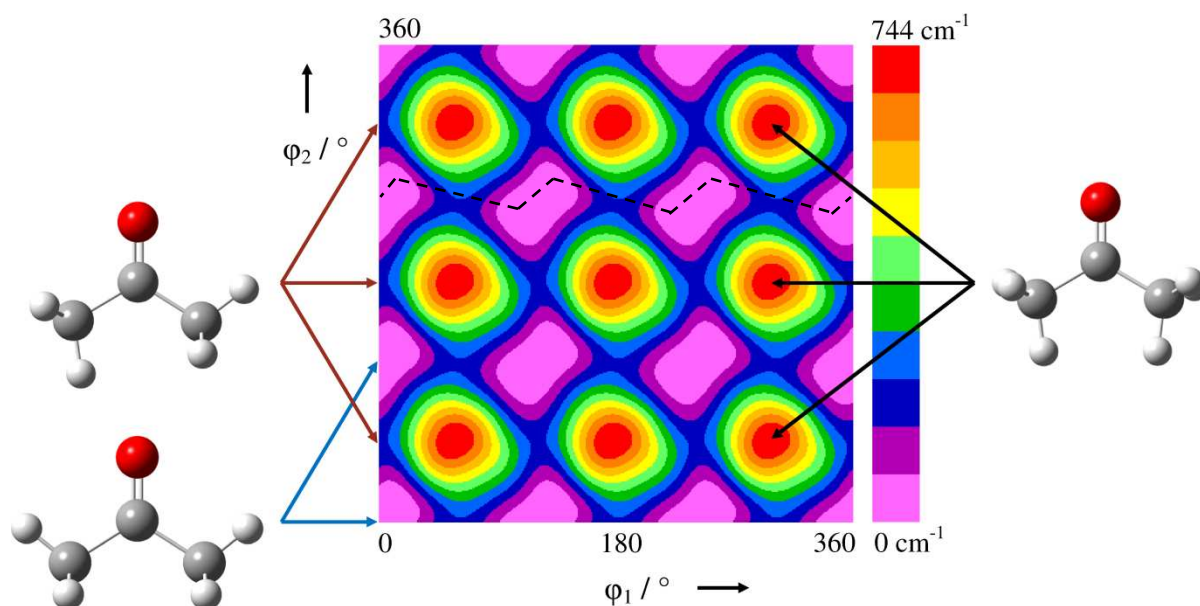
FIG. 2 The potential energy surface of acetone obtained by rotating both methyl groups by the torsional angles φ_1 and φ_2 calculated at the MP2/6-311++G(d,p) level.
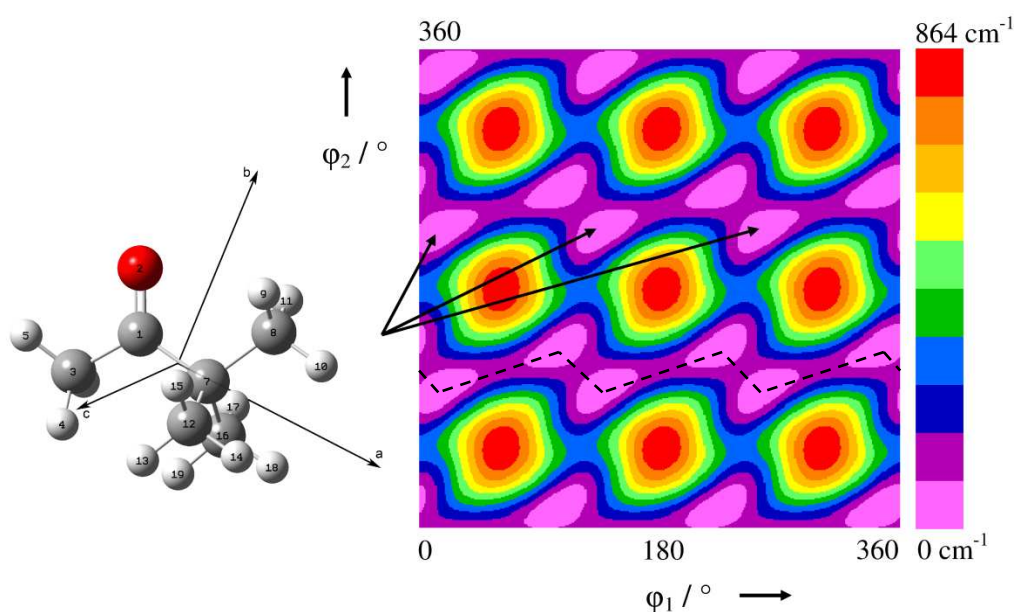
FIG. 3 The potential surface of pinacolone obtained by rotating the methyl and the *tert*-butyl group calculated at the basis set as given in Figure 2.

In agreement with Figure 3 of ref. [12], we found clearly non-circular energy minima. This can be considered as a consequence of the strong interaction between the two methyl groups. Figure 2 shows that the staggered – staggered conformer of ref. [9] is the global maximum in the energy potential surface and conformer I is a local maximum. An interesting result was found by comparing the potential surface of acetone with the one of a closely related
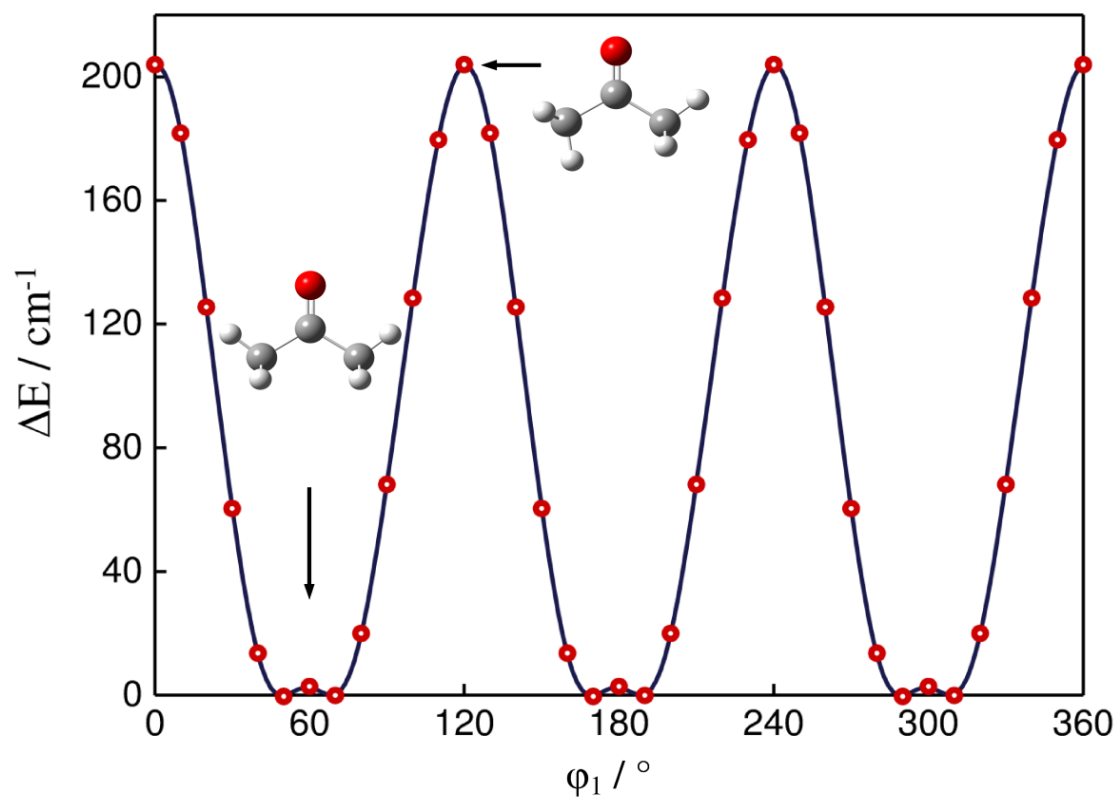
FIG. 4 The energy minimum path of acetone. The calculated stabilization energies are marked with red circles.
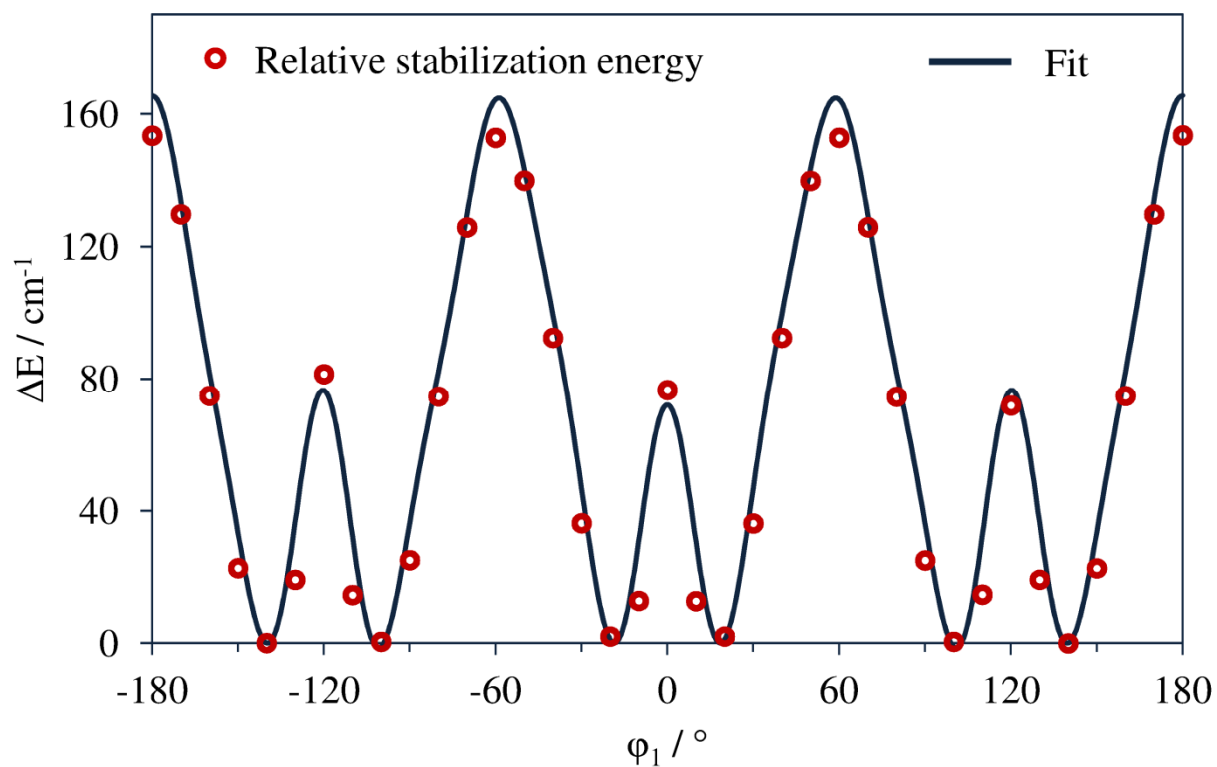
FIG. 5 The energy minimum path of pinacolone.[13]

molecule, pinacolone,[13] where a methyl group is exchanged by the also C_{3v} symmetric *tert*-butyl group. In the case of pinacolone, the regions around the equilibrium position show clearly to double minimum structure (Figure 3). A cut through the energy potential surfaces was carried out by varying the dihedral angel φ_1 in a grid of 10° whereas φ_2 was optimized. Thereby, the energy minimum path can be generated (marked with dashed lines in Figure 2 and Figure 3). The potential curves of acetone and pinacolone are given in Figure 4 and Figure 5, respectively, the Fourier coefficients in Table G-3. In the case of acetone, a small V_6 contribution to the potential can be identified. The optimized structure of conformer II becomes local maximum and the double minima are about 10° off from this structure. The V_6 potential is more pronounced in the case of pinacolone. This might be due to the steric hindering of the bulky *tert*-butyl group in pinacolone in contrast to the methyl group in acetone. However, the barrier to internal rotation of the methyl group in pinacolone has been determined to be 121.921(18) cm^{-1},[13] much lower than the value of 264.7(8) cm^{-1} found for acetone.[3] Obviously, the interaction between two methyl groups in acetone is stronger than between the methyl and the *tert*-butyl group in pinacolone in spite of the steric effect.

3. Microwave spectroscopy

Similar to the case of diethyl ketone, all rotational transitions of acetone are split into quartetts due to the internal rotation of two equivalent methyl groups. Using a modified version of the MB-FTMW spectrometer described in ref. [17,18] in the experimental setup section, 13 transitions with 51 torsional components were remeasured and fitted with the program XIAM with 8 independent molecular parameters to a standard deviation of 96.9 kHz (Table 1). A list of all fitted frequencies is given in Table G-4 in the Appendix.

Vacherand et al. reported standard deviations of 52 kHz, 266 kHz, 429 kHz, and 499 kHz for the AA, EE, AE, and EA species, respectively. The symmetry labels are given in ref. [5]. It should be noted that these symmetry labels are not identical with our local mode symmetry labels AA, EE, AE, and EE* described for the case of diethyl ketone (Chapter 6). A computer program based on the internal axis method has been developed for fitting acetone.[5] XIAM can fit the data set to a better standard deviation of 96.9 kHz, however, in both cases the standard deviation is larger than the experimental accuracy.

A standard deviation which is close to the experimental accuracy can be achieved by using the program Erham written by Groner. With this program, 1002 frequencies were fitted to determine 33 spectroscopic parameters. The dimensionless standard deviation is 1.58.[7]

Table 1

Spectroscopic constants of methyl propionate referred to the **PAM** system.

Parameter	Unit	XIAM	Erham[a]
A	GHz	10.186(12)	10.1652172(31)
B	GHz	8.516709(15)	8.5151631(18)
C	GHz	4.908679(16)	4.9101989(15)
Δ_K	kHz	20.1(18)	10.77(33)
V_3	cm^{-1}	269.0(10)	
	kJ/mol	3.218(12)	
I_α	$u\text{Å}^2$	3.187(14)	
$\angle(i,a)$	°	29.761(52)	
$\angle(i,b)$	°	60.239(53)	
$\angle(i,c)$	°	90.00 (fixed)	
D_{pi2K}	MHz	−1.15(62)	
σ	kHz	96.9	8.8
N_{tot}		51	51

[a] All other parameters were fixed to the values obtained from the fit in ref. [7].

Therefore, we also fitted our data set with the program Erham. Only the rotational constants and one centrifugal distortion constant Δ_K were fitted, all other parameters are kept fixed to the values obtained from Groner's fit given in ref. [7]. Totally, 51 torsional components could be fitted to a standard deviation of 8.8 kHz. This is somewhat larger than, however, still close to our experimental accuracy of 2 kHz. Unfortunately, similar to the case of isopropenyl acetate (Chapter 4), the potential barrier V_3 was not obtained. A list of all fitted frequencies is given in Table G-5.

It is interesting to compare the Erham fit of acetone with the fit of pinacolone. The standard deviation for 134 A species and 44 E species transitions of pinacolone is 9.4 and 12.6 kHz, respectively. Comparing to the standard deviation of 2.3 kHz achieved for isopropenyl acetate, in the cases of acetone and pinacolone, the strong interaction between the methyl groups within these molecules is not well understood.

There is a further effect which makes acetone more interesting. In many transitions, additional splittings on the order of a few ten kHz were observed (Figure 6a). In the presence of an inhomogeneous magnetic field with a maximum of five times the strength of the earth's magnetic field, these splittings vanished or changed their appearance (Figure 6b). In analogy to the case of isopropenyl acetate (Chapter 4), we concluded that these extra splittings result proton spin-rotation and spin-spin coupling of 6 protons. In the investigation of Oldag and
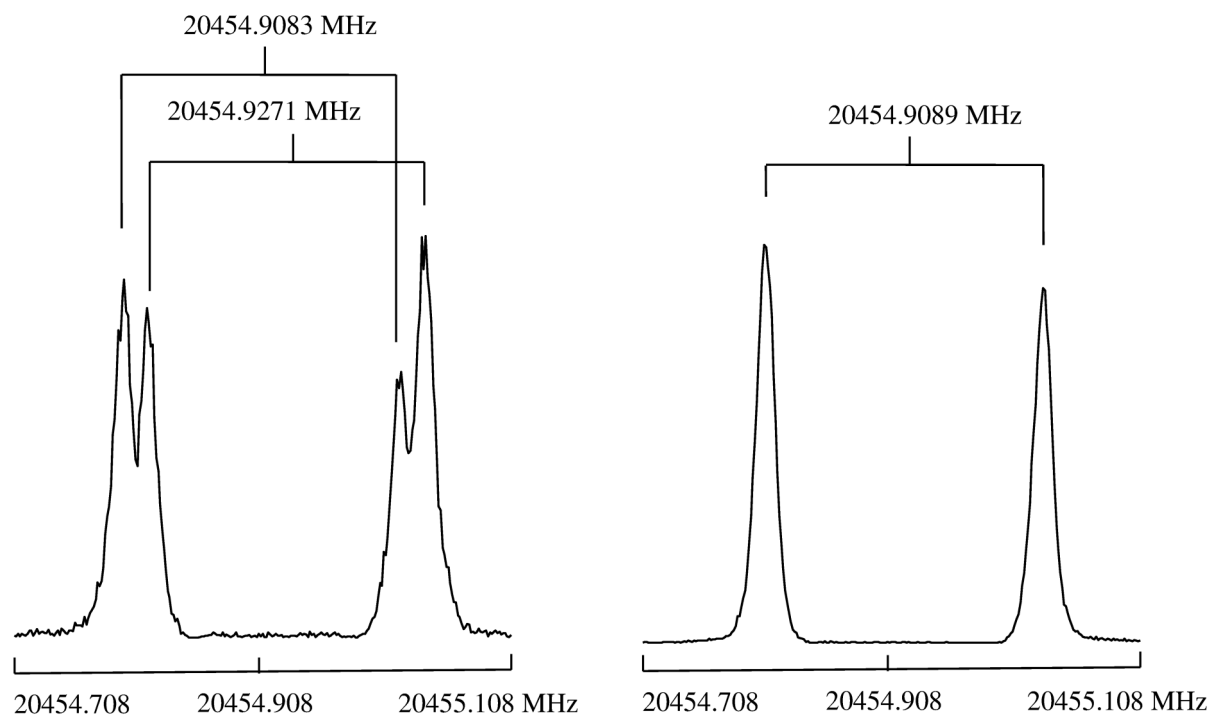
FIG. 6a (left hand-side) Additional splittings of the AA species of the $3_{12} \leftarrow 3_{03}$ transition of acetone. These splittings might be due to the proton spin-spin or spin-rotation coupling.

FIG. 6b (right hand-side) The splittings vanished in the presence of an inhomogeneous magnetic field of five times the strength of the earth's magnetic field.

Sutter,[6] the rotational Zeeman effect of acetone in exterior fields up to 2 Tesla was studied for the AA species. It is surprising that this effect can be observed even under the low external earth's magnetic field. Therefore, the spin-rotation and spin-spin coupling in acetone makes it a suitable test molecule for further studies in this area, where only few investigations were carried out so far due to the rather complicated theory needed to treat six coupled protons. These splittings also explain why the standard deviations obtained by XIAM and also by Erham are larger than expected. The line positions used in the fit were the mean values of the hyperfine multiplets rather than the exact AA species hyperfine-free line position.

4. Conclusion

The Fourier transform microwave spectrum of acetone was remearsured in the frequency range from 4 to 26.5 GHz. 51 torsional components were fitted with the program XIAM and Erham to a standard deviation of 96.9 kHz and 8.8 kHz, respectively. The standard deviation achieved by Erham is close to the experimental accuracy. Barrier to internal rotation was determined to be 269.0(10) cm^{-1} by the program XIAM. Additional splittings due to proton

spin-spin and spin-rotation coupling could be observed. The quantum chemical calculations were improved. The energy potential surface was recalculated with a higher resolution and larger basis set. The energy minimum path showed a double minimum potential which explains the rather oblong than circular minima region in the energy potential surface. The potential surface and energy minimum path were compared with pinacolone, where a methyl group is replaced by a steric *tert*-butyl group.

Acknowledgments

References

[1]F. Combes, M. Gerin, A. Wootten, G. Wlodarczak, F. Clausset, P. J. Encrenaz, *Astron. Astrophys.* **180**, 13 (1987).

[2]J. D. Swalen and C. C. Costain, *J. Chem. Phys.* **31**, 1562 (1959).

[3]R. Peter and H. Dreizler, *Z. Naturforsch.* **204**, 301 (1965).

[4]R. Nelson and L. Pierce, *J. Mol. Spectrosc.* **18**, 344 (1965).

[5]J. M. Vacherand, B. P. van Eijck, J. Burie, J. Demaison, *J. Mol. Spectrosc.* **118**, 355 (1986).

[6]F. Oldag and D. H. Sutter, *Z. Naturforsch.* **47a**, 527 (1992).

[7]P. Groner, S. Albert, E. Herbst, F. C. D. Lucia, F. J. Lovas, B. J. Drouin, J. C. Pearson, *ApJS* **142**, 145 (2002).

[8]D.Cremer, J. S. Brinkley, J. Pople, W. J. Hehre, *J. Am. Chem. Soc.* **96**, 6900 (1974)

[9]P. Bowers and L. Schäfer, *J. Mol. Struct.* **69**, 233 (1980).

[10]J. S. Crighton and S. Bell, *J. Mol. Spectrosc.* **118**, 383 (1986).

[11]A. G. Ozkabak, J. G. Philis, L. Goodmann, *J. Am. Chem. Soc.* **112**, 7854 (1990).

[12]Y. G. Smeyers, M. L. Senent, V. Botella, D. C. Moule, *J. Chem. Phys.* **98**, 2754 (1993).

[13]Y. Zhao, diploma thesis at the RWTH Aachen University under supervision of Prof. W. Stahl, **2009**.

Discussion

Internal rotation of some esters and ketones with one or two methyl internal rotors and different frame symmetries has been investigated. The V_3 barriers of the methyl groups which have been determined are listed in Table I.

The barrier to internal rotation of the acetyl methyl group is much lower than in the case of the methyl group in acetone, though they are both bound to a carbonyl group. In the case of ethyl acetate and allyl acetate, the barrier high is almost 100 cm^{-1}. It is somewhat higher in the case of isopropenyl acetate (135 cm^{-1}), vinyl acetate (158 cm^{-1}), and acetone (269 cm^{-1}), however, in comparison to the barrier of 1171.3(14) cm^{-1} found for the ethyl methyl group in ethyl fluoride,[1] these values are clearly much lower. The low barrier of the acetyl methyl group in acetates can be explained by symmetry consideration. In the case of the acetate anion, two mesomeric structures exist (Figure III). Therefore, it has a C_{2v} symmetry. In combination with the C_{3v} symmetry of the methyl group, a six fold potential arises (Figure IV).

Some molecules with V_6 potential like toluene and nitromethane have been investigated. The barrier to internal rotation is often very low in those cases. For nitromethane, **CH$_3$**–NO$_2$, a V_6 barrier potential of 2.098(11) cm^{-1} was reported by Tannenbaum et al.[2] already in 1954 and improved by Sørensen et al. (2.099649(10) cm^{-1}) 30 years later.[3,4] In toluene, C$_6$H$_5$–**CH$_3$**,[5] and its derivates p-chlorotoluene, Cl–C$_6$H$_4$–**CH$_3$**,[6] and p-fluorotoluene, F–C$_6$H$_4$–**CH$_3$**,[7,8] the methyl groups also has very low barriers to internal rotation of 4.876(35) cm^{-1}, 4.872(14) cm^{-1}, and 4.7700(63) cm^{-1}, respectively. In 1999, Walker et al. reported on a nearly free internal rotation of the methyl group in p-tolualdehyde, **CH$_3$**–C$_6$H$_4$–CHO, though the presence of the aldehyde group makes the V_3 term to be non-zero.[9] A global fit of approximately 800 transitions using the program Belgi-C$_S$ was carried out to determine the V_3 and V_6 barrier to be 28.370(17) cm^{-1} and 5.329(26) cm^{-1}, respectively.[10]

In the case of the acetyl methyl group in acetates, perturbation of the V_6 potential arises due to the non-C_{2v} symmetry of the COO- ester group. This perturbation is larger than in the case of p-tolualdehyde since the COO- group is attached directly to the methyl group, therefore the V_3 value should be larger than 28 cm^{-1} found for p-tolualdehyde. However, this could explain the relatively low barrier of about 100 cm^{-1} of the acetyl methyl group in acetates in comparison to the barrier of 1171.3(14) cm^{-1} found for the ethyl methyl group in ethyl fluoride.[1]

Table I

Barriers to internal rotation of the methyl groups in investigated esters and ketones

Molecule	Structure	Symmetry	Program	Barrier / cm^{-1}
ethyl acetate	**CH$_3$**-COO-CH$_2$-**CH$_3$**	C$_S$	XIAM Belgi-C$_S$	97.7844(45) 1061.4(68)
allyl acetate	**CH$_3$**-COO-CH$_2$-CH=CH$_2$	C$_1$	XIAM BELGI-C$_1$	98.093(12)
vinyl acetate	**CH$_3$**-COO-CH=CH$_2$	C$_S$	XIAM Erham	157.78(13)
isopropenyl acetate	**CH$_3$**-COO-C(**CH$_3$**)=CH$_2$	C$_1$	XIAM Erham	135.3498(38) 711.7(73)
methyl propionate	**CH$_3$**-CH$_2$-COO-**CH$_3$**	C$_S$	XIAM BELGI-C$_S$-2tops	429.324(23) 820.46(99)
diethyl ketone	**CH$_3$**-CH$_2$-(C=O)-CH$_2$-**CH$_3$**	C$_{2v}$	XIAM	771.93(27)
acetone	**CH$_3$**-(C=O)-**CH$_3$**	C$_{2v}$	XIAM Erham	269.0(10)

Note: the methyl group marked in boldface **black**, **red**, **blue**, and **green** is the **acetyl**, **ethyl**, **isopropenyl**, and **methoxy** methyl group, respectively. The barriers to internal rotation are given in corresponding colors.

The difference in the barriers found for three molecules containing a double bond, allyl acetate, isopropenyl acetate, and vinyl acetate, was attributed to the delocalization of π-electrons which extends from the vinyl double bond to the ester group, which increases the potential barrier in vinyl acetate and isopropenyl acetate, as discussed in Chapter 4. In the case of allyl acetate, the vinyl group is not involved in delocalization and the barrier remains near 100 cm^{-1}.

We attribute the different barriers found for the ethyl methyl group in ethyl acetate, methyl propionate, and diethyl ketone to the electronegativity of the neighbor group, which will be discussed later in Chapter 8 in detail.

Rotational constants obtained from quantum chemical calculations were in good agreement with the experimental data, therefore they could be used in all cases as good start values for the spectral assignment. Quantum chemical calculations were also helpful for identifying possible conformers, which is almost impossible by classical method like isotopic substitution
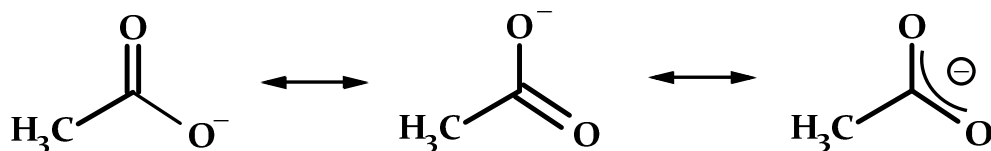
FIG. III Two mesomeric structures (left-hand side) and the C_{2v} structure (right-hand side) of the acetate ion.
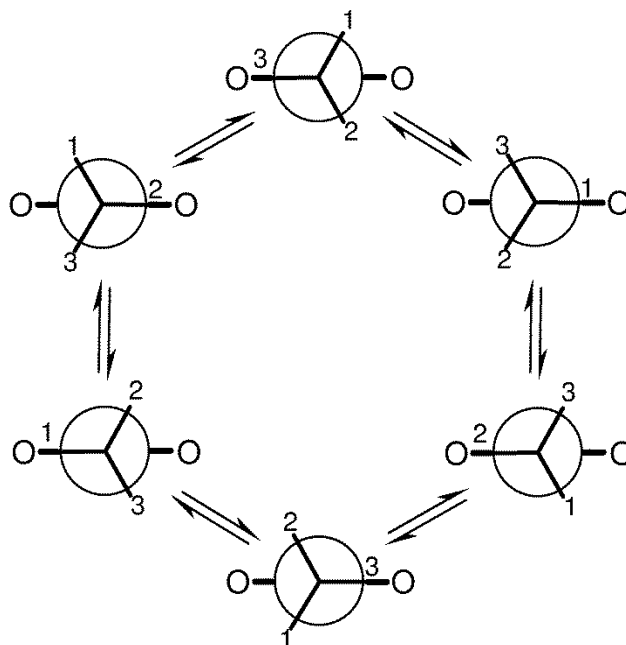
FIG. IV A six-fold potential arises from the combination of the C_{2v} symmetry of the COO$^-$ group and the C_{3v} symmetry of the methyl group.

for the investigated molecules due to the large number of atoms. However, it should be noted that in the case of vinyl acetate, methyl propionate, and diethyl ketone the results of quantum chemical calculations turned out to be strongly dependent on the methods and basis sets. Further investigations should be carried out to determine the most suitable methods and basis sets for calculations on esters and ketones.

For almost all molecules (except diethyl ketone) the three internal rotation programs XIAM, BELGI, and Erham were used. The programs BELGI and XIAM were compared in the case of ethyl acetate, allyl acetate, and methyl propionate. For ethyl acetate and allyl acetate, where the barrier to internal rotation is in the order of 100 cm^{-1}, XIAM can fit the A species to experimental accuracy. However, the predictive power for the E species is not satisfactory. The standard deviation of a global fit carried out with XIAM is 18.5 kHz and 54.0 kHz for ethyl acetate and allyl acetate, respectively, whereas BELGI can fit the whole data set with a standard deviation of only 2.3 kHz in both cases. In the case of methyl propionate, where the

barrier to internal rotation is intermediate or high, XIAM can fit both, the A and the E species, in a global fit to experimental accuracy. BELGI seems to have some difficulties in the high barrier case.

The program XIAM and Erham were used to fit the spectra of vinyl acetate, isopropenyl acetate, and acetone. In all cases Erham could fit the data set to experimental accuracy, whereas XIAM is not suitable for fitting internal rotation spectra for the low barrier case. Unfortunately, it is difficult to extract the barrier to internal rotation from the Erham fit. However, especially for the case of isopropenyl acetate, where the splitting due to the propenyl methyl group is in the same order of magnitude as the standard deviation obtained from the XIAM fit, Erham was a good choice to check the assignment, since the standard deviation was only 2.3 kHz if compared to the standard deviation of 75.5 kHz found in the XIAM fit.

References

[1]E. Fliege, H. Dreizler, J. Demaison, D. Boucher, J. Burie, A. Dubrulle, *J. Chem. Phys.* **78**, 3541 (1983).

[2]E. Tannenbaum, R. D. Johnson, R. J. Myers, W. D. Gwinn, *J. Chem. Phys.* **22**, 949 (1954).

[3]G. O. Sørensen and T. Pedersen, Studies in Physical and Theoretical Chemistry, Vol. 23, p. 219 – 236, Elsevier, Amsterdam 1983.

[4]G. O. Sørensen, T. Pedersen, H. Dreizler, A. Guarnieri, A. P. Cox, *J. Mol. Struct.* **97**, 77 (1983).

[5]H. D. Rudolph, H. Dreizler, A. Jaeschke, P. Wendling, *Z. Naturforsch.* **22a**, 940 (1967).

[6]G. Herberich, *Z. Naturforsch.* **22a**, 761 (1967).

[7]H. D. Rudolph and H. Seiler, *Z. Naturforsch.* **20a**, 1682 (1965).

[8]P. N. Ghosh, *J. Mol. Spectrosc.* **138**, 505 (1989).

[9]A. R. H. Walker, J. T. Hougen, J.-U. Grabow, *54th Ohio State Univ. Int. Symp. Mol. Spectrosc.* Columbus, Ohio (1999).

[10]H. Saal, J.-U. Grabow, A. R. Hight-Walker, J. T. Hougen, W. Caminati, I. Kleiner, *65th Ohio State Univ. Int. Symp. Mol. Spectrosc.* Columbus, Ohio (2010).

B. Nitrogen inversion tunneling

Introduction

The inversion process is well-known in the case of the ammonia molecule, NH_3.[1] There, it describes the tunneling of the nitrogen atom through the plane spanned by the three hydrogen atoms, thereby connecting two energetically equivalent forms of the molecule. The tunneling path itself has the shape of a double minimum potential.[2] In the microwave spectrum, rotational transitions of a certain symmetry show splittings due to inversion tunneling and for suitable model potentials the height of the tunneling barrier can be determined from these splittings. The effect of inversion is not only found in ammonia but also in bigger and more complex molecules or molecular systems like ethylene diamine, hydrazine, some dimers, and complexes.

Ethylene diamine, $\mathbf{NH_2}$–CH_2–CH_2–$\mathbf{NH_2}$, has been investigated for the first time by Marstokk and Møllendal.[3] They reported on two conformers, both of them showing large amplitude tunneling motions corresponding to an interchange of the donor and acceptor roles of the amino groups. The (+) and (−) energy levels were fitted separately. Inversion splittings of 86.356(21) MHz and 1.564(66) MHz for conformer I and II, respectively, (Figure 1 in ref.[3]) were observed. Later, theoretical improvements were made and a global fit was carried out on this interesting system by Merke and Coudert.[4] Another molecule with two amino groups, hydrazine, $\mathbf{NH_2}$–$\mathbf{NH_2}$, shows three large amplitude motions, namely inversion motions of both amino groups and an internal rotation around the N–N bond. The first assignment was carried out by Kasuja et al.[5] and improved by Tsunekawa and Hougen.[6,7] An inversion motion has been found in almost all primary amines like methyl amine, CH_3-$\mathbf{NH_2}$,[8,9] and aniline, C_6H_5–$\mathbf{NH_2}$.[10] Tunneling is not only linked to nitrogen containing molecules but it is also found in several "floppy" molecules like dimers and complexes. The theoretical studies of Ohashi and Hougen predicted 25 different possible tunneling motions besides internal rotation of two methyl groups in methanol dimer, $(CH_3OH)_2$.[11] Assignment of the rotational spectrum by Lovas et al. has shown that a-type R branch $K_a = 0$ transitions are split into 15 states due to these tunneling motions.[12] Obviously, considerably fewer studies on inversion tunneling have been reported in comparison to the large number of investigation on internal rotation. Furthermore, inversion tunneling often takes place in combination with internal rotation. For example, the proton inversion in primary amines is in almost all cases combined with internal

rotation of the primary amino group. Only in very few molecules like dimethyl amine, $CH_3-\mathbf{NH}-CH_3$,[13] and ethyl methyl amine, $CH_3-CH_2-\mathbf{NH}-CH_3$,[14] the inversion tunneling at the nitrogen is not accompanied by internal rotation, as will be discussed later in Chapter 8. To the best of our knowledge, no further investigation on this type of nitrogen inversion tunneling has been reported. This induced us to study proton inversion tunneling in secondary amines where, unlike the case of primary amines, additional internal rotation does not exist. We started our investigation with diethyl amine, $CH_3-CH_2-\mathbf{NH}-CH_2-CH_3$, a molecule with a similar structure as diethyl ketone (already discussed in Chapter 6) and then continued with methyl *tert*-butyl amine, $CH_3-\mathbf{NH}-(CH_3)_3$.

Moreover, besides splitting due to large amplitude motions, there are also effects originating from the nuclei which cause shifts and splittings of the energy levels and thereby also of the spectral lines. These splittings are due to the electric and magnetic nuclear multipole moments. Most important are the magnetic dipole moment which is responsible for splittings due to spin-rotation and spin-spin coupling and the electric quadrupole moment which causes a nuclear quadrupole hyperfine structure of the rotational lines.

For the observation of magnetic coupling effects it is necessary that the spin of the coupling nucleus is bigger than zero, i.e. for nuclei with $I = 1/2$ (^{1}H, ^{15}N, ^{19}F), 1 (^{2}H=D, ^{13}C, ^{14}N), 3/2 (^{35}Cl, ^{37}Cl, ^{79}Br, ^{81}Br), 2, 5/2, ... Some important nuclei are given as examples in braces. It should be noted that the ^{12}C nucleus has a spin of $I = 0$ and does not show any magnetic coupling effects. Different types of magnetic coupling can occur. In spin-rotation coupling, the magnetic moment of the nucleus interacts with the magnetic field generated by the molecule itself. The origins of this magnetic field are partial charges within the molecule which produce a magnetic field while the molecule rotates in space. The coupling energy depends on the spin state of the nucleus. For a nucleus with a spin I there are $2I + 1$ spin states $M_I = -I, -I + 1, ... , I - 1, I$, which describe the orientation of the nucleus in space. A second type of magnetic interaction is the spin-spin coupling, where two nuclei interact via their magnetic moments. Also in this case different combinations of the spin states of the respective nuclei result in different interaction energies. The size of the splittings depends on the nuclear magnetic moments. These are in units of nuclear magnetons 2.7928456 for ^{1}H, −0.2831892 for ^{15}N, 2.628867 for ^{19}F, 0.8574376 for D, 0.702411 for ^{13}C, and 0.4037607 for ^{14}N.[15] At our spectral resolution of typically 2 kHz, usually only splittings or line broadening due to spin-rotation or spin-spin coupling of ^{1}H and ^{19}F, which is on the order of 10 kHz, can

be observed. The magnetic moments of the other nuclei are too small to cause appreciable effects. Not only internal magnetic field can interact with the nuclear magnetic moment. The (nuclear) Zeeman effect is an interaction with an external magnetic field. This has been used as a diagnostic tool for the identification of magnetic coupling effects in this thesis. When an inhomogeneous magnetic field with a strength on the order of the earth's magnetic field caused modifications in the hyperfine structure of a line then this hyperfine structure was assumed to be due to magnetic coupling (as discussed in the part on internal rotation). Generally, the observed splittings were too small to be analyzed in detail. Therefore, no theoretical treatment is given here.

In the case of electric quadrupole coupling, a hyperfine structure can be observed if the spin of the coupling nucleus is bigger than 1/2, i.e. $I = 1$, 3/2, 2, ... Some basic principles of quadrupole hyperfine coupling are presented here because hyperfine splittings appear in the spectra of all amines due to the electric quadrupole moment $I = 1$ of the ^{14}N nucleus. The origin of the quadrupole coupling is the interaction of the electric nuclear quadrupole moment with the electric field, or more exact, the electric field gradient at the site of the nucleus. In an atom, the electron density around the nucleus has spherical symmetry, the field gradient is zero, and the same interaction energies are observed for different orientations of the nucleus with respect to the electric field. Within a molecule, the situation is usually different. Due to the chemical bond, the electric field around the nuclei is generally no longer of spherical symmetry. Therefore, different orientations of the nuclei within the electron shells cause different coupling energies and transitions between these hyperfine levels cause a hyperfine splitting of the rotational lines. The size of this splitting depends on both, the electric quadrupole moment of the coupling nucleus and the electric field gradient. Since the quadrupole moments are well known, the analysis of the quadrupole hyperfine structure yields information on the electric field gradient at the site of the respective nucleus and thereby also on the nature of the chemical bond. This can be easily seen in the case of the ^{35}Cl nucleus in NaCl and in HCl. In NaCl there is an ionic bond with an independent Cl^- ion with an almost sperical electronic field distribution and with a very small field gradient, in HCl the field distribution is no longer spherical due to a considerable covalent contribution in the H–Cl bond. However, the size of the coupling effects is mainly governed by the quadrupole moments of the nuclei, which are 0.2875 fm^2 for D, 1.56 fm^2 for ^{14}N, −8.249 fm^2 for ^{35}Cl, and −78.9 fm^2 for ^{127}I.[15] In the case of the ^{14}N nucleus splittings of the rotational lines on the order of 1 MHz can be expected, for the other nuclei the splittings are accordingly smaller or bigger.

The theoretical treatment of nuclear quadrupole coupling will not be given here in detail because it has been treated in many publications and textbooks (e.g. Gordy [2]). However, some important equations will be given since they have been the basis of the spectral analysis in this thesis and they provide an exact definition of the quantities obtained from the fits.

Within the irreducible (spherical) tensor formalism the quadrupole coupling Hamiltonian can be written as a scalar product of the second rank field gradient tensor $\mathbf{V}^{(2)}$ and the second rank quadrupole tensor $\mathbf{Q}^{(2)}$.

$$H_{NQ} = \mathbf{V}^{(2)} \cdot \mathbf{Q}^{(2)} \tag{1}$$

The Hamilton matrix is set up in the coupled basis $\vec{F} = \vec{J} + \vec{I}$ with the rotational angular momentum vector $\vec{J}$, the spin vector $\vec{I}$, and the total angular momentum vector $\vec{F}$. The values of possible F quantum numbers are in the range of $|J - I|, |J - I| + 1, \ldots, |J + I|$. The energy eigenvalues are obtained by direct diagonalization of the Hamilton matrix.

The elements of the field gradient tensor components $V_{q'}^{\prime(2)}$ can be expressed by the elements of the Cartesian field gradient tensor. The prime indicates that the tensors refer to the molecule fixed axis system.

$$2V_0^{\prime(2)} = V_{z'z'} \tag{2}$$

$$2V_{\pm 1}^{\prime(2)} = \mp\sqrt{\tfrac{2}{3}}(V_{x'z'} \pm iV_{y'z'}) \tag{3}$$

$$V_{\pm 2}^{\prime(2)} = \sqrt{\tfrac{1}{6}}(V_{x'x'} - V_{y'y'} \pm 2iV_{x'y'}) \tag{4}$$

The constants $eQV_{x'x'}$ etc. are identical to the quadrupole coupling constants $\chi_{x'x'}$ etc. Here, e is the charge of the electron and Q the nuclear quadrupole moment. The complete nuclear quadrupole coupling tensor is traceless, i.e. $\chi_{aa} + \chi_{bb} - \chi_{cc} = 0$, and symmetric, i.e. $\chi_{ab} = \chi_{ba}$, $\chi_{bc} = \chi_{cb}$, $\chi_{ac} = \chi_{ca}$. In a first order approximation, the quadrupole coupling energy depends only on the diagonal elements of the coupling tensor, therefore only two linear combinations of χ_{aa}, χ_{bb}, and χ_{cc} are needed. For this purpose, often $\chi_+ = \chi_{bb} + \chi_{cc}$ and $\chi_- = \chi_{bb} - \chi_{cc}$ are used. The off-diagonal elements χ_{ab}, χ_{bc}, and χ_{ac} contribute only in second order to the quadrupole coupling energy. They are associated with $\Delta J = 2$ matrix elements. Their effect is usually observed for strong coupling nuclei only, or if near degenerate energy levels enhance their contribution. This near degeneracy can exist between rotational energy levels of suitable

symmetry or, as shown in Chapter 8, for inversion energy levels. The determination of the complete quadrupole coupling tensor is important in order to find its principal axis system which often reflects the binding situation of the respective nucleus. In the case of diethyl amine, the z axis of the coupling tensor pointed into the direction of the lone pair of the nitrogen atom. The values of the principal coupling constants depend on the chemical environment of the nucleus, e.g. on the electronegativities of the neighboring atoms.

For comparison with other amines we decided to study the quadrupole hyperfine structure of triethyl amine, $(C_2H_5)_3\mathbf{N}$, a molecule related to diethyl amine, where instead of two protons all three protons of an ammonia molecule are replaced by ethyl groups. Nitrogen inversion tunneling does not occur in this case and only hyperfine splittings can be observed. Surprisingly, triethyl amine is a symmetric oblate top, whereas ammonia itself is a prolate top. Methyl *tert*-butyl amine, a very near prolate top ($\kappa = -0.994$), is another molecule which we studied for both, the nitrogen inversion as well as for its quadrupole hyperfine structure.

References

[1]G. R. Gunther-Mohr, R. L. White, A. L. Schawlow, W. E. Good, D. K. Coles, *Phys. Rev.* **94**, 1184 (1954).

[2]W. Gordy and R. L. Cook, Microwave Molecular Spectra, John Wiley & Sons, New York 1984, 3rd edition.

[3]K. M. Marstokk and H. Møllendal, *J. Mol. Struct.* **49**, 221 (1978).

[4]I. Merke and L. H. Coudert, *J. Mol. Spectrosc.* **237**, 174 (2006).

[5]T. Kasuja, *Sci. Papers Inst. Phys. Chem. Res. Tokyo* **56**, 1 (1962).

[6](a) S. Tsunekawa, *J. Phys. Soc. Japan* **41**, 2077 (1976); (b) S. Tsunekawa and T. Kojima, *J. Phys. Soc. Japan* **49**, 1957 (1980).

[7]S. Tsunekawa, T. Kojima, J. T. Hougen, *J. Mol. Spectrosc.* **95**, 133 (1982).

[8](a)T. Nishikawa, T. Itoh, K. Shimoda, *J. Chem. Phys.* **23**, 1735 (1955); (b) K. Takagi and T. Kojima, *J. Phys. Soc. Japan* **30**, 1145 (1971).

[9]M. Kreglewski, *J. Mol. Spectrosc.* **133**, 10 (1989).

[10]B. Kleibömer and D. H. Sutter, *Z. Naturforsch.* **43a**, 561 (1988).

[11]N. Ohashi and J. T. Hougen, *J. Mol. Spectrosc.* **170**, 493 (1995).

[12]F. J. Lovas, S. P. Belov, M. Yu. Tretyakov, W. Stahl, R. D. Suenram, *J. Mol. Spectrosc.* **170**, 478 (1995).

[13]J. E. Wollrab and V. W. Laurie, *J. Chem. Phys.* **48**, 5058 (1968).

[14]R. E. Penn and J. E. Boggs, *J. Mol. Spectrosc.* **47**, 340 (1973).

[15]E. R. Cohen, T. Cvitaš, J. G. Frey, B. Holmström, K. Kuchitsu, R. Marquardt, I. Mills, F. Pavese, M. Quack, J. Stohner, H. L. Strauss, M. Takami, A. J. Thor, Quantities, Units and Symbols in Physical Chemistry, Royal Society of Chemistry, Cambridge 2007, 3rd edition.

Chapter 8

DIETHYL AMINE

The effects of nitrogen inversion tunneling, methyl internal rotation, and ^{14}N quadrupole coupling

1. Introduction

This chapter deals with another type of large amplitude motions, the proton inversion tunneling which appears in several amines. Many studies on ammonia[1] and small aliphatic amines, such as methyl amine,[2] ethyl amine,[3] dimethyl amine,[4] trimethyl amine,[5] and methyl ethyl amine[6] have been carried out in the microwave region. The primary amines often show internal rotation of the asymmetric NH_2 rotor whereas the secondary amines might show proton inversion tunneling at the nitrogen atom. From investigations on dimethyl amine[4] and methyl ethyl amine,[6] we know that the inversion tunneling of the proton causes a splitting in the order of 2646.0 MHz and 1981.0 MHz, respectively, of all rotational lines. Therefore, it is interesting to study diethyl amine, $CH_3–CH_2–NH–CH_2–CH_3$, to understand more about this type of large amplitude motions. Due to its structure, which is similar to dimethyl amine and methyl ethyl amine, inversion splittings on the same order of magnitude were expected.

Although internal rotation of the methyl groups is not the main interest in this case, we expected that the splittings due to internal rotation of the two equivalent methyl groups in diethyl amine could also be resolved and would increase the complexity of the spectra. From our study on diethyl ketone which has been reported in Chapter 6, a barrier to internal rotation of the methyl groups of 771.93(27) cm^{-1} was determined. In diethyl amine, the carbonyl C=O- group was substituted by the secondary amino NH-group. It is interesting to find out, whether the torsional barrier of the methyl groups is significantly different if compared to diethyl ketone.

There is a further effect which makes this molecule even more interesting. The ^{14}N nucleus has a nuclear spin of $I = 1$. Due to its electric quadrupole moment, hyperfine splittings arise and have been reported for some amines. These splittings are usually on the order of 0.5 MHz. Since the experimental resolution of our spectrometer is about 2 kHz,[7] we expected to be able to resolve the ^{14}N quadrupole hyperfine splittings also in the case of diethyl amine.

2. Quantum chemistry

At the beginning of the experimental work quantum chemical calculations were carried out in order to obtain initial molecular parameters of diethyl amine for spectral assignment purposes. A fully optimized structure was calculated at the MP2/6-311++G(d,p) level of theory using the *Gaussian03* and *Gaussian09* program package. The nuclear coordinates referred to principal axes of inertia are given in the Appendix in Table H-1, the molecular structure is visualized in Figure 1.

It should be pointed out that all heavy atoms are almost located within one plane. A harmonic frequency calculation has proven the stationary point to be a minimum instead of a saddle point. The rotational constants of A = 17.7066 GHz, B = 2.1051 GHz, and C = 1.9831 GHz indicate that diethyl amine is a near prolate top with an asymmetry parameter of $\kappa = -0.9845$.[8] The molecular dipole moment was found to be $\mu = 1.089$ D with the components $\mu_a = 0.000$ D, $\mu_b = 0.502$ D, and $\mu_c = 0.967$ D referred to the principal axes of inertia. The *a* component is zero due to a *bc* mirror plane which is perpendicular to the *a* axis and which contains the nitrogen atom. Additionally, the electric field gradient tensor at the ^{14}N nucleus was calculated at the MP2/6-311++G(d,p) level of theory. Referred to principal axes of inertia its elements are $q_{aa} = -0.6064$ a.u., $q_{bb} = -0.2250$ a.u., $q_{cc} = 0.8314$ a.u., $q_{bc} = 0.7114$ a.u., and $q_{ab} = q_{ac} = 0$. Using an effective ^{14}N quadrupole moment of 19.41 mbarn,[13] the quadrupole coupling constants were calculated to be $\chi_{aa} = 2.766$ MHz, $\chi_{bb} = 1.026$ MHz, $\chi_{cc} = -3.792$ MHz, $|\chi_{bc}| = 3.244$ MHz, and $\chi_{ab} = \chi_{ac} = 0$.

3. Microwave spectrum

Due to the low boiling point of only 328.7 K, mixtures of 1% of diethyl amine in helium at a total pressure of 100 kPa could be easily prepared and served as a sample throughout all measurements. At the beginning, a broadband scan in the range from 14.5 to 16.5 GHz was recorded. All lines observed were remeasured under high resolution conditions. Each frequency is split into two Doppler components. The width of each single component was strongly dependent on the respective transition, however they were always clearly broader than 1 to 3 kHz which can be achieved with a molecule like carbonyl sulfide under comparable conditions.[7] This might be attributed to partly unresolved internal rotation splittings and hydrogen spin-rotation and spin-spin coupling effects. The microwave spectrum of diethyl amine was assumed to be similar to the spectrum of dimethyl amine extensively
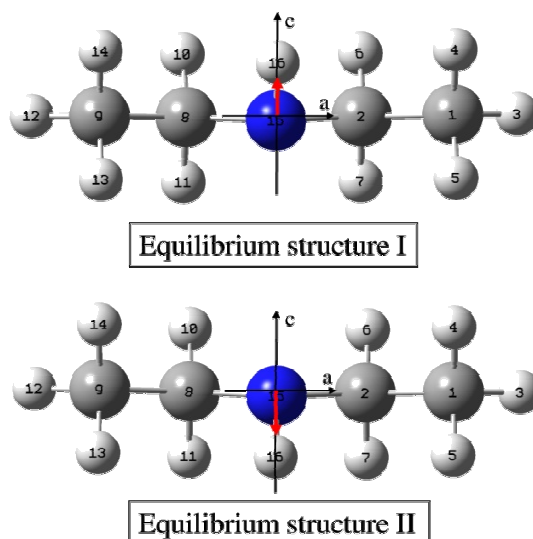
FIG. 1 Two equilibrium geometries of diethyl amine corresponding to the two energy minima of the nitrogen tunneling process. The principal a and c axes of inertia are indicated showing that the dipole component (red arrow) in c direction changes sign upon proton tunneling.

studied by Wollrab and Laurie.[4] The molecule has the same symmetry, a similar ratio of the dipole moment components, and also tunneling splittings arising from an inversion motion at the nitrogen atom were expected. Moreover, all lines should show a ^{14}N quadrupole hyperfine structure on the order of 0.5 MHz and a smaller additional splitting due to the internal rotation of two methyl groups. From the dipole moment components obtained from the quantum chemical calculations, the c-type spectrum was estimated to be by a factor of 4 stronger than the b-type spectrum, whereas a-type lines cannot be observed at all.

3.1. Overall rotation and nitrogen inversion tunneling

As mentioned before, all heavy atoms are located almost within one plane. The inversion motion can be considered as a tunneling of the amino hydrogen from one energy minimum at one side of this plane to an equivalent minimum on the other side of the plane (see equilibrium structure I and II in Figure 1). This causes the lowest vibrational level (v = 0) to split into a lower symmetric (+) sublevel and a higher antisymmetric (−) sublevel. In the equilibrium geometry, the c axis is only approximately perpendicular to the plane containing the heavy atoms and if the hydrogen atom moves during the tunneling process, the principal axes of inertia are not conserved. Therefore, Eckart conditions are applied to allow for reorientation of the principal axes while the molecule undergoes large amplitude motions.[9] The sign of the c dipole component is exchanged (compare Figure 1) during the tunneling motion causing the selection rules (+) ↔ (−) and (−) ↔ (+) for the c type transitions. The sign
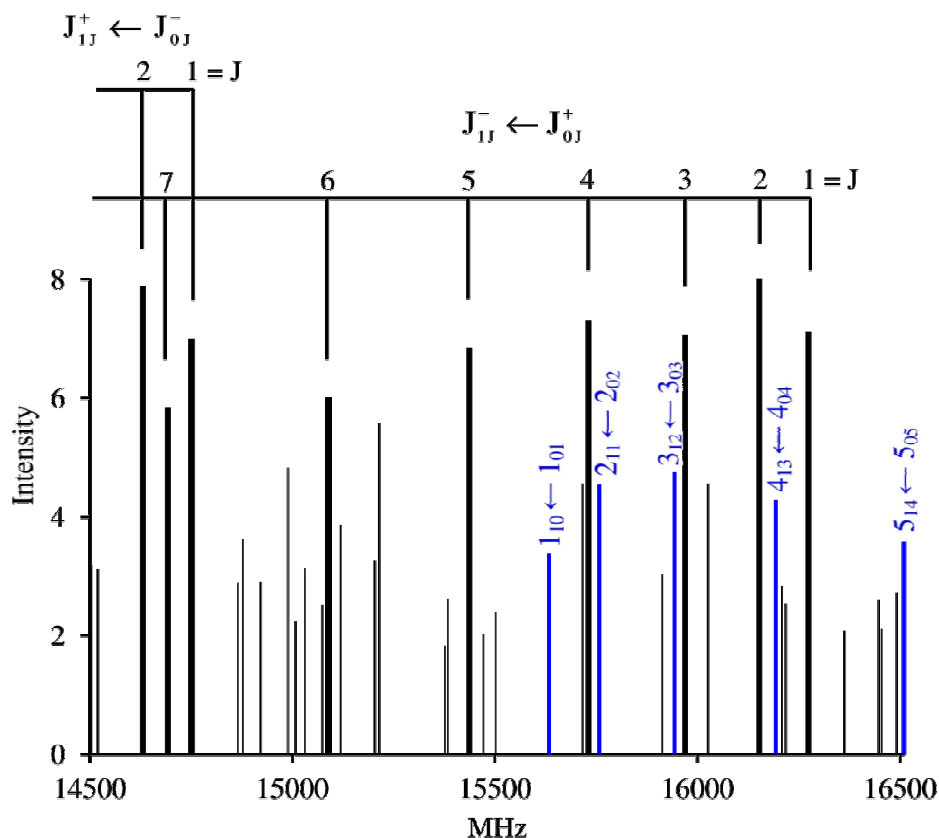
FIG. 2 Broadband scan of diethyl amine in the range of 14.5 to 16.5 GHz. Q branch b-type transitions are marked in blue. The c-type transitions are shown as thick lines. They are split into two components due to proton tunneling.

of the b dipole component does not change upon inversion and the selection rules $(+) \leftrightarrow (+)$ and $(-) \leftrightarrow (-)$ are obtained for b-type transitions.

These selection rules can be derived in detail by group theoretical methods. Diethyl amine has a C_S point group symmetry with a bc mirror plane. If proton tunneling is forbidden, there is only one feasible operator, the operator $(C_1C_4)(C_2C_3)(1\ 10)(29)(38)(46)(57)^*$. This operator is abbreviated as A*. For atom labels see Figure 1.

The operator A* has the same effect as a consecutive application of the operators E* and $(C_1C_4)(C_2C_3)(1\ 10)(29)(38)(46)(57)$, although both individual operators are not feasible (see Figure 3). The E operator is a neutral element and exists in every group. No further feasible operators exist in the case of rigid diethyl amine. Its molecular symmetry group is therefore $C_S(M) = \{E, A^*\}$.

If proton tunneling at the nitrogen atom is enabled, two further operators become feasible. The operator $(C_1C_4)(C_2C_3)(1\ 10)(28)(39)(47)(56)$ corresponds to a rotation of the whole
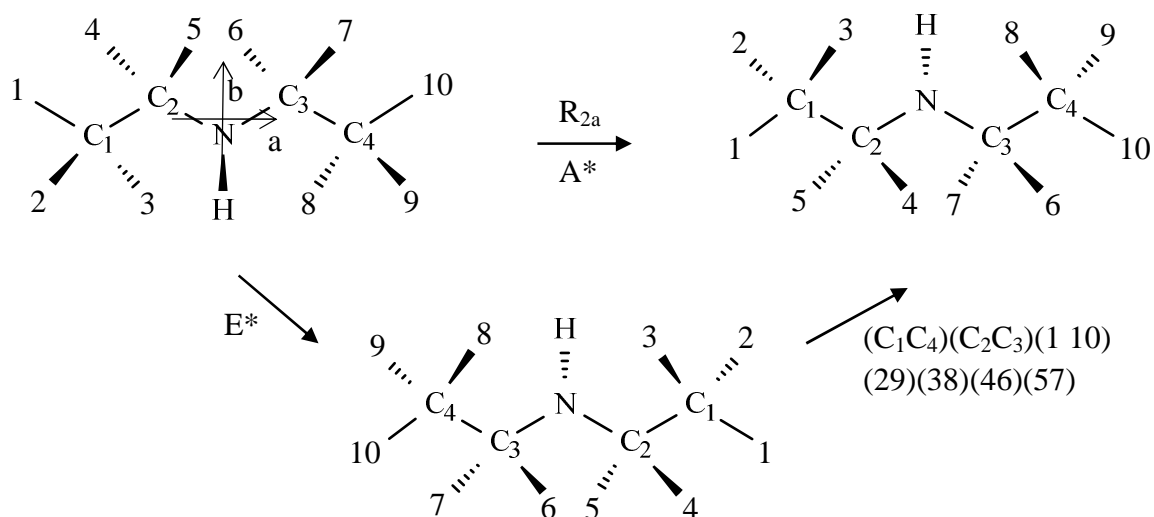
FIG. 3 Operator A* with the same effect as a consecutive application of the operators E* and $(C_1C_4)(C_2C_3)(1\ 10)(29)(38)(46)(57)$.
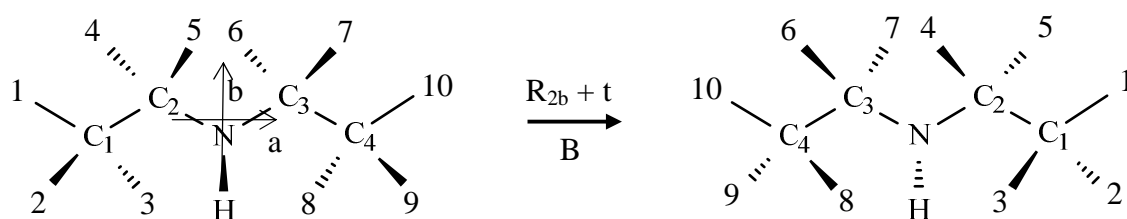
FIG. 4 Operator B with the same effect as a application of the operators $(C_1C_4)(C_2C_3)(1\ 10)(29)(38)$ $(46)(57)$ and proton tunneling (t) at the nitrogen atom.
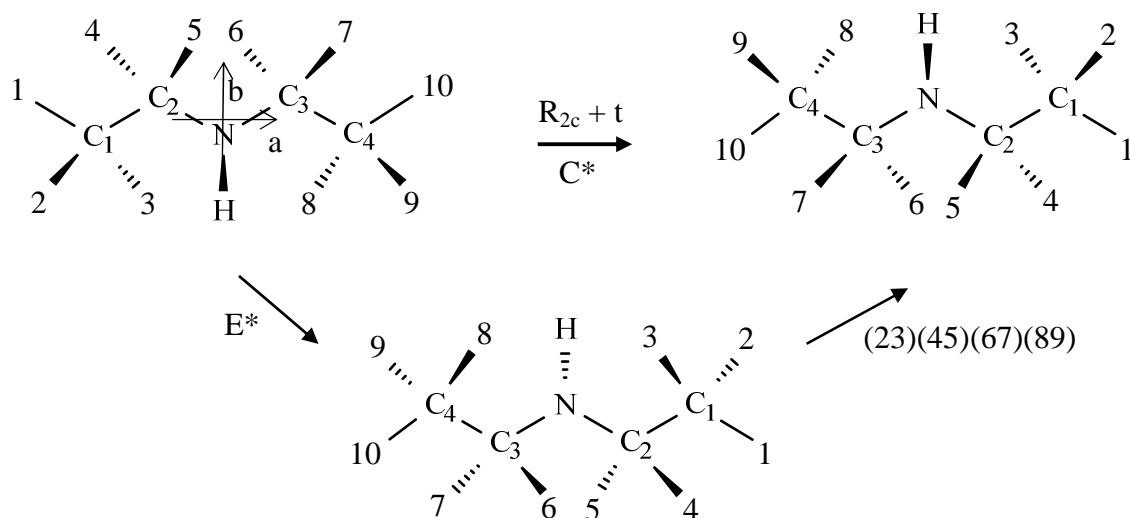
FIG. 5 Operator C* with the same effect as a consecutive application of the operators E* and $(23)(45)(67)(89)$.

Table 1

The multiplication table of the molecular symmetry group of diethyl amine. The operators R_{2a}, $R_{2b} + t$, and $R_{2c} + t$ are commutative.

	E	R_{2a}	$R_{2b} + t$	$R_{2c} + t$
E	E	R_{2a}	$R_{2b} + t$	$R_{2c} + t$
R_{2a}	R_{2a}	E	$R_{2c} + t$	$R_{2b} + t$
$R_{2b} + t$	$R_{2b} + t$	$R_{2c} + t$	E	R_{2a}
$R_{2c} + t$	$R_{2c} + t$	$R_{2b} + t$	R_{2a}	E

Table 2

The character table of the molecular symmetry group of diethyl amine which is isomorphic to the character table of the "Four group" (V).

V	E	R_{2a} A*	$R_{2b} + t$ B	$R_{2c} + t$ C*	μ	Ψ_{rot}	Ψ_t
A	1	1	1	1		ee	+
B_a	1	1	−1	−1		eo	−
B_b	1	−1	1	−1	μ	oo	
B_c	1	−1	−1	1		oe	

molecule by 180° around the *b* axes (see Figure 4). This operator will be called the B operator throughout this chapter.

Another feasible operator is (23)(45)(67)(89)*, abbreviated as C*. Like A*, this operator can be considered as a subsequent application of E* and (23)(45)(67)(89). This operator corresponds to a rotation of the whole molecules by 180° around the *c* axes (see Figure 5).

There are four feasible elements of „floppy" diethyl amine, {E, R_{2a}, $R_{2b} + t$, $R_{2c} + t$}. The multiplication table (Table 1) shows that these four elements generate a group, which is isomorphic to the V-group. Therefore, the molecular symmetry group of diethyl amine should be identical with the character table of the V-group (Table 2).

The selection rule for an allowed transition from the energy level *m* to *n* is

$$\int_{\tau} \Psi_m^* \hat{\mu} \Psi_n d\tau \neq 0 \ .$$

(1)

The symmetry species of the rotational tunneling wave function and the dipole moment operator obey:

Table 3

Selection rules for the rotation inversion transitions of diethyl amine

$\Gamma_{\Psi_{rot,m}}$	$\otimes$	$\Gamma_{\Psi_{t,m}}$	$\otimes$	Γ_{μ}	$\otimes$	$\Gamma_{\Psi_{rot,n}}$	$\otimes$	$\Gamma_{\Psi_{t,n}}$	$= A$	Selection rules	
A	$\otimes$	A	$\otimes$	B_b	$\otimes$	B_b	$\otimes$	A	$= A$	$A \leftrightarrow B_b$	$ee^+ \leftrightarrow oo^+$
B_a	$\otimes$	A	$\otimes$	B_b	$\otimes$	B_c	$\otimes$	A	$= A$	$B_a \leftrightarrow B_c$	$eo^+ \leftrightarrow oe^+$
A	$\otimes$	B_a	$\otimes$	B_b	$\otimes$	B_b	$\otimes$	B_a	$= A$	$A \leftrightarrow B_b$	$ee^- \leftrightarrow oo^-$
B_a	$\otimes$	B_a	$\otimes$	B_b	$\otimes$	B_c	$\otimes$	B_a	$= A$	$B_a \leftrightarrow B_c$	$eo^- \leftrightarrow oe^-$
A	$\otimes$	A	$\otimes$	B_b	$\otimes$	B_c	$\otimes$	B_a	$= A$	$A \leftrightarrow B_c$	$ee^+ \leftrightarrow oe^-$
B_a	$\otimes$	A	$\otimes$	B_b	$\otimes$	B_b	$\otimes$	B_a	$= A$	$B_a \leftrightarrow B_b$	$eo^+ \leftrightarrow oo^-$
A	$\otimes$	B_a	$\otimes$	B_b	$\otimes$	B_c	$\otimes$	A	$= A$	$A \leftrightarrow B_c$	$ee^- \leftrightarrow oe^+$
B_a	$\otimes$	B_a	$\otimes$	B_b	$\otimes$	B_b	$\otimes$	A	$= A$	$B_a \leftrightarrow B_b$	$eo^- \leftrightarrow oo^+$

$$\Gamma_{\Psi_{t,rot,m}} \otimes \Gamma_{\mu} \otimes \Gamma_{\Psi_{t,rot,n}} = A \tag{2}$$

If the representation of the rotation-inversion wave function $\Gamma_{\Psi_{t,rot}}$ is replaced by the product of the representations of the rotational wave function $\Gamma_{\Psi_{rot}}$ and the torsional wave function $\Gamma_{\Psi_{t}}$, one obtaines

$$\Gamma_{\Psi_{rot,m}} \otimes \Gamma_{\Psi_{t,m}} \otimes \Gamma_{\mu} \otimes \Gamma_{\Psi_{rot,n}} \otimes \Gamma_{\Psi_{t,n}} = A \ . \tag{3}$$

The dipole moment vector in the space fixed coordinate system transforms like B_b (the sign is changed under the inversion operations A* and C*). The symmetric tunneling wave function (+) transforms like A (the sign remains for all operations) and the antisymmetric function (−) transforms like B_b (the sign changes for operations containing the tunneling operation t). The selection rule for all possible combinations of $\Gamma_{\Psi_{rot,m}}$ and $\Gamma_{\Psi_{t,n}}$ are given in Table 3.

The *b*-type transitions $A \leftrightarrow B_b$ and $B_a \leftrightarrow B_c$ are always associated with $(+) \leftrightarrow (+)$ and $(-) \leftrightarrow (-)$ selection rules for the tunneling sublevels. The energy differences are the same for $(+) \leftrightarrow (+)$ and $(-) \leftrightarrow (-)$ transitions (see Figure 6), and therefore *b*-type transitions do not split in the rotational spectrum. In contrary, *c*-type transitions $A \leftrightarrow B_c$ and $B_a \leftrightarrow B_b$ are always associated with $(+) \leftarrow (-)$ and $(-) \leftarrow (+)$ transitions between the tunneling sublevel. As can be seen in Figure 7 the energy difference between the $(+) \leftarrow (-)$ and the $(-) \leftarrow (+)$ is $2\Delta E$, if ΔE indicates the tunneling splitting of a rotational energy level. Therefore, all *c*-type lines are split by $2\Delta E/h$.
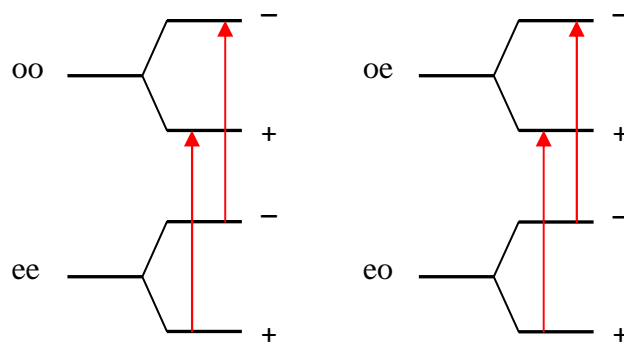
FIG. 6 Selection rules for *b*-type transitions
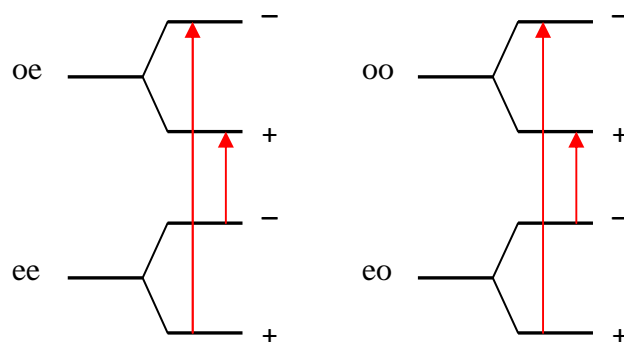
FIG. 7 Selection rules for *c*-type transitions

In the case of dimethyl amine, the separation between the (+) and the (−) sublevel was approximately 1.323 GHz causing the *c*-type lines to split into doublets separated by 2.646 GHz. The selection rules for the *b*-type transitions predict these lines to be unsplit, however, due to Coriolis interaction a narrow splitting usually below 100 kHz is observed.

For the assignment a broadband scan in the range from 14.5 to 16.5 GHz was recorded (Figure 2). As a first step, a rigid rotor spectrum based on the rotational constants from the quantum chemical calculations was predicted. The *b*-type Q branch lines $J_{1,J-1} \leftarrow J_{0,J}$ (marked in blue in Figure 2) were immediately identified and were used to improve the $A - (B + C)/2$ and the $B - C$ rotational constants. In a second step, the center frequencies of the *c*-type Q branch $J_{1,J} \leftarrow J_{0,J}$ were predicted. Since the inversion splitting was unknown at that time, the calculated spectrum was shifted to higher frequencies and at an offset of 0.761 GHz the observed and calculated spectra matched. This was confirmed by shifting the calculated frequencies by the same offset to lower frequencies, where the transitions $1_{11}^{+} \leftarrow 1_{01}^{-}$ and $2_{12}^{+} \leftarrow 2_{02}^{-}$ were found. Therefore, the splitting of the rotational lines due to inversion was found to be 1.522 MHz.

3.2. ^{14}N nuclear quadrupole coupling

All lines of the assigned c-type Q branch $J_{1J} \leftarrow J_{0J}$ appear as multiplets with a different number of lines. The two inversion components $(+) \leftarrow (-)$ and $(-) \leftarrow (+)$ of the $1_{11} \leftarrow 1_{01}$ transition are sextets. For $J = 2$ to $J = 5$ septets were found and for $J > 5$ only triplets could be measured. Therefore, we attribute these splittings to ^{14}N hyperfine quadrupole coupling. It was surprising that even for $J = 5$ septets could be observed, since the intensity of the $F \leftrightarrow F+1$ transitions should be only 1.09% of the total multiplet intensity.

3.3. Methyl internal rotation

All components of the ^{14}N quadrupole hyperfine multiplets were split again into triplets. These splittings are on the order of 20 kHz, which is the same order of magnitude Fliege et al. have reported for ethyl fluoride.[10] Therefore, we conclude that also in the case of diethyl amine the barrier should be on the order of 1171 cm^{-1} as in ethyl fluoride. The triplet structure is often found for molecules with two equivalent methyl groups with a high hindering potential.[11] A typical spectrum is shown in Figure 8.

4. Analysis and discussion

After the structure of the spectrum was roughly understood, a global analysis of the overall rotation, the N inversion tunneling, and the ^{14}N nuclear quadrupole coupling was carried out using the program *spfit* written by Pickett.[12] For this purpose the effective Hamiltonian was used.

$$H = \sum_{v=0}^{1} |v\rangle \left(H_R + H_\Delta^v + H_{NQ}(\chi_a, \chi_{bb} - \chi_{cc}) \right) \langle v | + \left(|0\rangle\langle 1| + |1\rangle\langle 0| \right) \left(H_C + H_{NQ}(\chi_{bc}) \right) \tag{4}$$

$|0\rangle$ and $|1\rangle$ represent the symmetric $(+)$ and the antisymmetric $(-)$ inversion state, respectively. The notation is similar to that used by Christen et al.[13]

The operator

$$H_R = AJ_a^2 + BJ_b^2 + CJ_c^2 - \Delta_J J^4 - \Delta_{JK} J^2 J_a^2 - \Delta_K J_a^4 \\ - \delta_J J^2 (J_+^2 + J_-^2) - \tfrac{1}{2}\delta_K [J_a^2, (J_+^2 + J_-^2)]_+ \tag{5}$$

with $J_\pm = J_b \pm iJ_c$ and the anti-commutator $[.., ..]_+$ describes the overall rotation and the centrifugal distortion in terms of Watson's A reduction in the I^r representation.[14]
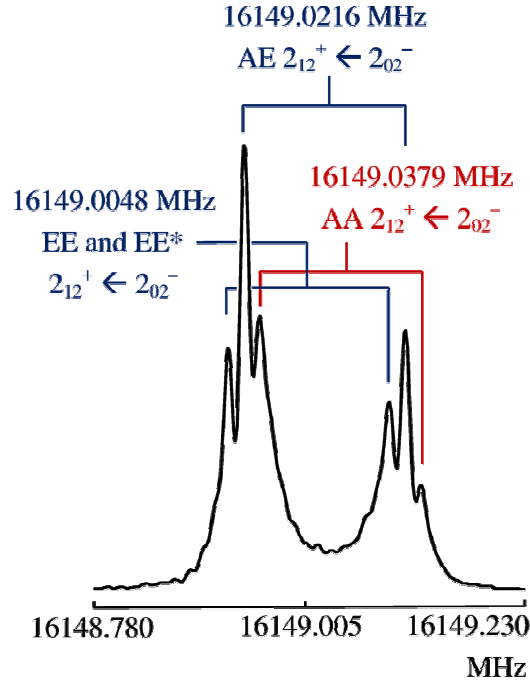
FIG. 8. The F: $1 \leftarrow 2$ hyperfine component of the $2^-_{12} \leftarrow 2^+_{02}$ transition of diethyl amine with splittings due to internal rotation of two methyl groups. Doppler splittings are marked by brackets. For symmetry labels see chapter 6.

The rotational constants A, B, C, and the centrifugal distortion constants Δ_J, Δ_{JK}, Δ_K, δ_J, δ_K are assumed to be the same for both, the $|0\rangle$ and $|1\rangle$ state.

The inversion splitting between the $|0\rangle$ and the $|1\rangle$ energy levels and its J and K dependence is expressed by the operator

$$H^v_\Delta = vE + \tfrac{1}{2}(-1)^v \left(E_J J^2 + E_K J^2_a + E_2 (J^2_+ + J^2_-) + E_{JK} J^2 J^2_a \right) \tag{6}$$

The Coriolis coupling operator is connecting the $|0\rangle$ and the $|1\rangle$ state. It is given by

$$H_C = F_{bc} (J_b J_c + J_c J_b) \ . \tag{7}$$

Finally, the operator of nuclear quadrupole coupling has both, diagonal and off-diagonal matrix elements in the inversion quantum number v. It is represented by the expression

$$H_{NQ} = V^{(2)} \cdot Q^{(2)} \ . \tag{8}$$

$V^{(2)}$ and $Q^{(2)}$ the second rank irreducible tensor operators of the electric field gradient tensor and the nuclear quadrupole tensor, respectively. Details of treating nuclear quadrupole

coupling using the irreducible tensor method is given in ref. [15]. Again, the nuclear quadrupole coupling constants χ_{fg}, f, g $\in \{a, b, c\}$ are assumed to be the same for both inversion states.

Matrix elements associated with the diagonal coupling constants χ_{aa} and $\chi_{bb} - \chi_{cc}$ are also diagonal in the $|0\rangle$ and in the $|1\rangle$ state, respectively. The influence of the off-diagonal constant χ_{bc} is only a second-order effect associated with the operator $J_b J_c + J_c J_b$. Its matrix elements diagonal in the inversion quantum number are zero, but as in the Coriolis coupling operator H_C they are non-zero for matrix element connecting the $|0\rangle$ and the $|1\rangle$ state.

It should be noted that the absolute sign of the Coriolis coupling constant F_{bc} and the off-diagonal nuclear quadrupole coupling constant χ_{bc} cannot be obtained from the experiment because it depends on how the directions of the principal axes of inertia are defined. However, the quantity sign(F_{bc}) / sign(χ_{bc}), which might be called the relative sign, is well-defined. Constants associated with the operators $J_a J_b + J_b J_a$ and $J_a J_c + J_c J_a$ are zero because the proton tunneling in diethyl amine is restricted to the bc plane.

A list of all transitions included in the fit is given in the Appendix in Table H-2. The fitted parameters and a comparison with quantum chemical calculations are shown in Table 4. The parameter definition (*.par) file of the program *spfit* is also in the Appendix (Table H-3).

All rotational constants agree better than 0.6% with the values obtained by quantum chemical calculations at the MP2/6-311++G(d,p) level of theory. This agreement is surprisingly good because the *ab initio* data refer to the equilibrium geometry of the molecule whereas the experimental constants are obtained for the vibrational ground state and no corrections were made. The quartic centrifugal distortion constants Δ_J, Δ_{JK}, and δ_J could be accurately determined. They have a reasonable order of magnitude for this kind of molecules. The constants Δ_K and δ_K were strongly correlated with other parameters and could not be determined.

The most important constant associated with the inversion tunneling is the separation between the lowest (v = 0) symmetric and antisymmetric inversion energy levels E, a slight *J* and *K* dependence of the level separation is described with the constants E_J, E_{JK}, E_K, and E_2. As in former studies on amines the constant E was used to determine the barrier to inversion using a double minimum potential. Here, we used a modified version of a potential proposed by

Table 4

Parameters describing the overall rotation, nitrogen inversion, and ^{14}N quadrupole coupling of diethyl amine.

Parameter	Unit	Obs.	Calc.	Obs. – Calc.
Overall rotation and centrifugal distortion				
A	GHz	17.61499170(11)	17.7066	−0.0916 (−0.52%)
B	GHz	2.103650248(49)	2.1051	−0.0015 (−0.07%)
C	GHz	1.981332501(47)	1.9831	−0.0018 (−0.09%)
Δ_J	kHz	0.23755(49)		
Δ_{JK}	kHz	−3.1638(25)		
δ_J	kHz	0.025850(44)		
Nitrogen inversion tunneling and Coriolis interaction				
E	MHz	760.77062(20)		
E_J	kHz	1.6114(64)		
E_{JK}	kHz	−0.4550(82)		
E_K	MHz	−0.059444(30)		
E_2	kHz	0.4602(48)		
F_{bc}	MHz	0.45747(28)		
^{14}N *quadrupole coupling*				
χ_{aa}	MHz	2.67576(37)	2.766	−0.090 (−3.4%)
$\chi_{bb}-\chi_{cc}$	MHz	4.34144(65)	4.818	−0.477 (−11.0%)
χ_{bc}	MHz	2.9199(92)	3.244	−0.324 (−11.1%)
Statistical information				
N		228		
σ	kHz	4.4		

Table 5

Calculated energy levels and splittings of diethyl amine.

v	E^+/(kJ/mol)	E^-/(kJ/mol)	$(E^- - E^+)$/(kJ/mol)	$(E^- - E^+)$/h
0	3.402	3.403	0.001	761 MHz
1	9.880	9.899	0.019	46.6 GHz
2	15.423	15.816	0.393	
3	19.514	21.521	2.007	
4	24.617	27.732	3.115	
5	31.102	34.612	3.510	

V_{max} = 18.31 kJ/mol, I_r = 1.013534 uÅ^2, θ_{min} = 54.842°, F/G = 1.5, m_{max} = 20.

Table 6

Potential barrier of proton tunneling in som amines.

	I_r/uÅ^2	θ_{min}/°	E/MHz	V_{max}/(kJ/mol)
dimethyl amine	1.000681	54.162	1323.0	17.17, 18.4(46)[4]
methyl ethyl amine	1.007155	54.528	990.5	17.77, 21.7[6]
diethyl amine	1.013534	54.842	760.771	18.31
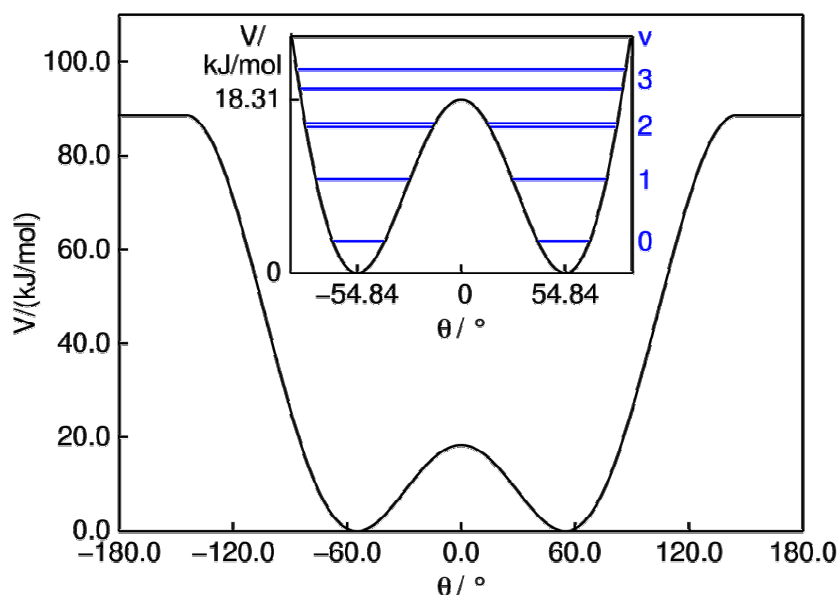
FIG. 9 The double minimum potential as defined in Appendix I used to describe the inversion tunneling at the nitrogen atom. The angle θ is the angle of the NH bond against the NCC plane. For the parameters see Table 6. In the inset, the angles for the calculated equilibrium geometries, the barrier height as determined from the $v = 0$ inversion splitting, and also the inversion levels (in blue) are shown. Each level marked by the v quantum number is split into a (+) and a (−) sublevel (see Table 5).

Weeks, Hecht, and Dennison for ammonia[16] and also used by Penn and Boggs for the inversion tunneling in methyl ethyl amine.[6] Details concerning the model and the method of calculation are given in Appendix I. For diethyl amine, a barrier of 18.31 kJ/mol was found. Some splittings of higher tunneling levels ($v = 1, 2, ...$) calculated with the same model are given in Table 5.

The shape of the double minimum potential and the inversion energy levels are shown in Figure 9. It should be noted that all calculations of the inversion barrier strongly depend on the model potential and on the equilibrium geometry of the molecule. Therefore, the barrier determined might contain a rather large systematic error. However it is useful if it is compared with inversion barriers of other amines determined exactly by the same method.

The results for dimethyl amine, methyl ethyl amine, and diethyl amine are given in Table 6. In all cases, the equilibrium geometry was obtained by quantum chemical calculations at the MP2/6-311++G(d,p) level of theory. All inversion barriers obtained by the same method were found within the narrow range of 17.7 ± 0.7 kJ/mol, whereas the agreement between the barriers reported earlier is worse.
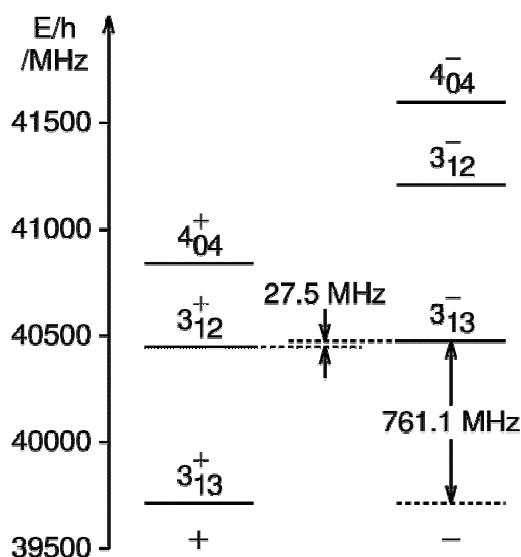
FIG. 10. Energy level diagram showing the near degenerate 3_{12}^+ and 3_{13}^- levels (27.5 MHz) and the inversion splitting of the 3_{13} level (761.1 MHz) into a symmetric (+) and an antisymmetric (−) inversion state. E/h is the rotation-inversion energy in frequency units.
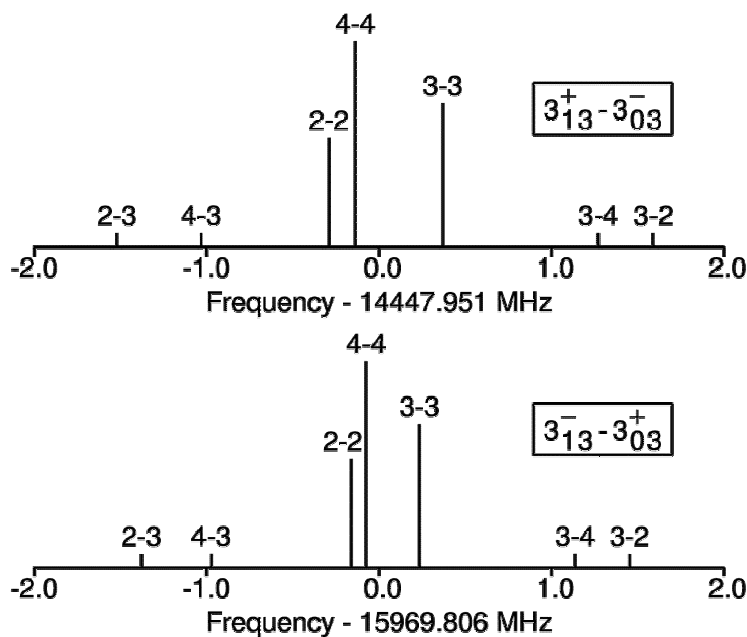
FIG. 11. ^{14}N quadrupole hyperfine structure of the $3_{13} \leftarrow 3_{03}$ transition. Different patterns arise from a perturbation of the 3_{13}^- level, which interacts with the only by 27.5 MHz lower 3_{12}^+ level.

The Coriolis coupling constant is associated with the operator $J_b J_c + J_c J_b$ which has matrix elements connecting the (+) and the (−) inversion state. In the case of diethyl amine the determination of F_{bc} is mainly due to a near degeneracy of the energy levels 3_{12}^+ and 3_{13}^- (Figure 10). These levels are separated by only 27.5 MHz.
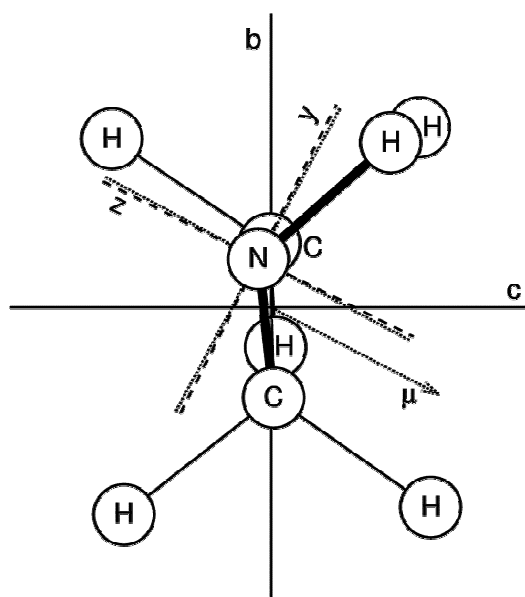
FIG. 12. Experimental and calculated (MP2/6-311++G(d,p)) principal axes x, y, z of the ^{14}N quadrupole coupling tensor. A part of the molecule is drawn as a projection on the bc plane. The bonds of the atoms directly bonded to the N atom are drawn as thick lines. The theoretical axes of the coupling tensor and also the theoretical dipole moment vector μ are dotted, the experimentally determined axes are dashed.

Moreover, the near degeneracy causes a perturbation in the ^{14}N quadrupole coupling splitting associated with one of these levels. An example is shown in Figure 11, where for the same rotational but different inversion transitions different hyperfine patterns are shown. It should be noted that also in other amines such degeneracies are found, e.g. in ^{15}N-dimethyl amine the 1_{10}^{+} and the 1_{11}^{+} level are separated by 66 MHz and by 204 MHz for the normal species.[4] However, these values are much bigger and in the case of ^{14}N dimethyl amine no perturbation of the nuclear quadrupole hyperfine structure has been reported.

The ^{14}N quadrupole coupling constants obtained from the global fit may be directly compared to the quantum chemical results. Here, the deviation of the χ_{aa} constant is only -3.4%. In contrast, the $\chi_{bb} - \chi_{cc}$ and the χ_{bc} constants both differ by -11%. These rather big deviations might have two reasons: (i) When the constants were calculated from the electric field gradient tensor as obtained by quantum chemical calculations, an effective ^{14}N nuclear quadrupole moment of 19.41 mbarn was used. This value depends on the method and basis set and might be not suitable in this case. (ii) The $\chi_{bb} - \chi_{cc}$ and the χ_{bc} constants are averaged under the influence of the inversion tunneling. The χ_{aa} constant is not affected by this averaging process since the tunneling path of the proton is located in the bc plane. The

Table 7

Comparison of principal quadrupole coupling constants (in MHz) of ^{14}N in ammonia and in amines.

	χ_{xx}	χ_{yy}	χ_{zz}	η
ammonia[1]	2.0421	2.0421	−4.0842	0
methyl amine[2]	2.4136	1.9805	−4.3941	−0.099
trans-ethyl amine[3]	2.93	1.75	−4.68	−0.25
dimethyl amine[4]	3.04	2.01	−5.05	−0.20
diethyl amine[a]	2.67576	2.30050	−4.97626	−0.075
trimethyl amine[5]	2.74	2.74	−5.47	0
quinuclidine[b, 17]	2.5958	2.5958	−5.1915	0

$\chi_{xx} \geq \chi_{yy} \geq \chi_{zz}$ (by definition). Asymmetry $\eta = (\chi_{xx}-\chi_{yy}) / \chi_{zz}$.
[a] this work, [b] also called ABCO, 1-azabicyclo[2.2.2]octane.

Table 8

Parameters describing the internal rotation of two methyl groups of diethyl amine.

Parameter	Unit	Value
V_3	kJ/mol	12.5816(68)
	cm^{-1}	1051.74(57)
	GHz	31530(17)
I_γ	uÅ^2	3.172 (fixed)[a]
$\angle(i_1,a)$	°	35.85 (fixed)[a]
$\angle(i_2,a)$	°	144.15 (fixed)[a,b]
$\angle(i_1,b) = \angle(i_2,b)$	°	125.84 (fixed)[a]
$\angle(i_1,c) = \angle(i_2,c)$	°	90.87 (fixed)[a]
N[c]		48
σ[d]	kHz	0.7

[a] calculated from structure optimized at the MP2/6-311++G(d,p) level
[b] $\angle(i_2,a) = 180°-\angle(i_1,a)$ (due to symmetry).
[c] number of torsional splittings
[d] standard deviation of the fit

quadrupole constants were transformed into its principal axes. This allows for comparison with other amines. The results are shown in Table 7. The χ_{zz} value of −4.97626 MHz found for diethyl amine is in excellent agreement with $\chi_{zz} = −5.05$ MHz reported for dimethyl amine. The corresponding absolute values of ammonia and primary amines are usually lower, those of tertiary amines a slightly higher. Unfortunately, in some cases the accuracy of the reported coupling constants is not sufficient for a more detailed comparison. In Figure 12, the orientation of the principal axes of the coupling tensor relative to the principal axes of inertia

Table 9

Barriers to internal rotation of the methyl groups in dependence of the electro negativity.

Molecule	Structure	Symmetry	Barrier / cm^{-1}	EN
methyl propionate	**CH$_3$**-CH$_2$-COO-CH$_3$	C$_S$	817.1(15)	C: 2.55
diethyl ketone	**CH$_3$**-CH$_2$-(C=O)-CH$_2$-**CH$_3$**	C$_{2v}$	771.93(27)	
diethyl amine	**CH$_3$**-CH$_2$-NH-CH$_2$-**CH$_3$**	C$_S$	1051.74(57)	N: 3.04
trans ethyl acetate	CH$_3$-COO-CH$_2$-**CH$_3$**	C$_S$	1061.4(68)	O: 3.44
ethyl fluoride[10]	**CH$_3$**-CH$_2$-F	C$_S$	1171.3(14)	F: 3.98

is shown. The *z* axis of the coupling tensor points into a direction where the maximum charge density of the nitrogen lone pair is expected. This also agrees nicely with the direction of the calculated dipole moment vector. To determine the barrier to internal rotation, some selected *c*-type transitions showing torsional splittings (also that one in Figure 8) were fitted with the program XIAM. Here, the splittings $\nu_{EE} - \nu_{AA}$, $\nu_{EE} - \nu_{AE}$, and $\nu_{EE} - \nu_{EE*}$ instead of the absolute line frequencies were fitted. For the nomenclature of the torsional substates see Chapter 6. All other parameters like the rotational constants and the angles between the internal rotor axes and the inertial axes were fixed and only the barrier to internal rotation was fitted. The result is given in Table 8. A list of all fitted lines is given in the Appendix (Table H-4).

The barrier to internal rotation was found to be approximately 1050 cm^{-1} which is in a good agreement with the barrier of about 1100 cm^{-1} of the methyl group found in ethyl fluoride[10] and ethyl acetate (Chapter 1), but much higher than the value of 772 cm^{-1} found in diethyl ketone (Chapter 6). The reason for a lower barrier in diethyl ketone might be due to the inductive effect of the carbonyl group (see Table 9).

5. Conclusion

From the microwave spectrum of diethyl amine as recorded under molecular beam conditions molecular parameters were determined which allowed to reproduce the observed spectrum within experimental accuracy. The analysis was carried out using an effective Hamiltonian accounting for overall rotation, centrifugal distortion, nitrogen inversion, and ^{14}N nuclear

quadrupole coupling. In contrast to previous work on dimethyl amine[4] and methyl ethyl amine,[6] the inversion splittings of diethyl amine were described with molecular parameters instead of reporting the splitting of each single rotational transition.

From the inversion splittings of diethyl amine and those splittings reported for dimethyl amine and methyl ethyl amine the barriers to nitrogen inversion were calculated. This analysis was based on simple model potential and on geometry parameters obtained by the same quantum chemical methods and basis sets for all three molecules. As a result, the inversion barriers were found consistently in a range of 17.7 ± 0.7 kJ/mol.

Due to a near degeneracy of the 3^-_{13} and the 3^+_{12} levels, which are separated by an energy difference of only 27.5 MHz, it became possible to determine the complete ^{14}N quadrupole coupling tensor. Thereby, also its principal axes could be determined without additional information from isotopic substitution. This is interesting because the z axis of the coupling tensor might be associated with the direction of the lone pair at the nitrogen atom. By comparison with the results of quantum chemical calculations the influence of vibrational averaging due to the nitrogen inversion could be identified.

Finally, due to the inherently high resolution of MB-FTMW spectroscopy narrow splittings due to internal rotation of the methyl groups were resolved and analyzed to give the torsional barrier of 12.5816(68) kJ/mol.

This work is also considered as a reference for future studies to be carried out on other amines. Most parameters have been determined with a higher accuracy compared to the studies on dimethyl amine and methyl ethyl amine. Again, this is mainly due to the inherently high resolution of the MB-FTMW spectroscopy, a method which was not available at the time the older studies were carried out. It is also due to the availability of the easy to use and extremely flexible programs *spfit* and *spcat* by Pickett. Finally, it is due to a perturbation between two rotorsional energy levels. Such perturbations are also found in the other amines, but there the energy levels do not come as close together as in diethyl amine. However, it is believed that remeasurement and reanalysis of the spectra of the other amines will significantly improve the molecular parameters.

6. Appendix I: Proton tunneling

In order to obtain the hindering barrier from the observed nitrogen inversion splitting a model potential was chosen, since the exact potential and the tunneling path is usually not known. Several double minimum potentials have been described, e.g. that of Manning[18] or that of Weeks, Hecht, and Dennison.[16] The latter one has already been used by Penn and Boggs for the inversion tunneling in methyl ethyl amine[6] and it will also be used here with slight modifications concerning the boundaries and the potential offset. The potential is assumed be periodic in 2π.

$$V(\theta) = \frac{F^2}{4G} + 2G - 2F\cos\frac{\theta}{L} + 2G\cos\frac{2\theta}{L} \quad \text{for} \quad -\pi L \le \theta \le \pi L \quad (9)$$

$$V(\theta) = \frac{F^2}{4G} + 2F + 4G \quad \text{for} \quad \left\{ \begin{array}{l} -\pi \le \theta < -\pi L \text{ and} \\ \pi L < \theta < \pi \end{array} \right. \quad (10)$$

The parameter L is determined by the angles θ_{min}, where the potential is $V(\theta_{min}) = 0$.

$$\cos\frac{\theta_{min}}{L} = \frac{F}{4G} \quad (11)$$

F and G are positive parameters. Following the method of Penn and Boggs,[6] they were fixed at a constant ratio of $F/G = 1.5$. However, the following expressions hold also for the general case of arbitrary F/G ratios. The height of the inversion barrier can be expressed as

$$V_{max}(\theta = 0) = \frac{F^2}{4G} + 4G - 2F. \quad (12)$$

With this potential the Hamiltonian has the same form as in ref. [16].

$$H = -D\frac{d^2}{d\theta^2} + V(\theta) \quad (13)$$

The parameter D is defined by

$$D = \frac{\hbar^2}{2I_r} \quad (14)$$

with the reduced moment of inertia I_r, which refers to the rotation of the amine H atom on a circular path around the N atom against the molecular frame. Likewise, D can be expressed in frequency units by the rotational constant $D_\nu = D/h$.

The Hamilton matrix was set up in the basis of the planar rotor wave functions

$$|m\rangle = \sqrt{\frac{1}{2\pi}} e^{im\theta}, \quad i^2 = -1 \tag{15}$$

and truncated at a certain $m = m_{max}$. The matrix elements are given by

$$
\begin{aligned}
\langle m | H | n \rangle &= Dm^2 f(n-m,\pi) \\
&\quad + \left(\frac{F^2}{4G} + 2G \right) f(n-m,\pi L) \\
&\quad - F \left[f(n-m+\tfrac{1}{L},\pi L) + f(n-m-\tfrac{1}{L},\pi L) \right] \\
&\quad + G \left[f(n-m+\tfrac{2}{L},\pi L) + f(n-m-\tfrac{2}{L},\pi L) \right] \\
&\quad + \left(\frac{F^2}{4G} + 2F + 4G \right) \left[f(n-m,\pi) - f(n-m,\pi L) \right]
\end{aligned}
\tag{16}
$$

with

$$f(r,A) = \frac{1}{2\pi} \int_{-A}^{A} e^{ir\theta} d\theta = \begin{cases} \frac{1}{\pi}A & \text{if} \quad r = 0 \\ \frac{1}{r\pi}\sin rA & \text{if} \quad r \neq 0. \end{cases} \tag{17}$$

The energy eigenvalues were obtained by diagonalization of the Hamilton matrix using the Jacobi method. The eigenvalues are labeled by 0^+, 0^-, 1^+, 1^-, 2^+, 2^-, ... in an ascending order of energy.

Acknowledgments

Publication statement

Part of this work is published in Journal of Chemical Physics under H. V. L. Nguyen and W. Stahl, *J. Chem. Phys.* **135**, 024310 (2011), doi:10.1063/1.3607992.

References

[1] G. R. Gunther-Mohr, R. L. White, A. L. Schawlow, W. E. Good, D. K. Coles, *Phys. Rev.* **94**, 1184 (1954).

[2] M. Kręglewski, W. Stahl, J.-U. Grabow, G. Wlodarczak, *Chem. Phys. Lett.* **196**, 155 (1992).

[3] E. Fischer and I. Botskor, *J. Mol. Spectrosc.* **91**, 116 (1982).

[4] J. E. Wollrab and V. W. Laurie, *J. Chem. Phys.* **48**, 5058 (1968).

[5] D. R. Lide, Jr. and D. E. Mann, *J. Chem. Phys.* **28**, 572 (1958).

[6] R. E. Penn and J. E. Boggs, *J. Mol. Spectrosc.* **47**, 340 (1973).

[7] J.-U. Grabow and W. Stahl, *Z. Naturfosch.* **45a**, 1043 (1990).

[8] B. S. Ray, *Z. Phys.* **78**, 74 (1932).

[9] C. Eckart, *Phys. Rev.* **47**, 552 (1935).

[10] E. Fliege, H. Dreizler, J. Demaison, D. Boucher, J. Burie, A. Dubrulle, *J. Chem. Phys.* **78**, 3541 (1983).

[11] H. Dreizler, *Z. Naturforsch.* **16a**, 1354 (1961).

[12] H. M. Pickett, *J. Mol. Spectrosc.* **148**, 371 (1991).

[13] D. Christen and H. S. P. Müller, *Phys. Chem. Chem. Phys.* **5**, 3600 (2003).

[14] J. K. G. Watson, J. R. Durig (Ed.), Vibrational Spectra and Structure, Vol. 6, Elsevier, Amsterdam, 1977.

[15] W. Gordy and R. L. Cook, Microwave Molecular Spectra, John Wiley & Sons, New York, 1984, 3rd edition, chapter XV.

[16] W. T. Weeks, K. T. Hecht, D. M. Dennison, *J. Mol. Spectrosc.* **8**, 30 (1962).

[17] D. Consalvo and W. Stahl, *J. Mol. Struct.* **447**, 119 (1998).

[18] M. F. Manning, *J. Chem. Phys.* **3**, 136 (1935).

Chapter 9

METHYL *tert*-BUTYL AMINE

Nitrogen inversion tunneling, ^{14}N nuclear quadrupole, and internal rotation in an almost prolate symmetric top $(\kappa = -0.994)$

1. Introduction

The investigation on diethyl amine was a strong motivation for further studies on secondary amines. As mentioned in Chapter 8, the proton inversion tunneling at the nitrogen atom was studied only in the cases of dimethyl amine,[1] ethyl methyl amine,[2] and diethyl amine so far. The resulting inversion splitting of all *c*-type rotational transitions is 2646.0 MHz, 1981.0 MHz, and 1521.542 MHz, respectively. A precondition for proton inversion tunneling is the existence of two equilibrium structures, i.e. a double minimum potential. Therefore, transition state of the molecule should have a symmetry plane.

In the case of methyl *tert*-butyl amine only a few geometries can be generated due to the C_{3v} symmetry of both the methyl group and the *tert*-butyl group. The molecule is an isomer of diethyl amine and can be considered as similar to dimethyl amine, a similarity as in the case of acetone (Chapter 7) and pinacolone.[3] Therefore, when we decided to investigate methyl *tert*-butyl amine we expected also in this case a splitting due to nitrogen inversion tunneling.

In Chapter 8, we found that the splitting due to internal rotation of two equivalent methyl groups in diethyl amine could be resolved. The barrier was determined to be 1051.74(57) cm^{-1}. The comparison in Table 9 (Chapter 8) has shown that the barrier to internal rotation does not only depend on the structure analogy, but also on the electronegativity of the neighboring group. The splittings due to internal rotation of the methyl group in methyl *tert*-butyl amine were expected to be in the same order as in the case of diethyl amine and, consequently, should be resolved with our spectrometer. It is interesting to determine the barrier, since the methyl group is attached directly to the nitrogen atom and no information about potential parameter was reported for dimethyl amine and ethyl methyl amine.

As in diethyl amine, the ^{14}N nucleus has a nuclear spin of $I = 1$ and hyperfine splittings on the order of 0.5 MHz were expected for all rotational transitions. With the combination of both
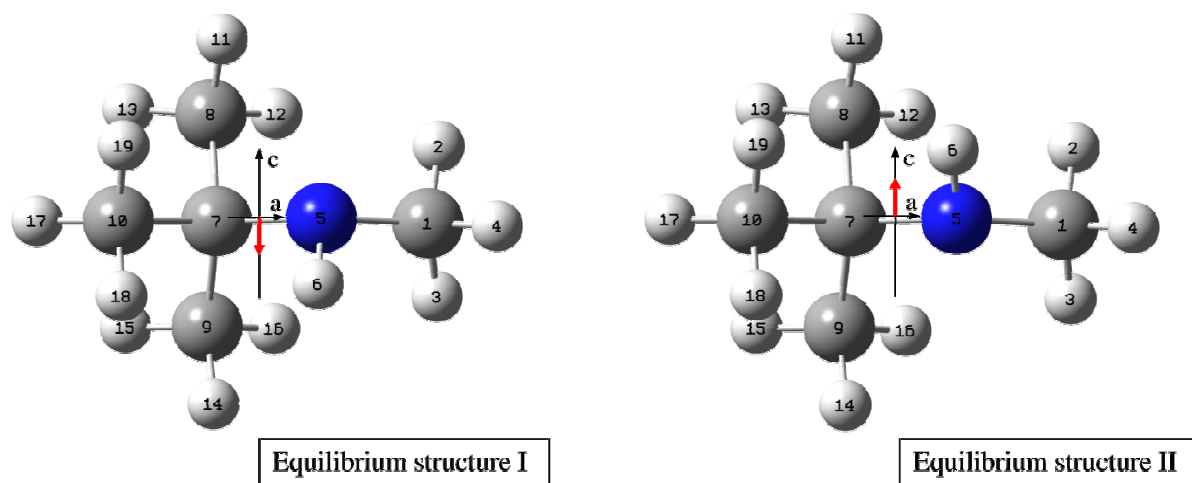
FIG. 1 Two equilibrium geometries of methyl *tert*-butyl amine corresponding to the two energy minima of the nitrogen tunneling process. The principal *a* and *c* axes of inertia are indicated showing that the dipole component (red arrow) in *c* direction changes sign upon proton tunneling.

effects, quadrupole hyperfine structure and internal rotation, methyl *tert*-butyl amine was expected to show an interesting and complicated rotational spectrum.

2. Quantum chemistry

In order to have reasonable rotational constants for the spectral assignment, quantum chemical calculations were carried out before the microwave spectrum was recorded. As mentioned in the introduction, due to the C_{3v} symmetry of the methyl and the *tert*-butyl group only a few start geometries can be generated. At the beginning, four different start geometries at the dihedral angle $\varphi = \angle(C_{10}, C_7, N, C_1) = 180°, 150°, 120°,$ and $90°$ (for atom numbers see Figure 1) were optimized at the MP2/6-311++G(d,p) level of theory using the program *Gaussian09*. Only one conformer was found. The Cartesian coordinates are available in Table I-1 in the Appendix. The two equivalent equilibrium structures connected by the tunneling path are given in Figure 1.

It should be noted that the equilibrium structure of methyl *tert*-butyl amine has almost a C_S symmetry if the proton attached to the nitrogen atom is neglected. The rotational constants were calculated to be A = 4.3700 GHz, B = 2.6375 GHz, and C = 2.6275 GHz. The B and C constants differ by only 10 MHz. Therefore, methyl *tert*-butyl amine is a very near prolate top with a Ray's parameter of $\kappa = -0.989 \approx -1.0$.[4] Consequently, the coarse structure of the microwave spectrum was expected to be quite clear. The rotational lines should form groups of lines, which will be call multiplets from now and exist within narrow frequency ranges.
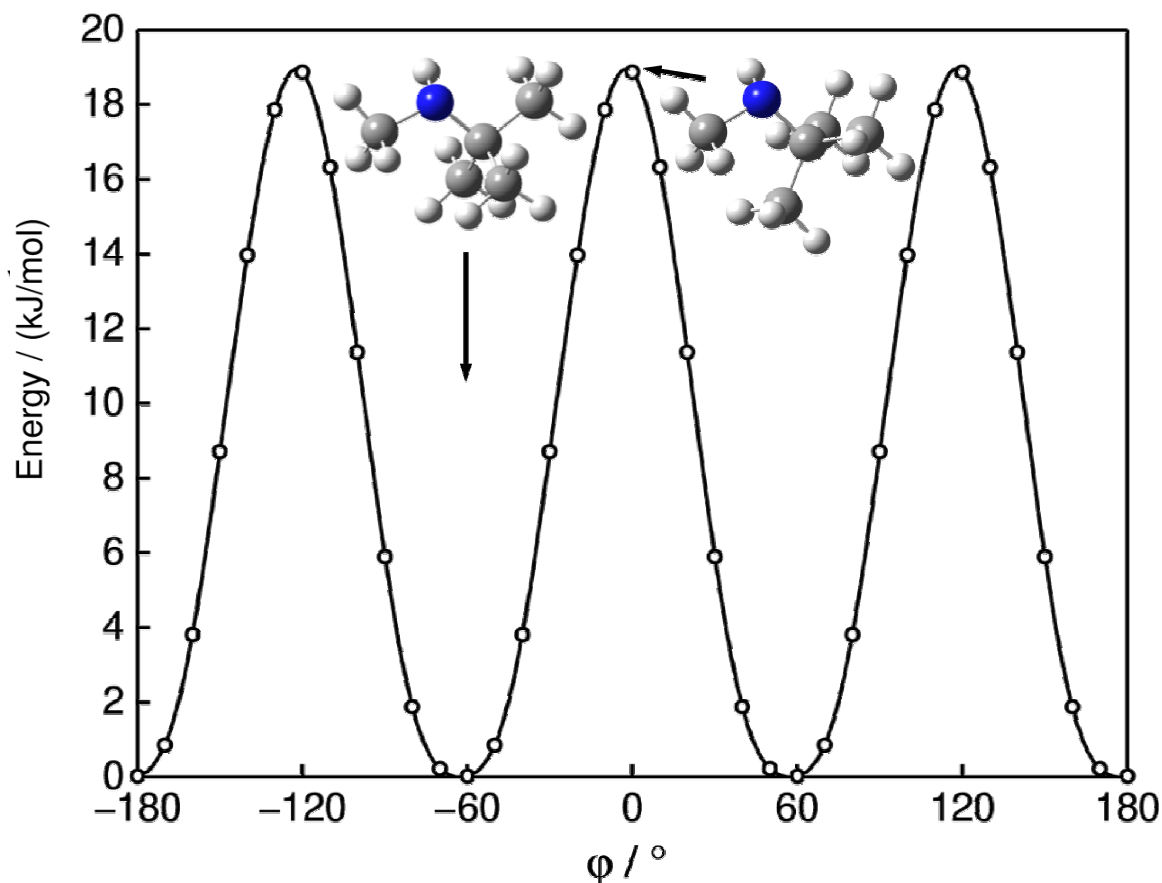
FIG. 2 The energy minimum path of methyl *tert*-butyl amine calculated at the MP2/6-311++G(d,p) level. The dihedral angle $\varphi = \angle(C_{10}, C_7, N, C_1)$ was fixed at different values and all other parameters were optimized.

This increases the complexity of the spectrum, since additional hyperfine splittings in the same order of magnitude arise for each single rotational transition due to the electric quadrupole moment of the ^{14}N nucleus.

In a next step, the energy minimum path was calculated by varying the dihedral angle $\varphi = \angle(C_{10}, C_7, N, C_1)$ at a certain fixed value in a 10° grid while all other parameters were optimized. Due to the C_{3v} symmetry of the *tert*-butyl group only one-third of a full rotation of 120° was needed. The resulting potential curve is shown in Figure 2. The Fourier coefficients used to parameterize the curve are given in Table I-2. The range from $\varphi = -60°$ to 0° and $\varphi = 0°$ to 60° are not symmetric since the equilibrium structure is not exactly C_S symmetry due to the proton at the nitrogen atom. The energy minima are slightly broader than the maxima. Comparing to pinacolone[3], where the V_6 ratio is approximately 45%, there is almost no interaction between the methyl and the *tert*-butyl group in this case. Obviously, these groups are separated much more by the secondary amino group than by a carbonyl group.
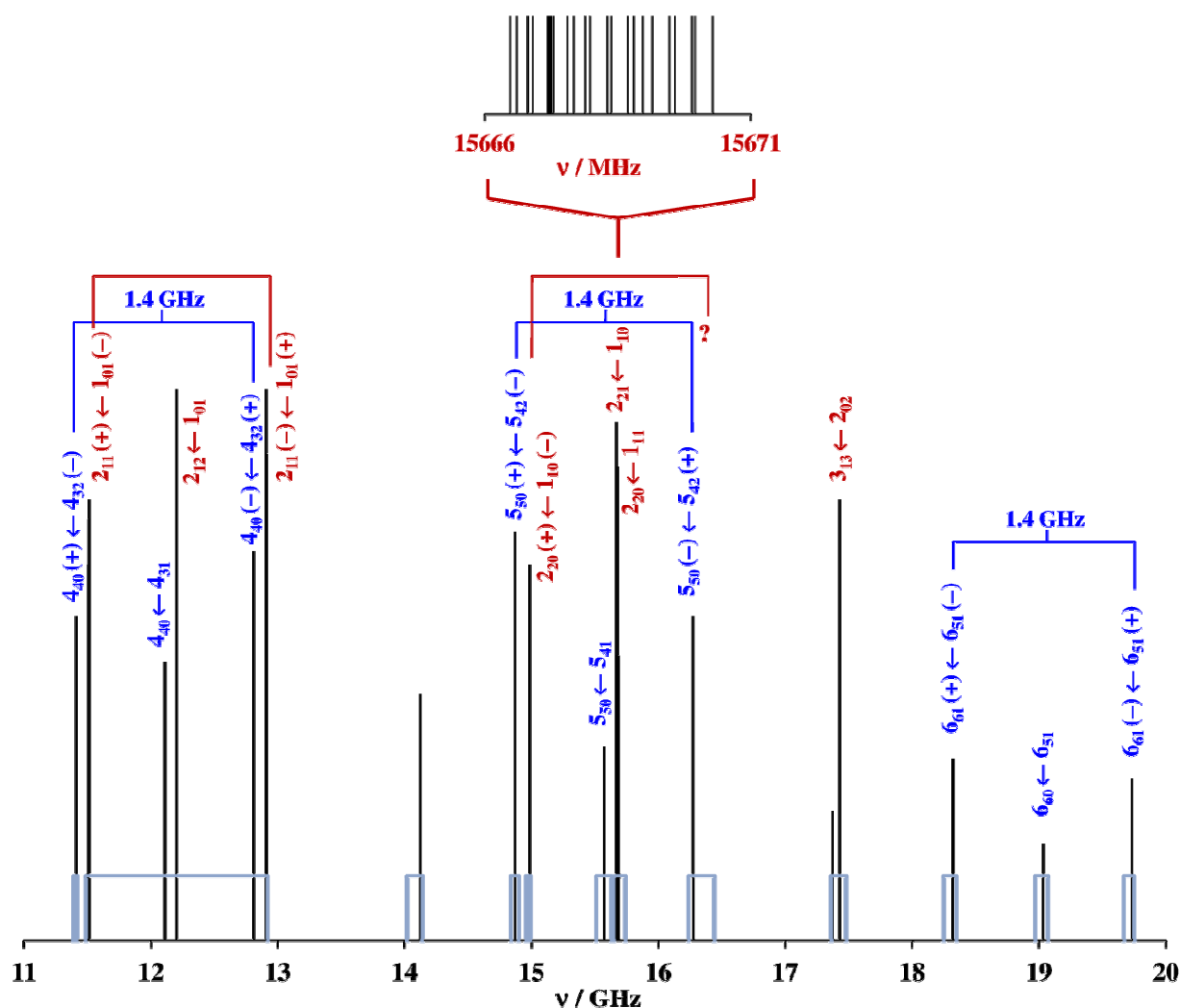
FIG. 3 The microwave spectrum of methyl *tert*-butyl amine in the range from 11 to 20 GHz. The broadband scans are marked with rectangles. *R* branch transitions are labeled in red, *Q* branch in blue. All *c*-type transitions appear as doublet (marked with brackets). The frequency range from 15666 to 15671 MHz is enlarged and the positions of all rotational lines in this area without regard to their intensity are shown.

3. Microwave spectrum

The rotational constants calculated by quantum chemical methods were used to predict the rotational spectrum of methyl *tert*-butyl amine using a rigid rotor program. At the beginning, a broadband scan in the frequency range from 11.5 GHz to 13.0 GHz was taken using a modified version of the MB-FTMW spectrometer described in ref. [17,18] in the experimental setup section. Five multiplets were found in this frequency range of 1.5 GHz. In addition, during the spectral assignment process some smaller ranges were scanned. All scanned ranges are given as rectangles in Figure 3. An example of the multiplets in the frequency range from

15666 MHz to 15671 MHz (*b*-type *R* branch $2_2 \leftarrow 1_1$ transitions) is visualized in a enlarge scale. Only the line positions are indicated without regard to the line intensity.

Similar to diethyl amine, proton inversion tunneling at the nitrogen atom is possible since there are also two equivalent equilibrium structures in this case (see Figure 1). The dipole moment in *c* direction changes sign upon proton tunneling, the *a* component is zero due to a *bc* mirror plane, and the dipole moment in *b* direction does not change its sign. Therefore, it is expected that all *c*-type transitions are split into doublet, whereas *b*-type transitions do not split and *a*-type transitions do not exist at all. It is difficult to predict the value of splittings of the *c*-type transitions. However, we expected a splitting on the order of 1.5 GHz like in the case of diethyl amine. Further theoretical details were discussed in Chapter 8 and will not be repeated here.

We tried to assign five multiplets found in the broadband scan by comparing the experimental and theoretical spectrum with regard to the splitting of *c*-type transitions. By trial and error, the *b*- and *c*-type *R* branch $2 \leftarrow 1$ and the *b*- and *c*-type *Q* branch $4 \leftarrow 4$ could be assigned. The tunneling splitting of *c*-type transitions is approximately 1400 MHz. Afterwards, only small scanned ranges were needed to find all other multiplets within the frequency range from 11 GHz to 20 GHz (see Figure 3). Unfortunately, the *c*-type 2_{20} (−) ← 1_{10} (+) transition, which should be very intensive, could not be found yet. The position of this transition is marked with a red question mark in Figure 3. All other transitions match almost exactly the predicted spectrum.

For analysis of the hyperfine structure and methyl internal rotation, all multiplets were remeasured in the high resolution mode. A range of about 5 MHz for each multiplet was measured in a step width of 0.25 MHz. A typical spectrum is shown in Figure 4. Doppler splittings are marked by brackets.

4. Results and discussion

After the structure of the spectrum was roughly understood as indicated in Figure 3, a preliminary fit containing the overall rotation and the nitrogen inversion tunneling was carried out using the program *spfit* written by Pickett.[5] The center of the multiplets was used for the fit. The fitted parameters are given in the column Fit I in Table 1, a list of all transitions included in the fit in Table 2. The parameter definition (*.par) file of the program *spfit* is also available in the Appendix (Table I-3).
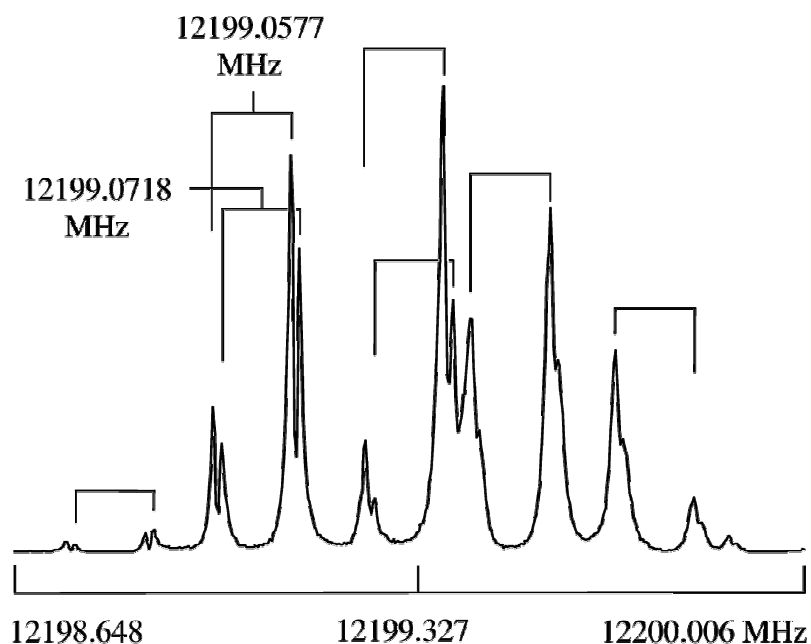
FIG. 4 A spectrum measured in the high resolution mode. Doppler splittings are marked by brackets. Each line appears as an A-E doublet due to internal rotation of the methyl group. For this spectrum 240 FIDs were co-added.

The experimental and calculated A, B, and C rotational constants are in good agreement with deviations of 29 MHz, 16 MHz, and 11 MHz, respectively. The deviations are below 0.7% in all cases (see Table 1). A better agreement is not expected since the quantum chemical results refer to the equilibrium structure whereas the experimental rotational constants are obtained for the ground vibrational state. The separation between the lowest (v = 0) symmetric and antisymmetric inversion energy levels E was determined to be 698.903(99) MHz. The predictive power of the fit is high since all multiplets could be easily found. Therefore, the assignment can be confirmed, even though the *c*-type 2_{20} (−) ← 1_{10} (+) transition component is absent. The reason is still unknown.

The splitting of 1397.81(20) MHz of all *c*-type transitions can be compare with the splitting of 2646.0 MHz, 1981.0 MHz, and 1521.542 MHz found for dimethyl amine,[1] ethyl methyl amine,[2] and diethyl amine (Chapter 8), respectively. The nitrogen inversion splitting of methyl *tert*-butyl amine is very close to that one of diethyl amine and smaller than in the case of dimethyl amine and ethyl methyl amine. As discussed in Chapter 8, the Hamilton operator consists of the kinetic and the potential energy (V_φ). The V_φ part is the same for these four molecules since the double minimum potential for the proton inversion tunneling should be very similar. The kinetic energy includes the reduced moment of inertia which is given by

Table 1

Parameters describing the overall rotation and nitrogen inversion of methyl *tert*-butyl amine obtained from a preliminary fit of the *spfit* program.

Parameter	Unit	Fit I (Obs.)	Fit II	Calc.	Obs. – Calc.
A−(B+C)/2	MHz	1730.126(34)	1730.134(34)		
(B+C)/2	MHz	2619.171(69)	2619.112(69)		
(B−C)/4	MHz	1.265(54)	−1.207(54)		
A[a]	GHz	4.349		4.370	−0.029 (−0.67%)
B[a]	GHz	2.622		2.638	−0.016 (−0.61%)
C[a]	GHz	2.617		2.628	−0.011 (−0.42%)
κ		−0.994		−0.989	
E	MHz	698.903(99)	698.901(99)		
E_K	MHz	−0.172(18)	−0.175(18)		
N[b]		24	24		
σ	MHz	2.8	3.0		

[a] derived parameter.
[b] number of multiplets.

$I_r = (I_H \cdot I_f) / (I_H + I_f)$, where I_f is the moment of inertia of the molecular frame. The smaller the molecule is, the smaller the reduced moment of inertia becomes and, consequently, the bigger the splitting is. Therefore, it appears reasonable that the largest splitting is observed in dimethyl amine and the splittings of diethyl amine and methyl tert-butyl amine (two isomers) are close to each other.

The fine analysis of both, the rotational spectrum and its ^{14}N hyperfine structure turned out to be a difficult task. Since the Ray's asymmetry parameter is $\kappa = -0.994$, which is very close to −1.0, methyl *tert*-butyl amine is an extremely near prolate top. The *Q* branch lines are extremely close to each other and overlap in their hyperfine strutures. The transitions labeled in blue in Figure 3 present only the band head of the *Q* branches. Each component of these *Q* branches splits into a multiplet due to the ^{14}N hyperfine structure. Consequently, the *Q* branch lines overlap and assignment is almost impossible. Furthermore, no identical ^{14}N hyperfine structures could be found for the (−) ← (+) and (+) ← (−) components of the same rotational transition. In the case of diethyl amine (Chapter 8), it has been shown that a perturbation of the ^{14}N quadrupole pattern arises in the case of a near degeneracy of two energy levels and different hyperfine patterns appear for the same rotational but different inversion states. In the case of methyl *tert*-butyl amine, many energy levels might be degenerated. In combination with the overlapping of many transitions in the spectrum a detailed assignment requires further investigation and an improved theoretical model.

Table 2

Observed centers of multiplets ($\nu_{Mult.}$) of methyl *tert*-butyl amine. $\nu_{Calc.}$ is the calculated value; $\nu_{Mult.} - \nu_{Calc.}$ values obtained after a fit with program *spfit* called Fit I in Table 1. *c*-type transitions are split. J, K_a, and K_c are the asymmetric top rotational quantum numbers, ν denotes the inversional sublevels, $\nu = 0$ and $\nu = 1$ correspond to the symmetric (+) state and the antisymmetric (−) state, respectively (for more detail see Chapter 8).

Upper level				Lower level				$\nu_{Mult.}$	$\nu_{Mult.} - \nu_{Calc.}$
J	K_a	K_c	ν	J	K_a	K_c	ν	MHz	MHz
3	3	0	0	3	2	1	0	8650.00	0.2
3	3	0	1	3	2	1	1	8650.00	−0.6
2	1	2	0	1	0	1	0	12200.25	1.2
2	1	2	1	1	0	1	1	12200.25	1.0
4	4	0	0	4	3	1	0	12110.75	1.0
4	4	0	1	4	3	1	1	12110.75	−0.2
5	5	0	0	5	4	1	0	15571.00	1.3
5	5	0	1	5	4	1	1	15571.00	−0.2
2	2	0	0	1	1	1	0	15676.50	7.4
2	2	0	1	1	1	1	1	15676.50	6.9
2	2	1	0	1	1	0	0	15668.00	4.0
2	2	1	1	1	1	0	1	15668.00	3.4
3	1	3	0	2	0	2	0	17426.50	−3.3
3	1	3	1	2	0	2	1	17426.50	−3.5
4	4	0	0	4	3	2	1	11410.00	0.7
4	4	0	1	4	3	2	0	12811.00	−0.4
2	1	1	0	1	0	1	1	11511.50	−3.8
2	1	1	1	1	0	1	0	12910.25	−3.1
5	5	0	0	5	4	2	1	14870.00	2.0
5	5	0	1	5	4	2	0	16273.00	0.1
6	6	1	0	6	5	1	1	18322.00	−4.4
6	6	0	0	6	5	1	0	19032.00	2.4
6	6	0	1	6	5	1	1	19032.00	0.5
6	6	1	1	6	5	1	0	19732.00	−2.7

Moreover, it is difficult to distinguish the *b* and the *c* axis due to the very near prolate top properties of methyl *tert*-butyl amine. The identification of the *b* and the *c* axis also depends on the position of the proton at the nitrogen atom, which additionally tunnels back and forth. It is not clear, whether *b* or *c*-type transitions split into doublets. A second fit was carried out where *b*-type instead of *c*-type transitions are split. The result is almost identical. The fitted parameters are given in column Fit II in Table 1, a list of all transitions in Table 3. The parameter definition (*.par) file of the program *spfit* is given in Table I-3 in the Appendix.

Table 3

$\nu_{\text{Obs.}} - \nu_{\text{Calc.}}$ values obtained after a fit with program *spfit* with reference to Fit II in Table 1. In this case, *b*-type transitions are split. For all other notes see Table 2.

Upper level				Lower level				$\nu_{\text{Mult.}}$	$\nu_{\text{Mult.}} - \nu_{\text{Calc.}}$
J	K_a	K_c	ν	J	K_a	K_c	ν	MHz	MHz
3	3	0	0	3	2	2	0	8650.00	0.1
3	3	0	1	3	2	2	1	8650.00	−1.0
2	1	1	0	1	0	1	0	12200.25	1.0
2	1	1	1	1	0	1	1	12200.25	0.8
4	4	0	0	4	3	2	0	12110.75	0.9
4	4	0	1	4	3	2	1	12110.75	−0.6
5	5	0	0	5	4	2	0	15571.00	1.2
5	5	0	1	5	4	2	1	15571.00	−0.7
2	2	0	0	1	1	0	0	15676.50	7.6
2	2	0	1	1	1	0	1	15676.50	6.9
2	2	1	0	1	1	1	0	15668.00	4.2
2	2	1	1	1	1	1	1	15668.00	3.5
3	1	2	0	2	0	2	0	17426.50	−3.8
3	1	2	1	2	0	2	1	17426.50	−4.0
4	4	0	0	4	3	1	1	11410.00	1.0
4	4	0	1	4	3	1	0	12811.00	−1.2
2	1	2	0	1	0	1	1	11511.50	−5.4
2	1	2	1	1	0	1	0	12910.25	−2.7
5	5	0	0	5	4	1	1	14870.00	2.5
5	5	0	1	5	4	1	0	16273.00	−1.1
6	6	1	0	6	5	2	1	18322.00	−3.5
6	6	1	0	6	5	1	0	19032.00	2.3
6	6	1	1	6	5	1	1	19032.00	−0.1
6	6	1	1	6	5	2	0	19732.00	−4.4

Finally, each single line measured in the high resolution mode has small additional splitting in the order of 20 kHz as can be seen in Figure 4. These splittings are in the same order of magnitude as the splittings due to methyl internal rotation observed for diethyl amine. Therefore, we consider these doublets to be A-E doublets due to the internal rotation of the methyl group. The barrier is expected to be approximately 1100 cm^{-1}, similar to the case of diethyl amine. An accurate analysis is not possible until the ^{14}N hyperfine structure has been accurately assigned.

5. Conclusion

The MB-FTMW spectrum of methyl *tert*-butyl amine was recorded and analyzed in combination with quantum chemical calculations. Methyl *tert*-butyl amine is a very near prolate top with $\kappa = -0.994$. In the microwave spectrum many rotational transitions overlap. All rotational transitions show ^{14}N hyperfine splittings. Perturbations of these splittings caused by near degeneracy of some energy levels make the spectral assignment a difficult task. Each single line in the spectrum appears as a narrow A-E doublet due to internal rotation of the methyl group. A preliminary fit including the overall rotation and nitrogen inversion tunneling was carried out. The splitting of all *c*-type transitions was determined to be 1397.81(20) MHz which is close to the value found for diethyl amine. A detailed assignment of the spectrum including the ^{14}N hyperfine structure, the overlapping rotational Q branch transitions, and the internal rotation of the methyl group is in progress.

Acknowledgment

References

[1]J. E. Wollrab and V. W. Laurie, *J. Chem. Phys.* **48**, 5058 (1968).

[2]R. E. Penn and J. E. Boggs, *J. Mol. Spectrosc.* **47**, 340 (1973).

[3]Y. Zhao, diploma thesis at the RWTH Aachen University under supervision of Prof. W. Stahl, **2009**.

[4]B. S. Ray, *Z. Phys.* **78**, 74 (1932).

[5]H. M. Pickett, *J. Mol. Spectrosc.* **148**, 371 (1991).

Chapter 10

TRIETHYL AMINE

Conformational landscape – the wind mill structure found in an oblate symmetric top

1. Introduction

Amines are important derivates of ammonia, where one or more protons are replaced by organic substituents. Small aliphatic amines are often used in the pharmaceutical, fertilizer industry, or as solvents. As described in Chapter 8, many studies on ammonia and its derivates have been carried out in the microwave region. Our investigation on diethyl amine, where two protons in ammonia are substituted by ethyl groups yielded many interesting effects. The most interesting effect is the proton tunneling at the nitrogen atom, which causes all c-type transitions to split into doublets. Furthermore, the quadrupole hyperfine splittings due to the nuclear spin of $I = 1$ of the ^{14}N nucleus and the splittings due to the internal rotation of the two equivalent methyl groups could be resolved. The barrier to internal rotation has been determined to be 1051.74(57) cm^{-1}. The ^{14}N quadrupole coupling constants were found to be $\chi_{aa} = 2.67576(37)$ MHz, $\chi_{bb} - \chi_{cc} = 4.34144(65)$ MHz, and $|\chi_{bc}| = 2.9199(92)$ MHz. This motivated us to study triethyl amine, a related molecule, where all the protons in ammonia are substituted by ethyl groups. We were interested to compare the ^{14}N quadrupole coupling constants of this molecule with ammonia and other amines (see Table 7 in Chapter 8). It is also interesting to figure out whether the barrier to internal rotation changes, i.e. whether splitting of three internal rotors can be observed.

By rotating the ethyl groups, a large number of different geometries of triethyl amine can be generated. To find out which of those geometries are stable conformers, which can be observed under molecular beam conditions, and which symmetry the most stable conformer has, a combination of MB-FTMW spectroscopy and quantum chemical calculations were carried out for this molecule.

The microwave spectrum of trimethyl amine, a molecule with very similar structure, was first studied by Linde Jr. and Mann[1] in 1957 and pursued by Wollrab and Laurie.[2] Microwave
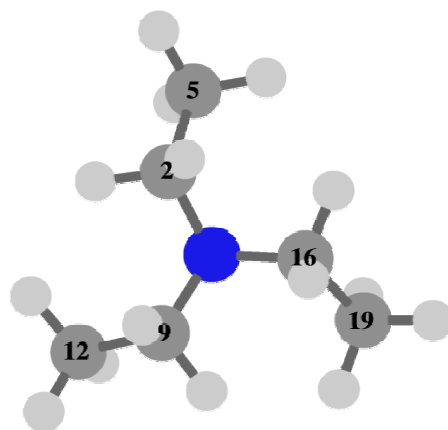
FIG. 1 Geometry of the observed conformer (most stable) of triethyl amine. Only C atoms are labeled. The nitrogen atom appears in blue.

spectroscopic results will be compared with those of trimethyl amine. A further motivation is the comparative quantum chemical studies on related molecules such as triethyl phosphine, triisopropyl amine, and tri-*tert*-butyl amine.

2. Quantum chemistry

Triethyl amine is a molecule with 22 atoms, which is too large for classical structure determination by isotopic substitution. A quite big number of geometries is possible, but not all of them are conformers. Quantum chemistry is a helpful method to calculate the conformers as well as giving reasonable start values of rotational constants to assign the microwave spectrum.

In total, 216 different start geometries were created by varying three dihedral angles $\alpha_1 = \angle(C_{16}, N, C_2, C_5)$, $\alpha_2 = \angle(C_{16}, N, C_9, C_{12})$, and $\alpha_3 = \angle(C_9, N, C_{16}, C_{19})$ in each case from $-120°$ to $180°$ in a grid of $60°$ and calculated using the program *Gaussian03*. Atom numbers are given in Figure 1. The MP2 method and the basis set 6-311++G(d,p) were used throughout, since it turned out to be reliable in many other molecules studied before.

From 216 start geometries, only 8 conformers were found. Frequency calculations for conformer VIII give an imaginary frequency, i.e. this conformer is a saddle point. Other conformers are stable. It should be noted that conformer I, II, III, and VII exist as an enantiomeric pair, whereas conformer IV and V have a structure with no possible enantiomer. All 7 stable conformers are indicated in Figure 2 in dependence on its relative energies. Their energy values, dipole moments, and rotational constants are given in Table 1. The nuclear coordinates in the principal axes system are available in Table J-1 in the Appendix.

Table 1

The energy values, dipole moments, and rotational constants of 7 stable conformers of triethyl amine.

Conf.	E_{MP2} Hartree	rel. E kJ/mol	μ_a / D	μ_b / D	μ_c / D	A / GHz	B / GHz	C / GHz
I	−291.555306	11.6310	0.330	0.264	0.577	3.044	2.010	1.519
II	−291.558563	3.0817	0.261	0.367	0.650	2.931	2.016	1.373
III	−291.559737	0.0000	0.000	0.000	0.781	2.319	2.319	1.326
IV	−291.558893	2.2143	0.000	0.416	0.643	3.387	1.855	1.407
V	−291.558517	3.2028	0.000	0.303	0.739	3.114	1.941	1.348
VI	−291.556593	8.2523	0.560	0.109	0.655	2.956	1.993	1.364
VII	−291.551129	22.5982	0.000	0.000	0.488	2.405	2.405	1.754
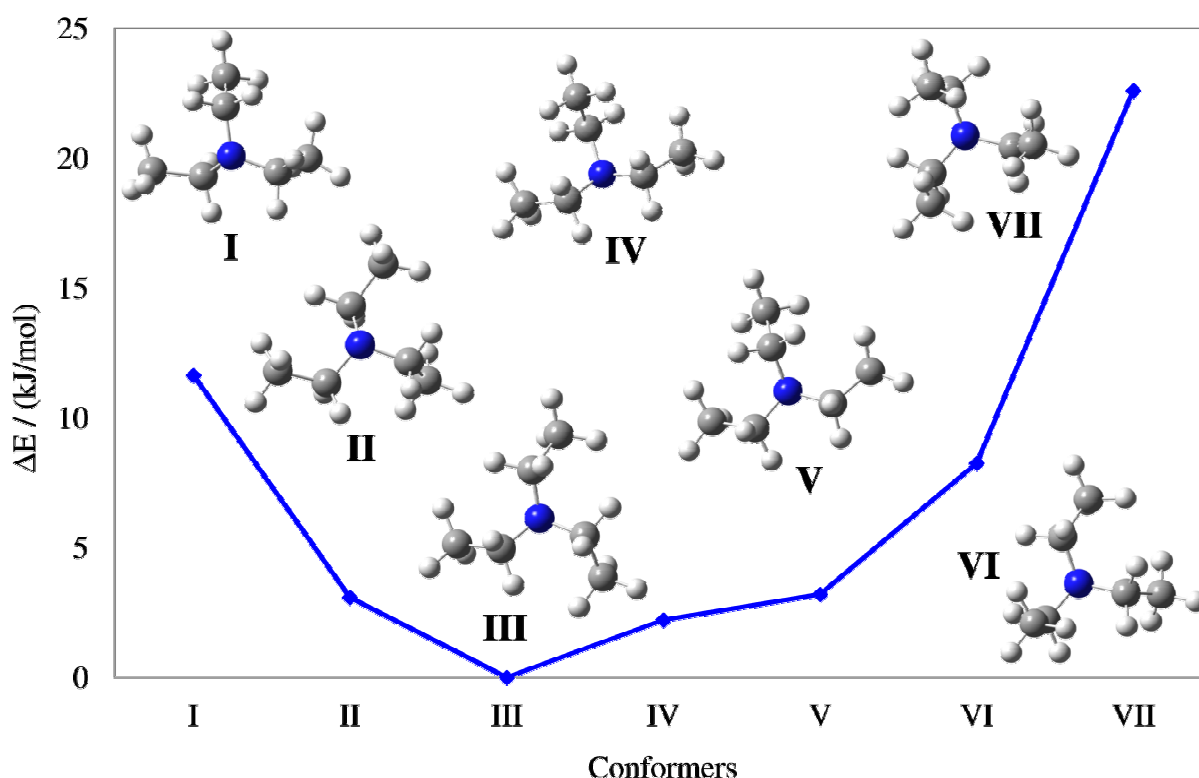
FIG. 2 Stable conformers of triethyl amine. The energy values are relative to the most stable conformer III (−291.559737 Hartree). Only one enantiomer of conformers I, II, III, and VII are indicated.

Conformer III is the most stable conformer with a C_3 symmetric, propeller-like structure (see also Figure 1). The methyl groups are titled into the direction of the free electron pair at the nitrogen atom by the same angle of 79.5 °. The A and B rotational constants are identical and a dipole moment exists only in c direction. Triethyl amine is consequently an oblate top with

$I_a = I_b < I_c$. Conformer VII is likewise an oblate top with the propeller structure. In this case, the methyl groups are title against the free electron pair. However, this conformer has an energy value of 22.6 kJ/mol higher than the one of conformer III and is very unlikely to be observed under molecular beam condition.

3. Microwave spectrum

3.1. Main isotopologue

Conformer III is the most stable conformer and therefore likely to be observed under molecular beam conditions, where the rotational temperature is often very low, approximately 10 K. Since this conformer is an oblate top, the rotational energy levels can be calculated easily using the rotational constants from quantum chemical results. Using the spectrometer described in ref. [17,18] in the experimental setup section, small scans of about 20 MHz around the predicted frequency of the transitions $J = 2 \leftarrow 1$ and $J = 3 \leftarrow 2$ were recorded. Approximately 5 MHz broad multiplets were found due to the hyperfine quadrupol splittings of the ^{14}N nucleus. These frequency ranges were remeasured in the high resolution mode in a grid of 0.25 MHz. A typical spectrum is shown in Figure 3, the complete scan of the $J = 3 \leftarrow 2$ transition in Figure 4. At the beginning, 10 lines of the $J = 2 \leftarrow 1$ and 12 lines of the $J = 3 \leftarrow 2$ transition were found and fitted with the program *spfit/spcat* by Pickett.[3] A more accurate theoretical spectrum could be predicted with the fitted parameters. Further lines of the transitions $J = 4 \leftarrow 3$ and $J = 5 \leftarrow 4$ could be measured directly in the high resolution mode. In total, 48 lines were found, assigned and fitted. A list of all transitions in the fit is given in Table 2, the fitted molecular parameters in Table 3. The parameter definition (*.par) file of the program *spfit* can be found in the Appendix (Table J-2).

3.2. ^{13}C isotopologue

In addition to the rotational spectrum of the main ^{12}C isotopologue, several lines of ^{13}C isotopologues could be observed. With 6 carbon atoms, many ^{13}C isotopologues are avaible, however, some of them are equivalent. They are the isotopologues with ^{13}C substituent at the C_2, C_9, and C_{16} positions and at the C_5, C_{12}, and C_{19} positions. In both cases, the frequency of occurrence increases from approximately 1.1% to 3.3%. Therefore, it is possible to measure these isotopologues in its natural concentration.
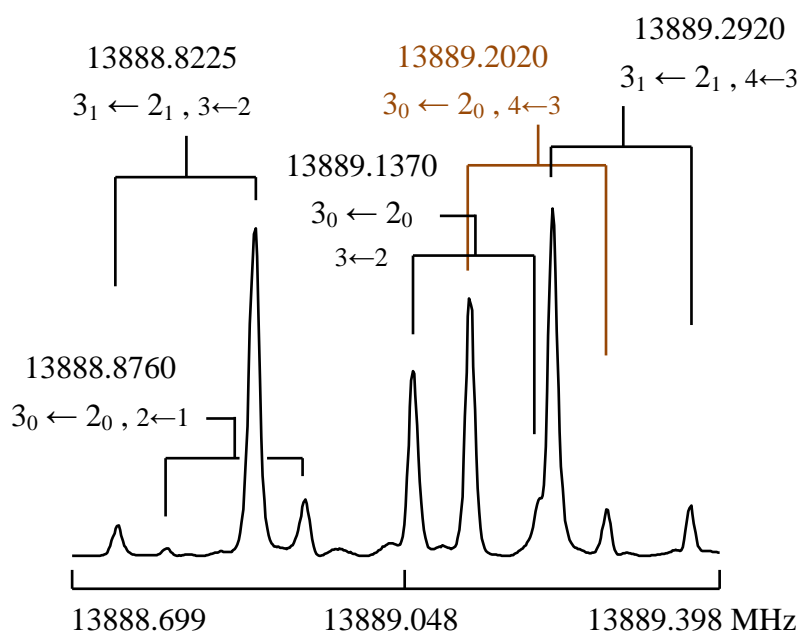
FIG. 3 A typical spectrum of the $3_K \leftarrow 2_K$, $F \leftarrow F$ transition of triethyl amine measured in the high resolution mode. Doppler splittings are marked by brackets.
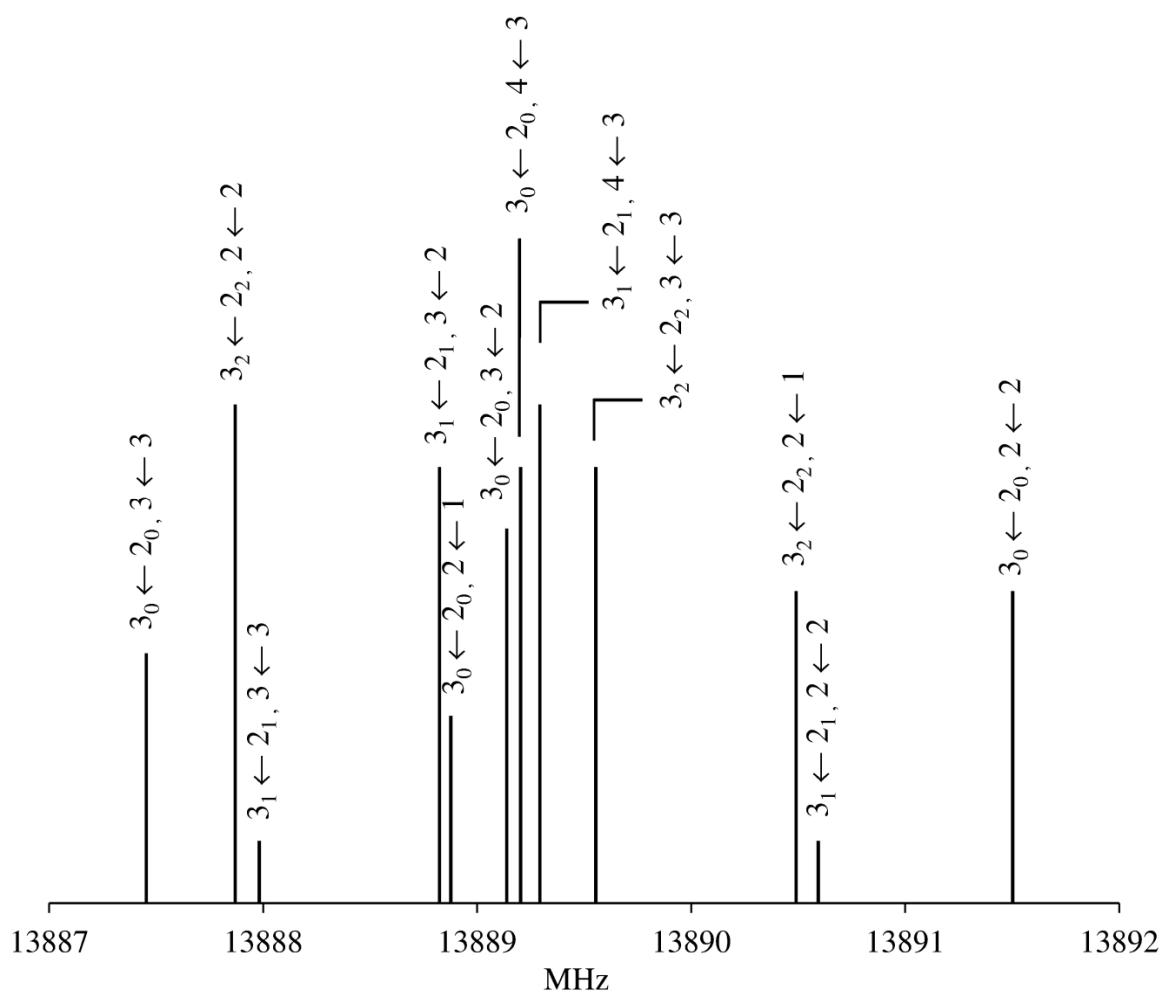
FIG. 4 The complete scan of the $3_K \leftarrow 2_K$, $F \leftarrow F$ transition of triethyl amine measured in high resolution mode in a grid of 0.25 MHz.

Table 2

Observed frequencies ($\nu_{Obs.}$) of the main isotopologue of triethyl amine. $\nu_{Calc.}$ is the calculated value; $\nu_{Obs.} - \nu_{Calc.}$ values obtained after a fit with the program *spfit*. J and K_c are the symmetric top rotational quantum numbers, F is the total angular momentum in the coupled basis with $F = J + I$.

Upper level			Lower level			$\nu_{Obs.}$ MHz	$\nu_{Obs.} - \nu_{Calc.}$ kHz
J	K_c	F	J	K_c	F		
2	0	3	1	0	2	9259.5790	1.5
2	0	2	1	0	1	9259.4630	−2.1
2	0	2	1	0	2	9257.8925	0.5
2	0	1	1	0	1	9262.0870	−0.6
2	0	1	1	0	2	9260.5150	0.6
2	1	1	1	1	0	9261.4380	−0.6
2	1	2	1	1	1	9258.1610	0.2
2	1	3	1	1	2	9259.7895	−0.5
2	1	2	1	1	2	9258.9470	−0.2
2	1	1	1	1	2	9260.2590	0.3
3	0	4	2	0	3	13889.2020	−0.4
3	0	3	2	0	2	13889.1370	−3.0
3	0	2	2	0	1	13888.8760	−1.7
3	0	3	2	0	3	13887.4530	−1.4
3	0	2	2	0	2	13891.5010	0.9
3	1	4	2	1	3	13889.2920	2.0
3	1	3	2	1	2	13888.8225	0.8
3	1	3	2	1	3	13887.9805	1.5
3	1	2	2	1	2	13890.5930	1.1
3	2	2	2	2	2	13887.8685	1.0
3	2	2	2	2	1	13890.4890	−0.5
3	2	3	2	2	3	13889.5535	0.7
4	0	4	3	0	3	18518.7440	−1.6
4	0	5	3	0	4	18518.7830	−2.3
4	0	4	3	0	4	18516.9990	1.5
4	0	3	3	0	3	18520.9940	0.7
4	1	5	3	1	4	18518.8370	1.2
4	1	4	3	1	3	18518.6245	−2.7
4	1	4	3	1	4	18517.3195	3.3
4	1	3	3	1	3	18520.5395	1.7
4	2	5	3	2	4	18518.9895	2.4
4	2	4	3	2	3	18518.2705	−1.5
4	2	3	3	2	2	18519.1690	−1.9
4	3	5	3	3	4	18519.2390	−0.4
4	3	4	3	3	3	18517.6805	0.4
4	3	3	3	3	2	18519.8430	−0.4
4	3	3	3	3	3	18516.8930	−0.6
5	0	5	4	0	4	23148.2570	−1.8

Table 2 continued

Upper level			Lower level			$\nu_{Obs.}$	$\nu_{Obs.} - \nu_{Calc.}$
J	K_c	F	J	K_c	F	MHz	kHz
5	1	6	4	1	5	23148.3220	−1.3
5	1	5	4	1	4	23148.2130	3.9
5	1	5	4	1	5	23146.6885	−1.0
5	3	6	4	3	5	23148.6180	−1.1
5	3	5	4	3	4	23147.8115	−0.3
5	3	4	4	3	3	23148.8185	1.6
5	3	5	4	3	5	23148.4380	0.4
5	4	6	4	4	5	23148.8770	−0.9
5	4	5	4	4	4	23147.4645	0.3
5	4	4	4	4	3	23149.3000	0.3

Table 3

Parameters describing the overall rotation and ^{14}N quadrupole coupling of triethyl amine as well as its $^{13}C_2$ and $^{13}C_5$ isotopologues fitted with the program *spfit*.

Parameter	Unit	Main isotopologue	Calc.	$^{13}C_2$ isotopologue	$^{13}C_5$ isotopologue
A	GHz	2.314873978(11)	2.3194	2.31293315(34)	2.31302815(28)
B	GHz	2.314873978(11)	2.3191	2.29283301(33)	2.25126785(40)
C	GHz	1.3262 (fixed)	1.3262	1.32681(96)	1.32989(18)
D_J	kHz	0.9619(17)		0.9694(88)	1.369(14)
D_{JK}	kHz	−1.5885(43)		−3.594(27)	1.988(25)
χ_{cc}	MHz	−5.2444(07)		−5.2660(40)	−5.947(98)
$\chi_{bb} - \chi_{aa}$	MHz	0.0[a]			−0.257(19)
N		43		16	10
σ	kHz	1.5		0.5	0.4

[a] due to symmetry

The Cartesian coordinates of conformer III was transformed in the principal axes coordinates. The mass of substituted ^{12}C atom was changed to the one of the ^{13}C atom. The rotational constants were calculated and used as start values to predict the theoretical spectrum with the program *spcat*. All lines were measured directly in the high resolution mode. In total, 16 transitions of the $^{13}C_2$- and 10 transitions of the $^{13}C_5$ isotopologue were assigned and fitted. It should be noted that the molecule becomes asymmetric due to the ^{13}C substituent and is no more an oblate top. Therefore, the C rotational constants could be determined. All fitted transitions are listed in Table 4 and 5. The molecular parameters can be found in the same

Table 4

Observed frequencies ($\nu_{Obs.}$) of the $^{13}C_2$ isotopologue of triethyl amine. For $\nu_{Calc.}$, $\nu_{Obs.} - \nu_{Calc.}$, J, K_a, K_c, and F see Table 3.

Upper level				Lower level				$\nu_{Obs.}$ MHz	$\nu_{Obs.} - \nu_{Calc.}$ kHz
J	K_a	K_c	F	J	K_a	K_c	F		
2	1	1	2	1	0	1	2	9191.0185	0.0
2	2	0	3	1	1	0	2	9211.9245	−0.1
2	2	1	2	1	1	1	1	9230.4292	0.1
2	2	1	1	1	1	1	1	9231.7460	−0.1
2	2	1	3	1	1	1	2	9232.0648	−0.2
3	3	0	2	2	2	0	1	13818.1711	−0.9
3	3	0	3	2	2	0	2	13818.4359	0.0
3	3	0	4	2	2	0	3	13818.4991	0.9
3	3	1	3	2	2	1	2	13847.4235	0.3
3	3	1	4	2	2	1	3	13847.8932	−0.1
4	4	0	3	3	3	0	2	18425.8052	−0.5
4	4	0	4	3	3	0	3	18425.9203	1.0
4	4	0	5	3	3	0	4	18425.9581	−0.5
4	4	1	4	3	3	1	3	18463.7852	0.0
4	4	1	3	3	3	1	2	18463.9261	0.1
4	4	1	5	3	3	1	4	18463.9943	−0.2

Table 5

Observed frequencies ($\nu_{Obs.}$) of the $^{13}C_5$ isotopologue of triethyl amine. For $\nu_{Calc.}$, $\nu_{Obs.} - \nu_{Calc.}$, J, K_a, K_c, and F see Table 3.

Upper level				Lower level				$\nu_{Obs.}$ MHz	$\nu_{Obs.} - \nu_{Calc.}$ kHz
J	K_a	K_c	F	J	K_a	K_c	F		
2	1	1	3	1	0	1	2	9067.0450	−0.4
3	2	1	4	2	1	1	3	13602.0519	0.4
3	1	2	2	2	0	2	1	13681.7775	0.0
3	3	0	2	2	2	0	1	13704.4148	−0.6
3	3	0	3	2	2	0	2	13704.6741	0.6
3	3	1	3	2	2	1	2	13786.7173	0.3
3	3	1	2	2	2	1	1	13787.1890	−0.4
3	3	1	2	2	2	1	3	13787.9226	0.1
4	3	1	4	3	2	1	3	18139.2802	0.2
4	3	1	3	3	2	1	2	18139.4766	−0.3

table with the main isotopologue (Table 3). The parameter definition (*.par) files of the program *spfit* are also given in Table J-2 in the Appendix.

4. Discussion

The structure of triethyl amine obtained by microwave spectroscopy yielded some interesting aspects. Even though this molecule is relatively large with 22 atoms, its most stable conformer is an oblate top. It has the propeller structure like a wind mill and is thereby chiral. The triethyl amine propeller can have a clockwise or anti-clockwise direction, dependent on the respective enantiomer.

The rotational transitions of the main isotopologue are located within several small frequency ranges and could be found easily in the spectrum. All recorded lines were assigned and fitted with a standard deviation of only 1.5 kHz, within the experimental accuracy. The A and B rotational constants calculated on the MP2/6-311++G(d,p) level are reasonable start values. The absolute deviation from the fitted one is only 4 MHz. Estimation about the C rotational constant is not possible, since it cannot be determined for an oblate top.

The symmetric top character of triethyl amine allows a direct comparison of the χ_{zz} quadrupole constant with other symmetric tops like nitrogen trifluoride, ammonia, trimethyl amine, and quinuclidine (see Table 6). The χ_{zz} value of triethyl amine is determined to be −5.2444 MHz, almost the same as the value of −5.1915 MHz found for quinuclidine.[4] The corresponding value of −5.47 MHz reported for trimethyl amine[1] is slightly higher. It is interesting to compare this value with the one of ammonia[5] and nitrogen trifluoride NF_3,[6] which is −4.0842 MHz and −7.903 MHz, respectively. The value of ammonia is much lower and the one of nitrogen trifluoride much higher. This effect might be due to the different inductive effect of these substituents. In the case of triethyl amine and quinuclidine, the substituents are carbon chains, whereas only the methyl groups exist in trimethyl amine. However, all these alkyl substituents have a positive inductive effect. In the case of ammonia, the protons have no inductive effect. For nitrogen trifluoride, the negative inductive effect of the fluor atoms might have influence on the quadrupole constant.

The rotational trantisions of the ^{13}C isotopologues could be fitted with an excellence standard deviation of lower than 0.5 kHz in both cases. The A rotational constant is almost the same as the one of the main isotopologue, however, the B constants are appreciably lower. The difference is 22.1 MHz and 63.6 MHz for the $^{13}C_2$ and the $^{13}C_5$ isotopologue, respectively. Unlike the ^{12}C isotopologue, the C rotational constant could be determined. The values of other parameters like centrifugal distorsional and quadrupole constants are similar to the main isotopologue.

Table 6

Comparison of the χ_{zz} quadrupole coupling constant (in MHz) of ^{14}N in triethyl amine with other symmetric tops.

	χ_{zz}[a]
nitrogen trifluoride[6]	−7.903
ammonia[5]	−4.0842
triethyl amine	−5.2444
quinuclidine[4]	−5.1915
trimethyl amine[1]	−5.47

[a] $\chi_{xx} = \chi_{yy} = -0.5\chi_{zz}$

Finally, it should be mentioned that no additional splittings were found in the spectrum. This means also, that the splittings due to internal rotation of the methyl groups are very small and cannot be resolved even in the high resolution mode.

5. Conclusion

Conformational studies with quantum chemistry yielded for the most stable conformer of triethyl amine a propeller-like structure belonging to the point group C_3, which is an oblate top. The microwave spectrum of this conformer was assigned and molecular parameters were determined. The observed spectrum could be reproduced within the experimental accuracy. The standard deviation of a global fit with 43 rotational transitions is only 1.4 kHz.

The propeller-like structure seems to be advantageous and therefore typical for related systems. Quantum chemical studies on similar molecules like triethyl phosphane, triisopropyl amine, tri-n-propyl amine, and tri-*tert*-butyl amine (see Appendix) yielded this structure for the most stable conformers in all cases.

Furthermore, several rotational transitions of two isotopologues, $^{13}C_2$ and $^{13}C_5$, could be measured in the natural concentration and fitted with an excellent standard deviation. The isotopologues are asymmetric top. Therefore, the C rotational constants could be determined.

6. Appendix: Quantum chemical calculations on related molecules

6.1. Triethyl phosphane

Analogue to triethyl amine, three dihedral angles $\alpha_1 = \angle(C_{16}, P, C_2, C_5)$, $\alpha_2 = \angle(C_{16}, P, C_9, C_{12})$, and $\alpha_3 = \angle(C_9, P, C_{16}, C_{19})$ were defined. In this case, only 8 start geometries were calculated, which were based on the structure of 8 conformers of triethyl amine (include the
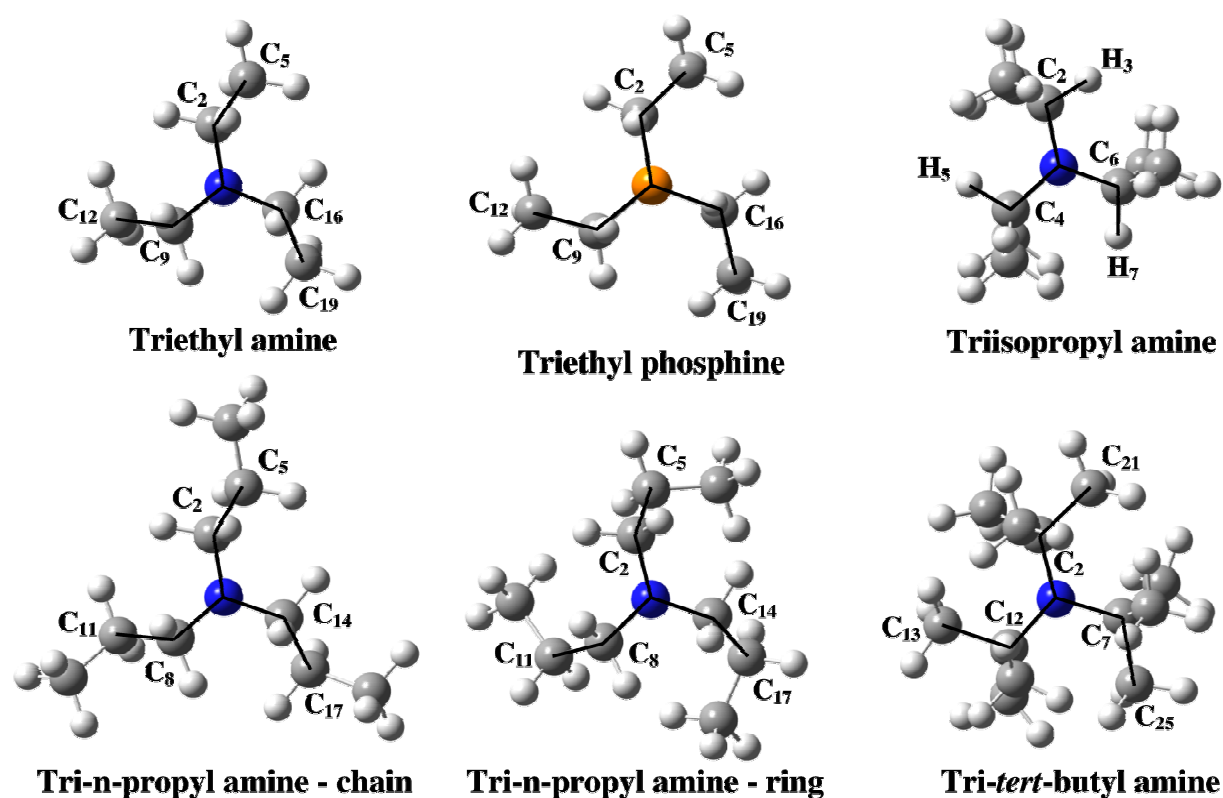
FIG. 5 The propeller structure found in triethyl amine and related molecules.

one with imaginary frequency). From these start geometries, 7 conformers were found. Only one conformer shows imaginary frequency, all other conformers should exist as stable ones. The most stable conformer of triethyl phosphine has the known propeller-like structure as in the case of triethyl amine and is consequently an oblate top. However, the ethyl groups are not tilted to the direction of the free electron pair, but located almost in a plane containing the phosphor atom.

6.2. Triisopropyl amine, tri-n-propyl amine, and tri-*tert*-butyl amine

In the case of triisopropyl amine, the dihedral angles were chosen to be $\alpha_1 = \angle(C_6, N, C_2, H_3)$, $\alpha_2 = \angle(C_6, N, C_4, H_5)$, and $\alpha_3 = \angle(C_4, N, C_6, H_7)$ in order to enable a direct comparison with the conformers of triethyl amine. From 7 start geometries, 7 conformers were found. Analogous to the case of triethyl phosphine, only one conformer shows imaginary frequency, whereas all other represent true minima. The structure of the most stable conformer is shown in Figure 5. Once again, a propeller-like structure was found.

The calculations are more complicate in the case of tri-n-propyl amine. Due to the long alkyl chains, a lot of start geometries are possible. Therefore, we started only with the start

geometries based on the most stable conformer III of triethyl amine. Two conformers were found, on the one hand with the zigzag chain structure, on the other hand the ring structure. The propeller structure is conserved in both cases.

For tri-*tert*-butyl amines, the optimized structures of all 7 start geometries are the same. Only one conformer, once again with the propeller structure, could be found which exists as an enantiomeric pair. For a better comparison, the most stable conformers of all related molecules are shown in Figure 5. It should be noted that all of them are oblate tops. The energy values, dipole moments, angles of torsion, bond lengths, and rotational constants of all conformers are given in Table J-3.

Acknowledgments

References

[1] D. R. Lide, Jr. and D. E. Mann, *J. Chem. Phys.* **28**, 572 (1958).

[2] J. E. Wollrab and V. W. Laurie, *J. Chem. Phys.* **51**, 1580 (1969).

[3] H. M. Pickett, *J. Mol. Spectrosc.* **148**, 371 (1991).

[4] D. Consalvo and W. Stahl, *J. Mol. Struct.* **447**, 119 (1998).

[5] G. R. Gunther-Mohr, R. L. White, A. L. Schawlow, W. E. Good, D. K. Coles, *Phys. Rev.* **94**, 1184 (1954).

[6] S. E. Novick, W. Chen, M. R. Munrow, K. J. Grant, *J. Mol. Spectrosc.* **179**, 219 (1996).

Summary

Within this thesis five esters, two ketones, and three amines showing two different types of large amplitude motions, internal rotation and nitrogen proton tunneling, have been investigated by a combination of molecular beam Fourier transform microwave spectroscopy and quantum chemical calculations. The molecular structure was characterized in terms of experimental rotational constants which have been used to validate the results from quantum chemical calculations. The molecular dynamics has been described by the barriers to internal rotation or inversion. These experimental data were supplemented by potential curves and two-dimensional potential energy surfaces obtained by quantum chemical calculations. Most results are provided as reference data for astrophysical research, atmospheric chemistry or general applications in gas phase analytics.

The esters and ketones were selected for different frame symmetries and different numbers of internal rotors. This large variety of molecules was important since they were also considered as test systems for the three computer programs XIAM, BELGI, and Erham which treat the internal rotation problem with different methods. In comparative studies the range of potential barriers, for which reliable results can be expected, were investigated. The programs BELGI and XIAM were compared for three molecules, ethyl acetate (one rotor, C_S), allyl acetate (one rotor, C_1), and methyl propionate (two rotors, C_S). XIAM is an user-friendly and extremely fast program. It can be used to fit rotational spectra of molecules with up to three internal rotors of an intermediate or high barrier to almost experimental accuracy. However, the program code needs to be improved for the low barrier case. For ethyl acetate and allyl acetate, where the barrier to internal rotation is on the order of 100 cm^{-1}, XIAM can fit the A species to experimental accuracy but the predictive power for the E species is not satisfactory. BELGI is also easy to use and has no problem with fitting spectra of molecules with low-barrier internal rotation. In contrast to XIAM, in the case of methyl propionate with a rather high barrier to internal rotation of 800 cm^{-1}, BELGI has shown problems with correlations between some internal rotation parameters. The XIAM code was also compared with the Erham code in the case of vinyl acetate (one rotor, C_S), isopropenyl acetate (two rotors, C_1), and acetone (two equivalent rotors, C_{2v}). Erham is very fast, the transitions frequencies can be usually fitted close to experimental accuracy even for the low barrier case. Especially in the case of isopropenyl acetate, where the splitting due to the propenyl methyl group is in the same order

of magnitude as the standard deviation obtained from the XIAM fit, Erham was a good choice to check the assignment. However, since Erham is based on an effective Hamiltonian, it is difficult to extract the rotational barrier. The physical meaning of the fitted parameters is less clear than in the other two programs.

Methyl acetate has been the only acetate investigated in the microwave region so far. Investigations of four new acetates within this thesis have shown that typically a low barrier on the order of 100 cm^{-1} can be expected for the acetyl methyl group. Some higher barriers were found for vinyl acetate (158 cm^{-1}) and isopropenyl acetate (135 cm^{-1}). This is probably due to electronic effects like delocalization within the π-electron system which extends from the vinyl double bond to the ester group.

Comparison of quantum chemical calculations using different methods and basis sets with the experimental results (rotational constants, angles between the internal axes and the principal axes) have shown, that currently no general purpose method and basis set for esters and ketones exists. This became especially clear in the case of diethyl ketone and methyl propionate. Therefore, the results of this thesis are also considered as reference data for future developments in quantum chemistry.

A combination of three interesting effects, nitrogen inversion tunneling, ^{14}N quadrupole coupling, and high barrier internal rotation was found in two amines, diethyl amine and methyl *tert*-butyl amine. Nitrogen inversion tunneling in secondary amines has been studied only for dimethyl amine and ethyl methyl amine before. In contrast to previous work, the inversion splittings were described with molecular parameters using the programs *spfit* and *spcat* by Pickett in a global fit instead of reporting the splitting of each single rotational transition. For diethyl amine, it was the first time that the complete ^{14}N nuclear quadrupole coupling tensor (i.e. also the off-diagonal coupling constant χ_{bc}) could be determined just from a perturbation due to a near degeneracy of two energy levels without additional information from isotopic substitution. ^{14}N quadrupole coupling was also studied in triethyl amine, an oblate top molecule with a propeller-like structure. Also in this case, quantum chemical calculations turned out to be very helpful to predict the stable conformers and to give reasonable start values for spectrum assignment, since many possible conformers can be generated by rotating the three ethyl groups.

Zusammenfassung

Im Rahmen dieser Arbeit wurden fünf Ester, zwei Ketone und drei Amine, die unterschiedliche Arten einer großamplitudigen Bewegung, nämlich der interne Rotation und der Inversion am Stickstoff zeigen, mit Hilfe einer Kombination von Molekularstrahl-Fouriertransform-Mikrowellenspektroskopie und quantenchemischen Rechnungen untersucht. Die molekulare Struktur wurde durch experimentell gewonnene Rotationskonstanten charakterisiert, die dann zur Validierung der quantenchemischen Rechnungen verwendet wurden. Die molekulare Dynamik wurde durch Angabe der Barrieren der internen Rotation und der Inversion beschrieben. Diese experimentellen Daten wurden durch Potentialkurven und zweidimensionalen Energieflächen ergänzt, die mit Hilfe quantenchemischer Rechnungen erhalten wurden. Die meisten Ergebnisse stellen Referenzdaten für die astrophysikalische Forschung, die Atmosphärenchemie oder allgemeine gasphasenanalytische Anwendungen dar.

Die Ester und Ketone wurden nach der Symmetrie und der Anzahl der internen Rotoren ausgewählt. Die große Vielfalt an Molekülen war wichtig, da diese als Testsysteme für drei verschiedene Computerprogramme, XIAM, BELGI und Erham, die das Problem der internen Rotation mit unterschiedlichen Methoden behandeln, dienen sollten. In vergleichenden Studien wurde der Bereich von Rotationsbarrieren, für den zuverlässige Ergebnisse erwartet werden können, untersucht. Die Programme BELGI und XIAM wurden für drei Moleküle, Ethylacetat (ein Rotor, C_S), Allylacetat (ein Rotor, C_1) und Methylpropionat (zwei Rotoren, C_S) verglichen. XIAM ist ein benutzerfreundliches und extrem schnelles Programm. Es kann zur Anpassung der Spektren von Molekülen mit bis zu drei internen Rotoren mit mittlerer oder hoher Barriere innerhalb experimenteller Genauigkeit verwendet werden. Dieses Programm muss jedoch für den Bereich niedriger Barrieren verbessert werden. Für Ethylacetat und Allylacetat, wo die Barrieren der internen Rotation eine Größenordnung von $100\,\mathrm{cm}^{-1}$ besitzen, kann XIAM die A-Spezies mit experimenteller Genauigkeit anpassen, jedoch ist die Vorhersagekraft für die E-Spezies nicht befriedigend. BELGI ist ebenfalls leicht zu verwenden und hat keine Probleme mit der Anpassung von Spektren von Molekülen mit niedriger Barriere. Jedoch zeigten sich bei BELGI im Gegensatz zu XIAM beim Methylpropionat, das eine relativ hohe Hinderungsbarriere der internen Rotation von $800\,\mathrm{cm}^{-1}$ besitzt, Probleme mit der Korrelation zwischen einigen Parametern der internen Rotation. Das Programm XIAM wurde für Vinylacetat (ein Rotor, C_S), Isopropenylacetat (zwei Rotoren, C_1)

und Aceton (zwei äquivalente Rotoren, C_{2v}) ebenfalls mit dem Programm Erham verglichen. Erham ist sehr schnell, die Übergangsfrequenzen können auch für den Fall niedriger Barrieren üblicherweise mit experimenteller Genauigkeit angepasst werde. Besonders im Fall von Isopropenylacetat, wo Aufspaltungen, die durch die Isopropenyl-Methylgruppe hervorgerufen werden, in der gleichen Größenordnung wie die Standardabweichung der Anpassung mit XIAM liegen, stellte Erham eine gute Möglichkeit zur Überprüfung der Zuordnung dar. Erham beruht lediglich auf einen effektiven Hamiltonoperator, daher ist es jedoch schwierig aus den Ergebnissen eine Rotationsbarriere zu erhalten. Die physikalische Bedeutung der angepassten Parameter ist weniger klar als bei den beiden anderen Programmen.

Methylacetat war das einzige Acetat, das bisher im Mikrowellengebiet untersucht wurde. Untersuchungen an vier neuen Acetaten, die im Rahmen dieser Arbeit durchgeführt wurden, zeigten, das für die Acetyl-Methylgruppe typischerweise eine Barriere von 100 cm^{-1} erwartet werden kann. Einige höhere Barrieren wurden für Vinylacetat (158 cm^{-1}) und Isopropenylacetat (135 cm^{-1}) gefunden. Dieses beruht wahrscheinlich auf elektronische Effekte, wie die Delokalisierung innerhalb des π-Elektronensystems, welches sich von der Vinyldoppelbindung bis zur Estergruppe erstreckt.

Ein Vergleich von quantenchemischen Rechnungen, die mit verschiedenen Methoden und Basissätzen durchgeführt wurden, mit der experimentellen Daten (Rotationskonstanten, Winkel zwischen der Achse des internen Rotors und den Hauptachsen des Moleküls) hat gezeigt, dass gegenwärtig eine Allzweckmethode bzw. ein Allzweckbasissatz für Ester und Ketone nicht existiert. Dieses wurde besonders im Fall des Diethylketons und des Methylpropionats deutlich. Deshalb können die Ergebnisse dieser Arbeit auch als Referenzdaten für zukünftige Entwicklungen in der Quantenchemie angesehen werden.

Eine Kombination von drei interessanten Effekten, der Inversion am Stickstoff, der ^{14}N-Quadrupolkopplung und der hochgehinderten internen Rotation wurde in zwei Aminen, dem Diethylamin und dem Methyl-*tert*-butylamin beobachtet. Die Inversion am Stickstoff innerhalb von sekundären Aminen wurde bisher nur am Dimethylamin und am Ethylmethylamin untersucht. Im Gegensatz zu vorherigen Arbeiten wurden Inversionsaufspaltungen am Stickstoff nicht für jeden einzelnen Übergang berichtet, sondern mit Hilfe molekularer Parameter beschrieben, die unter Verwendung der Programme spfit und spcat von Pickett in einem globalen Fit erhalten wurden. Für Diethylamin konnte zum ersten Mal der vollständige ^{14}N-Kerquadrupolkopplungstensor (d.h. einschließlich des Außer-

diagonalements χ_{bc}) bestimmt werden, wobei eine Störung aufgrund zweier nahezu entarteter Energieniveaus ausgenutzt wurde, ohne dass eine zusätzliche Information durch Isotopierung erforderlich war. Die ^{14}N-Quadrupolkopplung wurde ebenfalls am Triethylamin, einem oblate Top mit einer propellerartigen Struktur untersucht. Auch in diesem Fall erwiesen sich quantenchemische Rechnungen zur Vorhersage stabiler Konformere und um vernünftige Anfangswerte für die Zuordnung der Spektren zu erhalten, als sehr hilfreich, da durch Drehung der drei Ethylgruppen sehr viele Konformere erzeugt werden können.

Appendix

Chapter 1

ETHYL ACETATE

Table A-1

Cartesian nuclear coordinates in the principal inertial axes of the *trans* (assigned), *gauche* and *cis* conformer of ethyl acetate calculated at the MP2/6-311++G(d,p) level. The atoms are numbered according Figure A-1.

	trans conformer			*gauche* conformer		
	a /Å	b /Å	c /Å	a /Å	b /Å	c /Å
C1	–0.992923	0.081931	–0.000036	–0.861495	0.130741	–0.053438
O2	–1.179447	1.280087	0.000046	–0.674647	1.319355	–0.203973
O3	0.236786	–0.482697	–0.000085	0.095714	–0.811056	–0.229301
C4	–2.063158	–0.979275	0.000041	–2.159934	–0.509966	0.363444
H5	–1.953099	–1.613370	–0.882740	–2.387127	–1.359795	–0.282606
H6	–1.953017	–1.613324	0.882843	–2.060973	–0.882196	1.386728
H7	–3.043251	–0.504279	0.000076	–2.958556	0.229356	0.320143
C8	1.333536	0.455910	–0.000059	1.406768	–0.308727	–0.568837
H9	1.252861	1.093111	–0.884836	1.906437	–1.160387	–1.032496
H10	1.252733	1.093222	0.884623	1.301058	0.495378	–1.300212
C11	2.612330	–0.353021	0.000081	2.149231	0.164334	0.667918
H12	2.668424	–0.986643	–0.888002	3.165571	0.464762	0.395139
H13	3.473230	0.322070	0.000084	1.644349	1.022266	1.115441
H14	2.668312	–0.986507	0.888269	2.212297	–0.641839	1.403317

	cis conformer		
	a /Å	b /Å	c /Å
C1	–1.036711	–0.129698	–0.000069
O2	–1.883922	–0.990484	0.000124
O3	0.274363	–0.500016	–0.000877
C4	–1.347948	1.352378	0.001530
H5	–0.931708	1.838016	0.887943
H6	–0.926235	1.841535	–0.880308
H7	–2.430312	1.468033	–0.001423
C8	1.309407	0.496426	–0.003542
H9	1.223319	1.122937	–0.897525
H10	1.219932	1.131599	0.883938
C11	2.629891	–0.246193	0.002652
H12	2.712416	–0.881698	–0.881432
H13	3.457310	0.469563	0.000351
H14	2.709339	–0.872417	0.893615
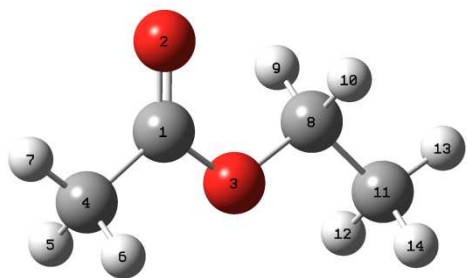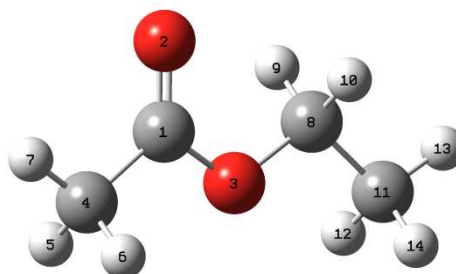
FIG. A-1

Table A-2

Observed A species frequencies ($\nu_{Obs.}$) of the *trans* ethyl acetate. $\nu_{Obs.} - \nu_{Calc.}$ values as obtained after a fit with BELGI-C$_S$ and XIAM are given in MHz.

Upper level			Lower level			$\nu_{Obs.}$	$\nu_{Obs.} - \nu_{Calc.}$	$\nu_{Obs.} - \nu_{Calc.}$
J	K_a	K_c	J	K_a	K_c	MHz	BELGI-C$_S$	XIAM
1	1	0	1	0	1	6785.923(5)	0.002	0.001
2	1	2	1	1	1	7297.734(5)	–0.003	–0.002
3	1	2	3	0	3	7761.041(5)	–0.005	–0.007
4	1	3	4	0	4	8606.360(5)	0.001	–0.003
4	0	4	3	1	3	9596.595(5)	0.001	0.002
1	1	1	0	0	0	10252.843(5)	–0.001	–0.002
3	1	3	2	1	2	10937.392(5)	0.002	0.003
6	1	5	6	0	6	11199.529(5)	0.004	–0.000
3	0	3	2	0	2	11432.550(5)	0.001	0.001
3	2	2	2	2	1	11492.364(5)	–0.001	0.000
3	2	1	2	2	0	11552.318(5)	–0.001	0.000
3	1	2	2	1	1	12028.748(5)	0.001	0.001
7	1	6	7	0	7	13019.715(5)	0.004	–0.000
2	1	2	1	0	1	13719.739(5)	0.001	–0.000
4	1	4	3	1	3	14566.520(5)	0.001	0.002
4	0	4	3	0	3	15174.526(5)	0.000	0.001
8	1	7	8	0	8	15216.818(5)	0.006	0.003
4	2	3	3	2	2	15311.440(5)	0.000	0.002
4	2	2	3	2	1	15460.220(5)	0.001	0.001
4	1	3	3	1	2	16019.842(5)	0.001	0.001
8	2	6	8	1	7	16536.543(5)	0.000	–0.002
3	1	3	2	0	2	17010.480(5)	–0.001	–0.001
5	2	3	5	1	4	17664.160(5)	0.001	0.000
5	1	5	4	1	4	18182.484(5)	0.001	0.002
4	2	2	4	1	3	18244.477(5)	0.002	0.000
5	0	5	4	0	4	18860.951(5)	0.002	0.002
5	2	4	4	2	3	19120.494(5)	0.000	0.001
5	3	3	4	3	2	19201.291(5)	0.002	0.002
5	3	2	4	3	1	19209.414(5)	–0.003	–0.001
5	1	4	4	1	3	19993.898(5)	0.000	–0.000
4	1	4	3	0	3	20144.449(5)	–0.002	–0.001
10	1	9	10	0	10	20695.264(5)	0.000	0.001
6	0	6	5	0	5	22484.955(5)	0.005	0.005
5	1	5	4	0	4	23152.406(5)	–0.002	0.000
6	1	5	5	1	4	23945.168(5)	0.001	0.000
7	4	4	6	4	3	26888.754(5)	–0.005	–0.003
7	4	3	6	4	2	26889.758(5)	0.004	0.005
7	3	5	6	3	4	26916.561(5)	–0.002	–0.000
7	3	4	6	3	3	26964.783(5)	0.000	0.001
10	1	9	9	2	8	27092.285(5)	–0.003	–0.005
12	3	9	12	2	10	27270.416(5)	0.000	0.001

Table A-2 continued

Upper level			Lower level			$\nu_{Obs.}$	$\nu_{Obs.} - \nu_{Calc.}$	$\nu_{Obs.} - \nu_{Calc.}$
J	K_a	K_c	J	K_a	K_c	MHz	BELGI-C_S	XIAM
2	2	1	1	1	0	27291.061(5)	–0.005	–0.007
7	2	5	6	2	4	27466.643(5)	–0.002	–0.002
19	3	16	19	2	17	27496.512(5)	0.001	0.001
2	2	0	1	1	1	27670.020(5)	0.003	–0.001
7	1	6	6	1	5	27866.926(5)	–0.004	–0.002
11	3	8	11	2	9	28286.297(5)	0.006	0.009
9	2	8	9	1	9	28308.881(5)	–0.008	–0.005
8	1	8	7	1	7	28935.729(5)	0.001	0.000
7	1	7	6	0	6	28957.711(5)	0.004	0.004
8	0	8	7	0	7	29554.342(5)	0.001	0.001
10	2	9	10	1	10	30218.414(5)	0.001	0.007
9	3	6	9	2	7	30283.488(5)	–0.008	–0.005
8	1	8	7	0	7	31846.691(5)	0.002	0.003
9	1	9	8	1	8	32487.266(5)	–0.003	–0.002
9	0	9	8	0	8	33021.551(5)	0.000	–0.002
3	3	1	3	2	2	33026.504(5)	–0.001	–0.002
10	1	10	9	1	9	36023.500(5)	0.001	–0.003
4	2	2	3	1	3	36447.434(5)	0.005	0.003
10	0	10	9	0	9	36463.980(5)	0.001	–0.003

Table A-3

Observed E species frequencies ($\nu_{Obs.}$) of the *trans* ethyl acetate. $\nu_{Obs.} - \nu_{Calc.}$ values as obtained after a fit with BELGI-C_S and XIAM are given in MHz.

Upper level			Lower level			$\nu_{Obs.}$	$\nu_{Obs.} - \nu_{Calc.}$	$\nu_{Obs.} - \nu_{Calc.}$
J	K_a	K_c	J	K_a	K_c	MHz	BELGI-C_S	XIAM
3	0	3	2	1	1	6458.119(5)	0.000	0.125
2	1	1	1	1	0	7581.513(5)	–0.001	0.011
2	0	2	1	0	1	7598.280(5)	–0.001	0.056
2	1	2	1	1	1	7745.219(5)	0.001	–0.033
2	1	2	2	0	2	8288.822(5)	–0.002	0.309
1	1	0	0	0	0	8734.429(5)	–0.007	0.007
5	1	5	5	0	5	10306.385(5)	–0.013	–0.005
3	1	2	2	1	1	11224.157(5)	0.003	0.057
3	0	3	2	0	2	11371.928(5)	0.000	0.061
3	2	2	2	2	1	11506.388(5)	–0.001	–0.005
3	2	1	2	2	0	11518.656(5)	0.000	–0.005
6	1	6	6	0	6	11639.611(5)	0.002	0.009
3	1	3	2	1	2	11734.432(5)	0.000	–0.065
2	1	1	1	0	1	12512.088(5)	–0.001	–0.010

Table A-3 continued

Upper level			Lower level			$\nu_{Obs.}$	$\nu_{Obs.} - \nu_{Calc.}$	$\nu_{Obs.} - \nu_{Calc.}$
J	K_a	K_c	J	K_a	K_c	MHz	BELGI-C$_S$	XIAM
7	1	7	7	0	7	13325.237(5)	0.003	0.050
5	0	5	4	1	3	14364.854(5)	−0.003	0.069
4	1	3	3	1	2	14783.518(5)	0.004	0.087
4	0	4	3	0	3	15111.373(5)	−0.001	0.050
4	3	2	3	3	1	15329.916(5)	0.000	0.001
4	3	1	3	3	0	15341.698(5)	0.000	0.001
4	2	3	3	2	2	15363.174(5)	0.000	−0.009
8	1	8	8	0	8	15374.878(5)	0.002	0.096
3	1	2	2	0	2	16137.964(5)	0.001	−0.010
9	1	9	9	0	9	17788.625(5)	0.003	0.117
9	2	8	9	1	9	17987.557(5)	−0.001	−0.294
8	2	7	8	1	8	18165.309(5)	0.000	−0.229
6	0	6	5	1	4	18480.793(5)	−0.003	−0.002
7	2	6	7	1	7	18601.234(5)	−0.001	−0.131
5	0	5	4	0	4	18803.029(5)	−0.002	0.031
5	4	2	4	4	1	19156.248(5)	0.000	0.005
5	4	1	4	4	0	19171.758(5)	−0.006	−0.004
5	3	3	4	3	2	19175.256(5)	−0.001	−0.004
6	2	5	6	1	6	19183.428(5)	0.001	−0.043
5	3	2	4	3	1	19192.643(5)	−0.002	−0.006
5	2	4	4	2	3	19241.271(5)	0.001	−0.016
5	2	3	4	2	2	19265.137(5)	−0.001	−0.020
4	1	3	3	0	3	19549.549(5)	0.001	0.013
5	2	4	5	1	5	19801.156(5)	0.000	0.002
10	1	10	10	0	10	20546.779(5)	0.004	0.087
6	1	5	5	1	4	21863.559(5)	0.002	0.072
6	0	6	5	0	5	22436.594(5)	−0.002	0.011
5	1	4	4	0	4	22758.828(5)	−0.003	0.040
6	4	3	5	4	2	22997.727(5)	0.001	0.000
6	4	2	5	4	1	23017.781(5)	−0.002	−0.006
6	3	4	5	3	3	23029.285(5)	0.001	−0.011
6	3	3	5	3	2	23054.098(5)	−0.001	−0.012
6	2	4	5	2	3	23151.313(5)	0.001	−0.028
11	1	11	11	0	11	23607.627(5)	−0.003	−0.002
7	1	6	6	1	5	25411.070(5)	0.002	0.057
7	3	5	6	3	4	26893.955(5)	0.000	−0.024
7	3	4	6	3	3	26928.352(5)	−0.002	−0.023
7	2	5	6	2	4	27018.654(5)	0.003	−0.034
7	1	7	6	1	6	27694.324(5)	−0.001	0.042
8	1	7	7	1	6	28956.043(5)	0.003	0.042
8	0	8	7	0	7	29524.801(5)	0.001	−0.002
8	1	8	7	1	7	31574.441(5)	0.000	0.045
9	1	8	8	1	7	32493.424(5)	0.001	0.025
9	0	9	8	0	8	32997.738(5)	0.000	−0.000

Table A-3 continued

Upper level			Lower level			$\nu_{Obs.}$	$\nu_{Obs.} - \nu_{Calc.}$	$\nu_{Obs.} - \nu_{Calc.}$
J	K_a	K_c	*J*	K_a	K_c	MHz	BELGI-C$_S$	XIAM
10	0	10	9	1	8	34731.359(5)	–0.006	–0.197
9	1	9	8	1	8	35411.484(5)	0.000	0.016
10	1	9	9	1	8	36020.824(5)	0.000	0.010
10	0	10	9	0	9	36443.426(5)	0.006	0.007
10	1	9	9	0	9	37732.883(5)	0.004	0.203
10	2	8	9	2	7	38233.402(5)	0.003	–0.065
11	0	11	10	1	9	38586.727(5)	–0.007	–0.200
10	1	10	9	1	9	39201.578(5)	0.004	–0.028

Table A-4

Observed splittings ($\nu_{Obs.}$) of transitions of *trans* ethyl acetate due to internal rotation of the ethyl methyl group;

$\nu_{Obs.} - \nu_{Calc.}$ values as obtained after a fit with XIAM.

Upper level			Lower level				$\nu_{Obs.}$	$\nu_{Obs.} - \nu_{Calc.}$
J	K_a	K_c	*J*	K_a	K_c		MHz	kHz
1	1	1	0	0	0	$\|\pm1,0>$	8734.4348	
						$\|\pm1,\pm1>$	0.0203	–3.4
						$\|\pm1,\mp1>$	–0.0265	1.1
1	1	0	1	0	1	$\|\pm1,0>$	8141.8851	
						$\|\pm1,\pm1>$	–0.0269	0.8
						$\|\pm1,\mp1>$	0.0209	–1.4
2	1	2	1	0	1	$\|\pm1,0>$	12512.0876	
						$\|\pm1,\pm1>$	0.0234	0.8
						$\|\pm1,\mp1>$	–0.0241	2.5
2	1	1	2	0	2	$\|\pm1,0>$	8288.8223	
						$\|\pm1,\pm1>$	–0.0256	0.0
						$\|\pm1,\mp1>$	0.0182	–2.1
3	0	3	2	1	2	$\|\pm1,0>$	6458.1190	
						$\|\pm1,\pm1>$	–0.0254	–1.5
						$\|\pm1,\mp1>$	0.0278	0.3
4	0	4	3	1	3	$\|\pm1,0>$	10345.3369	
						$\|\pm1,\pm1>$	–0.0222	–1.1
						$\|\pm1,\mp1>$	0.0249	0.3
6	2	4	6	1	5	$\|\pm1,0>$	19183.4273	
						$\|\pm1,\pm1>$	–0.0487	–1.7
						$\|\pm1,\mp1>$	0.0342	1.3

Table A-4 continued

Upper level			Lower level				$\nu_{Obs.}$	$\nu_{Obs.} - \nu_{Calc.}$
J	K_a	K_c	J	K_a	K_c		MHz	kHz
7	2	5	7	1	6	$\lvert \pm1,0 >$	18601.2349	
						$\lvert \pm1,\pm1 >$	–0.0485	–2.6
						$\lvert \pm1,\mp1 >$	0.0321	–0.2
8	2	6	8	1	7	$\lvert \pm1,0 >$	18165.3072	
						$\lvert \pm1,\pm1 >$	–0.0423	–0.2
						$\lvert \pm1,\mp1 >$	0.0262	–2.9
8	4	5	9	3	6	$\lvert 0,0 >$	11106.2714	
						$\lvert 0,\pm1 >$	–0.0198	–1.2

Chapter 2

ALLYL ACETATE

Table B-1

Some observed c type transitions ($\nu_{Obs.}$) of allyl acetate (not incl. in fit, see text). $\nu_{Calc.}$ values are obtained from a prediction with the program XIAM.

Upper level			Lower level			$\nu_{Obs.}$	$\nu_{Obs.} - \nu_{Calc.}$
J	K_a	K_c	J	K_a	K_c	MHz	MHz
2	1	1	1	0	1	11566.832	–0.001
3	1	2	2	0	2	14171.107	–0.004

Table B-2

Calculated geometry parameters in the *Gaussian*'s internal coordinate system (called standard orientation) and in the principal inertial axes of the assigned conformer (conformer I) of allyl acetate. The atoms are numbered according Figure 3.

	Gaussian internal coordinate system			principal inertial axes		
	a /Å	b /Å	c /Å	a /Å	b /Å	c /Å
C1	1.467027	0.122172	0.028940	1.443910	0.064319	0.030854
O2	1.655847	1.319410	0.036843	1.659633	1.256802	0.054154
O3	0.238421	–0.438187	–0.088803	0.202738	–0.466682	–0.091075
C4	2.523577	–0.944881	0.150083	2.476470	–1.027718	0.135031
H5	2.336801	–1.543576	1.044724	2.278367	–1.633941	1.022134
H6	2.476508	–1.611091	–0.714159	2.412404	–1.681120	–0.737852
H7	3.504815	–0.476558	0.211904	3.468137	–0.582419	0.200475
C8	–0.843356	0.513339	–0.211399	–0.857644	0.510454	–0.198172
H9	–0.889045	1.133186	0.688789	–0.887272	1.119114	0.710284
H10	–0.638888	1.163776	–1.067800	–0.640601	1.167494	–1.046399
C11	–2.100655	–0.27027	–0.400640	–2.132692	–0.242123	–0.394481
C12	–3.150290	–0.174671	0.427751	–3.177970	–0.134024	0.437873
H13	–2.140178	–0.926651	–1.267683	–2.189000	–0.885832	–1.270055
H14	–4.061668	–0.736328	0.251891	–4.102161	–0.672673	0.256978
H15	–3.120303	0.473325	1.299609	–3.131374	0.501453	1.318175

Table B-3

Observed A species frequencies ($\nu_{Obs.}$) of allyl acetate. $\nu_{Obs.} - \nu_{Calc.}$ values as obtained after a fit with

BELGI-C_1.

Upper level			Lower level			$\nu_{Obs.}$	$\nu_{Obs.} - \nu_{Calc.}$
J	K_a	K_c	J	K_a	K_c	MHz	MHz
1	1	1	0	0	0	8899.210	–0.001
3	2	2	4	1	3	9373.292	0.000
4	1	4	3	1	3	9386.164	0.001
4	0	4	3	0	3	9627.241	0.000
4	2	3	3	2	2	9644.523	0.001
4	3	2	3	3	1	9649.679	0.000
4	3	1	3	3	0	9649.783	0.001
4	2	2	3	2	1	9663.270	0.000
9	1	8	9	0	9	9887.376	0.001
4	1	3	3	1	2	9898.300	–0.001
3	2	1	4	1	4	10663.163	0.005
2	1	2	1	0	1	11182.648	–0.003
8	3	5	9	2	8	11201.637	0.002
5	1	5	4	1	4	11729.275	0.001
5	0	5	4	0	4	12020.039	0.001
2	2	1	3	1	2	12037.091	–0.003
5	2	4	4	2	3	12053.282	0.001
5	4	2	4	4	1	12061.602	–0.001
5	4	1	4	4	0	12061.602	–0.002
5	3	3	4	3	2	12063.718	0.000
5	3	2	4	3	1	12064.078	0.000
5	2	3	4	2	2	12090.701	–0.001
5	1	4	4	1	3	12369.212	–0.001
7	3	5	8	2	6	13162.001	0.001
3	1	3	2	0	2	13402.767	–0.001
7	3	4	8	2	7	13554.565	0.001
6	0	6	5	0	5	14403.657	0.001
6	2	5	5	2	4	14460.461	0.000
6	5	1	5	5	0	14473.555	0.001
6	5	2	5	5	1	14473.555	0.001
6	4	3	5	4	2	14475.263	0.002
6	4	2	5	4	1	14475.263	–0.003
6	3	4	5	3	3	14478.743	0.000
6	3	3	5	3	2	14479.706	0.001
6	2	4	5	2	3	14525.713	0.000
4	1	4	3	0	3	15561.932	–0.002
7	5	3	6	5	2	16886.945	–0.002
7	5	2	6	5	1	16886.945	–0.002
7	4	4	6	4	3	16889.637	–0.010
7	4	3	6	4	2	16889.672	0.010
7	3	5	6	3	4	16894.861	–0.001
7	3	4	6	3	3	16897.025	0.000

Table B-3 continued

Upper level			Lower level			$\nu_{Obs.}$	$\nu_{Obs.} - \nu_{Calc.}$
J	K_a	K_c	J	K_a	K_c	MHz	MHz
9	0	9	8	1	8	16935.998	–0.002
7	1	6	6	1	5	17302.818	0.000
9	2	7	9	1	8	17447.225	0.001
5	1	5	4	0	4	17663.965	–0.003
8	2	6	8	1	7	17781.213	0.000
8	1	8	7	1	7	18744.102	–0.001
5	2	3	5	1	4	18767.434	0.000
4	2	2	4	1	3	19045.941	–0.003
3	2	1	3	1	2	19280.973	–0.003
8	6	3	7	6	2	19298.738	0.003
8	6	2	7	6	1	19298.738	0.003
8	5	3	7	5	2	19300.866	0.001
8	5	4	7	5	3	19300.866	0.001
8	4	5	7	4	4	19304.883	0.005
8	4	4	7	4	3	19304.918	–0.003
8	3	6	7	3	5	19312.137	0.003
8	3	5	7	3	4	19316.453	–0.002
2	2	0	2	1	1	19464.381	–0.001
8	1	7	7	1	6	19764.250	0.000
2	2	1	2	1	2	19846.686	0.000
3	2	2	3	1	3	20039.941	0.003
4	2	3	4	1	4	20298.299	0.002
5	2	4	5	1	5	20622.305	0.001
2	2	1	1	1	0	24413.570	–0.001
2	2	0	1	1	1	24543.508	–0.002
10	1	10	9	0	9	27546.250	0.000
13	0	13	12	1	12	27827.837	–0.001
11	1	11	10	0	10	29457.917	0.004
14	0	14	13	1	13	30492.182	–0.005
5	2	4	4	1	3	31071.094	–0.002
13	3	10	13	2	11	31194.122	–0.004
13	2	12	12	2	11	31240.482	–0.004
13	4	10	12	4	9	31397.523	–0.001
13	4	9	12	4	8	31399.013	0.004
13	3	11	12	3	10	31414.015	0.000
13	3	10	12	3	9	31464.503	0.003
12	3	9	12	2	10	31568.823	–0.001
13	2	11	12	2	10	31839.203	0.006
11	3	8	11	2	9	31881.966	–0.002
13	1	12	12	1	11	31986.666	0.002
10	3	7	10	2	8	32135.379	–0.001
9	3	6	9	2	7	32333.364	0.002
5	2	3	4	1	4	32417.130	0.001
8	3	5	8	2	6	32482.065	0.003

Table B-3 continued

Upper level			Lower level			$\nu_{Obs.}$	$\nu_{Obs.} - \nu_{Calc.}$
J	K_a	K_c	J	K_a	K_c	MHz	MHz
7	3	4	7	2	5	32588.785	0.004
6	3	3	6	2	4	32661.306	0.002
14	1	14	13	1	13	32687.731	–0.001
5	3	2	5	2	3	32707.310	–0.002
4	3	1	4	2	2	32733.932	–0.003
3	3	0	3	2	1	32747.424	0.002
4	3	2	4	2	3	32761.945	0.000
5	3	3	5	2	4	32772.382	0.001
6	3	4	6	2	5	32790.665	0.002
7	3	5	7	2	6	32819.777	–0.003
8	3	6	8	2	7	32863.092	0.000
9	3	7	9	2	8	32924.273	0.000
10	3	8	10	2	9	33007.254	–0.001
14	0	14	13	0	13	33036.797	–0.003
11	3	9	11	2	10	33116.156	–0.004
6	2	5	5	1	4	33162.346	0.002
12	3	10	12	2	11	33255.236	0.006
13	1	13	12	0	12	33292.744	0.002
13	3	11	13	2	12	33428.764	0.005
14	3	12	14	2	13	33641.023	–0.005
15	3	13	15	2	14	33896.223	–0.006
14	1	14	13	0	13	35232.349	0.003
9	2	8	8	1	7	39061.637	–0.003

Table B-4

Observed E species frequencies ($\nu_{Obs.}$) of allyl acetate. $\nu_{Obs.} - \nu_{Calc.}$ values as obtained after a fit with

BELGI-C$_1$.

Upper level			Lower level			$\nu_{Obs.}$	$\nu_{Obs.} - \nu_{Calc.}$
J	K_a	K_c	J	K_a	K_c	MHz	MHz
1	1	1	0	0	0	7498.669	–0.002
6	0	6	5	1	5	9407.794	0.001
4	1	4	3	1	3	9550.206	0.001
4	0	4	3	0	3	9594.276	0.000
4	–2	2	3	–2	1	9646.692	0.000
4	2	3	3	2	2	9650.765	0.001
8	–1	7	8	0	8	9687.986	0.002
4	–1	3	3	–1	2	9734.043	–0.001
2	1	2	1	0	1	9910.385	–0.002
2	2	1	3	1	3	10851.832	0.000
3	–2	1	4	–1	3	11002.729	0.001

Table B-4 continued

Upper level			Lower level			$\nu_{Obs.}$	$\nu_{Obs.} - \nu_{Calc.}$
J	K_a	K_c	J	K_a	K_c	MHz	MHz
5	1	5	4	1	4	11881.648	0.002
5	0	5	4	0	4	11983.261	–0.001
5	–4	1	4	–4	0	12050.870	0.000
5	–3	2	4	–3	1	12053.754	0.000
5	4	2	4	4	1	12055.349	–0.001
5	3	3	4	3	2	12057.822	0.000
5	–2	3	4	–2	2	12062.555	0.001
5	2	4	4	2	3	12068.780	0.001
5	–1	4	4	–1	3	12212.008	0.000
3	1	3	2	0	2	12303.039	–0.002
2	–1	1	1	0	1	12707.988	–0.002
2	–2	0	3	–1	2	13503.676	0.000
9	2	8	9	–1	8	13830.993	0.001
8	2	7	8	–1	7	14186.638	0.000
6	–4	2	5	–4	1	14462.293	0.001
6	–3	3	5	–3	2	14466.840	0.003
6	4	3	5	4	2	14467.822	–0.001
6	3	4	5	3	3	14472.137	0.000
6	–2	4	5	–2	3	14481.385	0.000
7	2	6	7	–1	6	14505.325	0.002
4	1	4	3	0	3	14653.284	0.000
5	2	4	5	–1	4	14983.522	0.000
3	–1	2	2	0	2	15180.381	–0.002
7	–5	2	6	–5	1	16871.174	0.000
7	–4	3	6	–4	2	16874.395	0.000
7	5	3	6	5	2	16878.737	0.000
7	3	5	6	3	4	16887.959	0.000
5	1	5	4	0	4	16940.654	0.000
9	0	9	8	1	8	17177.818	–0.002
7	–1	6	6	–1	5	17183.961	0.001
2	2	1	2	1	2	18046.395	0.000
3	2	2	3	1	3	18087.371	0.000
4	2	3	4	1	4	18187.930	0.000
5	2	4	5	1	5	18375.061	–0.002
8	1	8	7	1	7	18816.622	0.000
10	–2	8	10	–1	9	18941.399	–0.001
8	–5	3	7	–5	2	19282.749	0.000
8	–4	4	7	–4	3	19287.294	0.000
8	4	5	7	4	4	19295.194	–0.002
8	–3	5	7	–3	4	19297.054	0.001
8	3	6	7	3	5	19305.548	–0.001
9	–2	7	9	–1	8	19313.538	–0.001
8	2	7	8	1	8	19600.841	–0.001
10	0	10	9	1	9	19838.711	0.002

Table B-4 continued

Upper level			Lower level			$\nu_{Obs.}$	$\nu_{Obs.} - \nu_{Calc.}$
J	K_a	K_c	J	K_a	K_c	MHz	MHz
5	–2	3	5	–1	4	20499.967	0.001
4	–2	2	4	–1	3	20649.422	0.003
3	–2	1	3	–1	2	20736.771	0.001
2	–2	0	2	–1	1	20777.977	0.000
2	2	1	1	1	1	22859.623	0.001
3	2	2	2	1	2	25281.934	0.001
2	–2	0	1	–1	0	25613.451	–0.002

Table B-5

Calculated geometry parameters in the principal inertial axes of conformer C_S, II, III, IV, and V of allyl acetate.
The atoms are numbered according Figure 3.

	Conformer C_S			Conformer II		
	a /Å	b /Å	c /Å	a /Å	b /Å	c /Å
C1	1.472110	0.095998	0.000015	–1.360641	–0.009327	0.000061
O2	1.610468	1.299973	–0.000009	–1.791783	–1.141533	–0.000046
O3	0.261855	–0.514079	0.000032	–0.037273	0.285801	0.000033
C4	2.577976	–0.926408	–0.000098	–2.180035	1.254297	–0.000022
H5	2.490103	–1.563293	0.883091	–1.937799	1.849603	0.883390
H6	2.489624	–1.563671	–0.882962	–1.937254	1.849885	–0.883091
H7	3.540557	–0.417187	–0.000452	–3.238506	0.998280	–0.000375
C8	–0.861578	0.386612	0.000120	0.827784	–0.857951	0.000021
H9	–0.802811	1.029020	0.884274	0.615223	–1.472574	0.881887
H10	–0.802878	1.029115	–0.883970	0.615191	–1.472583	–0.881833
C11	–2.107192	–0.455897	0.000118	2.253514	–0.401358	–0.000008
C12	–3.344010	0.059563	–0.000168	2.663953	0.873768	–0.000026
H13	–1.956924	–1.532949	0.000375	2.984514	–1.208870	–0.000014
H14	–4.216842	–0.583629	–0.000136	3.722583	1.110558	–0.000045
H15	–3.514436	1.133213	–0.000433	1.955003	1.693705	–0.000020

Table B-5 continued

	Conformer III			Conformer IV		
	a /Å	b /Å	c /Å	a /Å	b /Å	c /Å
C1	–1.128316	–0.088290	0.114620	1.443692	0.064425	–0.032424
O2	–1.028199	–0.610346	1.201505	1.659108	1.257102	–0.053672
O3	–0.200985	–0.210670	–0.873534	0.202778	–0.467016	0.088488
C4	–2.263461	0.787254	–0.346894	2.477169	–1.027013	–0.134285
H5	–1.908095	1.817626	–0.435485	2.437490	–1.654676	0.758935
H6	–2.611351	0.467127	–1.330756	2.259187	–1.659604	–0.997768
H7	–3.073413	0.742496	0.379807	3.465378	–0.580715	–0.235392
C8	0.972788	–0.956048	–0.522741	–0.857700	0.509796	0.200371
H9	0.696517	–1.783236	0.137604	–0.640096	1.163038	1.051343
H10	1.341800	–1.364511	–1.467576	–0.887736	1.122177	–0.705501
C11	2.023771	–0.102904	0.127999	–2.132583	–0.243804	0.394059
C12	1.935900	1.220275	0.313997	–3.178120	–0.132569	–0.437584
H13	2.915337	–0.640456	0.448789	–2.188537	–0.891051	1.267033
H14	2.740119	1.767505	0.793396	–4.102100	–0.672201	–0.258507
H15	1.062503	1.780290	–0.003842	–3.131972	0.506542	–1.315258

Table B-5 continued

	Conformer V		
	a /Å	b /Å	c /Å
C1	1.163821	0.180449	–0.078162
O2	0.766717	1.228094	–0.538666
O3	0.452615	–0.976328	–0.107514
C4	2.481761	–0.032311	0.619209
H5	2.303830	–0.070453	1.697738
H6	2.927742	–0.980669	0.315915
H7	3.148862	0.798919	0.393904
C8	–0.890694	–0.853733	–0.634400
H9	–0.887734	–0.171460	–1.487482
H10	–1.139430	–1.863293	–0.967200
C11	–1.831149	–0.376467	0.429467
C12	–2.459618	0.806594	0.364789
H13	–1.986385	–1.038986	1.279237
H14	–3.140203	1.128218	1.146784
H15	–2.290930	1.481966	–0.469079

Chapter 3

VINYL ACETATE

Table C-1

Calculated geometry parameters in the principal inertial axes of conformer I and conformer II of vinyl acetate calculated at the MP2/6-311++G(d,p) and the MP2/6-311++G level of theory. The atoms are numbered according Figure 1.

	Conformer I			Conformer II		
	MP2/6-311++G(d,p)			MP2/6-311++G(d,p)		
	a /Å	b /Å	c /Å	a /Å	b /Å	c /Å
C1	–2.036850	–0.926071	–0.000544	2.201035	–0.390876	0.101113
H2	–1.994965	–1.490165	0.934443	2.380710	–1.133192	–0.679142
H3	–1.886551	–1.628798	–0.822815	2.306584	–0.888304	1.068483
H4	–3.002306	–0.431508	–0.094791	2.919103	0.424055	0.022777
C5	–0.944356	0.106784	–0.008084	0.806589	0.162954	–0.024990
O6	–1.086153	1.305380	–0.031038	0.507528	1.328431	–0.107726
O7	0.277202	–0.518046	0.024940	–0.087210	–0.877433	–0.026717
C8	1.400623	0.290786	0.062798	–1.457976	–0.679103	–0.088363
C9	2.612854	–0.256917	–0.048387	–2.168393	0.431332	0.146960
H10	1.204112	1.348512	0.191386	–1.928719	–1.623165	–0.339283
H11	3.484667	0.382616	0.000819	–3.245182	0.339569	0.062587
H12	2.742601	–1.324381	–0.181127	–1.735961	1.387370	0.394194

Table C-2

Observed A and E species frequencies ($\nu_{Obs.}$) of vinyl acetate. $\nu_{Obs.} - \nu_{Calc.}$ values as obtained after a fit with XIAM.

Upper level			Lower level				$\nu_{Obs.}$	$\nu_{Obs.} - \nu_{Calc.}$
J	K_a	K_c	J	K_a	K_c		MHz	kHz
1	1	1	0	0	0	A	11268.6222	–12.8
1	1	0	1	0	1	A	7603.8433	–5.8
2	1	2	1	0	1	A	14933.3756	–19.3
2	1	1	2	0	2	A	8031.6904	–7.1

Table C-2 continued

Upper level			Lower level				$\nu_{\text{Obs.}}$	$\nu_{\text{Obs.}} - \nu_{\text{Calc.}}$
J	K_a	K_c	J	K_a	K_c		MHz	kHz
2	2	1	2	1	2	A	22811.0955	−9.4
2	2	0	2	1	1	A	21595.8734	−1.8
3	1	3	2	0	2	A	18399.3563	−16.4
3	1	2	3	0	3	A	8705.0798	−13.3
3	2	2	3	1	3	A	23437.6303	−11.1
3	2	1	3	1	2	A	21058.7305	9.8
4	1	4	3	0	3	A	21688.6018	−6.4
4	0	4	3	1	3	A	9892.0713	−20.6
4	1	3	4	0	4	A	9660.2102	−12.7
4	2	3	4	1	4	A	24278.6424	−8.4
4	2	2	4	1	3	A	20428.5134	19.2
5	1	5	4	0	4	A	24836.0883	10.8
5	0	5	4	1	4	A	14488.7614	−13.8
5	1	4	5	0	5	A	10940.7832	−18.4
5	2	4	5	1	5	A	25337.6845	−9.5
5	2	3	5	1	4	A	19776.2488	33.6
6	0	6	5	1	5	A	19093.3153	4.5
6	1	5	5	2	4	A	6347.2832	−8.5
5	3	3	6	2	4	A	11607.0384	8.2
6	3	4	7	2	5	A	6873.6837	−20.7
6	3	3	7	2	6	A	8938.4386	16.0
1	1	0	1	0	1	E	8035.7888	−0.1
2	1	1	2	0	2	E	8271.4547	0.8
3	1	2	3	0	3	E	8831.061	7.4
4	1	3	4	0	4	E	9728.2396	14.8
5	1	4	5	0	5	E	10974.2171	20.1
6	1	5	6	0	6	E	12597.8747	20.8
7	1	6	7	0	7	E	14629.2292	15.8
8	1	7	8	0	8	E	17084.5706	6.4
9	1	8	9	0	9	E	19956.699	−8.4
4	0	4	3	1	3	E	10075.6022	−17.0
5	0	5	4	1	4	E	14602.9388	−4.6
6	0	6	5	1	5	E	19167.5427	21.3
7	0	7	6	1	6	E	23701.7651	62.4
1	1	1	0	0	0	E	10736.7885	9.1
1	1	1	1	0	1	E	6665.8778	7.7
2	1	2	1	0	1	E	14601.2021	22.8
3	1	3	2	0	2	E	18191.0844	46.8
2	2	1	2	1	2	E	21645.6982	−90.8
2	2	0	2	1	1	E	22450.3789	54.7
3	2	2	3	1	3	E	22186.9891	−56.8
3	2	1	3	1	2	E	21997.1052	37.4
4	2	3	4	1	4	E	23048.4232	−9.8
4	2	2	4	1	3	E	21346.8343	11.2

Table C-2 continued

Upper level			Lower level				$\nu_{Obs.}$	$\nu_{Obs.} - \nu_{Calc.}$
J	K_a	K_c	J	K_a	K_c		MHz	kHz
5	2	4	5	1	5	E	24219.1932	48.7
5	2	3	5	1	4	E	20585.9822	–19.1
6	1	5	5	2	4	E	7546.2254	–5.4
6	2	4	6	1	5	E	19819.4664	–42.7
7	1	6	6	2	5	E	12650.9283	–28.4
7	2	5	7	1	6	E	19181.0944	–40.2
8	1	7	7	2	6	E	17856.2806	–22.4
8	2	6	8	1	7	E	18804.678	1.1

Table C-3

Observed A and E species frequencies ($\nu_{Obs.}$) of vinyl acetate. $\nu_{Obs.} - \nu_{Calc.}$ values as obtained after a fit with Erham.

Upper level		Lower level			$\nu_{Obs.}$	$\nu_{Obs.} - \nu_{Calc.}$
J	N	J	N		MHz	kHz
1	2	0	1	A	11268.6222	2.2
1	3	1	1	A	7603.8433	1.5
2	2	1	1	A	14933.3756	–0.1
2	3	2	1	A	8031.6904	1.7
2	4	2	2	A	22811.0955	–0.5
2	5	2	3	A	21595.8734	–0.9
3	2	2	1	A	18399.3563	1.2
3	3	3	1	A	8705.0798	–2.0
3	4	3	2	A	23437.6303	–2.9
3	5	3	3	A	21058.7305	1.8
4	2	3	1	A	21688.6018	1.7
4	1	3	2	A	9892.0713	0.3
4	3	4	1	A	9660.2102	2.2
4	4	4	2	A	24278.6424	–0.3
4	5	4	3	A	20428.5134	–0.6
5	2	4	1	A	24836.0883	0.0
5	1	4	2	A	14488.7614	–1.0
5	3	5	1	A	10940.7832	1.5
5	4	5	2	A	25337.6845	–0.2
5	5	5	3	A	19776.2488	–0.8
6	1	5	2	A	19093.3153	–2.6
6	3	5	4	A	6347.2832	2.1
5	6	6	5	A	11607.0384	1.5

Table C-3 continued

Upper level		Lower level			$\nu_{Obs.}$	$\nu_{Obs.} - \nu_{Calc.}$
J	*N*	*J*	*N*		MHz	kHz
6	6	7	5	A	6873.6837	0.7
6	7	7	4	A	8938.4386	–0.8
1	3	1	1	E	8035.7888	2.4
2	3	2	1	E	8271.4547	1.4
3	3	3	1	E	8831.061	2.0
4	3	4	1	E	9728.2396	1.4
5	3	5	1	E	10974.2171	0.3
6	3	6	1	E	12597.8747	–1.6
7	3	7	1	E	14629.2292	–3.3
8	3	8	1	E	17084.5706	–2.1
9	3	9	1	E	19956.699	2.8
4	1	3	2	E	10075.6022	–2.6
5	1	4	2	E	14602.9388	0.5
6	1	5	2	E	19167.5427	2.5
7	1	6	2	E	23701.7651	2.2
1	2	0	1	E	10736.7885	4.5
1	2	1	1	E	6665.8778	2.7
2	2	1	1	E	14601.2021	–2.2
3	2	2	1	E	18191.0844	–5.3
2	4	2	2	E	21645.6982	–0.7
2	5	2	3	E	22450.3789	1.9
3	4	3	2	E	22186.9891	0.3
3	5	3	3	E	21997.1052	0.7
4	4	4	2	E	23048.4232	–0.1
4	5	4	3	E	21346.8343	–1.1
5	4	5	2	E	24219.1932	0.2
5	5	5	3	E	20585.9822	–2.5
6	3	5	4	E	7546.2254	2.0
6	5	6	3	E	19819.4664	–2.1
7	3	6	4	E	12650.9283	0.4
7	5	7	3	E	19181.0944	0.5
8	3	7	4	E	17856.2806	–2.5
8	5	8	3	E	18804.678	2.8

Chapter 4

ISOPROPENYL ACETATE

Table D-1

Calculated geometry parameters in *Gaussian*'s internal coordinate system (called standard orientation) and in principal inertial axes of the only stable *trans* conformer of isopropenyl acetate. The atoms are numbered according Figure 1.

	Gaussian internal coordinate system			principal inertial axes		
	X	Y	Z	X	Y	Z
C1	–2.456605	–0.296326	–0.421510	–2.425088	–0.422861	–0.436122
H2	–3.255908	0.076339	0.217357	–3.246596	0.018566	0.126179
H3	–2.532445	–1.379677	–0.535245	–2.471608	–1.512745	–0.387894
H4	–2.535204	0.150876	–1.415758	–2.493937	–0.131138	–1.487242
C5	–1.125669	0.063724	0.182029	–1.116428	0.059791	0.129335
O6	–0.941835	0.757497	1.154205	–0.970268	0.895489	0.989851
O7	–0.116721	–0.516074	–0.535902	–0.078587	–0.592355	–0.476602
C8	1.194179	–0.190972	–0.136784	1.215194	–0.175259	–0.108355
C9	1.937047	–1.155120	0.414133	1.970078	–1.025628	0.593050
H10	2.970603	–0.961390	0.673754	2.992844	–0.766847	0.838315
H11	1.515654	–2.133324	0.612544	1.569043	–1.974634	0.928280
C12	1.631593	1.193774	–0.493882	1.625469	1.152394	–0.660970
H13	1.498210	1.359347	–1.567907	1.510528	1.152338	–1.749787
H14	1.038815	1.934609	0.048258	1.003260	1.949043	–0.245826
H15	2.685457	1.331354	–0.243342	2.670117	1.354882	–0.415943
[a]	$\lvert\mu_a\rvert$	$\lvert\mu_b\rvert$	$\lvert\mu_c\rvert$	$\lvert\mu_a\rvert$	$\lvert\mu_b\rvert$	$\lvert\mu_c\rvert$
	0.246	0.594	1.796	0.194	0.862	1.691

[a] dipole moments in Debye

Table D-2

Observed AA and AE[a] species frequencies ($\nu_{Obs.}$) of isopropenyl acetate. $\nu_{Obs.} - \nu_{Calc.}$ values as obtained after a fit with XIAM.[a]

Upper level			Lower level				$\nu_{Obs.}$	$\nu_{Obs.} - \nu_{Calc.}$
J	K_a	K_c	J	K_a	K_c		MHz	MHz
b-type transitions								
2	1	2	1	0	1	AA	9959.8164	–0.0433
						AE	0.0000	0.0026
2	2	1	2	1	2	AA	10057.0205	–0.0751
						AE	0.0000	0.0137
2	2	0	2	1	1	AA	9603.3064	–0.0502
						AE	0.0183	0.0065
3	1	3	2	0	2	AA	13189.0572	–0.0508
						AE	0.0000	0.0020
3	2	2	3	1	3	AA	10289.8003	–0.0758
						AE	0.0000	0.0096
3	2	1	3	1	2	AA	9398.5042	–0.0320
						AE	0.0000	–0.0069
4	0	4	3	1	3	AA	10933.5866	–0.0445
						AE	–0.0206	–0.0050
4	2	3	4	1	4	AA	10602.0080	–0.0689
						AE	–0.0232	–0.0101
5	2	4	5	1	5	AA	10994.8505	–0.0779
						AE	–0.0264	–0.0077
6	1	5	5	2	4	AA	12450.4934	–0.0789
						AE	–0.0333	0.0041
6	2	5	6	1	6	AA	11469.4823	–0.0890
						AE	–0.0302	–0.0045
7	2	6	7	1	7	AA	12026.7301	–0.1004
						AE	–0.0361	–0.0020
7	1	7	6	2	4	AA	11762.8077	0.0140
						AE	0.0399	0.0140
8	1	8	7	2	5	AA	14275.2581	0.0452
						AE	0.0309	–0.0103
8	2	6	7	3	5	AA	12082.6581	–0.0777
						AE	–0.0333	0.0051
8	2	7	7	3	4	AA	11009.3480	–0.0262
						AE	–0.0185	–0.0008
8	2	7	8	1	8	AA	12666.8765	–0.1079
						AE	–0.0470	–0.0032
9	2	8	8	3	5	AA	14291.1135	–0.0377
						AE	–0.0124	0.0003
9	2	8	9	1	9	AA	13389.4367	–0.1176
						AE	–0.0556	–0.0010
10	2	9	10	1	10	AA	14193.0199	–0.1187
						AE	–0.0713	–0.0048

Table D-2 continued

Upper level			Lower level				$\nu_{Obs.}$	$\nu_{Obs.} - \nu_{Calc.}$
J	K_a	K_c	J	K_a	K_c		MHz	MHz
10	3	8	9	4	5	AA	11773.4892	–0.0611
						AE	–0.0974	0.0031
11	1	10	11	0	11	AA	10401.8322	–0.1531
						AE	–0.1316	–0.0123
11	3	8	11	2	9	AA	14497.0406	0.0121
						AE	0.0362	–0.0017
12	1	11	12	0	12	AA	11868.5195	–0.1567
						AE	–0.1535	–0.0141
12	3	9	12	2	10	AA	14025.7513	0.0226
						AE	0.0411	–0.0010
13	2	11	13	1	12	AA	9339.4845	–0.0743
						AE	–0.0636	–0.0034
13	3	10	13	2	11	AA	13561.2335	0.0298
						AE	0.0401	–0.0032
14	2	12	14	1	13	AA	10044.8318	–0.0830
						AE	–0.0886	–0.0045
14	3	11	14	2	12	AA	13137.9726	0.0317
						AE	0.0386	–0.0018
15	2	13	15	1	14	AA	10937.1968	–0.0944
						AE	–0.1013	0.0097
15	3	12	15	2	13	AA	12791.1339	0.0269
						AE	0.0350	0.0021
16	2	14	16	1	15	AA	12016.4400	–0.0842
						AE	–0.1455	–0.0054
16	3	13	16	2	14	AA	12554.0436	0.0263
						AE	0.0212	0.0010
17	2	15	17	1	16	AA	13274.6123	–0.0682
						AE	–0.1758	–0.0055
17	3	14	17	2	15	AA	12456.3030	0.0242
						AE	0.0000	–0.0023
19	3	16	19	2	17	AA	12773.8743	0.0283
						AE	–0.0485	0.0004
c-type transitions								
2	1	1	1	0	1	AA	10418.9033	–0.0517
						AE	–0.0148	–0.0055
2	2	0	2	1	2	AA	10062.3929	–0.0590
						AE	0.0000	–0.0050
2	2	1	2	1	1	AA	9597.9457	–0.0545
						AE	0.0000	0.0070
3	1	2	2	0	2	AA	14107.1140	–0.0724
						AE	–0.0210	–0.0054
3	2	1	3	1	3	AA	10316.5392	–0.0755
						AE	0.0000	0.0067

Table D-2 continued

Upper level			Lower level				$\nu_{\text{Obs.}}$	$\nu_{\text{Obs.}} - \nu_{\text{Calc.}}$
J	K_a	K_c	J	K_a	K_c		MHz	MHz
3	2	2	3	1	2	AA	9371.7627	–0.0349
						AE	0.0000	–0.0039
4	0	4	3	1	2	AA	10015.5299	–0.0228
						AE	0.0000	0.0021
4	2	2	4	1	4	AA	10681.9157	–0.0720
						AE	–0.0255	–0.0113
5	0	5	4	1	3	AA	13072.0079	–0.0206
						AE	0.0000	–0.0023
5	2	3	5	1	5	AA	11179.9346	–0.0899
						AE	–0.0281	–0.0046
6	1	5	5	2	3	AA	12265.4101	–0.0660
						AE	–0.0314	0.0011
6	2	4	6	1	6	AA	11835.1186	–0.1147
						AE	–0.0474	–0.0115
7	1	7	6	2	5	AA	12128.4559	0.0003
						AE	0.0255	0.0098
7	2	5	7	1	7	AA	12672.7065	–0.1380
						AE	–0.0480	0.0042
8	2	6	7	3	4	AA	12058.2565	–0.0740
						AE	–0.0432	0.0033
8	2	6	8	1	8	AA	13715.7850	–0.1557
						AE	–0.0754	–0.0029
8	2	7	7	3	5	AA	11033.7425	–0.0370
						AE	0.0082	0.0178
9	2	8	8	3	6	AA	14344.5048	–0.0420
						AE	–0.0101	0.0007
10	3	8	9	4	6	AA	11776.2012	–0.0611
						AE	0.0463	0.0047
10	3	7	9	4	5	AA	11968.0216	–0.0728
						AE	–0.1050	0.0027
11	3	9	11	2	9	AA	14161.7815	0.0327
						AE	0.0477	–0.0038
12	3	10	12	2	10	AA	13478.2406	0.0519
						AE	0.0633	–0.0013
13	3	11	13	2	11	AA	12708.0680	0.0687
						AE	0.0786	0.0007
14	3	12	14	2	12	AA	11862.9315	0.0858
						AE	0.0897	–0.0013
15	3	13	15	2	13	AA	10956.3197	0.0897
						AE	0.1093	0.0058

[a] The AE species is referred to the AA species. The differences of these transitions are given and fitted.

Table D-3

Observed EA, EE[a] and EE*[a] species frequencies ($\nu_{Obs.}$) of isopropenyl acetate. $\nu_{Obs.} - \nu_{Calc.}$ values as obtained

after a fit with XIAM.[b]

Upper level			Lower level				$\nu_{Obs.}$	$\nu_{Obs.} - \nu_{Calc.}$
J	K_a	K_c	J	K_a	K_c		MHz	MHz
2	2	0	2	1	1	EA	10278.4778	0.0751
						EE	–0.1275	–0.0133
						EE*	0.0952	–0.0195
3	2	1	3	1	2	EA	10174.3478	0.0597
						EE	–0.1197	–0.0009
						EE*	0.1246	0.0004
4	2	2	4	1	3	EA	9985.5422	0.0510
						EE	–0.1277	–0.0030
						EE*	0.137	–0.0006
5	2	3	5	1	4	EA	9726.1519	0.0325
						EE	–0.1326	–0.0018
						EE*	0.1522	0.0005
6	2	4	6	1	5	EA	9426.0113	0.0103
						EE	–0.1442	–0.0053
						EE*	0.1646	–0.0020
13	2	11	13	1	12	EA	9601.8574	0.1151
						EE	–0.1714	0.0069
						EE*	0.0458	–0.0147
14	2	12	14	1	13	EA	10318.5082	0.2048
						EE	–0.1211	0.0137
						EE*	–0.0424	–0.0061
15	2	13	15	1	14	EA	11246.7876	0.3215
						EE	–0.065	0.0029
						EE*	–0.1778	–0.0140
2	1	1	1	0	1	EA	10790.1509	0.0515
						EE	–0.1258	–0.0025
						EE*	0.1075	–0.0014
3	1	2	2	0	2	EA	14373.131	0.0663
						EE	–0.1511	–0.0220
						EE*	0.0902	–0.0130
11	1	10	11	0	11	EA	10885.5465	0.2494
						EE	0.2259	–0.0065
						EE*	–0.4925	–0.0035
4	0	4	3	1	3	EA	11188.9078	0.0903
						EE	–0.0961	–0.0023
						EE*	0.0724	0.0041

Table D-3 continued

Upper level			Lower level				$\nu_{Obs.}$	$\nu_{Obs.} - \nu_{Calc.}$
J	K_a	K_c	J	K_a	K_c		MHz	MHz
4	0	4	3	1	2	EA	9715.724	0.0298
						EE	0.1157	–0.0014
						EE*	–0.1204	0.0057
5	0	5	4	1	3	EA	12831.8299	0.0381
						EE	0.0981	–0.0045
						EE*	–0.0949	0.0068
5	2	3	5	1	5	EA	12262.8913	0.1303
						EE	–0.354	–0.0007
						EE*	0.3113	–0.0049
6	2	4	6	1	6	EA	12769.6821	0.1509
						EE	–0.3924	–0.0012
						EE*	0.3293	–0.0051
7	2	5	7	1	7	EA	13422.9293	0.1935
						EE	–0.4544	–0.0049
						EE*	0.3584	–0.0086
8	2	6	8	1	8	EA	14245.7647	0.2583
						EE	–0.5286	–0.0019
						EE*	0.4026	–0.0079
2	1	2	1	0	1	EA	9545.1685	–0.0156
						EE	0.1027	0.0072
						EE*	–0.0985	0.0063
3	1	3	2	0	2	EA	12899.9357	–0.0058
						EE	0.0839	0.0021
						EE*	–0.0917	–0.0005
6	1	6	5	2	4	EA	10342.1717	0.0148
						EE	–0.0701	0.0016
						EE*	0.0951	0.0053
7	1	7	6	2	5	EA	13201.0868	–0.0529
						EE	0.0147	0.0258
						EE*	0.0553	0.0115
3	2	2	3	1	3	EA	9335.7049	–0.0385
						EE	0.118	–0.0011
						EE*	–0.1322	–0.0022
4	2	3	4	1	4	EA	9582.6487	–0.0155
						EE	0.1172	0.0045
						EE*	–0.1363	–0.0016
5	2	4	5	1	5	EA	9958.5346	0.0234
						EE	0.0897	–0.0004
						EE*	–0.1306	–0.0036

Table D-3 continued

Upper level			Lower level				$\nu_{Obs.}$	$\nu_{Obs.} - \nu_{Calc.}$
J	K_a	K_c	J	K_a	K_c		MHz	MHz
6	2	5	6	1	6	EA	10458.8427	0.0797
						EE	0.0438	–0.0031
						EE*	–0.1086	–0.0069
7	2	6	7	1	7	EA	11072.5664	0.1535
						EE	–0.0275	–0.0081
						EE*	–0.0647	–0.0094
9	2	8	9	1	9	EA	12558.9207	0.3375
						EE	–0.2072	0.0013
						EE*	0.0861	–0.0079
8	2	6	7	3	4	EA	11200.5755	0.0051
						EE	0.0867	0.0041
						EE*	–0.1479	0.0019
8	2	7	7	3	5	EA	12180.2347	0.1698
						EE	–0.1628	0.0031
						EE*	0.1244	0.0042
4	2	2	4	1	4	EA	11890.4497	0.1198
						EE	–0.3353	–0.0012
						EE*	0.3104	–0.0017
10	3	7	9	4	5	EA	11480.9229	–0.0594
						EE	0.0808	0.0041
						EE*	–0.1377	0.0047
13	3	10	13	2	11	EA	14519.5365	–0.2270
						EE	–0.139	–0.0045
						EE*	0.2415	0.00270
14	3	11	14	2	12	EA	13986.0631	–0.2885
						EE	–0.1594	–0.0060
						EE*	0.2595	–0.0006
16	3	13	16	2	14	EA	13144.2657	–0.3134
						EE	–0.2025	0.0049
						EE*	0.2742	–0.0040
10	3	8	10	2	8	EA	12560.7565	0.0401
						EE	0.5421	–0.0005
						EE*	–0.4893	0.0015
12	3	10	12	2	10	EA	11665.0935	0.0829
						EE	0.5143	0.0002
						EE*	–0.4194	0.0006
13	3	11	13	2	11	EA	11103.3946	0.0872
						EE	0.4906	0.0004
						EE*	–0.3745	0.0012

Table D-3 continued

Upper level			Lower level				$\nu_{Obs.}$	$\nu_{Obs.} - \nu_{Calc.}$
J	K_a	K_c	J	K_a	K_c		MHz	MHz
14	3	12	14	2	12	EA	10485.2186	0.0746
						EE	0.46	0.0021
						EE*	–0.3234	–0.0001
6	1	5	5	2	4	EA	13685.8451	0.1581
						EE	–0.3245	–0.0005
						EE*	0.2564	–0.0012
6	1	5	5	2	3	EA	11381.4867	0.0496
						EE	0.1259	0.0065
						EE*	–0.1829	0.0027
10	3	8	9	4	6	EA	12646.0536	0.3030
						EE*	0.0924	0.0013

[a] The EE and EE* species are referred to the EA species. The differences of these transitions are given and fitted.
[b] The frequency list is sorted to the branches.

Table D-4

Observed AA and AE species frequencies ($\nu_{Obs.}$) of isopropenyl acetate. $\nu_{Obs.} - \nu_{Calc.}$ values as obtained after a fit with Erham.

Upper level		Lower level			$\nu_{Obs.}$	$\nu_{Obs.} - \nu_{Calc.}$
J	N	J	N		MHz	MHz
2	2	1	1	AA	9959.8164	–0.0025
				AE	9959.8164	0.0006
2	3	1	1	AA	10418.9033	0.0032
				AE	10418.8883	–0.0018
2	4	2	2	AA	10057.0205	–0.0131
				AE	10057.0205	0.0016
2	4	2	3	AA	9597.9493	–0.0031
				AE	9597.9493	0.0046
2	5	2	3	AA	9603.3064	–0.0021
				AE	9603.3247	0.0050
2	5	2	2	AA	10062.3929	0.0033
				AE	10062.3929	–0.0010
3	2	2	1	AA	13189.0572	–0.0027
				AE	13189.0572	–0.0001
3	3	2	1	AA	14107.1140	0.0034
				AE	14107.0930	–0.0010

Table D-4 continued

Upper level		Lower level			$\nu_{Obs.}$	$\nu_{Obs.} - \nu_{Calc.}$
J	N	J	N		MHz	MHz
3	4	3	2	AA	10289.8034	–0.0052
				AE	10289.8034	0.0055
3	4	3	3	AA	9371.7636	0.0057
				AE	9371.7636	0.0024
3	5	3	2	AA	10316.5403	–0.0054
				AE	10316.5403	0.0023
3	5	3	3	AA	9398.5048	0.0098
				AE	9398.5048	0.0035
4	1	3	2	AA	10933.5866	0.0052
				AE	10933.5660	0.0008
4	1	3	3	AA	10015.5299	–0.0008
				AE	10015.5299	0.0014
4	4	4	2	AA	10602.0063	0.0039
				AE	10601.9849	–0.0033
4	5	4	2	AA	10681.9128	0.0040
				AE	10681.8904	–0.0030
5	4	5	2	AA	10994.8499	0.0042
				AE	10994.8243	–0.0014
5	5	5	2	AA	11179.9424	0.0103
				AE	11179.9063	–0.0008
5	1	4	3	AA	13072.0079	0.0028
				AE	13072.0079	0.0006
6	3	5	4	AA	12450.4934	–0.0025
				AE	12450.4601	0.0027
6	3	5	5	AA	12265.4101	0.0006
				AE	12265.3787	0.0027
6	4	6	2	AA	11469.4823	0.0024
				AE	11469.4521	–0.0005
6	5	6	2	AA	11835.1217	–0.0017
				AE	11835.0856	0.0000
7	2	6	5	AA	11762.8077	–0.0119
				AE	11762.8476	0.0013
7	2	6	4	AA	12128.4559	–0.0072
				AE	12128.4814	0.0021
7	4	7	2	AA	12026.7301	–0.0002
				AE	12026.6940	–0.0003
7	5	7	2	AA	12672.7065	–0.0071
				AE	12672.6585	–0.0005
8	2	7	5	AA	14275.2581	0.0104
				AE	14275.2890	–0.0012

Table D-4 continued

Upper level		Lower level			$\nu_{Obs.}$	$\nu_{Obs.} - \nu_{Calc.}$
J	*N*	*J*	*N*		MHz	MHz
8	5	7	6	AA	12082.6581	–0.0037
				AE	12082.6248	0.0023
8	4	7	6	AA	11033.7425	–0.0092
				AE	11033.7507	0.0087
8	4	7	7	AA	11009.3480	–0.0002
				AE	11009.3295	–0.0009
8	5	7	7	AA	12058.2565	–0.0018
				AE	12058.2133	0.0024
8	4	8	2	AA	12666.8765	0.0006
				AE	12666.8295	–0.0005
8	5	8	2	AA	13715.7850	–0.0010
				AE	13715.7096	–0.0008
9	4	8	6	AA	14344.5048	–0.0012
				AE	14344.4947	–0.0004
9	4	8	7	AA	14291.1135	–0.0008
				AE	14291.1011	–0.0005
9	4	9	2	AA	13389.4367	–0.0024
				AE	13389.3811	–0.0009
10	6	9	8	AA	11776.2012	–0.0018
				AE	11776.2475	0.0026
10	6	9	9	AA	11773.4892	–0.0020
				AE	11773.3918	0.0017
10	7	9	9	AA	11968.0222	–0.0010
				AE	11967.9168	0.0022
10	4	10	2	AA	14193.0199	0.0010
				AE	14192.9486	–0.0010
11	3	11	1	AA	10401.8322	0.0050
				AE	10401.7006	–0.0033
11	6	11	5	AA	14161.7815	0.0000
				AE	14161.8292	–0.0042
11	7	11	5	AA	14497.0406	–0.0013
				AE	14497.0768	–0.0030
12	3	12	1	AA	11868.5260	0.0118
				AE	11868.3658	–0.0044
12	6	12	5	AA	13478.2406	–0.0001
				AE	13478.3039	–0.0022
12	7	12	5	AA	14025.7513	–0.0009
				AE	14025.7924	–0.0020
13	5	13	3	AA	9339.4852	–0.0012
				AE	9339.4200	–0.0039

Table D-4 continued

Upper level		Lower level			$\nu_{Obs.}$	$\nu_{Obs.} - \nu_{Calc.}$
J	*N*	*J*	*N*		MHz	MHz
13	6	13	5	AA	12708.0680	–0.0001
				AE	12708.1466	–0.0006
13	7	13	5	AA	13561.2335	0.0003
				AE	13561.2736	–0.0031
14	5	14	3	AA	10044.8318	–0.0021
				AE	10044.7432	–0.0036
14	6	14	5	AA	11862.9303	0.0022
				AE	11863.0216	0.0009
14	7	14	5	AA	13137.9726	0.0004
				AE	13138.0112	–0.0016
15	5	15	3	AA	10937.1968	–0.0095
				AE	10937.0955	0.0039
15	6	15	5	AA	10956.3227	0.0006
				AE	10956.4299	0.0024
15	7	15	5	AA	12791.1339	–0.0030
				AE	12791.1689	–0.0008
16	5	16	3	AA	12016.4400	–0.0024
				AE	12016.2945	–0.0033
16	7	16	5	AA	12554.0436	–0.0001
				AE	12554.0648	0.0013
17	5	17	3	AA	13274.6123	0.0015
				AE	13274.4365	0.0013
17	7	17	5	AA	12456.3030	0.0012
				AE	12456.3030	–0.0002
19	7	19	5	AA	12773.8743	0.0042
				AE	12773.8258	0.0066

Table D-5

Observed EA, EE and EE* species frequencies ($\nu_{Obs.}$) of isopropenyl acetate. $\nu_{Obs.} - \nu_{Calc.}$ values as obtained after a fit with Erham.

Upper level		Lower level			$\nu_{Obs.}$	$\nu_{Obs.} - \nu_{Calc.}$
J	*N*	*J*	*N*		MHz	MHz
2	5	2	3	EA	10278.4778	0.0104
				EE	10278.3503	–0.0011
				EE*	10278.5730	–0.0095
2	2	1	1	EA	9545.1685	–0.0074

Table D-5 continued

Upper level		Lower level			$\nu_{Obs.}$	$\nu_{Obs.} - \nu_{Calc.}$
J	N	J	N		MHz	MHz
2	2	1	1	EE	9545.2712	–0.0009
				EE*	9545.0700	0.0008
2	3	1	1	EA	10790.1509	0.0052
				EE	10790.0251	0.0031
				EE*	10790.2584	0.0047
3	2	2	1	EA	12899.9357	–0.0037
				EE	12900.0196	–0.0027
				EE*	12899.8440	–0.0017
3	3	2	1	EA	14373.1310	0.0137
				EE	14372.9799	–0.0090
				EE*	14373.2212	0.0033
3	5	3	3	EA	10174.3478	–0.0010
				EE	10174.2281	0.0004
				EE*	10174.4721	–0.0020
3	4	3	2	EA	9335.7049	0.0021
				EE	9335.8229	0.0011
				EE*	9335.5727	0.0017
4	1	3	2	EA	11188.9078	0.0028
				EE	11188.8117	0.0045
				EE*	11188.9802	0.0039
4	1	3	3	EA	9715.7240	–0.0031
				EE	9715.8397	–0.0009
				EE*	9715.6036	–0.0004
4	4	4	2	EA	9582.6487	0.0006
				EE	9582.7659	0.0048
				EE*	9582.5124	0.0014
4	5	4	2	EA	11890.4497	0.0032
				EE	11890.1144	0.0043
				EE*	11890.7601	0.0013
4	5	4	3	EA	9985.5422	–0.0001
				EE	9985.4145	–0.0005
				EE*	9985.6792	–0.0023
5	1	4	3	EA	12831.8299	–0.0077
				EE	12831.9280	–0.0073
				EE*	12831.7350	–0.0055
5	4	5	2	EA	9958.5346	0.0006
				EE	9958.6243	–0.0003
				EE*	9958.4040	0.0001
5	5	5	2	EA	12262.8913	0.0034
				EE	12262.5373	0.0046

Table D-5 continued

Upper level		Lower level			$\nu_{Obs.}$	$\nu_{Obs.} - \nu_{Calc.}$
J	N	J	N		MHz	MHz
5	5	5	2	EE*	12263.2026	–0.0007
5	5	5	3	EA	9726.1519	–0.0025
				EE	9726.0193	–0.0017
				EE*	9726.3041	–0.0040
6	2	5	4	EA	10342.1717	–0.0024
				EE	10342.1016	0.0010
				EE*	10342.2668	0.0003
6	3	5	4	EA	13685.8451	0.0048
				EE	13685.5206	0.0055
				EE*	13686.1015	0.0044
6	3	5	5	EA	11381.4867	0.0003
				EE	11381.6126	0.0055
				EE*	11381.3038	0.0062
6	4	6	2	EA	10458.8427	0.0016
				EE	10458.8865	–0.0023
				EE*	10458.7341	–0.0015
6	5	6	2	EA	12769.6821	0.0011
				EE	12769.2897	0.0013
				EE*	12770.0114	–0.0022
6	5	6	3	EA	9426.0113	–0.0036
				EE	9425.8671	–0.0067
				EE*	9426.1759	–0.0072
7	2	6	4	EA	13201.0868	–0.0141
				EE	13201.1015	0.0138
				EE*	13201.1421	–0.0058
7	4	7	2	EA	11072.5664	0.0027
				EE	11072.5389	–0.0062
				EE*	11072.5017	–0.0022
7	5	7	2	EA	13422.9293	0.0020
				EE	13422.4749	–0.0020
				EE*	13423.2877	–0.0036
8	4	7	6	EA	12180.2347	–0.0105
				EE	12180.0719	–0.0069
				EE*	12180.3591	–0.0061
8	5	7	7	EA	11200.5755	0.0010
				EE	11200.6622	0.0036
				EE*	11200.4276	0.0056
8	5	8	2	EA	14245.7647	–0.0017
				EE	14245.2361	–0.0032
				EA	14246.1673	–0.0051

Table D-5 continued

Upper level		Lower level			$\nu_{Obs.}$	$\nu_{Obs.} - \nu_{Calc.}$
J	N	J	N		MHz	MHz
9	4	9	2	EA	12558.9207	0.0008
				EE	12558.7135	0.0017
				EE*	12559.0068	–0.0020
10	6	9	8	EA	12646.0536	0.0056
				EE	12646.1460	0.0072
10	7	9	9	EE*	11480.9229	–0.0054
				EA	11481.0037	–0.0021
				EE	11480.7852	0.0007
10	6	10	5	EE*	12560.7565	0.0020
				EA	12561.2986	0.0030
				EE	12560.2672	0.0027
11	3	11	1	EE*	10885.5465	–0.0021
				EA	10885.7724	–0.0033
				EE	10885.0540	–0.0012
12	6	12	5	EE*	11665.0935	0.0018
				EA	11665.6078	0.0040
				EE	11664.6741	–0.0003
13	5	13	3	EE*	9601.8574	–0.0034
				EA	9601.6860	–0.0042
				EE	9601.9032	–0.0058
13	6	13	5	EE*	11103.3946	–0.0008
				EA	11103.8852	0.0010
				EE	11103.0201	–0.0023
13	7	13	5	EE*	14519.5365	0.0057
				EA	14519.3975	0.0025
				EE	14519.7780	0.0060
14	5	14	3	EE*	10318.5082	–0.0028
				EA	10318.3871	0.0049
				EE	10318.4658	0.0035
14	6	14	5	EE*	10485.2186	–0.0021
				EA	10485.6786	0.0002
				EE	10484.8952	–0.0044
14	7	14	5	EE*	13986.0631	0.0067
				EA	13985.9037	0.0000
				EE	13986.3226	0.0056
15	5	15	3	EE*	11246.7876	0.0036
				EA	11246.7226	0.0034
				EE	11246.6098	0.0011
16	7	16	5	EA	13144.2657	–0.0052
				EE	13144.0632	–0.0066
				EE*	13144.5399	–0.0031

Chapter 5

METHYL PROPIONATE

Table E-1

Fourier coefficients of the potential function for a rotation of the entire ethyl group around the dihedral angle $\varphi = \angle(C_1, C_2, C_3, O_5)$ calculated in $10°$ steps at different level of theory (see Figure 2). The potential is expanded as $V(\varphi) = a_0 + \sum\limits_{i=1}^{15} a_i \cos(i\varphi)$

	MP2/6-311++G(d,p)		**MP2/6-31G(d,p)**		**B3LYP/6-311++G(d,p)**	
	Hartree	cm^{-1}	Hartree	cm^{-1}	Hartree	cm^{-1}
a_0	−306.940504703		−306.802454568		−307.798341297	
a_1	−0.000675069	−148.1605	−0.000662920	−145.4941	−0.000726464	−159.4404
a_2	0.000051026	11.1989	−0.000226583	−49.7292	−0.000175595	−38.5386
a_3	−0.000287240	−63.0419	−0.000368589	−80.8959	−0.000225083	−49.4000
a_4	0.000053587	11.7610	0.000099139	21.7585	−0.000008212	−1.8023
a_5	−0.000017496	−3.8399	0.000002107	0.4624	0.000003786	0.8309
a_6	0.000030772	6.7537	−0.000004225	−0.9273	0.000006250	1.3717
a_7	−0.000001419	−0.3114	−0.000000766	−0.1681	−0.000001116	−0.2449
a_8	0.000006983	1.5326	0.000002980	0.6540	0.000001189	0.2610
a_9	0.000001872	0.4109	−0.000000058	−0.0127	0.000001950	0.4280
a_{10}	0.000002153	0.4725	0.000000027	0.0059	−0.000000431	−0.0946
a_{11}	−0.000000257	−0.0564	0.000000253	0.0555	0.000000289	0.0634
a_{12}	0.000000727	0.1596	0.000000031	0.0068	−0.000000295	−0.0647
a_{13}	0.000000170	0.0373	0.000000008	0.0018	0.000002678	0.5878
a_{14}	0.000000152	0.0334	0.000000133	0.0292	−0.000000192	−0.0421
a_{15}	0.000000050	0.0110	−0.000000027	−0.0059	−0.000000051	−0.0112

Table E-3

Fourier coefficients of the potential function for a rotation of the terminal methyl groups. Here the Fourier series is written as $V(\varphi) = a_0 + a_3 \cos 3\varphi + a_6 \cos 6\varphi$. It should be noted that usually the peak-to-peak potential terms $V_3 = 2a_3$ and $V_6 = 2a_6$ are used.

	Methoxy methyl group		Propionyl methyl group	
	Hartree	cm^{-1}	Hartree	cm^{-1}
a_0	−306.940162		−306.939280	
a_3	0.001160	254.6	0.002178	478.1
a_6	−0.000021	−4.7	0.000115	25.3

Table E-2

Calculated geometry parameters in the principal inertial axes of the *trans* C_S and *trans* C_1 conformer of methyl propionate. The atoms are numbered according Figure 1.

	C_S conformer			C_1 conformer		
	MP2/6-311++G(d,p)			MP2/6-311++G(d,p)		
	a /Å	b /Å	c /Å	a /Å	b /Å	c /Å
C1	2.501465	0.077563	–0.000151	–2.165939	–0.587048	0.531141
C2	1.235037	–0.771148	0.000098	–1.392196	0.098712	–0.604309
C3	–0.021752	0.068325	0.000109	0.025253	0.383571	–0.176305
O4	–0.067486	1.279774	0.000074	0.442031	1.445184	0.237363
O5	–1.122878	–0.718968	0.000015	0.788384	–0.732037	–0.263938
C6	–2.364926	0.001879	–0.000119	2.137138	–0.563402	0.199318
H2	2.536915	0.720997	–0.881914	–1.708732	–1.546873	0.783689
H4	2.537049	0.721305	0.881382	–2.173131	0.042974	1.425000
H3	3.386765	–0.563534	–0.000110	–3.201676	–0.766109	0.231391
H6	1.192439	–1.427750	0.875705	–1.854699	1.054098	–0.860547
H7	1.192270	–1.428038	–0.875282	–1.377343	–0.542520	–1.489518
H12	–2.441774	0.630319	–0.889147	2.145132	–0.269696	1.250561
H13	–3.141422	–0.760726	–0.000725	2.611875	–1.533839	0.067311
H14	–2.442413	0.629522	0.889423	2.649889	0.199557	–0.388938

Table E-2 continued

	C_S conformer			C_1 conformer		
	MP2/6-31G(d,p)			MP2/6-31G(d,p)		
	a /Å	b /Å	c /Å	a /Å	b /Å	c /Å
C1	2.495852	0.077472	–0.000220	–2.142177	–0.707539	0.399484
C2	1.235345	–0.772141	0.000114	–1.417354	0.324508	–0.463813
C3	–0.019572	0.065561	0.000188	0.042171	0.448953	–0.106928
O4	–0.064168	1.284383	0.000110	0.608616	1.467228	0.253009
O5	–1.123902	–0.724663	0.000062	0.670987	–0.749850	–0.232493
C6	–2.363986	0.005815	–0.000210	2.070735	–0.712672	0.100430
H7	2.527391	0.718362	–0.878211	–1.711425	–1.695310	0.257696
H8	2.527610	0.718710	0.877506	–2.066069	–0.447964	1.454516
H9	3.380626	–0.556497	–0.000212	–3.197936	–0.746683	0.137279
H10	1.193609	–1.428267	0.871287	–1.856315	1.313619	–0.351558
H11	1.193339	–1.428604	–0.870788	–1.483456	0.040376	–1.515414
H12	–2.435418	0.634369	–0.884468	2.207937	–0.398835	1.132266
H13	–3.140227	–0.751207	–0.002308	2.425004	–1.727224	–0.044052
H14	–2.437493	0.631424	0.885992	2.598744	–0.022535	–0.552991

Table E-4

Observed AA, AE, EA, EE, and EE* species frequencies ($\nu_{Obs.}$) of methyl propionate.

$\nu_{Obs.} - \nu_{Calc.}$ values as obtained after a fit with XIAM and BELGI-C_S-2tops.

Upper level			Lower level				$\nu_{Obs.}$	$\nu_{Obs.} - \nu_{Calc.}$	$\nu_{Obs.} - \nu_{Calc.}$
J	K_a	K_c	J	K_a	K_c		GHz	XIAM / kHz	BELGI / kHz
1	1	1	0	0	0	AA	11.3296409	–4.4	–4
						AE	11.3296126	–2.3	–2
						EA	11.3265986	–2.9	–3
						EE	11.3266090	–0.3	0
						EE*	11.3265296	–3.2	–3
1	1	0	1	0	1	AA	7.7036481	5.6	6
						EA	7.7036010	–11.6	–11
						AE	7.7028364	–10.4	–11
						EE	7.7027803	1.5	2
						EE*	7.7028476	–7.6	–8
2	0	2	1	0	1	AA	7.9092523	–2.3	–2
						AE	7.9092523	–1.1	–1
						EA	7.9092159	–1.4	–1
						EE	7.9092159	0.1	0
						EE*	7.9092159	0.2	0
2	1	1	1	1	0	AA	8.2545474	6.6	6
						AE	8.2545359	–2.8	–3
						EA	8.2537307	–4.1	–4
						EE	8.2537560	–2.1	–2
						EE*	8.2537067	–0.5	–1
2	1	2	1	0	1	AA	14.9556371	–3.2	–3
						AE	14.9556083	–1.7	–2
						EA	14.9533494	–1.9	–2
						EE	14.9533328	–1.1	–1
						EE*	14.9533064	–1.8	–2
2	1	1	2	0	2	AA	8.0489291	0.5	1
						AE	8.0489033	5.3	6
						EA	8.0473667	2.4	2
						EE	8.0473217	0.8	1
						EE*	8.0473450	–1.3	–2
3	0	3	2	0	2	AA	11.8361779	–0.8	–1
						AE	11.8361779	1.0	1
						EA	11.8361179	–1.6	–2
						EE	11.8361179	0.3	0
						EE*	11.8361179	0.2	1
3	1	3	2	0	2	AA	18.4188113	–2.0	–2
						AE	18.4187831	–0.3	0

Table E-4 continued

Upper level			Lower level				$\nu_{Obs.}$	$\nu_{Obs.} - \nu_{Calc.}$	$\nu_{Obs.} - \nu_{Calc.}$
J	K_a	K_c	J	K_a	K_c		GHz	XIAM / kHz	BELGI / kHz
3	1	3	2	0	2	EA	18.4167427	13.1	13
						EE	18.4167162	9.9	10
						EE*	18.4166916	−1.7	−2
3	1	3	2	1	2	AA	11.3724272	−0.5	−1
						AE	11.3724272	0.4	0
						EA	11.3725961	0.4	0
						EE	11.3725875	−0.9	−1
						EE*	11.3726017	0.5	1
3	1	2	2	1	1	AA	12.3747333	−2.3	−3
						AE	12.3747333	0.5	1
						EA	12.3744628	1.1	1
						EE	12.3744628	−2.5	−2
						EE*	12.3744501	−2.3	−2
3	2	1	2	2	0	AA	11.9248619	−4.8	−5
						AE	11.9248327	−1.0	−1
						EA	11.9111444	−1.1	−1
						EE	11.9112613	−1.6	−2
						EE*	11.9110276	0.3	0
3	2	2	2	2	1	AA	11.8805106	0.3	0
						AE	11.8805367	−2.8	−3
						EA	11.8941345	0.2	0
						EE	11.8940118	−1.4	−1
						EE*	11.8942445	−4.3	−4
3	1	2	3	0	3	AA	8.5874855	0.0	0
						AE	8.5874562	2.3	3
						EA	8.5857075	1.0	0
						EE	8.5856674	−1.2	−1
						EE*	8.5856853	4.3	4
3	2	1	3	1	2	AA	21.6695336	−2.7	−3
						AE	21.6694540	−2.7	−3
						EA	21.6834757	−1.6	−1
						EE	21.6828622	−1.7	−1
						EE*	21.6839189	−0.2	0
3	2	2	3	1	3	EA	23.5935722	1.3	1
						EE	23.5940044	−1.7	−1
						EE*	23.5929491	−1.8	−1
4	0	4	3	0	3	AA	15.7303315	−0.5	−1
						AE	15.7303315	2.1	2
						EA	15.7302457	−1.6	−2
						EE	15.7302457	1.9	1
						EE*	15.7302457	0.8	1

Table E-4 continued

Upper level			Lower level				$\nu_{Obs.}$	$\nu_{Obs.} - \nu_{Calc.}$	$\nu_{Obs.} - \nu_{Calc.}$
J	K_a	K_c	J	K_a	K_c		GHz	XIAM / kHz	BELGI / kHz
4	0	4	3	1	3	AA	9.1477005	3.1	3
						AE	9.1477236	0.7	1
						EA	9.1496294	−7.8	−8
						EE*	9.1496689	0.3	1
4	1	3	3	1	2	AA	16.4861083	−5.1	−5
						AE	16.4861083	−1.3	−1
						AE	16.4859220	0.3	0
						EE	16.4859220	1.5	2
						EE*	16.4859220	6.7	7
4	1	4	3	0	3	AA	21.7334178	−2.7	−3
						AE	21.7333916	0.2	0
						EA	21.7314396	−3.5	−4
						EE	21.7314213	3.4	3
						EE*	21.7314090	−1.0	−
4	1	4	3	1	3	AA	15.1507870	1.0	1
						AE	15.1507870	2.2	2
						EA	15.1508328	0.2	0
						EE	15.1508328	3.6	4
						EE*	15.1508328	−1.5	−2
4	2	2	3	2	1	AA	15.9423758	3.1	3
						AE	15.9423647	−0.4	0
						EA	15.9310476	−0.1	−1
						EE	15.9313037	0.3	0
						EE*	15.9307879	−0.1	0
4	2	3	3	2	2	AA	15.8320186	2.6	2
						AE	15.8320186	−0.1	0
						EA	15.8432148	−0.6	−1
						EE	15.8429535	−1.4	−1
						EE*	15.8434699	0.3	0
4	3	1	3	3	0	AE	15.8631334	−0.1	0
						EA	15.8627644	−2.6	−3
						EE	15.8627644	−1.0	−1
						EE*	15.8627644	0.6	1
4	3	2	3	3	1	EA	15.8628083	−3.5	−4
						EE	15.8628083	−0.3	0
						EE*	15.8628083	−1.9	−2
4	1	3	4	0	4	AA	9.3432648	−2.1	−2
						AE	9.3432344	0.4	1
						EA	9.3413807	−0.1	−1
						EE	9.3413418	−2.6	−2
						EE*	9.3413585	7.0	6

Table E-4 continued

Upper level			Lower level				$\nu_{Obs.}$	$\nu_{Obs.} - \nu_{Calc.}$	$\nu_{Obs.} - \nu_{Calc.}$
J	K_a	K_c	J	K_a	K_c		GHz	XIAM / kHz	BELGI / kHz
4	2	2	4	1	3	AA	21.1257946	–1.0	–1
						AE	21.1257113	–0.9	–1
						EA	21.1286023	–1.0	–1
						EE	21.1282454	–1.3	–1
						EE*	21.1287925	0.7	1
4	2	3	4	1	4	AA	24.3001609	9.6	9
						AE	24.3000577	1.3	2
						EA	24.2859510	–2.4	–3
						EE	24.2861326	0.8	2
						EE*	24.2855850	–1.7	–1
5	0	5	4	0	4	AA	19.5822695	–0.9	–1
						AE	19.5822695	2.2	2
						EA	19.5821549	–1.4	–2
						EE	19.5821549	1.8	2
						EE*	19.5821549	1.7	2
5	0	5	4	1	4	AA	13.5791846	2.8	2
						AE	13.5792088	3.4	3
						EA	13.5809612	0.7	1
						EE	13.5809903	10.3	11
						EE*	13.5809903	2.3	3
5	1	4	4	1	3	AA	20.5851905	5.0	5
						AE	20.5851857	4.9	5
						EE	20.5849945	–1.0	–1
						EE*	20.5849907	–2.2	–2
5	1	5	4	0	4	AA	24.9222258	–8.0	–8
						AE	24.9222074	1.8	2
						EA	24.9203366	–4.6	–5
						EE	24.9203170	1.3	1
						EE*	24.9203170	6.7	6
5	1	5	4	1	4	EA	18.9191454	0.0	0
						EE	18.9191454	2.8	3
						EE*	18.9191454	0.2	0
5	2	3	4	2	2	AA	19.9946342	–0.3	–1
						AE	19.9946298	–0.2	0
						EA	19.9898620	–1.4	–2
						EE	19.9900092	1.3	1
5	2	4	4	2	3	AA	19.7761040	–0.4	–1
						AE	19.7761040	1.2	1
5	2	4	4	2	3	EA	19.7807231	–0.8	–1
						EE	19.7805738	0.5	1
						EE*	19.7808702	0.1	0

Table E-4 continued

\multicolumn{3}{c|}{Upper level}			\multicolumn{3}{c|}{Lower level}				$\nu_{Obs.}$	$\nu_{Obs.} - \nu_{Calc.}$	$\nu_{Obs.} - \nu_{Calc.}$
J	K_a	K_c	J	K_a	K_c		GHz	XIAM / kHz	BELGI / kHz
5	1	4	5	0	5	AA	10.3461762	–5.9	–6
						EA	10.3442233	–0.1	–2
						EE	10.3441931	6.3	7
						EE*	10.3441991	7.9	7
5	2	4	5	1	5	AA	25.1571167	6.2	6
						EA	25.1475382	6.4	6
						EE	25.1475578	–4.7	–4
						EE*	25.1473114	–0.3	0
5	2	3	5	1	4	AA	20.5352440	–0.5	0
						AE	20.5351609	–0.4	0
						EA	20.5334677	–0.2	0
						EE	20.5332603	1.1	1
						EE*	20.5335105	0.4	1
5	3	3	6	2	4	AA	13.3086619	1.1	1
						AE	13.3083715	–0.3	–1
6	0	6	5	0	5	AA	23.3850077	–1.3	–2
						AE	23.3850077	2.4	3
						EA	23.3848601	–1.6	–2
						EE	23.3848601	2.2	2
						EE*	23.3848601	2.1	2
6	0	6	5	1	5	AA	18.0450519	6.2	6
						AE	18.0450678	0.8	1
						EA	18.0466792	2.4	2
6	1	5	5	1	4	AA	24.6679807	–5.8	–6
						AE	24.6679807	–0.1	0
						EA	24.6677775	–3.3	–4
						EE	24.6677775	1.7	2
						EE*	24.6677775	3.1	3
6	1	6	5	1	5	AA	22.6758150	–1.6	–2
						AE	22.6758150	0.3	0
						EA	22.6757917	1.2	1
						EE	22.6757917	3.8	4
						EE*	22.6757917	2.3	2
6	2	4	5	2	3	AA	24.0867394	–2.5	–3
						AE	24.0867394	1.7	2
						EA	24.0847911	–2.1	–3
						EE	24.0848517	–0.4	0
						EE*	24.0847268	0.9	1
6	2	5	5	2	4	AA	23.7109440	–0.3	–1
						AE	23.7109440	2.1	3
						EA	23.7127166	–0.5	–1

Table E-4 continued

Upper level			Lower level				$\nu_{\text{Obs.}}$	$\nu_{\text{Obs.}} - \nu_{\text{Calc.}}$	$\nu_{\text{Obs.}} - \nu_{\text{Calc.}}$
J	K_a	K_c	J	K_a	K_c		GHz	XIAM / kHz	BELGI / kHz
6	2	5	5	2	4	EE	23.7126530	2.2	2
						EE*	23.7127766	–0.4	0
6	1	5	6	0	6	AA	11.6291544	–5.1	–5
						AE	11.6291281	4.9	6
						EA	11.6271406	–1.9	–4
						EE	11.6271066	1.9	3
						EE*	11.6271111	3.4	3
6	2	4	6	1	5	AA	19.9539999	0.0	0
						AE	19.9539184	0.2	0
						EA	19.9504791	–1.2	–1
						EE	19.9503367	1.2	1
7	0	7	6	1	6	AA	22.5047858	8.1	8
						AE	22.5047919	–4.6	–4
						EA	22.5062581	5.3	5
						EE	22.5062581	–11.5	–11
						EE*	22.5062581	–15.5	–14
7	1	6	6	2	5	AA	9.5361126	0.3	0
						AE	9.5361874	–1.2	0
						EA	9.5432949	–1.2	–2
						EE	9.5433061	–0.1	0
						EE*	9.5434355	–3.0	–3
7	1	6	7	0	7	AA	13.2235708	–2.0	–3
						AE	13.2235322	–2.0	–1
						EA	13.2214990	–2.7	–5
						EE	13.2214668	4.8	6
						EE*	13.2214668	2.6	2
7	2	5	7	1	6	AA	19.4437921	0.7	1
						AE	19.4437120	0.3	0
						EA	19.4395908	0.3	0
						EE	19.4394781	2.0	2
						EE*	19.4395426	–3.0	–3
6	3	3	7	2	6	AA	10.2690466	–0.7	–1
						AE	10.2689538	0.0	0
8	1	7	7	2	6	AA	14.6672631	0.5	–1
						AE	14.6673347	0.6	0
						EA	14.6734551	–0.8	–2
						EE	14.6734883	–3.1	–2
						EE*	14.6735649	–0.9	0
8	1	7	8	0	8	AA	15.1534592	–0.3	–2
						AE	15.1534144	–3.7	–2
						EA	15.1513266	–2.3	–4

Table E-4 continued

Upper level			Lower level				$\nu_{Obs.}$	$\nu_{Obs.} - \nu_{Calc.}$	$\nu_{Obs.} - \nu_{Calc.}$
J	K_a	K_c	J	K_a	K_c		GHz	XIAM / kHz	BELGI / kHz
						EE	15.1512804	–6.3	–5
						EE*	15.1512875	–0.9	–1
8	2	6	8	1	7	AA	19.0674393	0.8	1
						AE	19.0673615	0.3	1
						EA	19.0630090	–0.2	0
						EE	19.0629093	–2.1	–2
						EE*	19.0629539	1.5	1
9	1	8	8	2	7	AA	19.8913872	3.0	2
						AE	19.8914512	–1.9	–1
						EA	19.8969845	–2.3	–3
						EE	19.8970319	–1.2	0
						EE*	19.8970818	3.5	5
9	1	8	9	0	9	AA	17.4297980	1.5	0
						AE	17.4297532	1.5	3
						EA	17.4275831	–5.0	–7
						EE	17.4275456	3.0	5
						EE*	17.4275456	1.4	2
9	2	7	9	1	8	AA	18.8843503	–0.1	0
						AE	18.8842764	0.7	1
						EA	18.8799147	–0.6	–1
						EE	18.8798301	2.2	3
						EE*	18.8798499	–3.5	–4
10	1	9	10	0	10	AA	20.0464823	3.3	0
						AE	20.0464266	–3.5	–2
						EA	20.0441550	–3.4	–6
						EE	20.0441115	2.8	5
						EE*	20.0441115	1.2	3
10	2	8	10	1	9	AA	18.9474085	–1.0	–1
						AE	18.9473385	1.1	2
						EA	18.9430898	–0.9	–2
						EE	18.9430091	–1.4	–1
						EE*	18.9430303	3.4	2
11	1	10	11	0	11	EA	22.9766811	–1.5	–5
						EE	22.9766300	2.3	4
						EE*	22.9766300	0.6	3
11	2	9	10	3	8	AA	10.7512117	–1.0	–2
						AE	10.7513496	–2.9	–1
						EA	10.7689965	2.5	0
						EE	10.7688578	1.0	2
						EE*	10.7694128	2.6	3

Chapter 6

DIETHYL KETONE

Table F-1/A

Coefficients of the two-dimensional Fourier expansion for the energy potential surface calculated at the MP2/6-311++G(d,p) level of theory (Figure 2).

Nr	Coefficient	Value
1	1	$-271.0437055(49)$
2	$\cos(\varphi_1) + \cos(\varphi_2)$	$-0.0023296(48)$
3	$\cos(2\varphi_1) + \cos(2\varphi_2)$	$0.0006021(48)$
4	$\cos(3\varphi_1) + \cos(3\varphi_2)$	$-0.0009031(48)$
5	$\cos(4\varphi_1) + \cos(4\varphi_2)$	$-0.0002170(48)$
6	$\cos(5\varphi_1) + \cos(5\varphi_2)$	$-0.0000394(48)$
7	$\cos(6\varphi_1) + \cos(6\varphi_2)$	$0.0000288(48)$
8	$\cos(\varphi_1)\cos(\varphi_2)$	$0.0016448(94)$
9	$\sin(\varphi_1)\sin(\varphi_2)$	$-0.0006171(101)$
10	$\cos(\varphi_1)\cos(2\varphi_2) + \cos(2\varphi_1)\cos(\varphi_2)$	$-0.0007183(67)$
11	$\sin(\varphi_1)\sin(2\varphi_2) + \sin(2\varphi_1)\sin(\varphi_2)$	$0.0005676(71)$
12	$\cos(2\varphi_1)\cos(2\varphi_2)$	$0.0005917(95)$
13	$\sin(2\varphi_1)\sin(2\varphi_2)$	$-0.0005528(101)$
14	$\cos(\varphi_1)\cos(3\varphi_2) + \cos(3\varphi_1)\cos(\varphi_2)$	$0.0000660(67)$
15	$\sin(\varphi_1)\sin(3\varphi_2) + \sin(3\varphi_1)\sin(\varphi_2)$	$-0.0001243(71)$
16	$\cos(2\varphi_1)\cos(3\varphi_2) + \cos(3\varphi_1)\cos(2\varphi_2)$	$-0.0001930(67)$
17	$\sin(2\varphi_1)\sin(3\varphi_2) + \sin(3\varphi_1)\sin(2\varphi_2)$	$0.0001550(71)$
18	$\cos(3\varphi_1)\cos(3\varphi_2)$	$0.0005678(95)$
19	$\sin(3\varphi_1)\sin(3\varphi_2)$	$-0.0003813(99)$
20	$\cos(\varphi_1)\cos(4\varphi_2) + \cos(4\varphi_1)\cos(\varphi_2)$	$0.0001486(67)$
21	$\sin(\varphi_1)\sin(4\varphi_2) + \sin(4\varphi_1)\sin(\varphi_2)$	$-0.0001692(71)$
22	$\cos(2\varphi_1)\cos(4\varphi_2) + \cos(4\varphi_1)\cos(2\varphi_2)$	$-0.0001806(67)$
23	$\sin(2\varphi_1)\sin(4\varphi_2) + \sin(4\varphi_1)\sin(2\varphi_2)$	$0.0001792(71)$
24	$\cos(3\varphi_1)\cos(4\varphi_2) + \cos(4\varphi_1)\cos(3\varphi_2)$	$0.0002397(67)$
25	$\sin(3\varphi_1)\sin(4\varphi_2) + \sin(4\varphi_1)\sin(3\varphi_2)$	$-0.0002189(70)$

Table F-1/A continued

Nr	Coefficient	Value
26	$\cos(4\varphi_1)\cos(4\varphi_2)$	0.0001294(95)
27	$\sin(4\varphi_1)\sin(4\varphi_2)$	–0.0001102(99)
28	$\cos(\varphi_1)\cos(5\varphi_2) + \cos(5\varphi_1)\cos(\varphi_2)$	–0.0000049(67)
29	$\sin(\varphi_1)\sin(5\varphi_2) + \sin(5\varphi_1)\sin(\varphi_2)$	0.0000237(70)
30	$\cos(2\varphi_1)\cos(5\varphi_2) + \cos(5\varphi_1)\cos(2\varphi_2)$	0.0000722(67)
31	$\sin(2\varphi_1)\sin(5\varphi_2) + \sin(5\varphi_1)\sin(2\varphi_2)$	–0.0000717(70)
32	$\cos(3\varphi_1)\cos(5\varphi_2) + \cos(5\varphi_1)\cos(3\varphi_2)$	–0.0001440(67)
33	$\sin(3\varphi_1)\sin(5\varphi_2) + \sin(5\varphi_1)\sin(3\varphi_2)$	0.0001380(70)
34	$\cos(4\varphi1)\cos(5\varphi_2) + \cos(5\varphi_1)\cos(4\varphi_2)$	–0.0001121(68)
35	$\sin(4\varphi_1)\sin(5\varphi_2) + \sin(5\varphi_1)\sin(4\varphi_2)$	0.0001062(70)
36	$\cos(5\varphi_1)\cos(5\varphi_2)$	0.0001291(96)
37	$\sin(5\varphi_1)\sin(5\varphi_2)$	–0.0001385(99)
38	$\cos(\varphi_1)\cos(6\varphi_2) + \cos(6\varphi_1)\cos(\varphi_2)$	–0.0000196(67)
39	$\sin(\varphi_1)\sin(6\varphi_2) + \sin(6\varphi_1)\sin(\varphi_2)$	0.0000011(70)
40	$\cos(2\varphi_1)\cos(6\varphi_2) + \cos(6\varphi_1)\cos(2\varphi_2)$	0.0000058(67)
41	$\sin(2\varphi_1)\sin(6\varphi_2) + \sin(6\varphi_1)\sin(2\varphi_2)$	0.0000005(70)
42	$\cos(3\varphi_1)\cos(6\varphi_2) + \cos(6\varphi_1)\cos(3\varphi_2)$	0.0000508(68)
43	$\sin(3\varphi_1)\sin(6\varphi_2) + \sin(6\varphi_1)\sin(3\varphi_2)$	–0.0000762(70)
44	$\cos(4\varphi_1)\cos(6\varphi_2) + \cos(6\varphi_1)\cos(4\varphi_2)$	0.0000854(67)
45	$\sin(4\varphi_1)\sin(6\varphi_2) + \sin(6\varphi_1)\sin(4\varphi_2)$	–0.0000778(70)
46	$\cos(5\varphi_1)\cos(6\varphi_2) + \cos(6\varphi_1)\cos(5\varphi_2)$	–0.0000879(68)
47	$\sin(5\varphi_1)\sin(6\varphi_2) + \sin(6\varphi_1)\sin(5\varphi_2)$	0.0000832(69)
48	$\cos(6\varphi_1)\cos(6\varphi_2)$	0.0000521(96)
49	$\sin(6\varphi_1)\sin(6\varphi_2)$	–0.0000375(98)

Table F-1/B

Cartesian nuclear coordinates of the most stable conformer of diethyl ketone optimized at the MP2/6-311++G(d,p) level of theory (C_2 symmetry) in the *Gaussian*'s internal coordinate system (called standard orientation) and in the principal inertial axes.

	Gaussian internal coordinate system			principal inertial axes		
	a /Å	b /Å	c /Å	a /Å	b /Å	c /Å
C1	0.000003	0.078506	–0.000160	0.000002	0.038026	–0.000146
O2	0.000012	1.298824	–0.000219	0.000011	1.258344	–0.000179
C3	–1.284442	–0.726812	–0.118651	–1.284511	–0.767290	–0.117914
C4	–2.543444	0.114897	0.055447	–2.543413	0.074415	0.056928
H5	–1.243149	–1.547379	0.608666	–1.242798	–1.587873	0.609361
H6	–1.266481	–1.204900	–1.107877	–1.267120	–1.245357	–1.107161
H7	–3.438381	–0.502429	–0.059074	–3.438415	–0.542909	–0.057090
H8	–2.564408	0.577366	1.045413	–2.563806	0.536862	1.046916
H9	–2.573333	0.918214	–0.683312	–2.573728	0.877748	–0.681796
C10	1.284404	–0.726839	0.118417	1.284471	–0.767322	0.117672
C11	2.543476	0.114887	–0.054945	2.543443	0.074408	–0.056397
H12	1.243308	–1.547147	–0.609206	1.242956	–1.587614	–0.609945
H13	1.266071	–1.205333	1.107448	1.266709	–1.245837	1.106703
H14	3.438360	–0.502515	0.059569	3.438393	–0.542996	0.057587
H15	2.564756	0.577805	–1.044695	2.564152	0.537348	–1.046149
H16	2.573181	0.917884	0.684170	2.573574	0.877389	0.682718

Table F-2/A

Coefficients of the two-dimensional Fourier expansion for the energy potential surface calculated at the B3LYP /6–311++G(d.p) level of theory (Figure 5).

Nr	Coefficient	Value
1	1	–271.8628216(13)
2	$\cos(\varphi_1) + \cos(\varphi_2)$	–0.0023493(13)
3	$\cos(2\varphi_1) + \cos(2\varphi_2)$	0.0002507(13)
4	$\cos(3\varphi_1) + \cos(3\varphi_2)$	–0.0008071(13)
5	$\cos(4\varphi_1) + \cos(4\varphi_2)$	–0.0001849(13)
6	$\cos(5\varphi_1) + \cos(5\varphi_2)$	–0.0000245(13)
7	$\cos(6\varphi_1) + \cos(6\varphi_2)$	0.0000300(13)
8	$\cos(\varphi_1)\cos(\varphi_2)$	0.0014733(26)
9	$\sin(\varphi_1)\sin(\varphi_2)$	–0.0005921(27)
10	$\cos(\varphi_1)\cos(2\varphi_2) + \cos(2\varphi_1)\cos(\varphi_2)$	–0.0006350(19)
11	$\sin(\varphi_1)\sin(2\varphi_2) + \sin(2\varphi_1)\sin(\varphi_2)$	0.0004722(19)

Table F-2/A continued

Nr	Coefficient	Value
12	$\cos(2\varphi_1)\cos(2\varphi_2)$	0.0005024(26)
13	$\sin(2\varphi_1)\sin(2\varphi_2)$	−0.0004539(27)
14	$\cos(\varphi_1)\cos(3\varphi_2) + \cos(3\varphi_1)\cos(\varphi_2)$	0.0000639(19)
15	$\sin(\varphi_1)\sin(3\varphi_2) + \sin(3\varphi_1)\sin(\varphi_2)$	−0.0000543(19)
16	$\cos(2\varphi_1)\cos(3\varphi_2) + \cos(3\varphi_1)\cos(2\varphi_2)$	−0.0001415(19)
17	$\sin(2\varphi_1)\sin(3\varphi_2) + \sin(3\varphi_1)\sin(2\varphi_2)$	0.0001191(19)
18	$\cos(3\varphi_1)\cos(3\varphi_2)$	0.0004753(26)
19	$\sin(3\varphi_1)\sin(3\varphi_2)$	−0.0003669(27)
20	$\cos(\varphi_1)\cos(4\varphi_2) + \cos(4\varphi_1)\cos(\varphi_2)$	0.0001153(19)
21	$\sin(\varphi_1)\sin(4\varphi_2) + \sin(4\varphi_1)\sin(\varphi_2)$	−0.0001096(19)
22	$\cos(2\varphi_1)\cos(4\varphi_2) + \cos(4\varphi_1)\cos(2\varphi_2)$	−0.0001188(18)
23	$\sin(2\varphi_1)\sin(4\varphi_2) + \sin(4\varphi_1)\sin(2\varphi_2)$	0.0001186(19)
24	$\cos(3\varphi_1)\cos(4\varphi_2) + \cos(4\varphi_1)\cos(3\varphi_2)$	0.0001598(18)
25	$\sin(3\varphi_1)\sin(4\varphi_2) + \sin(4\varphi_1)\sin(3\varphi_2)$	−0.0001467(19)
26	$\cos(4\varphi_1)\cos(4\varphi_2)$	0.0000560(26)
27	$\sin(4\varphi_1)\sin(4\varphi_2)$	−0.0000555(27)
28	$\cos(\varphi_1)\cos(5\varphi_2) + \cos(5\varphi_1)\cos(\varphi_2)$	−0.0000148(18)
29	$\sin(\varphi_1)\sin(5\varphi_2) + \sin(5\varphi_1)\sin(\varphi_2)$	0.0000337(19)
30	$\cos(2\varphi_1)\cos(5\varphi_2) + \cos(5\varphi_1)\cos(2\varphi_2)$	0.0000663(18)
31	$\sin(2\varphi_1)\sin(5\varphi_2) + \sin(5\varphi_1)\sin(2\varphi_2)$	−0.0000665(19)
32	$\cos(3\varphi_1)\cos(5\varphi_2) + \cos(5\varphi_1)\cos(3\varphi_2)$	−0.0000984(18)
33	$\sin(3\varphi_1)\sin(5\varphi_2) + \sin(5\varphi_1)\sin(3\varphi_2)$	0.0000954(19)
34	$\cos(4\varphi1)\cos(5\varphi_2) + \cos(5\varphi_1)\cos(4\varphi_2)$	−0.0000546(18)
35	$\sin(4\varphi_1)\sin(5\varphi_2) + \sin(5\varphi_1)\sin(4\varphi_2)$	0.0000534(19)
36	$\cos(5\varphi_1)\cos(5\varphi_2)$	0.0000684(26)
37	$\sin(5\varphi_1)\sin(5\varphi_2)$	−0.0000666(27)
38	$\cos(\varphi_1)\cos(6\varphi_2) + \cos(6\varphi_1)\cos(\varphi_2)$	−0.0000072(18)
39	$\sin(\varphi_1)\sin(6\varphi_2) + \sin(6\varphi_1)\sin(\varphi_2)$	0.0000053(19)
40	$\cos(2\varphi_1)\cos(6\varphi_2) + \cos(6\varphi_1)\cos(2\varphi_2)$	−0.0000048(18)
41	$\sin(2\varphi_1)\sin(6\varphi_2) + \sin(6\varphi_1)\sin(2\varphi_2)$	0.0000040(19)
42	$\cos(3\varphi_1)\cos(6\varphi_2) + \cos(6\varphi_1)\cos(3\varphi_2)$	0.0000437(18)
43	$\sin(3\varphi_1)\sin(6\varphi_2) + \sin(6\varphi_1)\sin(3\varphi_2)$	−0.0000514(19)
44	$\cos(4\varphi_1)\cos(6\varphi_2) + \cos(6\varphi_1)\cos(4\varphi_2)$	0.0000468(19)
45	$\sin(4\varphi_1)\sin(6\varphi_2) + \sin(6\varphi_1)\sin(4\varphi_2)$	−0.0000501(19)
46	$\cos(5\varphi_1)\cos(6\varphi_2) + \cos(6\varphi_1)\cos(5\varphi_2)$	−0.0000494(19)
47	$\sin(5\varphi_1)\sin(6\varphi_2) + \sin(6\varphi_1)\sin(5\varphi_2)$	0.0000495(19)
48	$\cos(6\varphi_1)\cos(6\varphi_2)$	0.0000283(26)
49	$\sin(6\varphi_1)\sin(6\varphi_2)$	−0.0000271(27)

Table F-2/B

Cartesian nuclear coordinates of the most stable conformer of diethyl ketone optimized at the B3LYP/6-311++G(d,p) level of theory (C_{2v} symmetry) in the *Gaussian*'s internal coordinate system (called standard orientation) and in the principal inertial axes.

	Gaussian internal coordinate system			principal inertial axes		
	a /Å	b /Å	c /Å	a /Å	b /Å	c /Å
C1	0.000000	0.077013	0.000010	0.000000	0.036467	0.000010
O2	0.000000	1.289036	–0.000013	0.000000	1.248490	–0.000011
C3	–1.294225	–0.728282	0.000800	–1.294225	–0.768829	0.000794
C4	–2.560315	0.124092	–0.000368	–2.560315	0.083545	–0.000377
H5	–1.269282	–1.394909	0.872361	–1.269285	–1.435457	0.872354
H6	–1.269162	–1.397287	–0.868913	–1.269159	–1.437832	–0.868920
H7	–3.449941	–0.510510	0.000717	–3.449941	–0.551057	0.000704
H8	–2.597901	0.771700	0.877698	–2.597904	0.731152	0.877690
H9	–2.598154	0.768968	–0.880444	–2.598151	0.728423	–0.880452
C10	1.294225	–0.728282	–0.000812	1.294225	–0.768828	–0.000808
C11	2.560316	0.124091	0.000387	2.560316	0.083545	0.000397
H12	1.269278	–1.394867	–0.872405	1.269281	–1.435412	–0.872402
H13	1.269166	–1.397329	0.868869	1.269163	–1.437876	0.868872
H14	3.449941	–0.510510	–0.000747	3.449941	–0.551056	–0.000735
H15	2.597887	0.771752	–0.877641	2.597890	0.731207	–0.877630
H16	2.598168	0.768916	0.880502	2.598165	0.728369	0.880513

Table F-3

Observed frequencies ($\nu_{Obs.}$) of diethyl ketone in the frequency range from 31.4 to 36.0 GHz using the scan mode of the spectrometer described in ref. [19] in the experimental setup section; $\nu_{Obs.} - \nu_{Calc.}$ values as obtained after a fit with XIAM. The fitted rotational constants are given below the frequencies.

Upper level			Lower level			$\nu_{Obs.}$	$\nu_{Obs.} - \nu_{Calc.}$
J	K_a	K_c	J	K_a	K_c	GHz	MHz
8	1	8	7	0	7	31.62900	–0.4167
3	2	2	2	1	1	31.68750	0.0817
12	1	11	11	2	10	31.75963	–0.0149
15	1	14	15	0	15	32.02475	–0.1852
11	3	8	11	2	9	32.15600	–0.5596
10	0	10	9	1	9	32.35700	0.0422
3	2	1	2	1	2	32.58225	0.3415
10	3	7	10	2	8	32.97425	–0.3261
9	3	6	9	2	7	33.67625	–0.0614
8	3	5	8	2	6	34.24475	0.1448

Table F-3 continued

Upper level			Lower level			$\nu_{Obs.}$	$\nu_{Obs.} - \nu_{Calc.}$
J	K_a	K_c	J	K_a	K_c	GHz	MHz
7	3	4	7	2	5	34.67725	0.2270
4	2	3	3	1	2	34.88500	0.4553
6	3	3	6	2	4	34.98400	0.1270
5	3	2	5	2	3	35.18500	0.4845
4	3	1	4	2	2	35.30300	0.0645
3	3	0	3	2	1	35.36275	–0.8936
4	3	2	4	2	3	35.42875	–0.6203
4	3	1	4	2	3	35.43150	1.0064
5	3	3	5	2	4	35.47600	–0.0400
8	3	6	8	2	7	35.87175	0.0607
A / GHz						8.892310(28)	
B / GHz						1.954112(13)	
C / GHz						1.670162(14)	

Table F-4

Observed AA. AE. EE and EE* species frequencies ($\nu_{Obs.}$) of diethyl ketone. $\nu_{Obs.} - \nu_{Calc.}$ values as obtained after a fit with XIAM.

Upper level			Lower level				$\nu_{Obs.}$	$\nu_{Obs.} - \nu_{Calc.}$
J	K_a	K_c	J	K_a	K_c		GHz	kHz
1	1	1	0	0	0	AA	10.5626611	–2.7
						AE	10.5626240	–1.4
						EE	10.5625879	2.3
						EE*	10.5625879	–0.5
1	1	0	1	0	1	AA	7.2223052	3.2
						AE	7.2222687	3.7
						EE	7.2222299	0.4
						EE*	7.2222299	3.3
2	1	2	1	0	1	AA	13.9030136	–6.1
						AE	13.9029783	–3.5
						EE	13.9029417	–1.7
						EE*	13.9029417	–2.6
2	1	1	2	0	2	AA	7.5148153	–2.7
						AE	7.5147816	1.9
						EE	7.5147468	4.9
						EE*	7.5147468	5.8
2	2	1	2	1	2	AA	21.6668614	11.3

Table F-4 continued

Upper level			Lower level				$\nu_{Obs.}$	$\nu_{Obs.} - \nu_{Calc.}$
J	K_a	K_c	J	K_a	K_c		GHz	kHz
2	2	1	2	1	2	AE	21.6666480	3.8
						EE	21.6662637	0.5
						EE*	21.6666194	−5.3
2	2	0	2	1	1	EE	20.8235884	−6.3
						EE*	20.8232280	−5.2
3	1	3	2	0	2	AA	17.1046482	−10.5
						AE	17.1046178	−3.5
						EE	17.1045821	−1.6
						EE*	17.1045821	−2.1
3	2	1	3	1	2	AA	20.4370037	−0.5
						AE	20.4369109	−3.1
						EE	20.4368619	0.6
						EE*	20.4367900	3.7
4	0	4	3	1	3	AA	8.1466328	5.5
						AE	8.1466489	−9.9
						EE	8.1466900	−0.7
						EE*	8.1466900	−0.2
4	1	4	3	0	3	AA	20.1785087	−9.1
						AE	20.1784764	−5.0
						EE	20.1784462	1.4
						EE*	20.1784462	1.1
4	2	2	4	1	3	AA	19.9648948	−2.2
						AE	19.9647945	−1.5
						EE*	19.9646870	4.5
5	0	5	4	1	4	AA	12.1869861	−3.2
						AE	12.1870257	7.3
						EE	12.1870505	2.8
						EE*	12.1870505	3.1
5	1	4	5	0	5	AA	9.4441392	3.1
						AE	9.4440938	1.3
						EE	9.4440561	7.2
						EE*	9.4440561	7.3
5	1	5	4	0	4	AA	23.1420602	−4.3
						AE	23.1420278	−1.4
						EE	23.1420278	−1.6
						EE*	19.4435255	−1.1
5	2	3	5	1	4	AA	19.4434240	0.0
						AE	19.4433260	−0.7
						EE	19.4433260	9.9
5	2	4	5	1	5	AE	23.4025056	5.2

Table F-4 continued

Upper level			Lower level				$\nu_{Obs.}$	$\nu_{Obs.} - \nu_{Calc.}$
J	K_a	K_c	J	K_a	K_c		GHz	kHz
5	2	4	5	1	5	EE	23.4023716	–3.2
						EE*	23.4023921	6.7
5	3	2	6	2	5	AA	13.7734428	–3.3
						EE*	13.7730841	–2.8
5	3	3	6	2	4	AA	13.1822798	–1.5
						EE*	13.1819219	–1.0
6	0	6	5	1	5	AA	16.2662223	4.9
						AE	16.2662466	2.9
						EE	16.2662727	2.5
						EE*	16.2662727	2.8
6	1	5	6	0	6	AA	10.5138487	–4.4
						AE	10.5138061	–0.7
						EE	10.5137661	5.6
						EE*	10.5137661	5.7
6	2	4	6	1	5	AA	18.9166952	1.3
						AE	18.9165935	1.2
						EE	18.9164914	–1.9
						EE*	18.9164914	3.3
6	2	5	6	1	6	AA	24.2800517	0.0
						AE	24.2799344	4.2
						EE	24.2798129	6.8
						EE*	24.2798129	1.5
6	3	3	7	2	6	AA	10.2670098	–2.6
						AE	10.2669639	–1.4
						EE	10.2671635	–3.7
						EE*	10.2666510	–3.9
6	3	4	7	2	5	AA	9.2124080	0.4
						AE	9.2120982	0.1
						EE	9.2115388	–0.7
						EE*	9.2120518	0.0
7	0	7	6	1	6	AA	20.3515538	3.5
						AE	20.3515758	2.2
						EE	20.3515981	1.2
						EE*	20.3515981	1.3
7	1	6	6	2	5	AA	7.9116209	–3.9
						AE	7.9117183	–1.6
						EE	7.9118178	0.0
						EE*	7.9118178	5.5
7	1	6	7	0	7	AA	11.8401199	–6.3
						AE	11.8400733	–3.3

Table F-4 continued

Upper level			Lower level				$\nu_{Obs.}$	$\nu_{Obs.} - \nu_{Calc.}$
J	K_a	K_c	J	K_a	K_c		GHz	kHz
7	1	6	7	0	7	EE	11.8400266	–0.4
						EE*	11.8400266	–0.3
7	2	5	7	1	6	AA	18.4333419	0.8
						AE	18.4332438	2.3
						EE	18.4331450	1.6
						EE*	18.4331450	4.5
7	4	3	8	3	6	AA	20.4279288	–0.6
						EE*	20.4274312	–0.1
7	4	4	8	3	5	AA	20.3540660	–0.8
						EE*	20.3535687	0.2
8	1	7	7	2	6	AA	12.5466269	–3.8
						AE	12.5467188	–2.1
						EE	12.5468114	–1.4
						EE*	12.5468114	1.7
8	1	7	8	0	8	AA	13.4449660	–8.2
						AE	13.4449177	–3.0
						EE	13.4448677	0.6
						EE*	13.4448677	0.6
8	2	6	8	1	7	AA	18.0444029	0.6
						AE	18.0443052	0.0
						EE	18.0442084	–0.5
						EE*	18.0442084	1.2
8	4	5	9	3	6	AA	16.6092800	2.5
						AE	16.6077737	0.2
						EE*	16.6087806	–0.6
8	4	4	9	3	7	AA	16.7565454	0.5
						AE	16.7575524	–0.4
						EE*	16.7560490	0.0
9	1	8	8	2	7	AA	17.2684168	–0.9
						AE	17.2685038	0.8
						EE	17.2685855	–3.8
						EE*	17.2685855	–1.9
9	2	7	9	1	8	AA	17.7993752	1.2
						AE	17.7992806	1.0
						EE	17.7991871	1.4
						EE*	17.7991871	2.5
9	4	5	10	3	8	AA	13.0820864	–1.1
						AE	13.0826230	3.2
						EE	13.0838711	–1.5
						EE*	13.0815948	0.7

Table F-4 continued

Upper level			Lower level				$\nu_{Obs.}$	$\nu_{Obs.} - \nu_{Calc.}$
J	K_a	K_c	J	K_a	K_c		GHz	kHz
9	4	6	10	3	7	AA	12.8099088	0.4
						AE	12.8088815	−0.8
						EE	12.8071357	0.0
						EE*	12.8094150	0.9
10	1	9	9	2	8	AA	22.0594216	−6.9
						AE	22.0595062	−2.3
						EE	22.0595885	−0.7
						EE*	22.0595885	0.5
10	2	8	10	1	9	AA	17.7435254	0.6
						AE	17.7434338	0.8
						EE	17.7433402	−1.4
						EE*	17.7433402	−0.7
10	4	6	11	3	9	AA	9.4105200	0.4
						AE	9.4106677	−0.1
						EE	9.4114273	−0.8
						EE*	9.4100284	−0.4
10	4	7	11	3	8	AA	8.9375903	−0.3
						AE	8.9369498	−1.1
						EE	8.9356973	−1.7
						EE*	8.9370976	−0.8
11	2	9	10	3	8	AA	8.3347970	−0.8
						AE	8.3349727	−1.1
11	2	9	11	1	10	AA	17.9164614	−0.7
						AE	17.9163722	−0.5
						EE	17.9162772	−6.3
						EE*	17.9162772	−5.9
12	2	10	11	3	9	AA	13.1840171	3.7
						AE	13.1841836	0.7
						EE	13.1843620	1.9
						EE*	13.1843377	−7.3
12	2	10	12	1	11	AA	18.3520910	4.3
						AE	18.3520017	2.3
						EE	18.3519080	−4.2
						EE*	18.3519080	−4.0
13	2	11	12	3	10	AA	18.2057938	5.9
						AE	18.2059545	2.9
						EE	18.2061157	−4.3
						EE*	18.2061157	4.8
13	2	12	12	3	9	AA	8.3807029	3.2
						AE	8.3808728	1.4

Table F-4 continued

Upper level			Lower level				$\nu_{\text{Obs.}}$	$\nu_{\text{Obs.}} - \nu_{\text{Calc.}}$
J	K_a	K_c	J	K_a	K_c		GHz	kHz
13	2	12	12	3	9	EE	8.3810404	1.8
						EE*	8.3810404	−7.3
13	2	11	13	1	12	AA	19.0792351	0.0
						AE	19.0791485	−0.9
						EE	19.0790623	−1.5
						EE*	19.0790623	−1.4
14	2	13	13	3	10	AA	10.7653058	−1.1
						AE	10.7654794	0.5
						EE	10.7656528	4.7
						EE*	10.7656528	−1.0
14	2	12	14	1	13	AA	20.1220183	−1.0
						AE	20.1219340	−0.6
						EE	20.1218528	2.8
						EE*	20.1218528	3.0
14	5	9	15	4	12	AA	8.6936393	1.4
						AE	8.6944168	1.2
						EE	8.6960557	1.9
						EE*	8.6930175	−0.9
15	2	14	14	3	11	AA	12.8260643	2.3
						AE	12.8262337	−0.4
						EE	12.8264042	−0.2
						EE*	12.8264042	−3.9

Chapter 7

ACETONE

Table G-1

Calculated geometry parameters in the principal inertial axes of conformer I and conformer II of acetone calculated at the MP2/6-311++G(d,p) level of theory. The atoms are numbered according Figure 1.

	Conformer I			Conformer II		
	a /Å	b /Å	c /Å	a /Å	b /Å	c /Å
C1	–1.272892	–0.729501	0.000000	1.285837	–0.701424	0.000089
H2	–1.081814	–1.804351	–0.000100	2.145403	–0.030996	0.000400
H3	–1.862227	–0.463806	–0.881895	1.319655	–1.350297	0.881407
H4	–1.862119	–0.463956	0.882012	1.320337	–1.350354	–0.881161
C5	0.005052	0.094562	–0.000006	0.000000	0.101165	–0.000454
O6	–0.038031	1.313109	0.000001	0.000000	1.320810	0.000125
C7	1.312822	–0.667002	0.000001	–1.285837	–0.701424	0.000088
H8	1.359692	–1.315784	0.881198	–1.320318	–1.350390	–0.881134
H9	1.359719	–1.315752	–0.881219	–1.319675	–1.350260	0.881433
H10	2.154730	0.025637	0.000026	–2.145403	–0.030996	0.000356

Table G-2

Coefficients of the two-dimensional Fourier expansion for the energy potential surface calculated of acetone (Figure 2).

Nr	Coefficient	Value
1	1	–192.6543734
2	$\cos(3\varphi_1)$	–0.000842712
3	$\sin(3\varphi_1)$	0.000060634
4	$\cos(3\varphi_2)$	–0.0008575
5	$\sin(3\varphi_2)$	0.000023194
6	$\cos(6\varphi_1)$	0.000005413
7	$\sin(6\varphi_1)$	–0.00004765
8	$\cos(6\varphi_2)$	0.000029853
9	$\sin(6\varphi_2)$	–0.00000136
10	$\cos(3\varphi_1)\cos(3\varphi_2)$	0.000359391
11	$\sin(3\varphi_1)\sin(3\varphi_2)$	–0.000228804

Table G-2 continued

Nr	Coefficient	Value
12	$\cos(3\varphi_1)\sin(3\varphi_2)$	0.000016086
13	$\sin(3\varphi_1)\cos(3\varphi_2)$	–0.000043293
14	$\cos(6\varphi_1)\cos(3\varphi_2)$	0.00003598
15	$\sin(6\varphi_1)\sin(3\varphi_2)$	–0.000078232
16	$\cos(6\varphi_1)\sin(3\varphi_2)$	–0.000013
17	$\sin(6\varphi_1)\cos(3\varphi_2)$	0.000029221
18	$\cos(3\varphi_1)\cos(6\varphi_2)$	0.000002386
19	$\sin(3\varphi_1)\sin(6\varphi_2)$	–0.000053965
20	$\cos(3\varphi_1)\sin(6\varphi_2)$	–0.000033491
21	$\sin(3\varphi_1)\cos(6\varphi_2)$	–0.000007684
22	$\cos(6\varphi_1)\cos(6\varphi_2)$	0.000018939
23	$\sin(6\varphi_1)\sin(6\varphi_2)$	0.000037869
24	$\cos(6\varphi_1)\sin(6\varphi_2)$	0.000030439
25	$\sin(6\varphi_1)\sin(6\varphi_2)$	0.000020775

Table G-3

Potential functions for the rotation around the dihedral angle $\varphi_1 = \angle(H_2, C_1, C_5, O_6)$ (Figure 4). Energies were calculated in a 10° grid and parametrized as a Fourier series $V(\varphi) = a_0 + \sum_{i=1}^{15} a_i \cos(i\varphi)$.

	cm^{-1}
a_0	82.3802
a_3	104.1293
a_6	19.1976

Table G-4

Observed AA, AE, EE, and EE* species frequencies ($\nu_{Obs.}$) of acetone; $\nu_{Obs.} - \nu_{Calc.}$ values as obtained after a fit with XIAM.

Upper level			Lower level				$\nu_{Obs.}$	$\nu_{Obs.} - \nu_{Calc.}$
J	K_a	K_c	J	K_a	K_c		GHz	kHz
1	1	0	1	0	1	AA	5276.0582	3.5
						AE	5269.0711	32.6
						EE	5270.9075	–17.7
						EE*	5253.0496	184.1
4	3	1	4	2	2	AA	11583.0825	–219.1
						EE	11585.2358	–115.1
						EE*	11525.0518	226.9
3	2	1	3	1	2	AA	10762.7108	–124.4
						AE	10751.6624	–54.1
						EE	10749.9321	–122.1
						EE*	10731.3372	140.3
2	1	1	2	0	2	AA	11286.1453	–134.7
						AE	11272.4608	–75.4
						EE	11265.2549	–91.6
						EE*	11252.5027	–70.4
1	1	1	0	0	0	AA	15096.3277	–15.1
						AE	15074.0747	11.9
						EE	15038.5119	2.9
						EE*	15064.9267	–5.8
2	2	1	2	1	2	AA	15827.7432	74.7
						AE	15750.8557	126.6
						EE	15615.7336	31.4
						EE*	15736.2383	71.5
5	3	2	5	2	3	AA	16943.5266	–86.6
						AE	16937.6855	51.4
						EE	16943.5266	36.9
						EE*	16920.8730	222
4	2	2	4	1	3	AA	18667.5826	–27
						AE	18654.2970	93.9
						EE	18651.6569	104.8
						EE*	18630.8827	–9.9
3	1	2	3	0	3	AA	20454.9089	–82.4
						AE	20426.4864	25.2
						EE	20404.2354	17
						EE*	20392.1014	–24.7
3	2	2	3	1	3	AA	22468.8796	–74.5
						AE	22413.0439	–12.8
						EE	22346.2788	–89.8

Table G-4 continued

Upper level			Lower level				$\nu_{Obs.}$	$\nu_{Obs.} - \nu_{Calc.}$
J	K_a	K_c	J	K_a	K_c		GHz	kHz
3	2	2	3	1	3	EE*	22367.8725	–37.5
2	0	2	1	1	1	AA	22793.2803	–75.6
						AE	22800.3776	–24.4
						EE	22820.8286	24.8
						EE*	22794.3188	–14.8
4	3	2	4	2	3	AA	23549.0261	42.5
						AE	23469.2274	80.1
						EE	23352.2400	–40
						EE*	23426.9883	25.7
2	1	2	1	0	1	AA	24916.4873	–27.5
						AE	24899.5046	17.3
						EE	24876.5477	13.4
						EE*	24888.2479	78.5

Table G-5

Observed AA, AE, EE, and EE* species frequencies ($\nu_{Obs.}$) of acetone; $\nu_{Obs.} - \nu_{Calc.}$ values as obtained after a fit with Erham.

Upper level		Lower level			$\nu_{Obs.}$	$\nu_{Obs.} - \nu_{Calc.}$
J	N	J	N		MHz	kHz
1	3	1	1	EE	5253.0496	–13.9
				EE*	5269.0711	–0.6
				AE	5270.9075	3.3
				AA	5276.0582	1.5
3	5	3	3	EE	10731.3372	–20.7
				EE*	10749.9321	–8.1
				AE	10751.6624	–5.6
				AA	10762.7108	11.6
2	3	2	1	EE	11252.5027	0.0
				EE*	11265.2549	–11.5
				AE	11272.4608	–0.3
				AA	11286.1453	17.0
4	7	4	5	EE	11525.0518	–38.1
				EE*	11583.0825	12.2
				AA	11585.2358	0.8
1	2	0	1	EE*	15038.5119	–2.4
				EE	15064.9267	–0.8
				AE	15074.0747	–0.9

Table G-5 continued

Upper level		Lower level			$\nu_{Obs.}$	$\nu_{Obs.} - \nu_{Calc.}$
J	*N*	*J*	*N*		MHz	kHz
1	2	0	1	AA	15096.3277	–2.0
2	4	2	2	EE	15615.7336	5.2
				EE*	15736.2383	2.5
				AE	15750.8557	11.9
				AA	15827.7432	5.1
5	7	5	5	EE	16920.8730	–8.8
				EE*	16937.6855	–12.0
				AE	16943.5266	21.0
				AA	16943.5266	14.8
4	5	4	3	EE	18630.8827	–75.6
				EE*	18651.6569	–6.4
				AE	18654.2970	–2.1
				AA	18667.5826	33.1
3	3	3	1	EE	20392.1014	20.2
				EE*	20404.2354	–7.0
				AE	20426.4864	3.7
				AA	20454.9089	23.4
3	4	3	2	EE	22346.2788	–14.5
				EE*	22367.8725	–5.4
				AE	22413.0439	0.6
				AA	22468.8796	16.5
2	1	1	2	EE	22793.2803	21.9
				EE*	22794.3188	9.2
				AE	22800.3776	–0.4
				AA	22820.8286	–10.2
4	6	4	4	EE	23352.2400	–25.2
				EE*	23426.9883	–7.3
				AE	23469.2274	13.1
				AA	23549.0261	25.3
2	2	1	1	EE	24876.5477	–6.7
				EE*	24888.2479	–5.7
				AE	24899.5046	–5.9
				AA	24916.4873	1.0

Chapter 8

DIETHYL AMINE

Table H-1

Cartesian coordinates of the nuclei in diethyl amine in the principal axes of inertia as calculated at the MP2/6-311++G(d,p) level of theory. The atoms are numbered according Figure 1.

	a /Å	b /Å	c /Å
C1	2.451988	−0.368445	−0.006933
C2	1.217280	0.523378	0.016279
H3	3.365912	0.231591	0.028268
H4	2.458552	−1.041758	0.856914
H5	2.461655	−0.975631	−0.915403
H6	1.230935	1.157356	0.921422
H7	1.229163	1.199429	−0.846588
C8	−1.217318	0.523407	0.016223
C9	−2.451962	−0.368462	−0.006908
H10	−1.230930	1.157427	0.921312
H11	−1.229190	1.199341	−0.846723
H12	−3.365939	0.231476	0.028664
H13	−2.461812	−0.975437	−0.915509
H14	−2.458258	−1.041967	0.856792
N15	0.000005	−0.279132	−0.072153
C16	−0.000022	−0.953151	0.691174

Table H-2

Observed frequencies ($\nu_{Obs.}$) of diethyl amine. $\nu_{Calc.}$ is the calculated value; $\nu_{Obs.} - \nu_{Calc.}$ values obtained after a fit with program *spfit*. J, K_a, and K_c are the asymmetric top rotational quantum numbers, ν denotes the inversional inversion sublevels, $\nu = 0$ and $\nu = 1$ correspond to the symmetric (+) state and the antisymmetric (−) state, respectively, F is the total angular momentum in the coupled basis with $\boldsymbol{F} = \boldsymbol{J} + \boldsymbol{I}$.

Upper level					Lower level					$\nu_{Obs.}$ MHz	$\nu_{Obs.} - \nu_{Calc.}$ MHz
J	K_a	K_c	ν	F	J	K_a	K_c	ν	F		
1	1	1	1	2	1	0	1	0	2	16272.2349	−0.0037
1	1	1	1	1	1	0	1	0	2	16272.4911	0.0034
1	1	1	1	2	1	0	1	0	1	16271.4336	−0.0023
1	1	1	1	0	1	0	1	0	1	16271.0715	0.0051
1	1	1	1	1	1	0	1	0	0	16273.6939	0.0021
1	1	1	1	1	1	0	1	0	1	16271.6821	−0.0029
1	1	1	0	2	1	0	1	1	2	14750.6458	0.0043
1	1	1	0	1	1	0	1	1	2	14750.8976	0.0061
1	1	1	0	2	1	0	1	1	1	14749.8356	−0.0032
1	1	1	0	0	1	0	1	1	1	14749.4616	0.0012
1	1	1	0	1	1	0	1	1	0	14752.0939	−0.0016
1	1	1	0	1	1	0	1	1	1	14750.0883	−0.0004
2	1	2	1	3	2	0	2	0	3	16150.5074	0.0017
2	1	2	1	2	2	0	2	0	2	16150.7607	−0.0018
2	1	2	1	1	2	0	2	0	1	16150.3635	−0.0015
2	1	2	1	2	2	0	2	0	3	16151.6316	0.0035
2	1	2	1	3	2	0	2	0	2	16149.6419	0.0018
2	1	2	1	1	2	0	2	0	2	16149.0212	0.0025
2	1	2	1	2	2	0	2	0	1	16152.1123	0.0034
2	1	2	0	3	2	0	2	1	3	14628.9112	0.0009
2	1	2	0	2	2	0	2	1	2	14629.1740	−0.0003
2	1	2	0	1	2	0	2	1	1	14628.7625	−0.0005
2	1	2	0	2	2	0	2	1	3	14630.0409	0.0010
2	1	2	0	3	2	0	2	1	2	14628.0447	0.0000
2	1	2	0	1	2	0	2	1	2	14627.4159	−0.0007
2	1	2	0	2	2	0	2	1	1	14630.5195	−0.0011
3	1	3	1	4	3	0	3	0	4	15969.7336	−0.0055
3	1	3	1	3	3	0	3	0	3	15970.0418	0.0025
3	1	3	1	2	3	0	3	0	2	15969.6463	−0.0086
3	1	3	1	3	3	0	3	0	4	15970.9446	−0.0010
3	1	3	1	4	3	0	3	0	3	15968.8327	−0.0002
3	1	3	1	2	3	0	3	0	3	15968.4293	−0.0023
3	1	3	1	3	3	0	3	0	2	15971.2604	−0.0023
3	1	3	0	4	3	0	3	1	4	14447.8274	−0.0006

Table H-2 continued

Upper level					Lower level					$\nu_{Obs.}$ MHz	$\nu_{Obs.} - \nu_{Calc.}$ MHz
J	K_a	K_c	ν	F	J	K_a	K_c	ν	F		
3	1	3	0	3	3	0	3	1	3	14448.3213	0.0020
3	1	3	0	2	3	0	3	1	2	14447.6556	−0.0001
3	1	3	0	3	3	0	3	1	4	14449.2237	−0.0018
3	1	3	0	4	3	0	3	1	3	14446.9204	−0.0013
3	1	3	0	2	3	0	3	1	3	14446.4315	−0.0009
3	1	3	0	3	3	0	3	1	2	14449.5435	0.0009
4	1	4	1	5	4	0	4	0	5	15730.4802	−0.0016
4	1	4	1	4	4	0	4	0	4	15731.0834	0.0016
4	1	4	1	3	4	0	4	0	3	15730.3270	0.0001
4	1	4	1	4	4	0	4	0	5	15732.0207	0.0004
4	1	4	1	5	4	0	4	0	4	15729.5373	−0.0060
4	1	4	1	3	4	0	4	0	4	15729.1539	0.0068
4	1	4	1	4	4	0	4	0	3	15732.2638	0.0022
4	1	4	0	5	4	0	4	1	5	14208.9626	−0.0031
4	1	4	0	4	4	0	4	1	4	14209.5539	0.0024
4	1	4	0	3	4	0	4	1	3	14208.8129	−0.0020
4	1	4	0	4	4	0	4	1	5	14210.4911	0.0011
4	1	4	0	5	4	0	4	1	4	14208.0289	0.0017
4	1	4	0	3	4	0	4	1	4	14207.6346	−0.0005
4	1	4	0	4	4	0	4	1	3	14210.7343	0.0031
5	1	5	1	6	5	0	5	0	6	15435.9816	−0.0025
5	1	5	1	5	5	0	5	0	5	15436.6261	0.0041
5	1	5	1	4	5	0	5	0	4	15435.8548	0.0008
5	1	5	1	5	5	0	5	0	6	15437.5897	−0.0001
5	1	5	1	6	5	0	5	0	5	15435.0200	0.0036
5	1	5	1	4	5	0	5	0	5	15434.6886	−0.0005
5	1	5	1	5	5	0	5	0	4	15437.7879	0.0010
5	1	5	0	6	5	0	5	1	6	13914.4817	0.0022
5	1	5	0	5	5	0	5	1	5	13915.1090	−0.0011
5	1	5	0	4	5	0	5	1	4	13914.3452	−0.0058
5	1	5	0	5	5	0	5	1	6	13916.0747	−0.0032
5	1	5	0	6	5	0	5	1	5	13913.5108	−0.0009
5	1	5	0	4	5	0	5	1	5	13913.1804	−0.0057
5	1	5	0	5	5	0	5	1	4	13916.2790	0.0040
6	1	6	1	7	6	0	6	0	7	15088.5646	0.0034
6	1	6	1	6	6	0	6	0	6	15089.2185	0.0011
6	1	6	1	5	6	0	6	0	5	15088.4434	−0.0070
6	1	6	0	7	6	0	6	1	7	13567.0825	0.0023
6	1	6	0	6	6	0	6	1	6	13567.7338	0.0023

Table H-2 continued

Upper level					Lower level					$\nu_{Obs.}$ MHz	$\nu_{Obs.} - \nu_{Calc.}$ MHz
J	K_a	K_c	ν	F	J	K_a	K_c	ν	F		
6	1	6	0	5	6	0	6	1	5	13566.9682	−0.0020
7	1	7	1	8	7	0	7	0	8	14691.4760	0.0024
7	1	7	1	7	7	0	7	0	7	14692.1387	0.0035
7	1	7	1	6	7	0	7	0	6	14691.3808	0.0026
7	1	7	0	8	7	0	7	1	8	13170.0164	−0.0054
7	1	7	0	7	7	0	7	1	7	13170.6776	−0.0023
7	1	7	0	6	7	0	7	1	6	13169.9238	−0.0031
8	1	8	1	9	8	0	8	0	9	14248.5056	−0.0016
8	1	8	1	8	8	0	8	0	8	14249.1653	−0.0004
8	1	8	1	7	8	0	8	0	7	14248.4225	−0.0019
8	1	8	0	9	8	0	8	1	9	12727.0959	0.0068
8	1	8	0	8	8	0	8	1	8	12727.7466	0.0018
8	1	8	0	7	8	0	8	1	7	12727.0029	−0.0040
9	1	9	1	10	9	0	9	0	10	13763.9536	−0.0032
9	1	9	1	9	9	0	9	0	9	13764.6070	0.0013
9	1	9	1	8	9	0	9	0	8	13763.8913	0.0070
9	1	9	0	10	9	0	9	1	10	12242.5801	0.0041
9	1	9	0	9	9	0	9	1	9	12243.2185	−0.0042
9	1	9	0	8	9	0	9	1	8	12242.4965	−0.0072
10	1	10	1	11	10	0	10	0	11	13242.5868	−0.0075
10	1	10	1	10	10	0	10	0	10	13243.2278	−0.0010
10	1	10	1	9	10	0	10	0	9	13242.5388	0.0082
10	1	10	0	11	10	0	10	1	11	11721.2471	−0.0070
10	1	10	0	10	10	0	10	1	10	11721.8873	0.0006
10	1	10	0	9	10	0	10	1	9	11721.2046	0.0141
11	1	11	1	12	11	0	11	0	12	12689.6162	−0.0057
11	1	11	1	11	11	0	11	0	11	12690.2367	−0.0012
11	1	11	1	10	11	0	11	0	10	12689.5731	0.0074
11	1	11	0	12	11	0	11	1	12	11168.3286	0.0035
11	1	11	0	11	11	0	11	1	11	11168.9378	−0.0018
11	1	11	0	10	11	0	11	1	10	11168.2622	−0.0069
12	1	12	1	13	12	0	12	0	13	12110.6086	−0.0003
12	1	12	1	12	12	0	12	0	12	12111.2007	−0.0024
12	1	12	1	11	12	0	12	0	11	12110.5612	0.0020
12	1	12	0	13	12	0	12	1	13	10589.3573	−0.0005
12	1	12	0	12	12	0	12	1	12	10589.9489	−0.0018
12	1	12	0	11	12	0	12	1	11	10589.3113	0.0030
1	1	0	1	2	1	0	1	1	2	15633.9979	−0.0069
1	1	0	1	1	1	0	1	1	2	15632.9530	0.0012

Table H-2 continued

Upper level					Lower level					$\nu_{\text{Obs.}}$ MHz	$\nu_{\text{Obs.}} - \nu_{\text{Calc.}}$ MHz
J	K_a	K_c	ν	F	J	K_a	K_c	ν	F		
1	1	0	1	2	1	0	1	1	1	15633.2002	−0.0018
1	1	0	1	0	1	0	1	1	1	15634.7899	0.0052
1	1	0	1	1	1	0	1	1	0	15634.1524	−0.0035
1	1	0	1	1	1	0	1	1	1	15632.1463	−0.0028
1	1	0	0	2	1	0	1	0	2	15633.9446	0.0003
1	1	0	0	1	1	0	1	0	2	15632.8983	0.0061
1	1	0	0	2	1	0	1	0	1	15633.1329	−0.0087
1	1	0	0	0	1	0	1	0	1	15634.7142	−0.0011
1	1	0	0	1	1	0	1	0	0	15634.0968	0.0006
1	1	0	0	1	1	0	1	0	1	15632.0924	0.0029
2	1	1	1	2	2	0	2	1	2	15755.8616	−0.0027
2	1	1	1	1	2	0	2	1	2	15756.2897	0.0051
2	1	1	1	2	2	0	2	1	3	15756.7199	−0.0100
2	1	1	1	3	2	0	2	1	3	15756.9953	−0.0040
2	1	1	1	2	2	0	2	1	1	15757.2086	−0.0021
2	1	1	1	1	2	0	2	1	1	15757.6271	−0.0038
2	1	1	0	2	2	0	2	0	2	15755.8068	0.0033
2	1	1	0	1	2	0	2	0	2	15756.2071	−0.0029
2	1	1	0	2	2	0	2	0	3	15756.6663	−0.0028
2	1	1	0	3	2	0	2	0	3	15756.9383	0.0069
2	1	1	0	2	2	0	2	0	1	15757.1569	0.0071
2	1	1	0	1	2	0	2	0	1	15757.5542	−0.0022
3	1	2	1	4	3	0	3	1	4	15942.9205	0.0062
3	1	2	1	3	3	0	3	1	3	15941.9557	0.0037
3	1	2	1	2	3	0	3	1	2	15943.2507	−0.0009
3	1	2	0	4	3	0	3	0	4	15942.5135	−0.0035
3	1	2	0	3	3	0	3	0	3	15941.7414	−0.0044
3	1	2	0	2	3	0	3	0	2	15942.7564	−0.0098
4	1	3	1	5	4	0	4	1	5	16193.3329	0.0038
4	1	3	1	3	4	0	4	1	3	16193.5536	−0.0080
4	1	3	0	5	4	0	4	0	5	16193.3090	0.0001
4	1	3	0	5	4	0	4	0	4	16192.3727	0.0023
4	1	3	0	3	4	0	4	0	3	16193.5536	0.0081
5	1	4	1	6	5	0	5	1	6	16510.3800	0.0029
5	1	4	1	5	5	0	5	1	5	16509.5069	0.0121
5	1	4	1	4	5	0	5	1	4	16510.5509	−0.0062
5	1	4	0	6	5	0	5	0	6	16510.3474	0.0011
5	1	4	0	5	5	0	5	0	5	16509.4473	−0.0095
5	1	4	0	4	5	0	5	0	4	16510.5269	−0.0010

Table H-2 continued

Upper level					Lower level					$\nu_{Obs.}$ MHz	$\nu_{Obs.} - \nu_{Calc.}$ MHz
J	K_a	K_c	ν	F	J	K_a	K_c	ν	F		
6	1	5	1	6	6	0	6	1	6	16895.8369	0.0026
6	1	5	1	5	6	0	6	1	5	16896.8666	0.0044
6	1	5	0	7	6	0	6	0	7	16896.6869	0.0065
6	1	5	0	6	6	0	6	0	6	16895.7961	−0.0003
6	1	5	0	5	6	0	6	0	5	16896.8241	−0.0058
7	1	6	1	8	7	0	7	1	8	17355.4941	−0.0004
7	1	6	1	7	7	0	7	1	7	17354.6062	−0.0025
7	1	6	1	6	7	0	7	1	6	17355.6229	0.0006
7	1	6	0	8	7	0	7	0	8	17355.4653	0.0042
7	1	6	0	7	7	0	7	0	7	17354.5694	−0.0024
7	1	6	0	6	7	0	7	0	6	17355.5875	−0.0020
8	1	7	1	9	8	0	8	1	9	17890.3440	−0.0045
8	1	7	1	7	8	0	8	1	7	17890.4718	0.0097
8	1	7	0	9	8	0	8	0	9	17890.3178	0.0017
8	1	7	0	8	8	0	8	0	8	17889.4111	−0.0039
8	1	7	0	7	8	0	8	0	7	17890.4343	0.0045
9	1	8	1	10	9	0	9	1	10	18505.3419	0.0037
9	1	8	1	9	9	0	9	1	9	18504.4252	0.0022
9	1	8	1	8	9	0	9	1	8	18505.4354	−0.0052
9	1	8	0	10	9	0	9	0	10	18505.3046	−0.0033
9	1	8	0	9	9	0	9	0	9	18504.3918	0.0013
9	1	8	0	8	9	0	9	0	8	18505.4064	−0.0040
1	1	0	0	2	0	0	0	1	1	18958.0238	0.0004
1	1	0	0	1	0	0	0	1	1	18956.9694	−0.0019
1	1	0	0	0	0	0	0	1	1	18959.5951	−0.0020
1	1	0	1	2	0	0	0	0	1	20479.6279	0.0061
1	1	0	1	1	0	0	0	0	1	20478.5701	0.0012
1	1	0	1	0	0	0	0	0	1	20481.2054	0.0009
2	1	1	0	2	1	0	1	1	1	23164.2764	−0.0045
2	1	1	0	1	1	0	1	1	1	23164.6869	−0.0005
2	1	1	0	2	1	0	1	1	2	23165.0978	0.0142
2	1	1	0	3	1	0	1	1	2	23165.3456	−0.0003
2	1	1	0	1	1	0	1	1	0	23166.6912	−0.0030
2	1	1	1	2	1	0	1	0	1	24685.8676	−0.0025
2	1	1	1	3	1	0	1	0	2	24686.9452	0.0029
2	1	1	1	1	1	0	1	0	0	24688.2961	−0.0010
1	1	0	1	1	2	0	2	0	2	8223.6792	0.0075
1	1	0	1	2	2	0	2	0	2	8224.7244	−0.0002
1	1	0	1	1	2	0	2	0	1	8225.0252	0.0072

Table H-2 continued

Upper level					Lower level					$\nu_{Obs.}$	$\nu_{Obs.} - \nu_{Calc.}$
J	K_a	K_c	ν	F	J	K_a	K_c	ν	F	MHz	MHz
1	1	0	1	2	2	0	2	0	3	8225.5815	−0.0087
1	1	0	1	0	2	0	2	0	1	8227.6568	0.0031
1	1	1	0	0	0	0	0	0	1	19595.8745	−0.0057
1	1	1	1	0	0	0	0	1	1	19595.9556	0.0074
1	1	1	0	2	0	0	0	0	1	19596.2530	−0.0056
1	1	1	1	2	0	0	0	1	1	19596.3237	0.0061
1	1	1	0	1	0	0	0	0	1	19596.4978	−0.0107
1	1	1	1	1	0	0	0	1	1	19596.5689	0.0021
7	0	7	1	7	6	1	6	1	6	14225.7755	−0.0028
7	0	7	0	7	6	1	6	0	6	14225.8714	−0.0047
7	0	7	1	8	6	1	6	1	7	14226.4059	0.0009
7	0	7	0	8	6	1	6	0	7	14226.4955	−0.0025
8	0	8	1	8	7	1	7	1	7	18687.6234	0.0056
8	0	8	0	8	7	1	7	0	7	18687.7230	0.0068
8	0	8	1	9	7	1	7	1	8	18688.2546	0.0061
8	0	8	0	9	7	1	7	0	8	18688.3550	−0.0020
6	0	6	1	5	5	1	4	0	4	8734.6991	0.0000
6	0	6	1	7	5	1	4	0	6	8734.8508	−0.0010
6	0	6	1	6	5	1	4	0	5	8735.7679	−0.0021
6	0	6	0	5	5	1	4	1	4	7213.2465	0.0043
6	0	6	0	7	5	1	4	1	6	7213.3965	0.0033
6	0	6	0	6	5	1	4	1	5	7214.3065	0.0023
7	0	7	1	6	6	1	5	0	5	12418.1468	−0.0098
7	0	7	1	8	6	1	5	0	7	12418.2877	0.0019
7	0	7	1	7	6	1	5	0	6	12419.1960	−0.0033
7	0	7	0	6	6	1	5	1	5	10896.7381	0.0019
7	0	7	0	8	6	1	5	1	7	10896.8647	0.0002
7	0	7	0	7	6	1	5	1	6	10897.7830	0.0098
2	1	2	0	1	1	0	1	0	1	23557.4320	0.0096
2	1	2	1	1	1	0	1	1	1	23557.4968	0.0007
2	1	2	0	3	1	0	1	0	2	23558.8597	0.0065
2	1	2	1	3	1	0	1	1	2	23558.9216	0.0013
2	1	2	0	2	1	0	1	0	1	23559.1736	−0.0064
2	1	2	1	2	1	0	1	1	1	23559.2356	−0.0043
2	1	2	0	1	1	0	1	0	0	23559.4239	−0.0053
2	1	2	1	1	1	0	1	1	0	23559.5004	−0.0024
2	1	2	0	2	1	0	1	0	2	23559.9902	0.0074
2	1	2	1	2	1	0	1	1	2	23560.0379	−0.0048

Table H-3

Fitted parameters and their values from the *.par file of the *spfit* program.

```
19  228   30    0     0.0000E+000    1.0000E+006    1.0000E+000 1.0000000000
'a'  3  2  0 ,,,,,,,,,
         10099  1.761499169773003E+004 1.00000000E+036 /A
         20099  2.103650247881789E+003 1.00000000E+036 /B
         30099  1.981332500668718E+003 1.00000000E+036 /C
           299 -2.375483165772915E-004 1.00000000E+036 /-DJ
          1199  3.163781997943447E-003 1.00000000E+036 /-DJK
         40199 -2.584987545751301E-005 1.00000000E+036 /-delJ
            11  7.607706203556969E+002 1.00000000E+036 /E
           100  8.056991118960588E-004 1.00000000E+036 /0.5EJ
          -111 -8.056991118960588E-004 1.00000000E-037 /-0.5EJ
          1100 -2.275361838059720E-004 1.00000000E+036 /0.5EJK
         -1111  2.275361838059720E-004 1.00000000E-037 /-0.5EJK
          1000 -2.972234065302882E-002 1.00000000E+036 /0.5EK
         -1011  2.972234065302882E-002 1.00000000E-037 /-0.5EK
         40000  2.300661044190619E-004 1.00000000E+036 /0.5E2
        -40011 -2.300661044190619E-004 1.00000000E-037 /-0.5E2
        210001  4.574740606100134E-001 1.00000000E+036 /Fbc
     110010099  4.013637347470256E+000 1.00000000E+036 /1.5Xaa
     110040099  1.085358667014616E+000 1.00000000E+036 /0.25X_
     110210001  2.919882537090598E+000 1.00000000E+036 /Xbc_01
```

Table H-4

Observed AA, AE, EE, and EE* species frequencies of some rotational transitions of diethyl amine. For J, K_a, K_c, v, and F, see Table H-2. v_{EE} is the frequency of the EE component of the torsional multiplet, $\delta_{Obs.}$ is the splitting of the torsional multiplet with respect to the EE component ($v_{EE} - v_\Gamma$). $\delta_{Calc.}$ is the calculated value; $\delta_{Obs.} - \delta_{Calc.}$ values were obtained after a fit with the program XIAM.

Upper level					Lower level					Γ	v_{EE} MHz	$\delta_{Obs.}$ MHz	$\delta_{Obs.} - \delta_{Calc.}$
J	K_a	K_c	v	F	J	K_a	K_c	v	F				
1	1	0	1	1	0	0	0	0	1	EE	20478.5517		
										EE*		0.0000	−0.0004
										AE		0.0184	0.0004
										AA		0.0358	0.0001
1	1	0	0	1	0	0	0	1	1	EE	18956.9515		
										EE*		0.0000	−0.0004
										AE		0.0179	−0.0001
										AA		0.0360	0.0003
1	1	0	1	0	0	0	0	0	1	EE	20481.1875		
										EE*		0.0000	−0.0004

Table H-4 continued

Upper level					Lower level					Γ	ν_{EE} MHz	$\delta_{Obs.}$ MHz	$\delta_{Obs.} - \delta_{Calc.}$
J	K_a	K_c	ν	F	J	K_a	K_c	ν	F				
1	1	0	1	0	0	0	0	0	1	AE	20481.1875	0.0179	−0.0001
										AA		0.0360	0.0003
1	1	0	0	0	0	0	0	1	1	EE	18959.5770		
										EE*		0.0000	−0.0004
										AE		0.0181	0.0001
										AA		0.0365	0.0008
2	1	1	0	2	1	0	1	1	1	EE	23164.2561		
										EE*		0.0000	−0.0001
										AE		0.0203	0.0021
										AA		0.0366	0.0003
2	1	1	0	1	1	0	1	1	0	EE	23166.6726		
										EE*		0.0000	−0.0001
										AE		0.0186	0.0004
										AA		0.0380	0.0017
1	1	1	1	0	1	0	1	0	1	EE	16271.0523		
										EE*		0.0000	0.0004
										AE		0.0181	0.0006
										AA		0.0345	−0.0007
1	1	1	0	0	1	0	1	1	1	EE	14749.4430		
										EE*		0.0000	0.0004
										AE		0.0177	0.0002
										AA		0.0342	−0.0010
1	1	1	1	1	1	0	1	0	0	EE	16273.6765		
										EE*		0.0000	0.0004
										AE		0.0176	0.0001
										AA		0.0345	−0.0007
1	1	1	0	1	1	0	1	1	0	EE	14752.0766		
										EE*		0.0000	0.0004
										AE		0.0178	0.0003
										AA		0.0350	−0.0002
2	1	2	1	1	2	0	2	0	2	EE	16149.0048		
										EE*		0.0000	0.0001
										AE		0.0168	−0.0006
										AA		0.0331	−0.0018
2	1	2	0	1	2	0	2	1	2	EE	14627.3989		
										EE*		0.0000	0.0001
										AE		0.0175	0.0001
										AA		0.0341	−0.0008

Chapter 9

METHYL *tert*-BUTYL AMINE

Table I-1

Calculated geometry parameters in the principal inertial axes of the only stable conformer of methyl *tert*-butyl amine. The atoms are numbered according Figure 1.

	a /Å	b /Å	c /Å
C1	–2.085233	–0.031084	0.004995
H2	–2.200183	0.739118	–0.761391
H3	–2.185463	0.445264	0.992064
H4	–2.911582	–0.736638	–0.116142
N5	–0.831278	–0.753696	–0.203081
H6	–0.810791	–1.558025	0.420085
C7	0.413105	0.010154	0.001078
C8	0.528749	0.622978	1.406526
C9	1.558198	–0.981157	–0.212181
C10	0.497436	1.115503	–1.054090
C11	–0.249852	1.370380	1.587674
C12	0.445043	–0.157252	2.172568
H13	1.498491	1.117976	1.529099
H14	1.493780	–1.418004	–1.212976
H15	2.527372	–0.484426	–0.099669
H12	1.506532	–1.792923	0.523777
H13	1.476343	1.603802	–1.006529
H14	0.362559	0.689433	–2.053051
H15	–0.264245	1.885299	–0.896137

Table I-2

Potential functions for the rotation around the dihedral angle $\varphi = \angle(C_{10}, C_7, N, C_1)$ (Figure 1). Energies were calculated in a 10° grid and parametrized as a Fourier series $V(\varphi) = a_0 + \sum_{i=1}^{15} a_i \cos(i\varphi)$.

	Hartree	cm^{-1}
a_0	−252.374103451	82.3802
a_3	0.003639326	104.1293
a_6	0.000405939	19.1976

Table I-3

Fitted parameters and their values from the *.par file of the *spfit* program.

A. Concerning Fit I in Table 1

```
5   25   10    0    0.0000E+000    1.0000E+006    1.0000E+000 1.0000000000
'a'  1  2  0
        1099  1.730125922927999E+003 1.00000000E-001 /A-(B+C)/2
         199  2.619170944807567E+003 1.00000000E-001 /(B+C)/2
       40099  1.264555349239291E+000 1.00000000E-001 /(B-C)/4
          11  6.989034261445589E+002 1.00000000E-001 /E
        1000 -1.722751459902137E-001 1.00000000E-001 /EK
```


B. Concerning Fit II in Table 1

```
5   25   10    0    0.0000E+000    1.0000E+006    1.0000E+000 1.0000000000
'a'  1  2  0
        1099  1.730133946676466E+003 1.00000000E-001 /A-(B+C)/2
         199  2.619112140270308E+003 1.00000000E-001 /(B+C)/2
       40099 -1.207362571709949E+000 1.00000000E-001 /(B-C)/4
          11  6.989008748244427E+002 1.00000000E-001 /E
        1000 -1.748742905671537E-001 1.00000000E-001 /EK
```

Chapter 10

TRIETHYL AMINE

Table J-1

Cartesian nuclear coordinates of 7 stable conformers of triethyl amine in the principal axes of inertia as calculated at the MP2/6-311++G(d,p) level of theory.

	Conformer I			Conformer II		
	a /Å	b /Å	c /Å	a /Å	b /Å	c /Å
N1	−0.025346	−0.323840	0.580016	−0.174363	0.020183	0.392375
C2	−0.199295	1.119037	0.752136	0.253764	1.117371	−0.475894
H3	0.588598	1.451659	1.437939	−0.599315	1.791841	−0.591073
H4	−1.149774	1.289321	1.273328	0.508366	0.757177	−1.491363
C5	−0.183514	1.997897	−0.509110	1.423501	1.910470	0.098585
H6	−1.009583	1.748752	−1.181472	2.355552	1.339377	0.086685
H7	−0.303073	3.046849	−0.216550	1.583033	2.815417	−0.495635
H8	0.748820	1.905574	−1.069618	1.207830	2.204312	1.129969
C9	−0.851757	−0.918473	−0.462254	0.898701	−0.931283	0.699021
H10	−0.605416	−1.986681	−0.490667	0.470921	−1.678452	1.377282
H11	−0.633795	−0.518743	−1.468839	1.668471	−0.404276	1.271489
C12	−2.341837	−0.760590	−0.169732	1.548307	−1.643282	−0.495769
H13	−2.930022	−1.314243	−0.908374	2.302187	−2.350871	−0.135112
H14	−2.570297	−1.148980	0.826747	0.812469	−2.205656	−1.078101
H15	−2.656415	0.285872	−0.212579	2.048307	−0.937774	−1.165926
C16	1.358650	−0.788064	0.566542	−1.357160	−0.651227	−0.149074
H17	1.830998	−0.433411	1.490797	−1.224981	−0.919190	−1.214391
H18	1.321614	−1.882727	0.633784	−1.477516	−1.589981	0.403819
C19	2.242300	−0.399211	−0.629927	−2.629957	0.177669	0.011574
H20	3.197145	−0.933004	−0.567907	−2.612307	1.082154	−0.601316
H21	1.770068	−0.665939	−1.580253	−3.499415	−0.412152	−0.296380
H22	2.461034	0.671435	−0.639252	−2.754023	0.469112	1.057932

Table J-1 continued

	Conformer III			Conformer IV		
	a /Å	b /Å	c /Å	a /Å	b /Å	c /Å
N1	0.000042	–0.000034	–0.026249	–0.000046	–0.409887	–0.274148
C2	–0.644863	1.233365	0.434748	–0.000004	1.007500	–0.649776
H3	–0.402276	1.423763	1.498352	–0.871533	1.180605	–1.287838
H4	–1.727923	1.089413	0.381951	0.871435	1.180466	–1.288006
C5	–0.273824	2.440354	–0.421518	0.000205	2.022552	0.501673
H6	–0.565999	2.262101	–1.459577	0.886148	1.917970	1.135220
H7	–0.788992	3.335318	–0.057307	0.000313	3.038656	0.093498
H8	0.800441	2.641628	–0.398527	–0.885660	1.918215	1.135356
C9	–0.745677	–1.175277	0.434559	1.194863	–0.813362	0.468367
H10	–1.031548	–1.060710	1.498297	1.102475	–1.892104	0.640239
H11	–0.079570	–2.041293	0.381301	1.238699	–0.340598	1.468242
C12	–1.976730	–1.457141	–0.421469	2.493520	–0.541625	–0.284084
H13	–2.493807	–2.351144	–0.057628	3.324442	–1.039780	0.224694
H14	–2.688431	–0.627683	–0.397702	2.426083	–0.930818	–1.304205
H15	–1.676552	–1.620296	–1.459730	2.728972	0.524807	–0.331811
C16	1.390622	–0.058295	0.434785	–1.194962	–0.813140	0.468476
H17	1.807453	0.951659	0.382140	–1.102608	–1.891840	0.640605
H18	1.434200	–0.363723	1.498356	–1.238724	–0.340120	1.468222
C19	2.250436	–0.982971	–0.421591	–2.493600	–0.541509	–0.284081
H20	3.283029	–0.984445	–0.057247	–2.426026	–0.930789	–1.304156
H21	1.887535	–2.013925	–0.398875	–3.324551	–1.039638	0.224664
H22	2.242311	–0.640578	–1.459575	–2.729102	0.524904	–0.331946

Table J-1 continued

	Conformer V			Conformer VI		
	a /Å	b /Å	c /Å	a /Å	b /Å	c /Å
N1	–0.000256	–0.287941	–0.066036	0.073814	–0.009432	0.374452
C2	0.000384	0.976562	0.689094	–0.463659	–1.046339	–0.517106
H3	0.876351	1.010685	1.351755	0.317939	–1.788309	–0.723708
H4	–0.876017	1.011888	1.351081	–0.735928	–0.612240	–1.492058
C5	0.001426	2.198366	–0.226126	–1.668020	–1.761084	0.094333
H6	–0.882205	2.191969	–0.869695	–2.477141	–1.056728	0.299869
H7	0.002298	3.124038	0.361020	–2.042681	–2.538076	–0.582194
H8	0.884888	2.190477	–0.869904	–1.380934	–2.228605	1.040416
C9	–1.208132	–1.073226	0.185244	–0.201458	1.347150	–0.090185
H10	–1.345146	–1.266133	1.267974	0.168905	1.515068	–1.119198
H11	–1.073604	–2.045837	–0.300337	0.348221	2.032864	0.566006
C12	–2.456772	–0.405753	–0.382343	–1.687748	1.687490	–0.038303

Table J-1 continued

	Conformer V			Conformer VI		
	a /Å	b /Å	c /Å	a /Å	b /Å	c /Å
H13	–3.331529	–1.043658	–0.219891	–1.842914	2.734092	–0.320197
H14	–2.654550	0.557215	0.096614	–2.263271	1.068440	–0.732257
H15	–2.335682	–0.238921	–1.456187	–2.076434	1.530493	0.971558
C16	1.207055	–1.074199	0.184898	1.486742	–0.211165	0.701919
H17	1.343800	–1.267811	1.267527	1.735451	0.471946	1.523374
H18	1.071899	–2.046418	–0.301293	1.586351	–1.228251	1.098718
C19	2.456241	–0.407272	–0.382123	2.484104	–0.007354	–0.447072
H20	2.654803	0.555194	0.097489	2.482091	1.028209	–0.798297
H21	3.330451	–1.046050	–0.220129	3.498275	–0.244275	–0.108557
H22	2.335398	–0.239650	–1.455870	2.252288	–0.657110	–1.296885

Table J-1 continued

	Conformer VII		
	a /Å	b /Å	c /Å
N1	0.073814	–0.009432	0.374452
C2	–0.463659	–1.046339	–0.517106
H3	0.317939	–1.788309	–0.723708
H4	–0.735928	–0.612240	–1.492058
C5	–1.668020	–1.761084	0.094333
H6	–2.477141	–1.056728	0.299869
H7	–2.042681	–2.538076	–0.582194
H8	–1.380934	–2.228605	1.040416
C9	–0.201458	1.347150	–0.090185
H10	0.168905	1.515068	–1.119198
H11	0.348221	2.032864	0.566006
C12	–1.687748	1.687490	–0.038303
H13	–1.842914	2.734092	–0.320197
H14	–2.263271	1.068440	–0.732257
H15	–2.076434	1.530493	0.971558
C16	1.486742	–0.211165	0.701919
H17	1.735451	0.471946	1.523374
H18	1.586351	–1.228251	1.098718
C19	2.484104	–0.007354	–0.447072
H20	2.482091	1.028209	–0.798297
H21	3.498275	–0.244275	–0.108557
H22	2.252288	–0.657110	–1.296885

Table J-2

Fitted parameters and their values from the *.par file of the *spfit* program

A. Main isotopologue

```
6    48    30    0    0.0000E+000    1.0000E+006    1.0000E+000 1.0000000000
's'  -3 -1  0    30    0    6    2    2    0    1    0
         10000  2.314873978171599E+003 1.00000000E+037 /A
        -20000  2.314873978171599E+003 1.00000000E-037 /B
         30000  1.326200000000000E+003 1.00000000E-037 /C
     110030000 -7.866604626405583E+000 1.00000000E+037 /1.5eqQ
           200 -9.619265665507071E-004 1.00000000E+037 /-DJ
          1100  1.588482320026774E-003 1.00000000E+037 /-DJK
```

B. $^{13}C_2$ isotopologue

```
6    16    30    0    0.0000E+000    1.0000E+006    1.0000E+000 1.0000000000
'a'   3 -2  0 ,,,,,,,,
         10000  2.312933148388725E+003 1.00000000E+037 /A
         20000  2.292833008304470E+003 1.00000000E+037 /B
         30000  1.326805735176605E+003 1.00000000E+037 /C
     110030000 -7.899035842546669E+000 1.00000000E+037 /1.5eqQ
           200 -9.693832871525565E-004 1.00000000E+037 /-DJ
          1100  3.594275012304982E-002 1.00000000E+037 /-DJK
```

C. $^{13}C_5$ isotopologue

```
7    10    30    0    0.0000E+000    1.0000E+006    1.0000E+000 1.0000000000
'a'   3 -2  0 ,,,,,,,,
         10000  2.313028148094109E+003 1.00000000E+037 /A
         20000  2.251267851743531E+003 1.00000000E+037 /B
         30000  1.329893199268403E+003 1.00000000E+037 /C
     110030000 -8.920996876517142E+000 1.00000000E+037 /1.5eqQ
     110040000 -5.641992532481138E-001 1.00000000E+036 /0.25X-
           200 -1.369036407949056E-003 1.00000000E+037 /-DJ
          1100 -1.987760643678322E-002 1.00000000E+037 /-DJK
```

Table J-3

The energy values, dipole moments, and rotational constants of the stable conformers of related molecules as calculated at the MP2/6-311++G(d,p) level of theory.

A. Triethyl phosphane

Conf.	rel. E kJ/mol	μ_a /D	μ_b /D	μ_c /D	α_1 /°	α_2 /°	α_3 /°	A /GHz	B /GHz	C /GHz	Freq. calc.
I	12.8898	−0.490	0.585	1.314	80.5	176.5	56.2	2.314	1.608	1.299	0
II	1.9084	−0.288	−0.525	1.336	−167.2	54.1	−178.8	2.344	1.590	1.159	0
III	0.0000	0.000	0.000	1.407	67.0	168.0	67.0	1.892	1.892	1.040	0
IV	0.4886	0.000	0.715	1.273	50.7	−168.9	168.9	2.778	1.468	1.157	0
V	6.0054	0.000	−0.319	1.394	129.4	176.0	−176.0	2.364	1.545	1.033	1
VI	6.7048	−0.611	0.111	1.344	155.4	175.4	−50.8	2.263	1.607	1.151	0
VII	27.3810	0.000	0.000	1.558	−77.9	30.3	−77.9	1.862	1.862	1.551	0
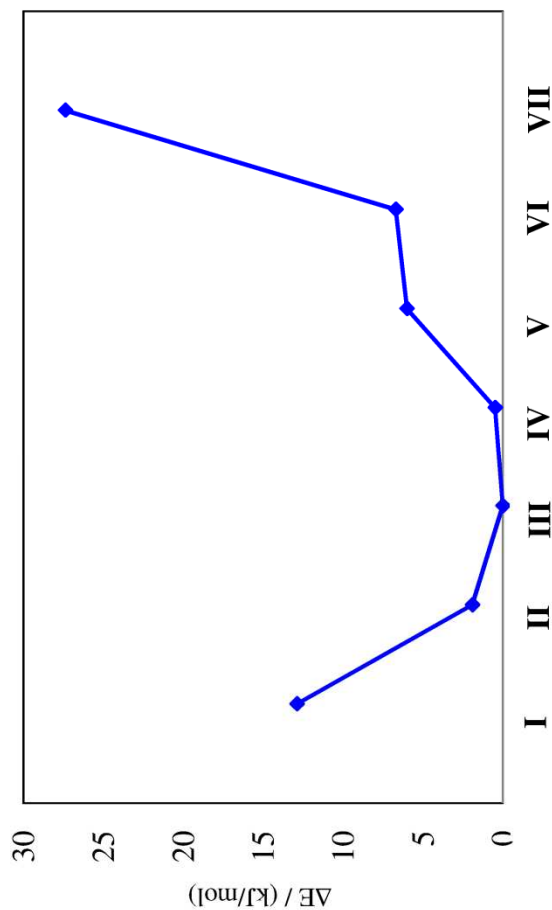
FIG. J-1 Stable conformers of triethyl phosphine. The energy values are relative to the most stable conformer III (−577.8018180 Hartree).

Table J-3/A. continued

Cartesian nuclear coordinates of conformer III (most stable) in the *Gaussian03* internal coordinate system (called

standard orientation)

Number	Atomic number	a /Å	b /Å	c /Å
1	6	−0.966140	−1.315831	0.299141
2	1	−0.784949	−1.246439	1.380952
3	1	−0.583746	−2.286420	−0.034972
4	6	−2.467839	−1.238127	0.001931
5	1	−2.654105	−1.254363	−1.076749
6	1	−2.997439	−2.085318	0.448260
7	1	−2.910051	−0.323319	0.405783
8	6	1.622539	−0.178783	0.299018
9	1	1.471852	−0.057020	1.380882
10	1	2.271654	0.637980	−0.034811
11	6	2.306431	−1.517855	0.001273
12	1	3.304885	−1.552889	0.447683
13	1	1.735439	−2.358540	0.404687
14	1	2.413751	−1.670532	−1.077466
15	6	−0.656558	1.494595	0.298692
16	1	−1.688249	1.648633	−0.035650
17	1	−0.687265	1.303251	1.380546
18	6	0.161616	2.756195	0.001322
19	1	−0.307412	3.638546	0.447290
20	1	1.174875	2.681913	0.405433
21	1	0.240936	2.925322	−1.077388
22	15	−0.000031	−0.000132	−0.584849

Table J-3 continued

B. Triisopropyl amine

| Conf.	rel. E kJ/mol	μ_a / D	μ_b / D	μ_c / D	A / GHz	B / GHz	C / GHz	Freq. calc.
I	27.7414	−0.071	−0.383	0.747	1.474	1.068	0.855	0
II	8.8007	0.292	0.165	0.747	1.310	1.194	0.867	0
III	18.8596	0.000	0.000	0.194	1.265	1.265	0.890	0
IV	20.9184	−0.117	0.263	0.647	1.400	1.144	0.844	0
V	22.3288	0.269	−0.112	0.336	1.430	1.076	0.902	1
VI	29.8116	−0.077	−0.280	−0.839	1.352	1.183	0.814	0
VII	0.0000	0.000	0.000	0.555	1.186	1.186	0.953	0
VIII	15.6744	0.105	-0.356	0.392	1.387	1.087	0.911	0
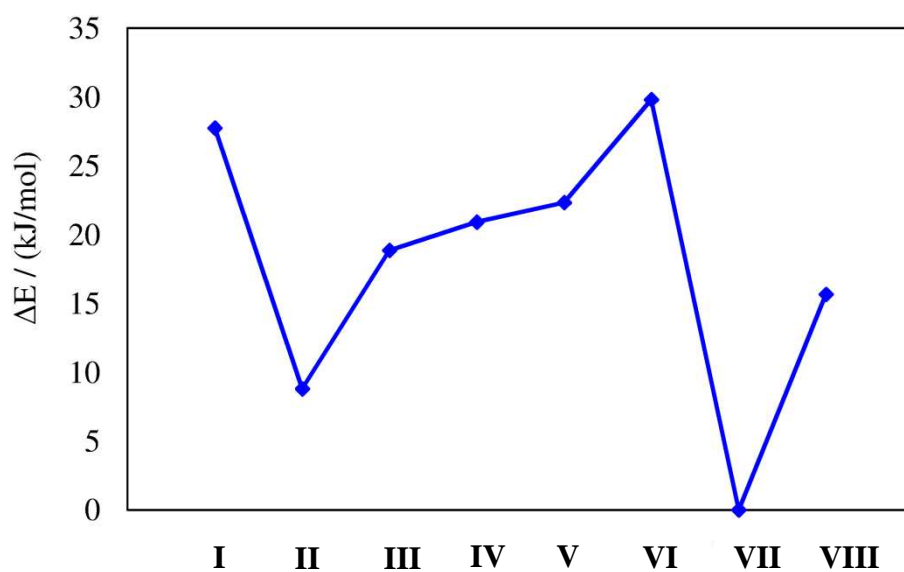
FIG. J-2 Stable conformers of triisopropyl amine. The energy values are relative to the most stable conformer VII (−409.1508669 Hartree).

Table J-3/B. continued

Cartesian nuclear coordinates of conformer VII (most stable) in the *Gaussian03* internal coordinate system

(called standard orientation)

Number	Atomic number	a /Å	b /Å	c /Å
1	7	0.000039	−0.000007	−0.325707
2	6	−0.932943	1.098862	−0.067962
3	1	−1.937174	0.662320	−0.125409
4	6	−0.485187	−1.357397	−0.067945
5	1	0.394971	−2.008852	−0.125149
6	6	1.418161	0.258503	−0.067800
7	1	1.542213	1.346474	−0.125029
8	6	−0.805949	1.778119	1.306973
9	1	−1.582844	2.543757	1.415116
10	1	−0.917011	1.062408	2.125124
11	1	0.163780	2.276900	1.410066
12	6	−0.837931	2.145389	−1.184491
13	1	0.152950	2.612528	−1.201232
14	1	−1.010388	1.674039	−2.155787
15	1	−1.578218	2.939755	−1.035391
16	6	−1.438803	−1.798433	−1.184626
17	1	−0.944170	−1.712222	−2.155828
18	1	−1.756677	−2.836695	−1.035494
19	1	−2.338767	−1.173835	−1.201608
20	6	−1.137260	−1.586863	1.306868
21	1	−0.462085	−1.325125	2.125145
22	1	−2.054079	−0.996390	1.409685
23	1	−1.411946	−2.642469	1.415066
24	6	1.942831	−0.191388	1.307080
25	1	1.889955	−1.280614	1.409925
26	1	2.994324	0.098614	1.415367
27	1	1.378464	0.262443	2.125291
28	6	2.277069	−0.346797	−1.184390
29	1	1.955134	0.038393	−2.155635
30	1	3.335132	−0.102849	−1.035185
31	1	2.186240	−1.438496	−1.201339

Table J-3 continued

C. Tri-n-propyl amine

Conf.	E_{MP2} / Hartree	μ_a / D	μ_b / D	μ_c / D	A / GHz	B / GHz	C / GHz	Freq. calc.
chain	−409.1473522	0.000	0.000	0.547	0.913	0.913	0.485	0
ring	−409.1413649	0.000	0.000	0.674	1.121	1.121	0.656	0

Table J-3/B. continued

Cartesian nuclear coordinates of the *chain* tri-n-propyl amine and the *ring* tri-n-propyl amine in the *Gaussian03* internal coordinate system (called standard orientation)

Nr.	Atomic number	*chain* tri-n-propyl amine			*ring* tri-n-propyl amine		
		a /Å	b /Å	c /Å	a /Å	b /Å	c /Å
1	7	−0.000003	−0.000013	−0.057498	0.000078	−0.000067	0.366425
2	6	1.269563	−0.571150	0.399921	1.400942	0.145269	0.790525
3	1	1.192267	−0.903324	1.454912	1.575865	−0.387183	1.744228
4	1	2.030052	0.217381	0.376346	1.589456	1.203905	0.991907
5	6	1.751648	−1.724021	−0.477117	2.414207	−0.321330	−0.256693
6	1	1.879708	−1.344519	−1.496632	2.262952	0.272093	−1.165707
7	1	0.984890	−2.505383	−0.523539	3.416925	−0.081637	0.122757
8	6	−0.140197	1.385038	0.399878	−0.826205	1.140343	0.790842
9	1	0.185973	1.484206	1.454915	−0.452492	1.557841	1.744620
10	1	−1.203320	1.649393	0.376141	−1.837249	0.774221	0.992202
11	6	0.617308	2.378945	−0.477079	−0.928812	2.251397	−0.256115
12	1	1.677368	2.105581	−0.523365	−1.637813	2.999785	0.123500
13	1	0.224746	2.300091	−1.496643	−1.367049	1.823881	−1.165242
14	6	−1.129406	−0.813961	0.399832	−0.574384	−1.285950	0.790570
15	1	−0.826773	−1.866828	0.376032	0.248221	−1.978575	0.991570
16	1	−1.378366	−0.581130	1.454885	−1.122612	−1.171311	1.744488
17	6	−2.368916	−0.654879	−0.477105	−1.485504	−1.929987	−0.256411
18	1	−2.662208	0.399841	−0.523395	−1.779118	−2.918288	0.122969
19	1	−2.104385	−0.955437	−1.496673	−0.896303	−2.095532	−1.165680
20	6	3.061252	−2.319544	0.042423	2.351851	−1.807536	−0.608746
21	1	3.414123	−3.128123	−0.604134	2.494493	−2.431936	0.280401
22	1	3.845820	−1.556504	0.084871	1.390853	−2.064629	−1.061094
23	1	2.933513	−2.725810	1.051196	3.137245	−2.064482	−1.326478
24	6	0.478205	3.810868	0.042421	0.389427	2.940673	−0.607956

Table J-3/B. continued

Nr.	Atomic number	*chain* tri-n-propyl amine			*ring* tri-n-propyl amine		
		a /Å	b /Å	c /Å	a /Å	b /Å	c /Å
25	1	1.002108	4.520734	−0.604086	0.858793	3.376188	0.281330
26	1	−0.574891	4.108823	0.084740	1.092635	2.237137	−1.060472
27	1	0.893794	3.903385	1.051242	0.219237	3.749503	−1.325474
28	6	−3.539448	−1.491282	0.042442	−2.741572	−1.132843	−0.607829
29	1	−4.416162	−1.392526	−0.604068	−3.353280	−0.944330	0.281600
30	1	−3.270942	−2.552267	0.084803	−2.483930	−0.171966	−1.060126
31	1	−3.827354	−1.177586	1.051249	−3.357075	−1.684435	−1.325398

Table J-3 continued

D. Tri-tert-butyl amine

Conf.	E_{MP2} / Hartree	μ_a / D	μ_b / D	μ_c / D	A / GHz	B / GHz	C / GHz	Freq. calc.
I	−526.694531	0.000	0.000	0.521	0.840	0.840	0.5848	0

Table J-3/B. continued

Cartesian nuclear coordinates of the *chain* tri-n-propyl amine and the *ring* tri-n-propyl amine in the *Gaussian03* internal coordinate system (called standard orientation)

Number	Atomic number	a /Å	b /Å	c /Å
1	7	−0.000005	−0.000008	−0.304005
2	6	−1.389865	−0.541522	−0.029630
3	6	−1.771151	−1.630607	−1.075898
4	1	−1.491757	−2.643440	−0.796632
5	1	−2.858229	−1.632924	−1.207805
6	1	−1.312923	−1.385318	−2.038238
7	6	0.225952	1.474413	−0.029621
8	6	1.687607	1.934757	−0.241193
9	1	1.708829	3.002692	−0.003396
10	1	2.415483	1.454755	0.407625
11	1	1.995941	1.824767	−1.282662
12	6	1.163904	−0.932896	−0.029627

Table J-3/B. continued

Number	Atomic number	a /Å	b /Å	c /Å
13	6	2.297704	−0.718556	−1.075913
14	1	2.843217	−1.658845	−1.207888
15	1	1.856155	−0.444294	−2.038228
16	1	3.035178	0.029783	−0.796615
17	6	−2.519349	0.494151	−0.241214
18	1	−3.454848	−0.021464	−0.003580
19	1	−2.467681	1.364440	0.407704
20	1	−2.578138	0.816283	−1.282657
21	6	−1.613606	−1.084873	1.402331
22	1	−2.625030	−1.505085	1.467932
23	1	−0.917375	−1.873525	1.683383
24	1	−1.534954	−0.286823	2.145549
25	6	−0.132754	1.939833	1.402345
26	1	−1.163846	1.731137	1.683407
27	1	0.519088	1.472731	2.145554
28	1	0.008971	3.025867	1.467953
29	6	−0.526544	2.349156	−1.075908
30	1	−1.543365	2.613666	−0.796640
31	1	0.015031	3.291724	−1.207852
32	1	−0.543265	1.829642	−2.038230
33	6	1.746349	−0.854956	1.402328
34	1	2.081199	0.142337	1.683366
35	1	1.015909	−1.185879	2.145555
36	1	2.615997	−1.520740	1.467928
37	6	0.831751	−2.428902	−0.241182
38	1	0.052177	−2.819278	0.407693
39	1	0.582254	−2.640919	−1.282636
40	1	1.746025	−2.981238	−0.003462